COMBINED UNTARGETED AND TARGETED LC-MS ANALYSIS OF THE FATTY ACID AND OXYLIPIN PATTERN IN PHOSPHOLIPIDS

Dissertation

to obtain the academic degree

Doctor rerum naturalium

(Dr. rer. nat.)

Faculty of Mathematics and Natural Sciences

of the

Bergische Universität Wuppertal

by

Laura Carpanedo

Avignon (France)

- 2025 -

First reviewer: ..... Prof. Dr. Nils Helge Schebb

Second reviewer: ..... Prof. Dr. Dieter Steinhilber

Third reviewer: .....Prof. Dr. Julia Bornhorst

Day of the oral examination: 18. 08. 2025

Promotion Day: 18. 08. 2025

Pour ma famille

Table of Contents

Chapter 1

Introduction and Scope

Lipids are a structurally diverse group of molecules including glycerolipids, phospholipids (PL), sphingolipids (SL), fatty acids (FA), and sterols [1]. Among them, cholesterol and triglycerides are hydrophobic, whereas PL are amphiphilic – possessing both hydrophobic and hydrophilic regions. This structural diversity underlies a wide range of biological functions. Triacylglycerols' (TG) primary role is energy storage in adipose tissue [2] while cholesterol contributes to membrane stability and also serves as a precursor to steroid hormones [3], such as estrogen [4]. PL are the main component of cellular membranes [5] and also play a crucial role in cell signaling [6, 7]. SL, including sphingomyelin (SM), are also important constituents of the lipid membrane [8, 9]. They act as a selective barrier between the extracellular and intracellular environments, regulating the transport of substances inside the cells [10]. The amphiphilic property of PL drives the formation of bilayer or monolayer structures including micelles, lipid droplets, and lipoproteins [11, 12]. The shape of these self-assembled structures varies, but they typically contain a hydrophobic core surrounded by a hydrophilic surface [11]. The hydrophobic region consists of two non-polar fatty acyl chains, while the hydrophilic region comprises a phosphate group and an organic moiety [9]. These regions are commonly referred to as the hydrophobic tails and the polar head group, respectively.

In PL, the polar head group is linked to a glycerol backbone at the *sn*-3 position via the phosphate group (Fig. 1.1) [8]. The two fatty acyl chains are attached at the *sn*-1 and *sn*-2 positions through their carboxyl ends. Fatty acyl chains can be chemically attached through an ester bond, and at the *sn*-1 position, they can also be linked via an ether bond or a vinyl-ether bond, forming ether PL (PL-O) and plasmalogen PL (PL-P), respectively [13].

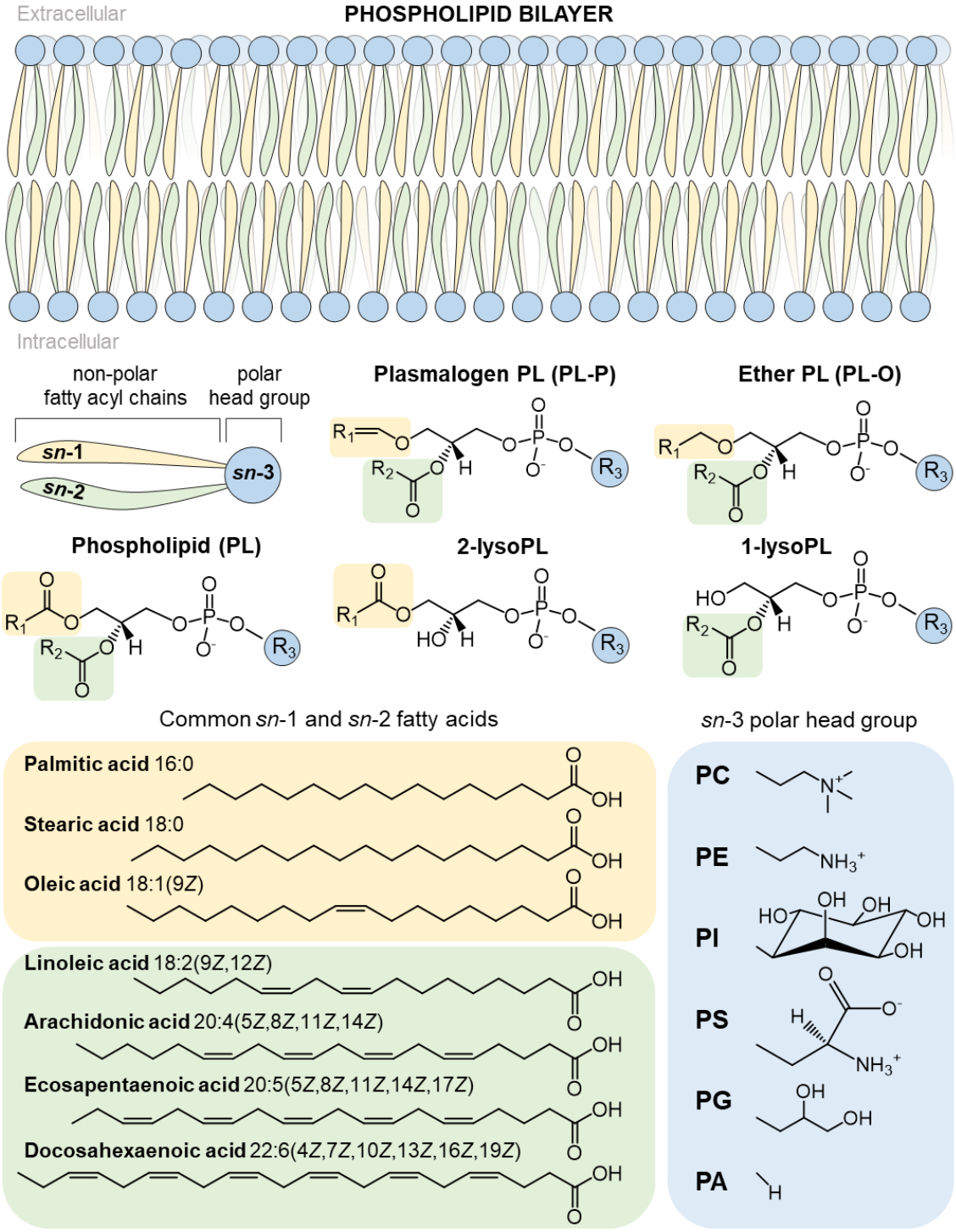

Fig. 1.1: Structure of PL. Shown is a simplified schematic representation of the PL bilayer, including the structures of different PL molecules, the typical FA at the *sn*-1 and *sn*-2 positions, and the head group attached at the *sn*-3 position.

In the case of lysoPL, only one fatty acyl chain is bound either on the *sn*-1 or *sn*-2 position. In PL, the *sn*-1 position is typically occupied by saturated or mono-unsaturated fatty acyl chains such as palmitic acid, stearic acid, or oleic acid [14, 15]. In contrast, the *sn*-2 position comprises *cis*-unsaturated fatty acyl chains such as n6-polyunsaturated FA (PUFA) including linoleic acid (LA), dihomo-γ-linolenic acid (DGLA), arachidonic acid (ARA), and adrenic acid (AdA); and n3-PUFA including α-linolenic acid (ALA), eicosapentaenoic acid (EPA), and docosahexaenoic acid (DHA).

PL are classified according to their distinctive head group at the *sn*-3 position into phosphatidylcholine (PC), phosphatidylethanolamine (PE), phosphatidylinositol (PI), phosphatidylserine (PS), phosphatidylglycerol (PG), and phosphatidic acid (PA) [8, 16]. PI 4-phosphate (PIP), PI 4,5-bisphosphate (PIP_2), and PI 3,4,5-trisphosphate (PIP_3) – which bear additional phosphate group(s) on the inositol ring – are phosphorylated derivatives of PI and are summarized as phosphoinositides. SM are also classified as a PL due to the presence of a phosphate group [8] but differs from other PL in its unique backbone structure and fatty acyl chain composition. Indeed, SM are derived from a sphingosine backbone [8] and commonly contain longer and more saturated fatty acyl chains compared to other PL [13, 17]. In mammalian cells, PC is the most abundant lipid, accounting on average for 45 – 55% of the total lipids, and PE is the second most abundant, ranging from 15% to 25% [18]. Cholesterol and PI contribute 10 – 20% and 10 – 15%, respectively, of the lipid membrane. PS and SM are present in similar amounts with 5 – 10% of the lipids. PA, PG, and phosphorylated derivatives of PI – i.e., PIP, PIP_2, and PIP_3 – are minor components, accounting each for approximately 1% of the total. PL classes are asymmetrically distributed across the cellular membranes [19, 20]. In human erythrocyte membrane, approximately 65 – 75% of PC and more than 85% of SL are located on the outer leaflet of the membrane, i.e., oriented toward the extracellular space [19, 21]. In contrast, PE, PS, PA, PI, and its phosphorylated derivatives are nearly exclusively (> 80%) found on the inner leaflet, i.e. facing the cytoplasm [19, 22-24].

PL can be synthesized *de novo* in mammalian cells [18, 25]. The synthesis of all PL requires either a diacylglycerol (DG) or a cytidine diphosphate-DG (CDP-DG) unit. These two-lipid species are generated from PA. First, lysoPA is formed from glycerol 3-phosphate via glycerol-3-phosphate acyltransferases. Then, a fatty acyl chain is incorporated into lysoPA via lysoPA acyl transferase enzymes, forming PA. Subsequently, DG and CDP-DG are generated via PA phosphatase-1 and CDP-DG synthetases, respectively. PC and PE are synthesized via the Kennedy's pathway using DG as an intermediate [26] while CDP-DG serves as a precursor for the synthesis of PI and PG. PS synthesis is made from PC or PE via a base-exchange reaction catalyzed by PS synthases [18, 27] while SM is formed from ceramide and PC via SM synthase 1 [18]. In mammalian cells, most PL synthesis occurs in the endoplasmic reticulum (ER) with a few exceptions – PS is synthesized in an ER subdomain called mitochondria-associated membranes, and SM synthesis is made in the Golgi apparatus. Following their synthesis, the fatty acyl chain composition of PL is modulated by diacylation and reacylation reactions [25, 28].

Remodeling of the fatty acyl chains in PL occurs through the exchange of FA, involving the formation of a lysoPL intermediate, followed by reacylation – known as the Lands' cycle [29]. Specifically, fatty acyl chains are selectively deacylated either at the *sn*-1 position by phospholipases 1 (PLA_1) or at the *sn*-2 position by PLA_2, generating 2-acyl-lysoPL or 1-acyl-lysoPL, respectively [30-32]. Subsequently, lysoPL acyltransferases (LPLAT) catalyze the reacylation of the FA into 2-lysoPL or 1-lysoPL [33, 34]. Incorporation of FA into the lysoPL by LPLAT enzymes commonly requires the activation of the FA [30, 35] through its coupling to coenzyme A (CoA) by the acyl-CoA synthetase (ACS) enzymes in a two-step reaction [36]. In the first step, the ACS catalyzes the reaction between the FA and adenosine triphosphate, resulting in the formation of an acyl-adenosine monophosphate (AMP). The subsequent acyl-AMP intermediate reacts with CoA, forming the acyl-CoA. Based on the chain length of the preferred acyl groups, ACS can be divided into five subfamilies: short-chain (C2 – C4), medium-chain (C4 – C12), long-chain (ACSL) (C12 – C22), bubblegum (C14 – C24), and very long-chain (C18 – C26) [36].

Activation of PUFA including LA, ARA, EPA, and DHA can be mediated by the isoenzymes of the ACSL family encoded by five genes, i.e., ACSL1, ACSL3, ACSL4, ACSL5, and ACSL6 [35, 36]. These exhibit differences in substrate preferences. Both ACSL1 and ACSL5 preferred substrates are palmitic acid, palmitoleic acid, oleic acid, and LA [37]. In contrast, both ACSL3 and ACSL4 preferentially take ARA and EPA as substrates, and also myristic acid is preferred by ACSL3 [38, 39]. ACSL6 can use both unsaturated and FA substrates including palmitic acid, oleic acid, ARA, and EPA as substrate [36].

Upon activation, LPLAT enzymes catalyze the acylation of lysoPL using (ox)FA-CoA as a donor, leading to the generation of PL species [33, 34]. LPLATs are membrane-bound enzymes primarily localized to the ER [40]. They regulate the fatty acyl composition of PL through the Kennedy pathway and/or the Lands' cycle, depending on their specific enzymatic activities [25, 40]. A total of 14 distinct LPLAT have been identified to date [40]. Based on their structures, they can be classified into two main families: the 1-acylglycerol-3-phosphate O-acyltransferase (AGPAT) family [41] and the membrane-bound O-acyltransferase (MBOAT) family [42]. LPLATs exhibit distinct acyl-CoA substrate specificities and lysoPL enzymatic activities [25, 40]. LPLAT1, LPLAT2, LPLAT3, and LPLAT4 contribute to the de novo pathway by incorporating a variety of acyl-CoA into lysoPA [43-46], a key intermediate in the PL synthesis [25]. Following PL synthesis, LPLAT6, LPLAT7, or LPLAT8 regulate the incorporation of saturated FA-CoA into various lysoPL [40]. LPLAT6 preferentially incorporates 18:0 into 2-acyl-lysoPI [47], LPLAT7 incorporates 16:0, 18:0, and 18:1 into lysoPG [48], while LPLAT8 mainly generates PC containing 16:0 [49]. Incorporation of PUFA can be mediated by LPLAT9, LPLAT11, or LPLAT12 [40]. LPLAT9 preferentially incorporates 20:4-CoA into lysoPC [50] while LPLAT11 transfers both 20:4- and 20:5-CoA into lysoPI [51]. LPLAT12 has the ability to incorporate both 18:2- and 20:4-CoA into lysoPC, lysoPE, and lysoPS [52]. The acyl-CoA and lysoPL enzymatic activities of the different LPLAT contribute greatly to the remarkable molecular diversity of PL species [33, 40].

The composition of the fatty acyl chains in PL influences the properties of the cellular membranes [53]. Saturated fatty acids increase membrane rigidity whereas PUFA enhance membrane fluidity through the *cis*-configuration of their double bonds [54, 55]. However, several studies have highlighted that n3- and n6-PUFA have different biological effects: While n6-PUFA typically act pro-inflammatory, n3-PUFA exhibit anti-inflammatory and beneficial health effects [56-58]. n3-PUFA have been reported to reduce the risk of cardiovascular events such as sudden cardiac death by lowering plasma TG levels. Moreover, their anti-inflammatory actions may be mediated through alteration of membrane fluidity and disruption of lipid rafts involved in pro-inflammatory signaling. Specifically, n3-PUFA has been shown to reduce nuclear factor kappa B activation – responsible for the production of pro-inflammatory cytokines – by interfering with the recruitment of toll-like receptor 4 [59, 60]. The n3- and n6-PUFA ratio is primarily influenced by diet [61] or supplementation [62, 63]. The Western diet is characterized by a high dietary intake of n-6 PUFA, primarily due to the consumption of soybean, sunflower, and corn oils [64, 65]. In contrast, the intake of n-3 PUFA – e.g., from flaxseed oil and fatty fish such as salmon – remains low [61]. This results in a high n6- to n3-PUFA ratio of > 10:1 instead of the recommended ratio i.e., 2:1 [65], which may promote a pro-inflammatory state. In **Chapter 2**, an untargeted LC-high resolution (HR)MS method for the analysis of PL was developed and applied to investigate the effect of one year of n3-PUFA supplementation on the PL pattern in human plasma. This method enabled the characterization of specific PL and lysoPL species, which could be used as possible biomarkers for consumption of fatty fish or fish oils.

PUFA can undergo oxidation processes leading to the formation of eicosanoids and other oxylipins [58]. Eicosanoids are formed from ARA through the well-described “ARA cascade” and also EPA through analogous pathways [66]. Oxylipins can also be derived from other non-20-carbon FA, such as n6-PUFA including LA and DGLA, as well as n3-PUFA including ALA and DHA [58]. They can be present in biological samples as non-esterified forms, but the major part is found esterified to lipids, e.g., PL, TG, or lipoproteins [63, 67-69].

Formation of oxPL is not well understood and could occur through two distinct pathways (Fig. 1.2) – Indirect oxidation in which a formed oxPUFA is incorporated into a 1-lysoPL through the Lands' cycle, and direct oxidation of an intact PL [70]. Indirect formation of oxPL requires first the release of the PUFA through the hydrolysis of the PL at the *sn*-2 position by PLA_2 [32]. Oxygenation of non-esterified PUFA can occur via three main enzymatic pathways or non-enzymatically via autoxidation processes. Enzymatic conversion of PUFA by cyclooxygenases (COX), lipoxygenases (LOX), or cytochrome P450 monooxygenases (CYP) leads to the generation of regioselectively and stereospecifically oxygenated products, such as hydroxy-PUFA or epoxy-PUFA [58, 71-71]. This results in a large number of distinct products. Following their formation, several non-esterified oxPUFA are incorporated into the lipid membranes by the combined action of ACSL and LPLAT enzymes [70]. In contrast, direct oxidation of PUFA esterified at the *sn*-2 position of an intact PL can be catalyzed by the 12-LOX, 15-LOX-1, and 15-LOX-2 enzymes or non-enzymatically via lipid peroxidation.

Conversion of non-esterified PUFA by COX forms prostanoids i.e., prostaglandins (PG) and thromboxanes [75]. Oxidation of ARA by COX yields the unstable hydroperoxy endoperoxide PGG_2, which is then reduced to the alcohol PGH_2. Conversion of PGH_2 to PGE_2 can be catalyzed by cytosolic PGE synthase, microsomal PGE synthase-1 or microsomal PGE synthase-2, or even non enzymatically [76]. In addition to PG synthesis, COX enzymes produce in minor amounts 11(*R*)-hydroxyeicosatetraenoic acid (HETE) from ARA [73]. COX exists primarily in two isoforms: COX-1 and COX-2 [77]. COX-1 is constitutively expressed in nearly all tissues under basal conditions and is responsible for the production of PG involved in tissue homeostasis, among other functions [78]. In contrast, COX-2 expression is induced at inflammation sites by pro-inflammatory cytokines such as interleukin 1 or tumor necrosis factor alpha [79].

Oxidation of non-esterified PUFA by CYP isoforms can lead to the formation of *cis*-epoxy-PUFAs via epoxygenase activity and/or hydroxy-PUFAs via ω(-1, -2)-hydroxylase activity, i.e., oxygenation at the methyl end of the PUFA [80].

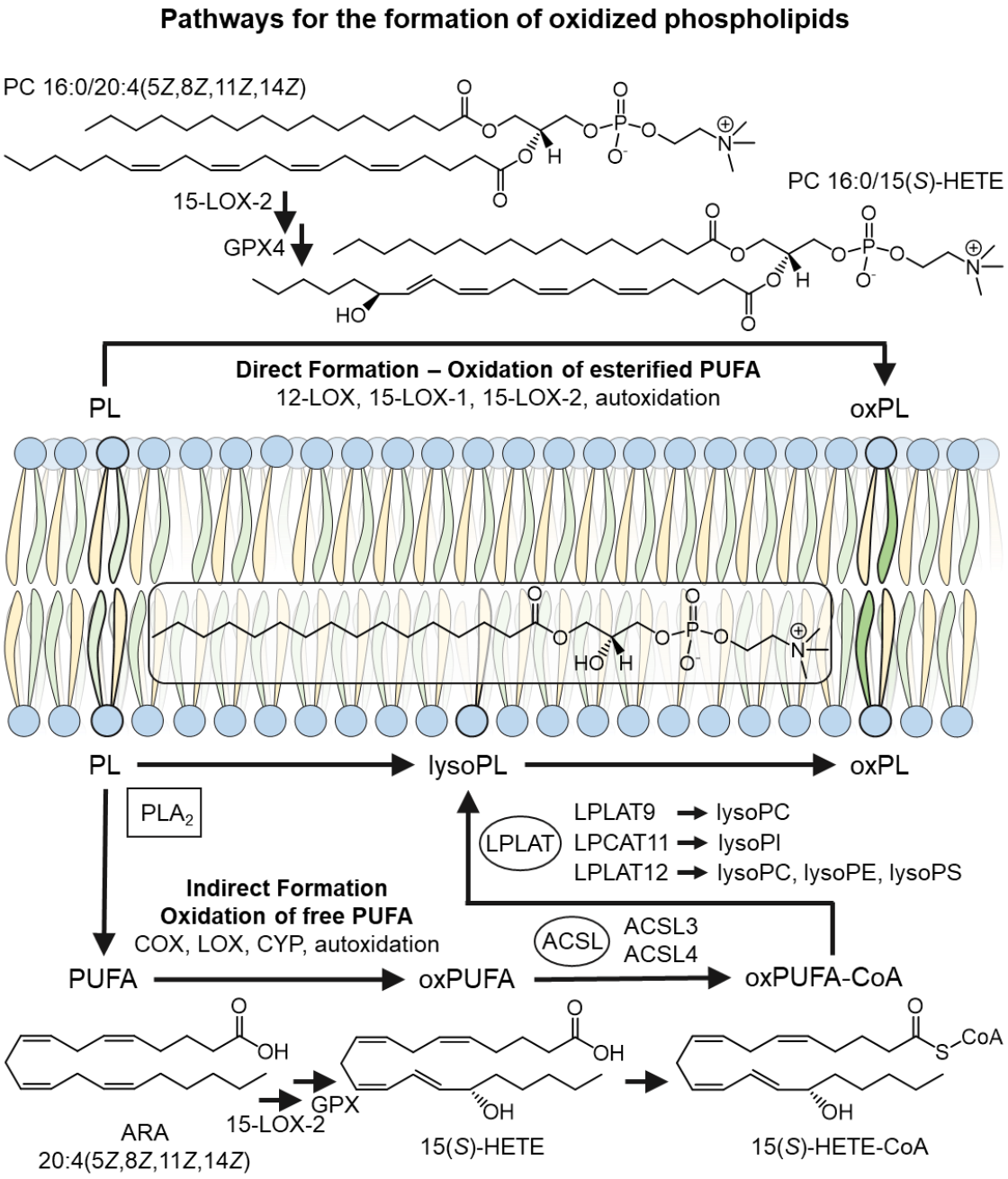

Fig. 1.2: Direct and indirect pathways for the formation of oxPL. The enzymes involved in the release of PUFA are framed, while those responsible for PL remodelling are enclosed in circles. As an example, the formation of PC 16:0/15(*S*)-HETE via 15-LOX-2 is depicted, demonstrating both a direct oxidation pathway and an indirect route. Following the release of the ARA by PLA_2, the non-esterified (free) ARA is oxygenated by 15-LOX-2, followed by the subsequent re-esterification of the activated 15(*S*)-HETE-CoA into lysoPC 16:0/0:0 by LPLAT enzymes.

The different CYP isoforms including CYP4F2, CYP4A11, CYP2E1, CYP1A1, CYP3A4 and the CYP2C-subfamily, give rise to distinct oxylipin products [81]. CYP4F2 and CYP4A11 form mainly 20-HETE from ARA via ω-hydrolase activity, while CYP2E1 and CYP1A1 produce predominantly 19-HETE via (ω-n)-hydrolase activity. Oxidation of PUFA by CYP3A4 via epoxygenase activity can occur at each double bond, yielding 14(15)-, 11(12)-, 8(9)-, and 5(6)-epoxyeicosatrienoic acid (EpETrE) from ARA. In contrast, CYP2C8 produce mainly 14(15)- and 11(12)-EpETrE [81]. These epoxy-PUFA can be converted to the corresponding vicinal dihydroxy-PUFA by soluble epoxide hydrolase (sEH) [82].

LOX enzymes catalyze the formation of stereo- and regioselective hydroperoxy-PUFA, which are reduced to more stable hydroxy-PUFA by glutathione peroxidase (GPX) enzymes [58, 83]. Six different LOX genes – ALOX5, ALOX12, ALOX12B, ALOX15, ALOX15B, and ALOXE3 – have been identified in the human genome [73, 83]**.** These encode for the enzymes 5-LOX, 12-LOX, 12R-LOX, 15-LOX-1, 15-LOX-2, and epidermis-type LOX-3, respectively, exhibiting differences in cell/tissue distribution. 5-LOX is primarily expressed in leukocytes, including neutrophils, macrophages, and dendritic cells [84]. 12-LOX is mainly found in blood platelets and, to a lesser extent, in skin tissue [83, 85]. 15-LOX-1 is present in eosinophils, reticulocytes, and differentiated macrophages [86-88], while 15-LOX-2 is mainly found in epithelial cells of the prostate, skin tissue, and hair roots [89, 90]. 12-LOX, 15-LOX-1, and 15-LOX-2 enzymes can oxygenate both non-esterified PUFA and PUFA esterified to intact lipids [91, 92] unlike other enzymes that require non-esterified PUFA as substrate such as 5-LOX, CYP, or COX. Oxidation of ARA from 15-LOX-1 predominantly yields 15(*S*)-hydroperoxyeicosatetraenoic acid (HpETE), but also produces minor amounts of 12(*S*)-HpETE due to its dual positional activity [93, 94]. In contrast, 5-LOX, 12-LOX, and 15-LOX-2 exclusively produce one product from ARA, i.e., 5(*S*)-HpETE, 12(*S*)-HpETE, and 15(*S*)-HpETE, respectively [89, 94-96].

Subsequent metabolization of these hydroperoxy-PUFA by LOX or other enzymes can form dihydroxy-PUFA and trihydroxy-PUFA and other oxylipins including leukotrienes, lipoxins, and resolvins [74, 84, 97]. 5-LOX enzyme is a key enzyme for the leukotriene synthesis [84]. Leukotriene A_4 (LTA_4) is formed from 5(*S*)-HpETE by 5-LOX and LTA_4 can be further converted to LTB_4 by LTA_4 hydrolase. Dihydroxy-PUFA, such as 5(*S*),15(*S*)-DiHETE, is formed from 5(S)-HpETE via 15-LOX-2 followed by the subsequent reduction of 5(*S*),15(*S*)-DiHpETE to the alcohol by GPX [98]. Dihydroxy- and trihydroxy-PUFA derived from n-3 PUFA, known as resolvins, can also be synthesized through the coordinated actions of various LOX isoforms, although the biosynthetic formation for several resolvins remains unclear [99]. 5(*S*),15(*S*)-DiHEPE, commonly referred to as resolvin E4 (RvE_4), is formed from EPA via a two-step reaction. First, EPA is oxidized to 15(*S*)-HpEPE by 15-LOX-1/-2, which is then converted to 5(*S*),15(*S*)-DiH(p)EPE via 5-LOX. 5(*S*),15(*S*)-DiHEPE (RvE_4) is obtained by subsequent reduction of 5(*S*),15(*S*)-DiH(p)EPE to the alcohol.

Oxylipins are signaling molecules that exhibit a wide range of biological activities, including vasodilatory, pro-thrombotic, pro-inflammatory, and anti-inflammatory effects [67]. Changes in the oxylipin pattern have been associated with several diseases including diabetes [100], atherosclerosis [101], and coronary artery disease [102]. Specifically, PGE_2 is one of the main pro-inflammatory prostanoids by its ability to bind to G-protein-coupled receptors i.e., PGE_2 subtype receptor (EP_1, EP_2, EP_3, and EP_4) [103]. PGE_2 upregulation induces pain hypersensitivity in inflamed tissues, which can be relieved by COX inhibitors such as aspirin [103, 104]. Leukotrienes play a key role in the pathogenesis of several chronic inflammatory diseases such as asthma, atherosclerosis, and cancer [74]. LTB_4 promotes atherosclerosis via the recruitment of monocytes to the vascular wall. Subbano *et al.* showed that actions of LTB_4 are likely mediated by binding to the G protein-coupled receptors BLT-1 [105]: Using BLT-1-deficient mice crossed with apolipoprotein-E-deficient mice, they observed a significant reduction in early atherosclerosis plaque formation. Other oxylipins, especially those derived from n3-PUFA, can have protective effects and be involved in the resolution of inflammation.

Rohwer *et al.* showed that the 15-LOX derived product of EPA 15-HEPE protects wild-type mice against chemically induced colitis [106]. Moreover, 15-HEPE and 17-HDHA serve as precursors to 5(*S*),15(*S*)-DiHEPE (RvE_4) and 7(*S*),17(*S*)-DiHDHA (RvD_5), respectively, which are discussed to play an important role in the resolution of inflammation [98, 99]. However, these specialized pro-resolving mediators (SPM) are either present in low levels or are not detectable in biological samples when state-of-the-art LC-MS methods are applied. Also, strong evidence showing the actions of SPM on specific receptors remains to be provided. Overall, oxylipins are believed to act in non-esterified form, although their physiological actions are not well understood. However, research on the biological functions of esterified oxylipins has been limited, and few studies have evaluated their incorporation into lipids.

In the 1990s, the incorporation of eicosanoids into lipids was investigated using thin-layer chromatography (TLC) with radioactively labeled oxylipins in various biological samples [107-115]. Brezinski *et al.* described a preferential incorporation of [^{3}H]15-HETE into PI, while [^{3}H]5-HETE and [^{3}H]12-HETE were predominantly found in TG of human primary neutrophils [113]. VanRollins *et al.* reported that [$^{14}C_1$]14(15)-EpETrE was primarily found in PI, while [$^{14}C_1$]11(12)-EpETrE and [$^{14}C_1$]8(9)-EpETrE were mostly detected in PC of endothelial cells supplemented with EpETrE regioisomers [115]. These studies offered an initial insight into the lipid incorporation pattern of eicosanoids, however, information on the specific molecular species in which oxylipins are esterified remains scarce. Moreover, this approach does not allow for the analysis of unlabeled oxylipins present in biological samples. Since the late 2010s, endogenous esterified oxylipins have been analyzed as non-esterified oxylipins, following alkaline hydrolysis, by targeted liquid chromatography (LC) coupled to tandem mass spectrometry (MS/MS) [116, 117]. In this analysis, esterified oxylipins are quantified through the parallel analysis of non-esterified and total oxylipins after the cleavage of the ester bond by alkaline hydrolysis [88, 116, 118, 119]. A multiple of targeted LC-MS/MS methods covering the comprehensive analysis of the oxylipins pattern in various biological samples have been developed [88, 116, 118, 119].

These methods allow the sensitive, precise, and accurate quantification of the sum of each esterified oxylipins [120]. Using this approach, Scholz *et al.* showed that esterified erythro- and threo-dihydroxy-FA increase in HepG2 cells exposed to oxidative stress [121]. Shen *et al.* demonstrated a reduction in esterified oxylipins during the early stages of Alzheimer's pathogenesis in transgenic rats [122]. Nevertheless, the analysis of esterified oxylipins using targeted LC-MS remains limited compared to non-esterified oxylipins. Also, this indirect analysis does not allow to draw conclusions about the lipid class, lipid species, or the *sn*-position in which the oxylipins are esterified. In parallel in the 2010s, esterified oxylipins began to be analyzed directly as intact oxPL using targeted LC-MS/MS [123, 124]. With this approach, 12-HETE and 15-HETE were identified in four PE(-P) species, respectively, in activated human monocytes and murine organs [123, 124]. In addition, Slatter *et al.* employed untargeted LC-high-resolution MS (LC-HRMS) to characterize 111 oxPL species in the human platelet lipidome [125]. Despite these advances, only a few direct approaches provide quantitative data on oxPL, and the separation of isobaric and isomeric oxPL species remains a significant challenge.

To learn more about the presence, the origin, and the effects of oxPL in the human organism, the development of state-of-the-art LC-MS/MS methods covering the analysis and quantification of a large number of oxPL is primordial. Direct analysis of oxPL represents a challenge for several reasons, including the presence of many isobaric and isomeric oxPL with the same mass-to-charge ratio (*m/z)*. Isomeric PL species bearing regioisomers of oxylipins can only be differentiated based on the MS^2 spectra through the alpha cleavage occurring at the oxidation group of the esterified oxylipins. Moreover, certain isomeric oxPL species present simultaneously the same *m/z* and fragmentation behavior. In **Chapter 3**, an untargeted LC-HRMS method for the semi-quantification of oxPL in human serum and cells was developed. The chromatographic separation of isobaric and isomeric oxPL species was optimized, enabling their differentiation and characterization based on MS^2 spectra and retention time. This method was applied to characterize the incorporation of oxylipins into PL classes using supplementation with high concentrations of oxylipins in human embryonic kidney

293T (HEK293T) cells. These data show a distinct incorporation of regioisomers into PL classes. However, incorporation of those exogenously added oxylipins into lipids might not reflect the incorporation of endogenously formed oxylipins within biological cells.

In **Chapter 4**, the incorporation of oxylipins into lipids of human cells was further investigated using both indirect and direct analysis of esterified oxylipins. The incorporation pattern of exogenously and endogenously formed oxylipins into PL was compared using supplementation with oxylipins and HEK293T cells genetically modified to overexpress 15-LOX-2 enzyme. Esterified oxylipins were indirectly quantified in lipid fractions separated using hydrophilic interaction liquid chromatography (HILIC)-based cartridges. Based on the untargeted LC-HRMS method developed in Chapter 3, a new targeted LC-MS/MS method for the quantification of oxPL was developed and validated. This targeted method allowed the sensitive detection and accurate quantification of oxPL species formed following supplementation, as well as those formed via 15-LOX-2 within the cells.

Overall, this thesis improves our understanding of the formation of oxylipins and their incorporation into the PL classes and molecular species using combined new state-of-the-art untargeted and targeted LC-MS methods. This work also provides deep insights into the fragmentation behaviour and chromatographic separation of (ox)PL.

1.1 References

1. Fahy E, Subramaniam S, Brown HA, Glass CK, Merrill Jr AH, Murphy RC, et al. (2005) A comprehensive classification system for lipids. *European journal of lipid science and technology*. **107**, 337-64.
2. Ahmadian M, Duncan RE, Jaworski K, Sarkadi-Nagy E, Sook Sul H (2007) Triacylglycerol metabolism in adipose tissue. *Future lipidology*. **2**, 229-37.
3. Cui J, Shen Y, Li R (2013) Estrogen synthesis and signaling pathways during aging: from periphery to brain. *Trends in molecular medicine*. **19**, 197-209.
4. de Meyer F, Smit B (2009) Effect of cholesterol on the structure of a phospholipid bilayer. *Proceedings of the National Academy of Sciences*. **106**, 3654-8.
5. Sj S (1972) The fluid mosaic model of the structure of cell membranes. *Science*. **175**, 720-31.
6. Epand RM (2017) Features of the phosphatidylinositol cycle and its role in signal transduction. *The Journal of membrane biology*. **250**, 353-66.
7. Song G, Ouyang G, Bao S (2005) The activation of Akt/PKB signaling pathway and cell survival. *Journal of cellular and molecular medicine*. **9**, 59-71.
8. Li J, Wang X, Zhang T, Wang C, Huang Z, Luo X, et al. (2015) A review on phospholipids and their main applications in drug delivery systems. *Asian journal of pharmaceutical sciences*. **10**, 81-98.
9. Fox CF (1972) The structure of cell membranes. *Scientific American*. 226, 30-9.
10. Zhang Q, Li S, Yang Y, Shan Y, Wang H (2021) Studying structure and functions of cell membranes by single molecule biophysical techniques. *Biophysics Reports*. **7**, 384.
11. Thiam AR, Farese Jr RV, Walther TC (2013) The biophysics and cell biology of lipid droplets. *Nature reviews Molecular cell biology*. **14**, 775-86.
12. Van Meer G, Voelker DR, Feigenson GW (2008) Membrane lipids: where they are and how they behave. *Nature reviews Molecular cell biology*. **9**, 112-24.
13. Vaňková Z, Peterka O, Chocholoušková M, Wolrab D, Jirásko R, Holčapek M (2022) Retention dependences support highly confident identification of lipid species in human plasma by reversed-phase UHPLC/MS. *Anal Bioanal Chem*. **414**, 319-31.
14. Beermann C, Möbius M, Winterling N, Schmitt JJ, Boehm G (2005) sn-Position determination of phospholipid-linked fatty acids derived from erythrocytes by liquid chromatography electrospray ionization ion-trap mass spectrometry. *Lipids*. **40**, 211-8.
15. Christie W, Clegg R, Calvert D, Noble R (1984) The positional distributions of fatty acids in the triacylglycerols and phosphatidylcholines of the intestinal and popliteal lymph and plasma of sheep. *Lipids*. **19**, 982-6.
16. O'Donnell VB, Rossjohn J, Wakelam MJ (2019) Phospholipid signaling in innate immune cells. *The Journal of clinical investigation*. **128**, 2670-9.
17. Quehenberger O, Armando AM, Brown AH, Milne SB, Myers DS, Merrill AH, et al. (2010) Lipidomics reveals a remarkable diversity of lipids in human plasma. *J Lipid Res*. **51**, 3299-305.
18. Vance JE (2015) Phospholipid synthesis and transport in mammalian cells. *Traffic*. **16**, 1-18.
19. Zachowski A (1993) Phospholipids in animal eukaryotic membranes: transverse asymmetry and movement. *Biochemical Journal*. **294**, 1.

20. Lorent JH, Levental KR, Ganesan L, Rivera-Longsworth G, Sezgin E, Doktorova M, et al. (2020) Plasma membranes are asymmetric in lipid unsaturation, packing and protein shape. *Nature chemical biology*. **16**, 644-52.
21. Verkleij AJ, Zwaal RF, Roelofsen B, Comfurius P, Kastelijn D, van Deenen LL (1973) The asymmetric distribution of phospholipids in the human red cell membrane. A combined study using phospholipases and freeze-etch electron microscopy. *Biochimica et Biophysica Acta -Biomembranes*. **323**, 178-93.
22. Bretscher MS (1972) Phosphatidyl-ethanolamine: differential labelling in intact cells and cell ghosts of human erythrocytes by a membrane-impermeable reagent. *Journal of molecular biology*. **71**, 523-8.
23. Gascard P, Tran D, Sauvage M, Sulpice J-C, Fukami K, Takenawa T, et al. (1991) Asymmetric distribution of phosphoinositides and phosphatidic acid in the human erythrocyte membrane. *Biochimica et Biophysica Acta-Biomembranes*. **1069**, 27-36.
24. Gordesky SE, Marinetti G, Love R (1975) The reaction of chemical probes with the erythrocyte membrane. *The Journal of membrane biology*. **20**, 111-32.
25. Shindou H, Shimizu T (2009) Acyl-CoA: lysophospholipid acyltransferases. *Journal of biological chemistry*. **284**, 1-5.
26. Kennedy EP, Weiss SB (1956) The function of cytidine coenzymes in the biosynthesis of phospholipides. *Journal of Biological Chemistry*. **222**, 193-214.
27. Vance JE, Tasseva G (2013) Formation and function of phosphatidylserine and phosphatidylethanolamine in mammalian cells. *Biochimica et Biophysica Acta-Molecular and Cell Biology of Lipids*. **1831**, 543-54.
28. Shindou H, Hishikawa D, Harayama T, Yuki K, Shimizu T (2009) Recent progress on acyl CoA: lysophospholipid acyltransferase research. *J Lipid Res*. **50**, S46-S51.
29. Lands WE (1958) Metabolism of glycerolipides: a comparison of lecithin and triglyceride synthesis. *Journal of Biological chemistry*. **231**, 883-8.
30. O'Donnell VB (2022) New appreciation for an old pathway: the Lands Cycle moves into new arenas in health and disease. *Biochemical Society Transactions*. **50**, 1-11.
31. Richmond GS, Smith TK (2011) Phospholipases A1. *International journal of molecular sciences*. **12**, 588-612.
32. Dennis EA, Cao J, Hsu Y-H, Magrioti V, Kokotos G (2011) Phospholipase A2 enzymes: physical structure, biological function, disease implication, chemical inhibition, and therapeutic intervention. *Chemical reviews*. **111**, 6130-85.
33. Valentine WJ, Shimizu T, Shindou H (2023) Lysophospholipid acyltransferases orchestrate the compositional diversity of phospholipids. *Biochimie*. **215**, 24-33.
34. Wang B, Tontonoz P (2019) Phospholipid remodeling in physiology and disease. *Annu Rev Physiol*. **81**, 165-88.
35. Klett EL, Chen S, Yechoor A, Lih FB, Coleman RA (2017) Long-chain acyl-CoA synthetase isoforms differ in preferences for eicosanoid species and long-chain fatty acids. *J Lipid Res*. **58**, 884-94.
36. Soupene E, Kuypers FA (2008) Mammalian long-chain acyl-CoA synthetases. *Experimental biology and medicine*. **233**, 507-21.
37. Oikawa E, Iijima H, Suzuki T, Sasano H, Sato H, Kamataki A, et al. (1998) A novel acyl-CoA synthetase, ACS5, expressed in intestinal epithelial cells and proliferating preadipocytes. *The journal of biochemistry*. **124**, 679-85.

38. Fujino T, Kang M-J, Suzuki H, Iijima H, Yamamoto T (1996) Molecular characterization and expression of rat acyl-CoA synthetase 3. *Journal of Biological Chemistry*. **271**, 16748-52.
39. Kang M-J, Fujino T, Sasano H, Minekura H, Yabuki N, Nagura H, et al. (1997) A novel arachidonate-preferring acyl-CoA synthetase is present in steroidogenic cells of the rat adrenal, ovary, and testis. *Proceedings of the National Academy of Sciences*. **94**, 2880-4.
40. Valentine WJ, Yanagida K, Kawana H, Kono N, Noda NN, Aoki J, et al. (2022) Update and nomenclature proposal for mammalian lysophospholipid acyltransferases, which create membrane phospholipid diversity. *Journal of Biological Chemistry*. **298**, 101470.
41. Lewin TM, Wang P, Coleman RA (1999) Analysis of amino acid motifs diagnostic for the sn-glycerol-3-phosphate acyltransferase reaction. *Biochemistry*. **38**, 5764-71.
42. Shindou H, Eto M, Morimoto R, Shimizu T (2009) Identification of membrane O-acyltransferase family motifs. *Biochemical and biophysical research communications*. **383**, 320-5.
43. Aguado Ba, Campbell RD (1998) Characterization of a human lysophosphatidic acid acyltransferase that is encoded by a gene located in the class III region of the human major histocompatibility complex. *Journal of Biological Chemistry*. **273**, 4096-105.
44. Agarwal AK, Sukumaran S, Cortés VA, Tunison K, Mizrachi D, Sankella S, et al. (2011) Human 1-acylglycerol-3-phosphate O-acyltransferase isoforms 1 and 2: biochemical characterization and inability to rescue hepatic steatosis in Agpat2−/− gene lipodystrophic mice. *Journal of Biological Chemistry*. **286**, 37676-91.
45. Hollenback D, Bonham L, Law L, Rossnagle E, Romero L, Carew H, et al. (2006) Substrate specificity of lysophosphatidic acid acyltransferase β—evidence from membrane and whole cell assays. *J Lipid Res*. **47**, 593-604.
46. Koeberle A, Shindou H, Harayama T, Shimizu T (2010) Role of lysophosphatidic acid acyltransferase 3 for the supply of highly polyunsaturated fatty acids in TM4 Sertoli cells. *The FASEB Journal*. **24**, 4929-38.
47. Imae R, Inoue T, Nakasaki Y, Uchida Y, Ohba Y, Kono N, et al. (2012) LYCAT, a homologue of C. elegans acl-8, acl-9, and acl-10, determines the fatty acid composition of phosphatidylinositol in mice. *J Lipid Res*. **53**, 335-47.
48. Yang Y, Cao J, Shi Y (2004) Identification and Characterization of a Gene Encoding Human LPGAT1, an Endoplasmic Reticulum-associated Lysophosphatidylglycerol Acyltransferase. *Journal of Biological Chemistry*. **279**, 55866-74.
49. Kawana H, Kano K, Shindou H, Inoue A, Shimizu T, Aoki J (2019) An accurate and versatile method for determining the acyl group-introducing position of lysophospholipid acyltransferases. *Biochimica et Biophysica Acta-Molecular and Cell Biology of Lipids*. **1864**, 1053-60.
50. Shindou H, Hishikawa D, Nakanishi H, Harayama T, Ishii S, Taguchi R, et al. (2007) A single enzyme catalyzes both platelet-activating factor production and membrane biogenesis of inflammatory cells: cloning and characterization of acetyl-CoA: LYSO-PAF acetyltransferase. *Journal of Biological Chemistry*. **282**, 6532-9.
51. Caddeo A, Hedfalk K, Romeo S, Pingitore P (2021) LPIAT1/MBOAT7 contains a catalytic dyad transferring polyunsaturated fatty acids to lysophosphatidylinositol. *Biochimica et Biophysica Acta-Molecular and Cell Biology of Lipids*. **1866**, 158891.

52. Hishikawa D, Shindou H, Kobayashi S, Nakanishi H, Taguchi R, Shimizu T (2008) Discovery of a lysophospholipid acyltransferase family essential for membrane asymmetry and diversity. *Proc Natl Academy Sci*. **105**, 2830-5.
53. Stubbs CD, Smith AD (1984) The modification of mammalian membrane polyunsaturated fatty acid composition in relation to membrane fluidity and function. *Biochimica et Biophysica Acta-Reviews on Biomembranes*. **779**, 89-137.
54. Hąc-Wydro K, Wydro P (2007) The influence of fatty acids on model cholesterol/phospholipid membranes. *Chemistry and physics of lipids*. **150**, 66-81.
55. Salem N, Niebylski CD (1995) The nervous system has an absolute molecular species requirement for proper function. *Molecular membrane biology*. **12**, 131-4.
56. Calder PC (2010) Omega-3 fatty acids and inflammatory processes. *Nutrients*. **2**, 355-74.
57. Calder PC (2012) Mechanisms of action of (n-3) fatty acids. *The Journal of nutrition*. **142**, 592S-9S.
58. Gabbs M, Leng S, Devassy JG, Monirujjaman M, Aukema HM (2015) Advances in our understanding of oxylipins derived from dietary PUFAs. *Advances in nutrition*. **6**, 513-40.
59. Calder PC (2015) Marine omega-3 fatty acids and inflammatory processes: Effects, mechanisms and clinical relevance. *Biochimica et Biophysica Acta-Molecular and Cell Biology of Lipids*. **1851**, 469-84.
60. Mozaffarian D, Hao T, Rimm EB, Willett WC, Hu FB (2011) Changes in diet and lifestyle and long-term weight gain in women and men. *New England journal of medicine*. **364**, 2392-404.
61. Welch AA, Shakya-Shrestha S, Lentjes MA, Wareham NJ, Khaw K-T (2010) Dietary intake and status of n–3 polyunsaturated fatty acids in a population of fish-eating and non-fish-eating meat-eaters, vegetarians, and vegans and the precursor-product ratio of α-linolenic acid to long-chain n–3 polyunsaturated fatty acids: Results from the EPIC-Norfolk cohort. *The American journal of clinical nutrition*. **92**, 1040-51.
62. Browning LM, Walker CG, Mander AP, West AL, Madden J, Gambell JM, et al. (2012) Incorporation of eicosapentaenoic and docosahexaenoic acids into lipid pools when given as supplements providing doses equivalent to typical intakes of oily fish. *The American journal of clinical nutrition*. **96**, 748-58.
63. Schebb NH, Ostermann AI, Yang J, Hammock BD, Hahn A, Schuchardt JP (2014) Comparison of the effects of long-chain omega-3 fatty acid supplementation on plasma levels of free and esterified oxylipins. *Prostaglandins & other lipid mediators*. **113**, 21-9.
64. Blasbalg TL, Hibbeln JR, Ramsden CE, Majchrzak SF, Rawlings RR (2011) Changes in consumption of omega-3 and omega-6 fatty acids in the United States during the 20th century. *The American journal of clinical nutrition*. **93**, 950-62.
65. Kris-Etherton PM, Taylor DS, Yu-Poth S, Huth P, Moriarty K, Fishell V, et al. (2000) Polyunsaturated fatty acids in the food chain in the United States. *The American journal of clinical nutrition*. **71**, 179S-88S.
66. Bogatcheva NV, Sergeeva MG, Dudek SM, Verin AD (2005) Arachidonic acid cascade in endothelial pathobiology. Microvascular research. **69**, 107-27.
67. Gladine C, Ostermann AI, Newman JW, Schebb NH (2019) MS-based targeted metabolomics of eicosanoids and other oxylipins: Analytical and inter-individual variabilities. *Free Radical Biology and Medicine*. **144**, 72-89.

68. Goebel B, Carpanedo L, Reif S, Göbel T, Schebb NH, Steinhilber D, et al. (2023) Development of a cell-based model system for the investigation of ferroptosis. *Front Cell Death*. **2**, 1182239.
69. Morrow JD, Awad JA, Boss HJ, Blair IA, Roberts 2nd L (1992) Non-cyclooxygenase-derived prostanoids (F2-isoprostanes) are formed in situ on phospholipids. *Proc Natl Academy Sci*. **89**, 10721-5.
70. O'Donnell VB, Aldrovandi M, Murphy RC, Krönke G (2019) Enzymatically oxidized phospholipids assume center stage as essential regulators of innate immunity and cell death. *Science Signaling*. **12**, eaau2293.
71. Funk CD (2001) Prostaglandins and leukotrienes: advances in eicosanoid biology. *science*. **294**, 1871-5.
72. Yin H, Zhou Y, Zhu M, Hou S, Li Z, Zhong H, et al. (2013) Role of mitochondria in programmed cell death mediated by arachidonic acid-derived eicosanoids. *Mitochondrion*. **13**, 209-24.
73. Buczynski M, Dumlao D, Dennis E (2009) An integrated omics analysis of eicosanoid biology. Thematic review series: proteomics. *J Lipid Res*. **50**, 1015-38.
74. Haeggstrom JZ, Funk CD (2011) Lipoxygenase and leukotriene pathways: biochemistry, biology, and roles in disease. *Chemical reviews*. **111**, 5866-98.
75. Marnett LJ (2000) Cyclooxygenase mechanisms. *Current opinion in chemical biology*. **4**, 545-52.
76. Park JY, Pillinger MH, Abramson SB (2006) Prostaglandin E2 synthesis and secretion: the role of PGE2 synthases. Clinical immunology. **119**, 229-40.
77. Morita I (2002) Distinct functions of COX-1 and COX-2. *Prostaglandins & other lipid mediators*. **68**, 165-75.
78. Korbecki J, Baranowska-Bosiacka I, Gutowska I, Chlubek D (2014) Cyclooxygenase pathways. *Acta Biochimica Polonica*. **61**, 639-49.
79. Feng L, Xia Y, Garcia G, Hwang D, Wilson C (1995) Involvement of reactive oxygen intermediates in cyclooxygenase-2 expression induced by interleukin-1, tumor necrosis factor-alpha, and lipopolysaccharide. *The Journal of clinical investigation*. **95**, 1669-75.
80. Arnold C, Markovic M, Blossey K, Wallukat G, Fischer R, Dechend R, et al. (2010) Arachidonic acid-metabolizing cytochrome P450 enzymes are targets of ω-3 fatty acids. *Journal of Biological Chemistry*. **285**, 32720-33.
81. Kampschulte N, Alasmer A, Empl MT, Krohn M, Steinberg P, Schebb NH (2020) Dietary polyphenols inhibit the cytochrome P450 monooxygenase branch of the arachidonic acid cascade with remarkable structure-dependent selectivity and potency. *Journal of agricultural and food chemistry*. **68**, 9235-44.
82. Norman JE, Nuthikattu S, Milenkovic D, Rutledge JC, Villablanca AC (2023) Sex-specific response of the brain free oxylipin profile to soluble epoxide hydrolase inhibition. *Nutrients*. **15**, 1214.
83. Kuhn H, Banthiya S, Van Leyen K (2015) Mammalian lipoxygenases and their biological relevance. *Biochimica et Biophysica Acta (BBA)-Molecular and Cell Biology of Lipids*. **1851**, 308-30.
84. Rådmark O, Werz O, Steinhilber D, Samuelsson B (2015) 5-Lipoxygenase, a key enzyme for leukotriene biosynthesis in health and disease. *Biochimica et Biophysica Acta-Molecular and Cell Biology of Lipids*. **1851**, 331-9.

85. Funk CD, Furci L, FitzGerald GA (1990) Molecular cloning, primary structure, and expression of the human platelet/erythroleukemia cell 12-lipoxygenase. Proceedings of the *National Academy of Sciences*. **87**, 5638-42.
86. Sigal E, Grunberger D, Cashman JR, Craik CS, Caughey GH, Nade JA (1988) Arachidonate 15-lipoxygenase from human eosinophil-enriched leukocytes: partial purification and properties. *Biochemical and biophysical research communications*. **150**, 376-83.
87. Sigal E, Dicharry S, Highland E, Finkbeiner WE (1992) Cloning of human airway 15-lipoxygenase: identity to the reticulocyte enzyme and expression in epithelium. *American Journal of Physiology-Lung Cellular and Molecular Physiology*. **262**, L392-L8.
88. Hartung NM, Mainka M, Pfaff R, Kuhn M, Biernacki S, Zinnert L, et al. (2023) Development of a quantitative proteomics approach for cyclooxygenases and lipoxygenases in parallel to quantitative oxylipin analysis allowing the comprehensive investigation of the arachidonic acid cascade. *Anal Bioanal Chem*. **415**, 913-33.
89. Brash AR, Boeglin WE, Chang MS (1997) Discovery of a second 15 S-lipoxygenase in humans. *Proceedings of the National Academy of Sciences*. **94**, 6148-52.
90. Benatzy Y, Palmer MA, Brüne B (2022) Arachidonate 15-lipoxygenase type B: Regulation, function, and its role in pathophysiology. *Frontiers in Pharmacology*. **13**, 1042420.
91. Brash AR (1999) Lipoxygenases: occurrence, functions, catalysis, and acquisition of substrate. *Journal of Biological Chemistry*. **274**, 23679-82.
92. O'Donnell VB, Aldrovandi M, Murphy RC, Krönke G (2019) Enzymatically oxidized phospholipids assume center stage as essential regulators of innate immunity and cell death. *Sci Signal*. **12**, eaau2293.
93. Bryant RW, Bailey JM, Schewe T, Rapoport S (1982) Positional specificity of a reticulocyte lipoxygenase. *J biol Chem*. **257**, 6050-5.
94. Kutzner L, Goloshchapova K, Heydeck D, Stehling S, Kuhn H, Schebb NH (2017) Mammalian ALOX15 orthologs exhibit pronounced dual positional specificity with docosahexaenoic acid. *Biochimica et Biophysica Acta-Molecular and Cell Biology of Lipids*. **1862**, 666-75.
95. Borgeat P, Hamberg M, Samuelsson B (1976) Transformation of arachidonic acid and homo-gamma-linolenic acid by rabbit polymorphonuclear leukocytes. Monohydroxy acids from novel lipoxygenases. *Journal of Biological Chemistry*. **251**, 7816-20.
96. Falardeau P, Hamberg M, Samuelsson B (1976) Metabolism of 8, 11, 14-eicosatrienoic acid in human platelets. *Biochimica et Biophysica Acta-Lipids and Lipid Metabolism*. **441**, 193-200.
97. Serhan CN, Petasis NA (2011) Resolvins and protectins in inflammation resolution. *Chemical reviews*. **111**, 5922-43.
98. Kahnt AS, Schebb NH, Steinhilber D (2023) Formation of lipoxins and resolvins in human leukocytes. *Prostaglandins & other lipid mediators*. **166**, 106726.
99. Schebb NH, Kühn H, Kahnt AS, Rund KM, O'Donnell VB, Flamand N, et al. (2022) Formation, signaling and occurrence of specialized pro-resolving lipid mediators—what is the evidence so far? *Frontiers in pharmacology*. **13**, 838782.

100. Buckner T, Vanderlinden LA, DeFelice BC, Carry PM, Kechris K, Dong F, et al. (2021) The oxylipin profile is associated with development of type 1 diabetes: the Diabetes Autoimmunity Study in the Young (DAISY). *Diabetologia*. **64**, 1785-94.
101. Bojic LA, McLaren DG, Harms AC, Hankemeier T, Dane A, Wang S-P, et al. (2016) Quantitative profiling of oxylipins in plasma and atherosclerotic plaques of hypercholesterolemic rabbits. *Analytical and bioanalytical chemistry*. **408**, 97-105.
102. Chiang K-M, Chen J-F, Yang C-A, Xiu L, Yang H-C, Shyur L-F, et al. (2022) Identification of serum oxylipins associated with the development of coronary artery disease: a nested case-control study. *Metabolites*. **12**, 495.
103. Chen L, Yang G, Grosser T (2013) Prostanoids and inflammatory pain. *Prostaglandins & other lipid mediators*. **104**, 58-66.
104. Boutaud O, Sosa IR, Amin T, Oram D, Adler D, Hwang HS, et al. (2016) Inhibition of the biosynthesis of prostaglandin E2 by low-dose aspirin: implications for adenocarcinoma metastasis. *Cancer Prevention Research*. **9**, 855-65.
105. Subbarao K, Jala VR, Mathis S, Suttles J, Zacharias W, Ahamed J, et al. (2004) Role of leukotriene B4 receptors in the development of atherosclerosis: potential mechanisms. *Arterioscler Thromb Vasc Biol*. **24**, 369-75.
106. Rohwer N, Chiu CY, Huang D, Smyl C, Rothe M, Rund KM, et al. (2021) Omega-3 fatty acids protect from colitis via an Alox15-derived eicosanoid. *The FASEB Journal*. **35**, e21491.
107. Fang X, Kaduce TL, Spector AA (1999) 13-(S)-Hydroxyoctadecadienoic acid (13-HODE) incorporation and conversion to novel products by endothelial cells 1. *J Lipid Res*. **40**, 699-707.
108. Alpert SE, Walenga RW, Mandal A, Bourbon N, Kester M (1999) 15-HETE-substituted diglycerides selectively regulate PKC isotypes in human tracheal epithelial cells. *American Journal of Physiology-Lung Cellular and Molecular Physiology*. **277**, L457-L64.
109. Girton RA, Spector AA, Gordon JA (1994) 15-HETE: selective incorporation into inositol phospholipids of MDCK cells. *Kidney international*. **45**, 972-80.
110. Cho Y, Ziboh VA (1994) Incorporation of 13-hydroxyoctadecadienoic acid (13-HODE) into epidermal ceramides and phospholipids: phospholipase C-catalyzed release of novel 13-HODE-containing diacylglycerol. *J Lipid Res*. **35**, 255-62.
111. Alpert SE, Walenga RW (1993) Human tracheal epithelial cells selectively incorporate 15-hydroxyeicosatetraenoic acid into phosphatidylinositol. *American journal of respiratory cell and molecular biology*. **8**, 273-281.
112. Legrand A, Lawson J, Meyrick B, Blair I, Oates J (1991) Substitution of 15-hydroxyeicosatetraenoic acid in the phosphoinositide signaling pathway. Journal of *Biological Chemistry*. **266**, 7570-7.
113. Brezinski ME, Serhan CN (1990) Selective incorporation of (15S)-hydroxyeicosatetraenoic acid in phosphatidylinositol of human neutrophils: agonist-induced deacylation and transformation of stored hydroxyeicosanoids. Proceedings of the National *Academy of Sciences*. **87**, 6248-52.
114. Stenson W, Nickells M, Atkinson J (1983) Esterification of monohydroxyfatty acids into the lipids of a macrophage cell line. Prostaglandins. **26**, 253-64.
115. VanRollins M, Kaduce T, Knapp H, Spector A (1993) 14, 15-Epoxyeicosatrienoic acid metabolism in endothelial cells. *J Lipid Res*. **34**, 1931-42.

116. Ostermann AI, Koch E, Rund KM, Kutzner L, Mainka M, Schebb NH (2020) Targeting esterified oxylipins by LC–MS-Effect of sample preparation on oxylipin pattern. *Prostaglandins & Other Lipid Mediators*. **146**, 106384.
117. Quehenberger O, Dahlberg-Wright S, Jiang J, Armando AM, Dennis EA (2018) Quantitative determination of esterified eicosanoids and related oxygenated metabolites after base hydrolysis. *J Lipid Res.* **59**, 2436-45.
118. Rund KM, Ostermann AI, Kutzner L, Galano J-M, Oger C, Vigor C, et al. (2018) Development of an LC-ESI (-)-MS/MS method for the simultaneous quantification of 35 isoprostanes and isofurans derived from the major n3-and n6-PUFAs. *Anal Chimica Acta.* **1037**, 63-74.
119. Kutzner L, Rund K, Ostermann A, Hartung N, Galano J, Balas L, et al. (2019) Development of an optimized LC-MS method for the detection of specialized pro-resolving mediators in biological samples. *Front Pharmacol.* **10**, 169.
120. Mainka M, Dalle C, Pétéra M, Dalloux-Chioccioli J, Kampschulte N, Ostermann AI, et al. (2020) Harmonized procedures lead to comparable quantification of total oxylipins across laboratories. *J Lipid Res.* **61**, 1424-36.
121. Scholz L, Wende LM, Chromik MA, Kampschulte N, Schebb NH (2025) Oxidative stress leads to the formation of esterified erythro-and threo-dihydroxy-fatty acids in HepG2 cells. *Redox Biology.* **82**, 103589.
122. Shen Q, Patten KT, Valenzuela A, Lein PJ, Taha AY (2022) Probing changes in brain esterified oxylipin concentrations during the early stages of pathogenesis in Alzheimer's Disease transgenic rats. *Neuroscience letters.* **791**, 136921.
123. Maskrey, B. H., Bermudez-Fajardo, A., Morgan, A. H., StewartJones, E, Dioszeghy, V., Taylor, G. W., et al. (2007) Activated platelets and monocytes generate four hydroxyphosphatidylethanolamines via lipoxygenase. *J. Biol. Chem.* **282**, 20151–20163.
124. A.H. Morgan, V. Dioszeghy, B.H. Maskrey, C.P. Thomas, S.R. Clark, S.A. Mathie, et al. (2009) Phosphatidylethanolamine-esterified eicosanoids in the mouse: tissue localization and inflammation-dependent formation in Th-2 disease, *J. Biol. Chem*. **284**, 21185–21191.
125. Slatter, D. A., Aldrovandi, M., O'Connor, A., Allen, S. M., Brasher, C. J., Murphy, R. C., et al. (2016) Mapping the human platelet lipidome reveals cytosolic phospholipase A2 as a regulator of mitochondrial bioenergetics during activation. *Cell. Metab.* **23**, 930–944.

Chapter 2

LC-ESI-HRMS — lipidomics of phospholipids

Characterization of extraction, chromatography and detection parameters *

Lipids are a diverse class of molecules involved in many biological functions including cell signaling or cell membrane assembly. Owing to this relevance, LC-MS/MS-based lipidomics emerged as a major field in modern analytical chemistry. Here, we thoroughly characterized the influence of MS and LC settings — of a Q Exactive HF operating in Full MS/data-dependent MS^2 TOP *N* acquisition mode — in order to optimize the semi-quantification of polar lipids. Optimization of MS-source settings improved the signal intensity by a factor 3 compared to default settings. Polar lipids were separated on an ACQUITY Premier CSH C18 reversed-phase column during an elution window of 28 min, leading to a sufficient number of both data points across the chromatographic peaks, as well as MS^2 spectra. Analysis was carried out in positive and negative ionization mode enabling the detection of a broader spectrum of lipids and to support the structural characterization of lipids. Optimal sample preparation of biological samples was achieved by liquid–liquid extraction using MeOH/MTBE, resulting in an excellent extraction recovery > 85% with an intra-day and inter-day variability < 15%. The optimized method was applied on the investigation of changes in the PL pattern in plasma from human subjects supplemented with n3-PUFA (20:5 and 22:6). The strongest increase was observed for lipids bearing 20:5, while 22:4 bearing lipids were lowered. These results were confirmed by targeted LC-MS/MS using commercially available PL as standards.

* modified from Rund K. M.[#], Carpanedo L.[#], Lauterbach R., Wermund T., West A. L., Wende L. M., Calder P. C., and Schebb N. H. (2024) *Anal and BioAnal Chem.* **416**, 925-944; doi: 10.1007/s00216-023-05080-0. [#]both authors contributed equally.

Author contributions: **KR:** Writing – review & editing, Writing – original draft, Visualization, Methodology, Investigation, Formal analysis, Data curation and Conceptualization. **LC:** Writing – review & editing, Writing – original draft, Visualization, Methodology, Investigation, Formal analysis, Data curation and Conceptualization. **RL:** Writing – review & editing, investigation, Formal analysis. **TM:** Writing – review & editing, investigation, Formal analysis. **ALW:** Writing – review & editing, resources. **LMW:** Writing – review & editing, Investigation, Formal analysis. **PCC:** Writing – review & editing Resources. **NHS:** Writing – review & editing, Writing – original draft, Supervision, Project administration, Investigation, Funding acquisition, Conceptualization.

2.1 Introduction

Lipids are lipophilic small molecules involved in many biological functions including cell membrane assembly, energy metabolism, cell signaling, and regulation of inflammation. They are classified in eight major lipid categories: FA, SL, glycerolipids, glyceroPL, sterol lipids, prenol lipids, saccharolipids, and polyketides [1]. FA can be saturated, e.g., stearic acid, monounsaturated, or polyunsaturated of the n3, n6, or n9 series, e.g., EPA (20:5(5*Z*,8*Z*,11*Z*,14*Z*,17*Z*)), ARA (20:4(5*Z*,8*Z*,11*Z*,14*Z*)), or oleic acid (18:1(9*Z*)) [2]. FA are the major components of PL which are the main constituents of the cellular membrane [3, 4]. Driven by the biological importance, lipidomics has emerged as a major field of research in life sciences in the past decades. However, due to the structural diversity of lipids, a simultaneous analysis of “all”, i.e., a comprehensive set of lipids in untargeted lipidomics is challenging.

Compared to shotgun lipidomics, LC-MS allows the separation of overlapping isomeric and isobaric lipid species in complex biological matrices [5]. The separation of lipids can be carried out by normal phase-LC (NP-LC) and HILIC allowing the separation based on the lipid classes, e.g., by the head group of PL, or by reversed-phase-LC (RP-LC) where the separation of the lipids is based on their hydrophobicity, i.e., the length of the fatty acyl chains and degree of unsaturation [6]. RP-LC comprising about 71% of all lipidomics applications has been most widely used for the analysis of complex lipids using C8 [7], C18 [8, 9], or C30 [10] modified silica columns. Criscuolo *et al.* showed that a C18 column achieved a better separation for polar lipids such as lysoPL, SM, or glyceroPL compared to a C30 column [11]. Separation of isobaric PL species was previously achieved using C18 columns, e.g., ACQUITY UPLC BEH C18 [12] or ACQUITY Premier CSH C18 [13].

For MS detection, untargeted analysis using high resolution and acquisition in Full MS mode is a promising approach as it allows simultaneous and comprehensive monitoring of a broad range of lipids extracted from a biological sample. Additionally, using data-dependent fragmentation, product ion spectra are obtained helping to identify the individual lipid species based on distinct fragmentation behavior. The processing of this huge amount of data generated during untargeted analysis is performed with bioinformatic software in two steps including first peak detection and peak alignment, and subsequent lipid annotation using comprehensive databases [6, 14]. Different software packages for the processing of lipid data have been developed and are available open source, as well as commercially [15].

Targeted LC-MS/MS analysis only allows the detection of preselected analytes of interest. During method development, a focus is set on the optimization of LC and MS parameters, assuring an optimal specific and sensitive detection of these analytes, e.g., eicosanoids and other oxylipins [16] or peptides [17]. Among the large number of LC-HRMS methods which have been described for the analysis of lipids in biological samples such as plasma [8, 11], serum [18], or liver [10], only few characterize and optimize the instrumental parameters including source parameters for ionization efficiency as well as parameter settings for Full MS and data-dependent acquisition. For example, Narváez-Rivas *et al.* optimized the MS parameters of the Q Exactive HF for the analysis of PL in rat plasma but provided no information about the effects of the parameters [10].

Overall, the main focus of method development/characterization of current lipidomics approaches is set on the bioinformatic processing of the LC-MS data. For example, the performance of extraction procedures [19, 20] and chromatographic separation [8, 11] is usually evaluated based on the number of identified lipid species by the bioinformatic software. However, characterization of ionization efficiency and extraction yield of representative lipid species as it is carried out in targeted LC-MS/MS analysis is limited and only described in few untargeted approaches [21].

The aim of this work was developing and optimizing extraction, separation, and detection of an untargeted LC-HRMS method for the identification and semi-

quantitative analysis of lipids with a focus on PL. The careful optimization of the MS parameters allowed to improve the ionization efficiency of the PL. The optimization of the chromatographic separation on two different columns aimed to achieve a broad elution range for PL allowing to detect more analytes by Full MS/ddMS^2 acquisition. Combined with the ionization in both modes, it enabled to acquire a broader spectrum of lipids and to confirm the characterization of tentatively identified lipids. Semi-quantification of polar lipids was performed using one internal standard (IS) per lipid class. Two liquid–liquid extraction (LLE) protocols were compared and evaluated regarding the extraction efficiency of IS and intra- and inter-day variability. Matrix effects were investigated by ion suppression analysis using two different pools of plasma, unveiling ion suppression as well as ion enhancement effects. Finally, the method was applied to investigate the effects of n3-PUFA supplementation on the human plasma lipidome. Here, we could identify distinct PL that were increased and decreased by 12 months of n3-PUFA supplementation.

2.2 Materials and methods

2.2.1 Chemicals

SPLASH Lipidomix Mass Spec Standard mixture containing deuterium-labeled lipids from 14 different lipid classes (lysoPC 18:1[D7]/0:0, lysoPE 18:1[D7]/0:0, monoacylglycerol (MG) 18:1[D7]/0:0/0:0, PS 15:0/18:1[D7], PI 15:0/18:1[D7], PG 15:0/18:1[D7], PA 15:0/18:1[D7], SM 18:1;2O/18:1[D9], PC 15:0/18:1[D7], PE 15:0/18:1[D9], DG 15:0/18:1[D7]/0:0, TG 15:0/18:1[D7]/15:0, cholesteryl ester (Chol Ester) 18:1[D7] and free cholesterol [D7]; 550 nmol L^{-1} – 5 µmol L^{-1}; concentrations relative to ratios in human plasma, for individual concentrations of the standards in the plasma extract see Table 2.1) and PL standards PC 16:0/20:4(5*Z*,8*Z*,11*Z*,14*Z*), PE 18:1(9*Z*)/18:1(9*Z*), and PE 14:0/14:0 were purchased from Avanti Polar Lipids (local supplier: Merck KGaA, Darmstadt). PC 18:2(9*Z*,12*Z*)/18:2(9*Z*,12*Z*),

PC 18:0/20:5(5*Z*,8*Z*,11*Z*,14*Z*,17*Z*), PC 18:0/22:6(4*Z*,7*Z*,10*Z*,13*Z*,16*Z*,19*Z*), PE 18:0/20:4(5*Z*,8*Z*,11*Z*,14*Z*), and PE 18:0/22:4(7*Z*,10*Z*,13*Z*,16*Z*) used for targeted LC-MS/MS were from Cayman Chemical (local supplier: Biomol, Hamburg, Germany).

Acetonitrile (ACN) LC-MS grade, methanol (MeOH) LC-MS grade, isopropanol (IPA) LC-MS grade, chloroform ($CHCl_3$) HPLC grade, formic acid LC-MS grade, and *n*-hexane HPLC grade were obtained from Fisher Scientific (Schwerte, Germany). Ultra-pure H_2O (18.2 MΩ cm) was generated using the Barnstead Genpure Pro system from Thermo Fisher Scientific (Langenselbold, Germany). Ammonium formate was supplied by Sigma-Aldrich (Schnelldorf, Germany). All other chemicals, including *tert*-butyl methyl ether (MTBE), were purchased from Merck KGaA (Darmstadt, Germany).

For method characterization, three different pools of human plasma were generated. The blood was collected from healthy human subjects in accordance with the guidelines of the Declaration of Helsinki and approved by the ethics committee of the University of Wuppertal. The blood was collected in ethylenediaminetetraacetic acid (EDTA) tubes and centrifuged (4 °C, 10 min, 1200 × *g*). The plasma was collected, aliquoted, and stored at – 80 °C as described in [22].

2.2.2 Lipid extraction

Extraction using MeOH and MTBE Lipids in plasma were extracted using a modified LLE based on Matyash *et al.* [23, 24]. Briefly, 10 µL freshly thawed plasma was transferred to glass tubes followed by the addition of 10 µL SPLASH IS. 225 µL MeOH was added and samples were vortexed shortly. Then, 750 µL MTBE was added and samples were thoroughly vortexed for 2 min. Phase separation was induced by the addition of 188 µL 150 mmol L^{-1} ammonium acetate and centrifugation (4 °C, 10 min, 1000 × *g*). The upper organic phase was carefully collected in glass tubes containing 6 µL 30% glycerol in MeOH and the lower phase was re-extracted by the addition of 300 µL MTBE. The samples were vortexed for 1 min and centrifuged again (4 °C, 5 min, 1000 × *g*). The

combined upper phases were evaporated to dryness using a vacuum concentrator (1 mbar, 30 °C, ~ 70 min; Christ, Osterode am Harz, Germany). The residue was reconstituted in 50 µL of 50/50 mobile phase (A/B, v/v without modifier, i.e., IPA/ACN/H_2O (45/35/20, v/v/v)) containing 200 nmol L^{-1} PE 14:0/14:0 as IS2. Samples were sonicated, centrifuged, and transferred to vials for LC-HRMS analysis.

Extraction using IPA, *n*-hexane, $CHCl_3$, and MeOH [25]. Lipids in plasma were extracted using a two-step LLE [26, 27]. 10 µL freshly thawed plasma was transferred to glass tubes followed by the addition of 10 µL IS (SPLASH) and 185 µL H_2O. After addition of 1 µL glacial acetic acid, the phase separation was induced with 500 µL 1 mol L^{-1} acetic acid/IPA/*n*-hexane (2/20/30, v/v/v), and samples were vortexed for 1 min. 500 µL *n*-hexane was then added, samples were vortexed again for 1 min and centrifuged (room temperature, 10 min, 1000 × *g*). The upper phase was carefully collected in glass tubes containing 6 µL 30% glycerol in MeOH. The lower phase was washed with 500 µL *n*-hexane, vortexed for 1 min, and centrifuged again (room temperature, 10 min, 1000 × *g*) and the upper layers were combined. In the second step of the extraction, 750 µL $CHCl_3$/MeOH (1/2, v/v) was added to the lower aqueous phase and samples were vortexed for 1 min. 250 µL $CHCl_3$ was further added and samples were vortexed again for 1 min. Phase separation was induced by the addition of 250 µL 150 mmol L^{-1} ammonium acetate and centrifugation (room temperature, 10 min, 1000 × *g*). The upper phase was discarded and the lower phase was collected and combined with the upper phases from the first extraction step. The combined organic phases containing the lipids of both extraction steps were evaporated to dryness using a vacuum concentrator (1 mbar, 30 °C, ~ 70 min). The residue was reconstituted in 50 µL IPA/ACN/H_2O (45/35/20, v/v/v) containing 200 nmol L^{-1} PE 14:0/14:0 as IS2, sonicated, centrifuged, and transferred to vials for LC-HRMS analysis.

2.2.3 Untargeted LC-HRMS instrument method

Untargeted lipidomics analysis was performed on a Vanquish Horizon ultra-high-performance liquid chromatography system composed of an autosampler, a binary pump, and a column oven coupled to a hybrid quadrupole-orbitrap mass spectrometer (Q Exactive HF) (Thermo Fisher Scientific, Dreieich, Germany). Samples (5 µL) were injected into the LC-HRMS system using an autosampler equipped with a 25-µL sample loop. The sample rack was kept at 10 °C. Two columns were tested for the separation, i.e., ZORBAX Eclipse Plus RRHT C18 (2.1 × 150 mm, 1.8 µm, 95 Å; Agilent, Waldbronn, Germany) and ACQUITY Premier CSH C18 (2.1 × 100 mm, 1.7 µm, 130 Å; Waters, Eschborn, Germany) (Fig. 2.2). A binary gradient was used with eluent A (H_2O/ACN, 40/60, v/v) and eluent B (IPA/ACN, 90/10, v/v, 1% H_2O), both containing 10 mmol L^{-1} ammonium formate and 0.1% formic acid. The optimized chromatographic separation was carried out on the ACQUITY Premier CSH C18 column equipped with a guard column (2.1 × 5 mm, 1.7 µm) at 40 °C using the following gradient with a flow rate of 260 µL min^{-1}: 0–0.7 min 30% B; 0.7–0.8 min 30–52.5% B; 0.8–11 min 52.5% B; 11–20 min 52.5–60% B; 20–22 min 60–99% B; 22–26 min 99% B; 26–28 min 30% B for column washing and re-equilibration. The total analysis time was 28 min.

Lipids were analyzed following positive and negative electrospray ionization in two separate runs using a heated electrospray ionization (ESI) source. For optimization of ionization parameters, PC 16:0/20:4(5*Z*,8*Z*,11*Z*,14*Z*) and PE 18:1(9*Z*)/18:1(9*Z*) were chosen as representative lipids for two abundant PL classes found in plasma. Optimization was done in positive and negative mode by infusion of the standards (each 300 nmol L^{-1}) (Fig. 2.1) *via* a syringe pump with 5 µL min^{-1} combined *via* a T-piece with an LC flow of 260 µL min^{-1} at an eluent composition of 70% B. Alternatively, also flow injection analysis injecting 5 µL of the standards in the LC flow (i.e., 260 µL min^{-1}) was used. Optimized settings are summarized in Fig. 2.1 and Fig. 8.1 of the appendix. These standards were also used for the optimization of the normalized collision energy (NCE) (Fig. 2.3). As sheath gas, auxiliary gas, sweep gas, and collision gas

nitrogen was used, generated from compressed air further purified with the purifier RAMS05Z, and combined with the NGM33 nitrogen generator (CMC instruments, Eschborn, Germany). The offset of the sprayer was side-to-side + 1, front-to-back 1.75 µm, and depth between C and D-ring.

MS detection was carried out in Full MS data-dependent (dd) MS^2 TOP *N* mode (Full MS/ddMS^2). For Full MS scans, data were acquired over a mass range of *m/z* 200 – 1200, for both positive and negative ionization modes. The Full MS scans were recorded at a resolution setting of 60,000 with the automatic gain control (AGC) target set to 1×10^6 and a maximum ion injection time (IT) of 160 ms. Data-dependent scans from the TOP *N m/z* detected in the Full MS scans were triggered based on an exclusion and inclusion list specific for positive and negative ionization (Appendix Tables 8.1 and 8.2) and a minimum AGC target of 2×10^3 considering an apex trigger of 1 – 4 s and a dynamic exclusion time of 4 s. MS^2 scans were acquired from the triggered *m/z* with an isolation window of *m/z* 1.5 using NCE combining 20 and 25 relative to *m/z* 500, at a resolution setting of 15,000 with an AGC target of 5×10^4 and a maximum IT of 80 ms. In order to ensure enough data points across the chromatographic peaks in Full MS mode for semi-quantitative evaluation, the analysis time was split into segments with different numbers of MS^2 scans triggered during one duty cycle: between 0 and 7 min TOP 5, between 7 and 12 min TOP 10, and between 12 and 28 min TOP 15.

Mass accuracy was assured using the following lock masses at the beginning of the run: in positive mode *m/z* 391.2843 (polytetrafluoroethylene) between 1.1 and 1.2 min and in negative mode *m/z* 265.1479 (sodium dodecyl sulfate) between 1.6 and 1.7 min. Mass calibration was carried out every 72 h by infusion of Pierce LTQ Velos ESI Positive Ion Calibration Solution and Pierce ESI Negative Ion Calibration Solution (Thermo Fisher Scientific, Langenselbold, Germany).

For data acquisition and instrument control Chromeleon software (version 7.2.11, Thermo Fisher Scientific) was used.

2.2.4 Targeted LC-MS/MS instrument method

Targeted LC-MS/MS analysis of selected PL was carried out using a 1290 Infinity II (Agilent, Waldbronn, Germany) LC system composed of an autosampler, a binary pump, and a column oven. The separation of the lipids was achieved using the same chromatographic conditions described for the untargeted LC-HRMS method. The LC system was coupled to a QTRAP 6500+ mass spectrometer (Sciex, Darmstadt, Germany) operated in negative electrospray ionization mode with the following settings: ion spray voltage – 4500 V, source temperature 650 °C, nebulizer gas (gas 1, compressed air purified with RAMS05Z; CMC instruments, Eschborn, Germany) 60 psi and drying gas (gas 2, purified compressed air) 60 psi, curtain gas (nitrogen, generated with the nitrogen generator Eco Inert-ESP4; DWT, Bottrop, Germany) 35 psi, collision gas (nitrogen) 6 psi. MS detection was carried out in scheduled multiple reaction monitoring (MRM) mode, acquiring two transitions per PL: one for quantification and one for qualification resulting from the cleavage of the individual fatty acyl chains. The detection window was set to 180 s around the retention time and the cycle time to 0.4 s. Declustering potentials (DP), entrance potentials (EP), collision cell exit potentials (CXP), and collision energies (CE) were optimized for each of the PL and transitions using flow injection analysis with standards (Appendix Fig. 8.2).

MS parameters for targeted PL analysis can be found in Table 8.3. Analyst (Sciex, version 1.7) was used for instrument control and data acquisition, and Multiquant (Sciex, version 2.1.1) for data evaluation.

For calibration, stock solutions of the individual PL PC 18:2(9*Z*,12*Z*)/18:2(9*Z*,12*Z*), PC 18:0/20:5(5*Z*,8*Z*,11*Z*,14*Z*,17*Z*), PC 18:0/22:6(4*Z*,7*Z*,10*Z*, 13*Z*,16*Z*,19*Z*), PE 18:0/20:4(5*Z*,8*Z*,11*Z*,14*Z*), and PE 18:0/22:4(7*Z*,10*Z*,13*Z*,16*Z*) were mixed and diluted in glass volumetric flasks (5 mL) with ACN/IPA (50/50, v/v) at 9 concentration levels. Each calibration level contained the same amount of the IS (SPLASH) comprising one labeled PL from each lipid class (400 nmol L^{-1} for PC 15:0/18:1[D7] and 15 nmol L^{-1} for PE 15:0/18:1[D7]). Calibration curves were calculated using linear least square

regression (weighting: $1/x^2$). Analyte quantification was carried out based on the analyte to corresponding IS peak area ratio using the obtained calibration curves. Linearity was assessed using standard solutions covering a concentration range from 0.2 to 1000 nmol L^{-1}. The limit of detection (LOD) was determined as the concentration yielding a signal-to-noise ratio (*S*/*N*, peak to peak) ≥ 3. The concentration with an *S*/*N* ≥ 5 and an accuracy of 80 – 120% within the calibration curve was defined as the lower limit of quantification (LLOQ) and set as the lowest concentration of the calibration curve (Appendix Table 8.3).

2.2.5 Method characterization of the untargeted LC-HRMS method

Two established LLE protocols used in the lipidomics field were tested and compared regarding their extraction recovery of major lipid classes from plasma: A protocol using MeOH/MTBE based on a modified procedure according to Matyash *et al.* [23], and a two-step extraction using acetic acid/IPA/*n*-hexane based on Hara *et al.* [27] for the first step and $CHCl_3$/MeOH based on Bligh and Dyer [26] for the second [25].

Extraction efficiency was evaluated for both protocols on three different days by determining the recovery of the IS spiked to the sample prior to extraction normalized to the IS2 (i.e., PE 14:0/14:0), which was added in the last step before LC-HRMS analysis. The recovery was calculated relative to the recovery of an IS solution directly injected.

Further lipid extraction was carried out using MeOH/MTBE. Robustness of the extraction was assessed by three different operators on three different days using three different pools of plasma. Effects of the matrix were investigated by assessing the extraction recovery of IS added to plasma prior to or post extraction and also using different volumes of plasma for extraction. Furthermore, matrix effects were determined by ion suppression analysis by post-columnly infusing a diluted (0.37 – 10 µmol L^{-1}) SPLASH solution (5 µL min^{-1}) mixed *via* a T-piece with the LC flow (260 µL min^{-1}) after injection of a plasma extract without IS (Fig. 2.4 and 2.5).

2.2.6 n3-PUFA supplementation study

The effects of n3-PUFA supplementation on the lipid pattern were investigated in plasma samples derived from a double-blinded, randomized, controlled intervention trial [28]. A subset of human plasma samples from 20 participants (9 males, 11 females, age 23 – 72 years) out of 42 subjects who received n3-PUFA capsules containing EPA and DHA corresponding to 4 portions of fatty fish per week (1.5 g EPA and 1.8 g DHA as TG per portion) was selected. Criteria for the inclusion/exclusion of subjects are summarized in Figure 8.3. Plasma samples of the individual participants at baseline (before supplementation) and after 12 months of supplementation were extracted using the LLE with MeOH/MTBE and analyzed by the untargeted LC-HRMS method in randomized order.

2.2.7 Data processing

Raw data acquired in positive and negative ionization modes by untargeted LC-HRMS analysis were processed using MS-DIAL software (version 4.70) [29] for feature detection, spectra deconvolution, and peak alignment between samples. Parameter settings for data processing by MS-DIAL are summarized in Table 8.4 of the appendix. Each detected feature was manually reviewed and assigned to a putative lipid class and to one of the three different categories (i.e., Confidence, Unsettled, or Unknown) based on its retention time and fragmentation spectrum according to following criteria: lipid class assignment was done based on following plausible retention times: lysoPL (≤ 8 min), PL (≥ 4 min), SM (≥ 4 min), DG (≥ 12 min), and TG (≥ 15 min). Features assigned to one of the mentioned lipid classes with a retention time outside the defined range were flagged as “Unknown” and were not further evaluated. An “Unsettled” feature with an identification score between 70 and 75% was flagged as “Confidence” if its fragmentation spectrum contained in positive mode (i) the precursor ion, (ii) a fragment of a neutral loss of a fatty acyl (e.g., ketene), and (iii) characteristic fragments of the lipid class (e.g., *m/z* 184.0733 for PC) [30].

In negative mode, a feature was assigned to “Confidence” if its fragmentation spectrum contained (i) the fragment(s) of the fatty acyl(s), (ii) a fragment of a neutral loss of a fatty acyl (e.g., ketene), and (iii) characteristic fragments of the lipid class (e.g., *m/z* 168.0426 for PC) [30]. In case one of the criteria mentioned above was not fulfilled, the feature remained assigned “Unsettled”. Likewise, features having an identification score between 67 and 70% were rated as “Unsettled”. All features assigned to “Confidence” and “Unsettled” were included in the further data evaluation. For additional confidence of lipid identification, the retention time of a logical series of lipid species from the same lipid class was plotted against the sum of the fatty acyl chain length or the sum of the number of double bonds according to Vaňková *et al.* [12] (Appendix Fig. 8.4, 8.5).

The peak heights of features detected in positive and/or negative mode derived from MS-DIAL data evaluation were normalized to peak heights of the IS from the same lipid class. For the individual features, fold changes between baseline (before supplementation) and after 12 months of supplementation were calculated for individual participants and the mean fold changes were determined. Using *t*-test, for the individual features, *p*-values for the means of the normalized peak heights before and after supplementation were determined. Volcano plots were created by plotting the log2 (fold change) against the – log10 (*p*-value).

Putatively identified PL, which changed most after n3-PUFA supplementation and were commercially available, were quantified by targeted LC-MS/MS using the same plasma extracts diluted 1:50 in ACN/IPA (50/50, v/v).

2.2.8 Lipid notation

The shorthand notation of the lipids is based on Liebisch *et al*., using the separator “_” if the *sn*-position of the fatty acyl(s) chain is unknown, while the separator “/” indicates a proven *sn*-position (with *sn*-1/*sn*-2) [31]. The position of the double bonds, e.g., PC 16:0/20:4(5*Z*,8*Z*,11*Z*,14*Z*), was specified only if confirmed by authentic standards.

2.3 Results and Discussion

2.3.1 Optimization of mass spectrometric parameters

Sensitive as well as selective mass spectrometric analysis of PL in biological samples requires careful optimization of instrument parameters. Mass spectrometric detection of PL is feasible after positive (ESI(+)) and negative (ESI(-)) electrospray ionization due to their polar head group by forming different types of adducts [6], while DG, TG, and Chol Ester can only be efficiently ionized in positive mode [8, 32]. Analysis of lipids was carried out in positive and negative modes in two separate runs to enable characterization of the lipid class as well as the fatty acyl chains based on characteristic fragmentation behavior. The instrument software sets default settings for the source parameters based on the LC flow rate. Starting from these settings, the source parameters of the HESI source (i.e., spray voltage, sheath gas, auxiliary gas, auxiliary gas heater temperature, sweep gas, capillary temperature) and the S-lens RF level were optimized in both ionization modes, and compared with the default settings and the settings described in an application note for lipidomics analysis with the same flow rate (260 µL min^{-1}) from the instrument manufacturer [33]. The optimization of the spray voltage, the sheath gas, the sweep gas, and the capillary temperature showed only a minor impact on the signal intensity, and is described in detail in the supplementary information (Appendix Fig. 8.1).

The heated auxiliary gas flow was optimized in combination with the auxiliary gas heater temperature and showed the greatest impact among all source parameters on spray stability in both ionization modes. It was optimized in a range of 4 – 14 arbitrary units (Fig. 2.1A). A value of 4 resulted in a noisy and unstable spray, and increasing the auxiliary gas flow decreased the noise but also decreased the signal intensity. A value of 12 was selected for both ionization modes in order to minimize the noise of the spray without losing too much sensitivity.

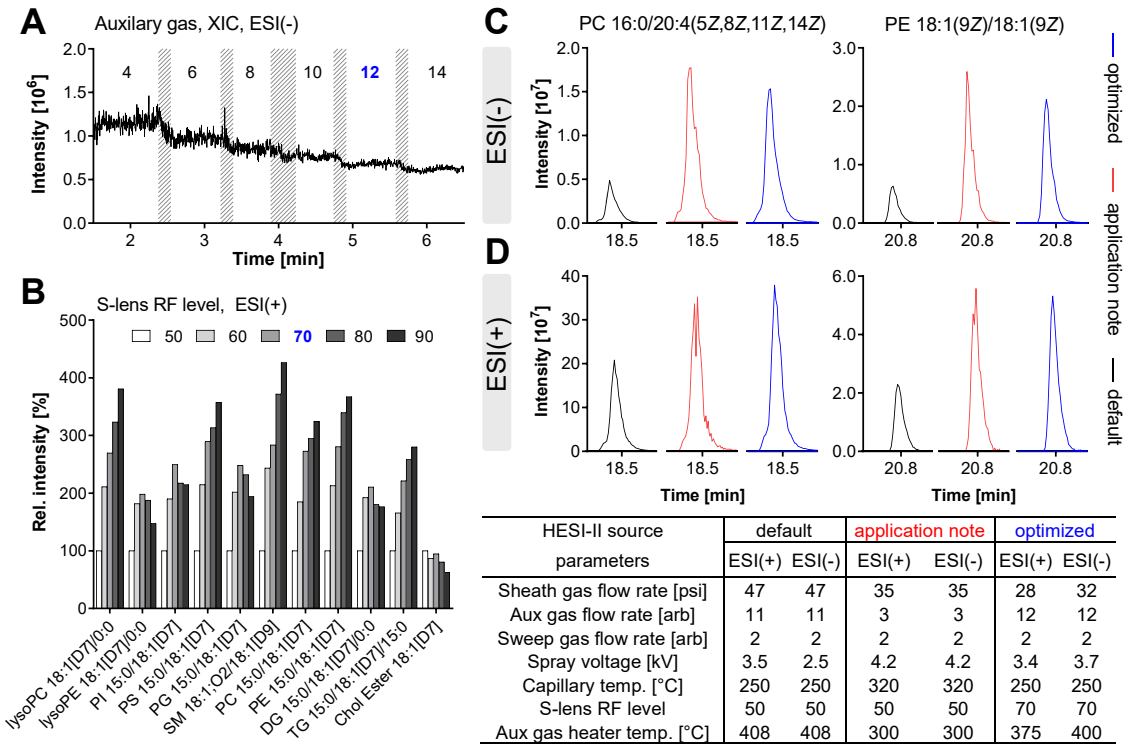

HESI-II source parameters	default		application note		optimized	
	ESI(+)	ESI(-)	ESI(+)	ESI(-)	ESI(+)	ESI(-)
Sheath gas flow rate [psi]	47	47	35	35	28	32
Aux gas flow rate [arb]	11	11	3	3	12	12
Sweep gas flow rate [arb]	2	2	2	2	2	2
Spray voltage [kV]	3.5	2.5	4.2	4.2	3.4	3.7
Capillary temp. [°C]	250	250	320	320	250	250
S-lens RF level	50	50	50	50	70	70
Aux gas heater temp. [°C]	408	408	300	300	375	400

Fig. 2.1: Effect of selected ion source parameters on intensity and stability of the ESI-MS signal. Shown is **A** the influence of the auxiliary gas flow rate on the signal in ESI(-) mode during infusion of a PL standard containing PC 16:0/20:4(5*Z*,8*Z*,11*Z*,14*Z*) and PE 18:1(9*Z*)/18:1(9*Z*) while other parameters were set to default; **B** the effect of the S-lens RF level on signal intensity relative to a value of 50 for different deuterium-labeled lipids; **C**, **D** peak intensity and shape of PC 16:0/20:4(5*Z*,8*Z*,11*Z*,14*Z*) and PE 18:1(9*Z*)/18:1(9*Z*) in (*top*, **C**) ESI(-) and (*bottom*, **D**) ESI(+) mode using default parameters, parameters of an application note for lipidomics from the manufacturer [33], or parameters after optimization.

The value selected for the auxiliary gas flow is close to the default settings (i.e., 11), but clearly higher than the value used in the application note (i.e., 3) [33]. However, the peak shape of the PL is clearly improved when a higher value is used (Fig. 2.1C, D). Our results are in line with previous studies employing with the same instrument an auxiliary gas flow of 10 for the analysis of PL in serum at an LC flow rate of 400 µL min^{-1} [34], or in pituitary adenoma tissues at an LC flow rate of 260 µL min^{-1} [7]; or an auxiliary gas flow of 15 for the analysis of human plasma lipids at an LC flow rate of 325 µL min^{-1} [11].

Transfer of ions from the ion transfer tube to the ion optics through the S-lens is achieved by the RF amplitude applied to the electrodes of the S-lens. The S-lens RF level is a numerical factor affecting transmission, i.e., a higher S-lens RF level increases transmission of ions with higher *m/z,* while also fragmentation of fragile ions in the S-lens occurs. Optimization of the S-lens RF level was performed using deuterium-labeled lipids (SPLASH) from different lipid classes(Fig. 2.1B). Increasing the S-lens RF level from the default value, i.e., 50, increased the ion transmission of all IS except Chol Ester 18:1[D7]. For an S-lens RF level of 80 and 90, a decrease in the signal of lysoPE 18:1[D7]/0:0, PI 15:0/18:1[D7], PG 15:0/18:1[D7], and DG 15:0/18:1[D7]/0:0 was observed. Thus, an S-lens RF level of 70 for both ionization modes was chosen, which massively improved the ion transmission of the PL (Fig. 2.1B). The default S-lens RF level of 50 is used in several lipidomic methods using a Q Exactive HF instrument [7, 9, 35]. However, our results show that optimization of this parameter has a great impact on the ion transmission and signal intensity and should thus be carefully optimized.

Overall, the optimization of the source parameters minimized the noise resulting in a better peak shape, and increased the sensitivity by a factor of 3 in ESI(+) and ESI(-) compared to the default parameters.

2.3.2 Optimization of chromatographic separation

Liquid chromatographic separation of lipids covering the range from polar lipids, such as lysoPL, to the very hydrophobic ones, e.g., neutral lipids (NL), can be performed using RP-LC [5, 8, 34, 36]. We aimed to optimize the chromatographic conditions in order to achieve an efficient separation between different lipid species with a focus on PL (Fig. 2.2). Since numerous isobaric lipid species, i.e., with the same *m/z* are present in biological samples, LC separation is crucial for their characterization. An isocratic step was included in the gradient to extend the elution window for PL, thereby enabling the acquisition of more MS^2 spectra for their characterization in Full MS/ddMS^2 mode.

For the liquid chromatographic optimization, we selected three critical pairs of isobaric PL: PC 18:2_20:4/PC 18:1_20:5, PC 18:1_18:2/PC 16:0_20:3, and PC 18:0_18:2/PC 18:1_18:1. These are highly abundant in human plasma and have different retention times between 10 and 20 min under the applied RP-LC conditions. Two RP C18 columns with fully porous sub-2-µm particles for high separation efficiency and sample loading capacity were tested using a lipid extract from human plasma. We chose two columns which were previously successfully used in lipidomics applications, i.e., the ZORBAX Eclipse Plus RRHT C18 [37, 38] and the ACQUITY Premier CSH C18 column [7, 9, 34, 38, 39].

Using the ZORBAX Eclipse Plus RRHT C18 column (2.1 × 150 mm, 1.8 µm, 95 Å) with an optimized gradient (Fig. 2.2A), lipids from a human plasma extract eluted as relatively broad peaks with a full width at half maximum (FWHM) for the labeled IS PS 15:0/18:1[D7], PC 15:0/18:1[D7], and PE 15:0/18:1[D7] of 17.4 s, 19.8 s, and 18.9 s, respectively (Fig. 2.2A, middle). PL also showed an asymmetric peak shape with a tailing factor for the labeled PL between 1.6 and 4.4. Overall, this mediocre separation of the lipids is reflected by incomplete separation of the selected critical pairs, i.e., PC 18:2_20:4/PC 18:1_20:5 and PC 18:1_18:2/PC 16:0_20:3 with a resolution of 0.64 and 1.1, respectively. Additionally, the pair PC 18:0_18:2/PC 18:1_18:1 was not fully separated (R = 1.2) (Fig. 2.2A, bottom).

The separation on the ACQUITY Premier CSH C18 column (2.1 × 100 mm, 1.7 µm, 130 Å) was carried out with adjusted elution power of the gradient during the isocratic step by lowering the percentage of eluent B from 60% to 52.5% (Fig. 2.2B). With this column, the same elution order was observed; however, the peak shape of the lipids was considerably improved showing narrower peaks and better peak symmetry. No peak tailing was observed for the PL, except for the acidic PS 15:0/18:1[D7] (i.e., tailing factor 1.8) (Fig. 2.2B, middle), which is known in RP-LC even when a high aqueous percentage is used for the initial conditions [40]. The better performance of this column might be explained by the charged surface of its particles improving peak symmetry with low ionic-strength mobile phases.

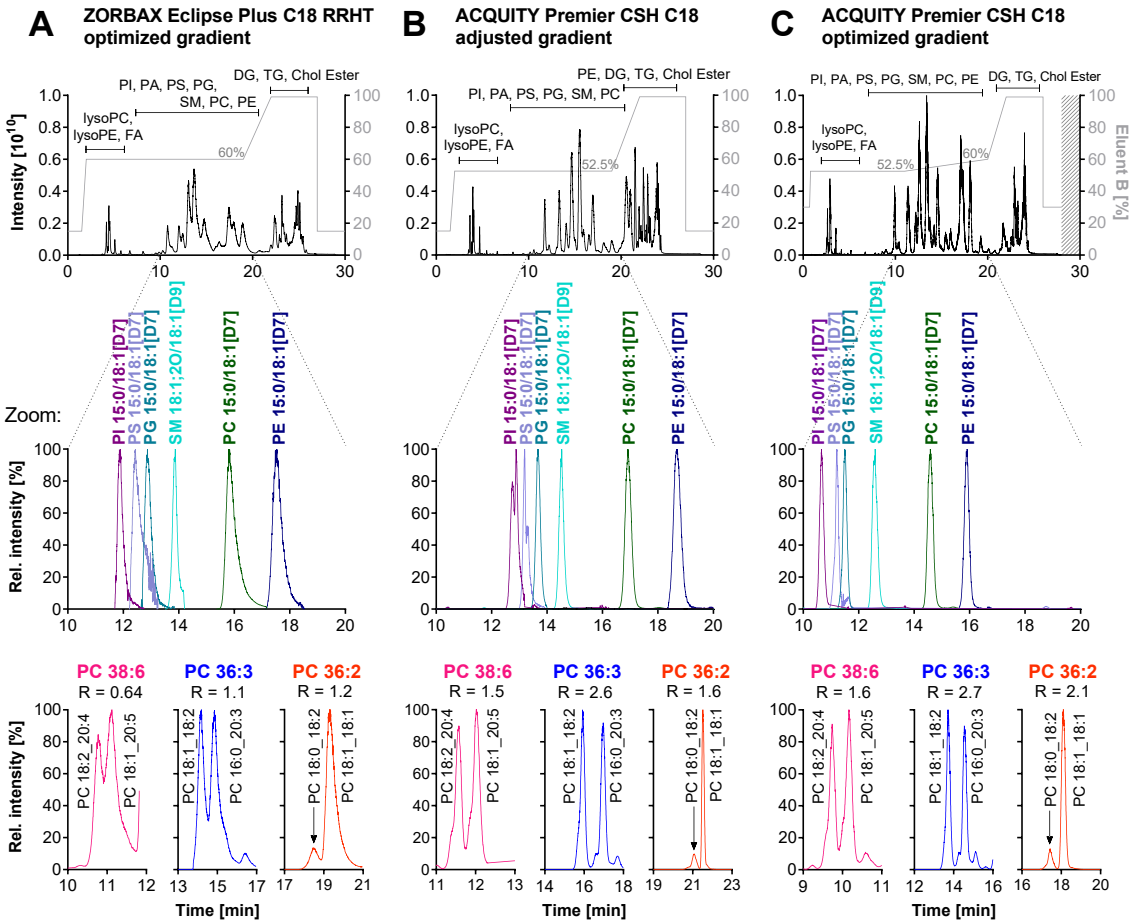

Fig. 2.2: Chromatographic separation efficiency of lipids. Shown is the separation of (**top**) a lipid extract from human plasma (Full MS scan *m/z* 200 – 1200), (**middle**) deuterium-labeled IS (respective extracted ion chromatogram (XIC)), and (**bottom**) isobaric PL species PC 38:6 (*m/z* 806.5694), PC 36:3 (*m/z* 784.5851), and PC 36:2 (*m/z* 786.6007) acquired in ESI(+) mode using **A** an optimized gradient on a ZORBAX Eclipse Plus RRHT C18 column (2.1 × 150 mm, 1.8 µm, 95 Å), **B** an ACQUITY Premier CSH C18 column (2.1 × 100 mm, 1.7 µm, 130 Å) and a gradient with adjusted elution power, and **C** an optimized gradient on the latter column. Mobile phases for all separations were eluent A (H_2O/ACN (40/60, v/v)) and eluent B (IPA/ACN (90/10, v/v), 1% H_2O), both containing 10 mmol L^{-1} ammonium formate and 0.1% formic acid. The fatty acyl chains of the isobaric PL (bottom) were characterized based on the fragmentation spectra acquired in ESI(-) mode.

Separation of PL was also considerably improved with a resolution ≥ 1.5 for the selected critical pairs, e.g., PC 18:2_20:4/PC 18:1_20:5 (R = 1.5) (Fig. 2.2B, bottom). However, using this gradient (Fig. 2.2B), late-eluting PC and PE species still showed broad peaks, e.g., PE 15:0/18:1[D7] eluting at the end of the isocratic step with a FWHM of 16.8 s.

Also, more hydrophobic PL eluting after the isocratic step, e.g., PE 18:0_20:4 at 21.7 min or PC 18:0_20:3 at 21.9 min, co-eluted with other late-eluting PL as indicated in the total ion chromatogram (TIC) (Fig. 2.2B, top).

Thus, the gradient was further optimized by including a shallow linear increase to 60% B after the isocratic step and adjusting the initial percentage of B as well as the time for the final elution and re-equilibration step (Fig. 2.2C): The more hydrophobic PL eluted earlier, e.g., PE 18:0_20:4 at 18.6 min and PC 18:0_20:3 at 19.7 min, and their separation was improved. For the starting conditions, 30% B was used as isocratic preconcentration step to focus the analytes at the beginning of the column. With a capacity factor $k > 1$, the retention of the polar lysoPC 18:1[D7]/0:0 ($k = 2.7$) was sufficient.

Overall, with this optimized gradient, the peak shape was further improved yielding FWHM for all labeled PL between 10 and 13 s, also for PE 15:0/18:1[D7] (Table 2.1). Moreover, separation of the critical pairs was optimal with a resolution ≥ 1.5, i.e., PC 18:2_20:4/PC 18:1_20:5 (R = 1.6), PC 18:1_18:2/PC 16:0_20:3 (R = 2.7), and PC 18:0_18:2/PC 18:1_18:1 (R = 2.08) (Fig. 2.2C, bottom). The isocratic step at 99% B at the end of the gradient was held for 4 min, which was sufficient to elute the NL, i.e., TG, DG, and Chol Ester (leading to minimal carry-over for TG 18:1_18:1_18:1 to the next injection (< 1%)). Only 2-min re-equilibration was required, resulting in stable retention times for the lysoPL in the following injection. Including re-equilibration, the final run time of the optimized method was 28 min covering polar as well as NL and the method showed stable retention times with an inter-batch (n = 92, 6 days) relative standard deviation (RSD) < 0.71% (0.08 min) (Table 2.1).

Table 2.1 (Next page): Characterization of mass spectrometric and chromatographic parameters of deuterium-labeled lipids used as IS. Shown are the molecular formula, the *m/z* of the most intense adduct measured in ESI(+) and ESI(-) mode, the concentration of the IS in the plasma extract, the t_R, and the FWHM of the chromatographic peak using the LC-HRMS method.

analyte	molecular formula	ESI(-) *m/z*	ESI(-) adduct type	ESI(+) *m/z*	ESI(+) adduct type	conc. [µmol L^{-1}]	t_R ± SD [min][1]	FWHM[1] ± SD [s]
lysoPC 18:1[D7]/0:0	$C_{26}H_{45}D_7NO_7P$	573.3903	$[M + HCOO]^-$	529.3994	$[M + H]^+$	4.5	2.88 ± 0.01	3.98 ± 0.46
lysoPE 18:1[D7]/0:0	$C_{23}H_{39}D_7NO_7P$	485.338	$[M – H]^-$	487.3524	$[M + H]^+$	1.0	2.97 ± 0.01	4.15 ± 0.65
PI 15:0/18:1[D7]	$C_{42}H_{75}D_7NO_{13}P$	828.563	$[M – H]^-$	847.6036	$[M + H]^+$	1.0	10.6 ± 0.04	10.04 ± 0.48
PS 15:0/18:1[D7]	$C_{39}H_{67}D_7NO_{10}P$	753.542	$[M – H]^-$	755.5562	$[M + H]^+$	0.50	11.1 ± 0.08	12.55 ± 1.02
PG 15:0/18:1[D7]	$C_{39}H_{68}D_7O_{10}P$	740.5464	$[M – H]^-$	759.5875	$[M + NH_4]^+$	3.5	11.4 ± 0.05	10.75 ± 1.19
SM 18:1;2O/18:1[D9]	$C_{41}H_{72}D_9N_2O_6P$	782.6379	$[M + HCOO]^-$	738.6470	$[M + H]^+$	4.0	12.8 ± 0.05	11.92 ± 1.00
PC 15:0/18:1[D7]	$C_{41}H_{73}D_7NO_8P$	797.6049	$[M + HCOO]^-$	753.6134	$[M + H]^+$	20	14.9 ± 0.05	12.25 ± 1.50
PE 15:0/18:1[D7]	$C_{38}H_{67}D_7NO_8P$	709.5519	$[M – H]^-$	711.5664	$[M + H]^+$	0.75	16.2 ± 0.05	12.33 ± 0.39
DG 15:0/18:1[D7]/0:0	$C_{36}H_{61}D_7O_5$	[2]	-	605.5844	$[M + NH_4]^+$	1.5	22.4 ± 0.02	3.98 ± 0.53
TG 15:0/18:1[D7]/15:0	$C_{51}H_{89}D_7O_6$	[2]	-	829.7985	$[M + NH_4]^+$	6.5	24 ± 0.01	3.60 ± 0.36
Chol Ester 18:1[D7]	$C_{45}H_{71}D_7O_2$	[2]	-	675.6779	$[M + NH_4]^+$	50	24.4 ± 0.01	3.87 ± 0.47

[1] t_R and FWHM were determined as mean in plasma extracts which were pre-spiked with IS mixture and measured on 6 different days (n = 92)

[2] DG 15:0/18:1[D7]/0:0, TG 15:0/18:1[D7]/0:0, Chol Ester 18:1[D7] are only detected in ESI(+) mode

2.3.3 Optimization of parameters for Full MS/dd MS² (TOP N) acquisition

Acquisition of data in Full MS/ddMS² TOP *N* mode allows, in addition to the determination of the exact mass of the detected lipid species by HRMS, their characterization based on characteristic product ion spectra. In this mode, one full scan (the survey scan) is recorded, followed by the acquisition of a distinct number (*N*) of product ion spectra of selected precursor ions. For reliable analysis of lipids using data-dependent acquisition, it is important to balance between (i) the acquisition of as many product ion spectra as possible to characterize as many precursor ions as possible, and (ii) an appropriate cycle time (frequency) enabling to record enough data points (12 to 20) for the semi-quantification in Full MS mode.

Table 2.2: Data points across the peaks using Full MS/ddMS² (TOP *N*) acquisition. Shown are the numbers of MS scans across the full chromatographic peak width using different numbers of data-dependent triggered fragment spectra (TOP *N*), and the FWHM (mean ± SD, n = 4) for selected deuterium-labeled IS. Resolution settings were Full MS: R = 60,000; ddMS²: R = 15,000. Bold values indicate the TOP *N* selected for the optimized method.

	ESI(-)				
analyte	**MS scans over the full peak width**				**FWHM ± SD [s]**
	TOP 5	**TOP 10**	**TOP 15**	**TOP 20**	
lysoPC 18:1[D7]/0:0	**13**	7	4	3	2.93 ± 0.13
lysoPE 18:1[D7]/0:0	**13**	7	5	3	3.17 ± 0.07
PI 15:0/18:1[D7]	32	**17**	12	9	10.6 ± 0.5
PS 15:0/18:1[D7]	34	**17**	11	7	10.5 ± 0.4
PG 15:0/18:1[D7]	34	**15**	11	8	8.03 ± 0.86
SM 18:1;2O/18:1[D9]	44	21	**14**	11	13.2 ± 0.5
PC 15:0/18:1[D7]	44	23	**15**	11	13.4 ± 1.0
PE 15:0/18:1[D7]	41	21	**13**	9	11.7 ± 0.6

The effect of the number of triggered ddMS² (TOP *N*) on the data points across the chromatographic peaks of different labeled lysoPL and PL eluting over the chromatographic range was investigated (Table 2.2).

As expected, with increasing number of the TOP *N*, fewer data points in Full MS were recorded, and TOP 20 resulted in an insufficiently low number of data points (i.e., 3 to 11 points) per peak. For analytes with narrow peaks, e.g., the early eluting lysoPL with a FWHM of 3 s, only the TOP 5 acquisition led to sufficient data points (i.e., 13 points). However, for later eluting PL, this resulted in a high number of data points (> 31 points) due to their broader peaks (FWHM > 8 s). Thus, a higher TOP *N* was chosen for PL yielding more comprehensive qualitative data without forfeiting peak accuracy for quantification. Consequently, the number of $ddMS^2$ triggered was adjusted in relation to the FWHM determined for the IS taking the cycle time into account using for Full MS R = 60,000 and for $ddMS^2$ R = 15,000, i.e., 0.8 s for TOP 5 (1 Full MS + 5 $ddMS^2$), 1.4 s for TOP 10 (1 Full MS + 10 $ddMS^2$), and 2.2 s for TOP 15 (1 Full MS + 15 $ddMS^2$). For the elution window of the lysoPL (i.e., 0 – 7 min) TOP 5 was selected (Table 2.2); TOP 10 precursor ions were triggered from 7 to 12 min covering PL eluting with a FWHM of 8 – 10 s; and from 12 min until the end of the analysis TOP 15 was chosen covering PL eluting with a FWHM > 11 s. As this study focuses on PL, no optimization was done for the late-eluting NL (i.e., DG, TG, Chol Ester).

Because one MS^2 spectrum per lipid species, ideally at the apex of the peak, is sufficient for characterization, the apex trigger was set from 1 to 4 s and the dynamic exclusion to 4 s allowing on the one hand the acquisition of meaningful spectra at high intensity of the precursor ions and on the other hand the trigger of many different precursor ions. So far, the number of MS^2 scans (TOP *N*) triggered during one duty cycle has not been split into segments over the analysis time in previous studies. Instead, they used constant TOP *N* ranging from 2, 3, 10, or 20 for the whole analysis time [7–11, 34, 35, 39, 41, 42]. Our data shows that the optimization of this parameter is crucial to acquire as many product ion spectra as possible for characterization while keeping sufficient data points for semi-quantification in Full MS. The use of an exclusion list covering common contaminants, such as polysiloxanes, alkane polymers, or phthalates, prevents the acquisition of $ddMS^2$ of abundant background ions containing no useful information (Appendix Table 8.1).

Additionally, using an inclusion list comprising lipids of interest, i.e., PC and PE bearing biologically relevant PUFA (Appendix Table 8.2), ascertains that their ddMS^2 are recorded and thus reliably allows the characterization of their presence in biological samples.

2.3.4 Optimization of normalized collision energy

In order to obtain meaningful product ion spectra enabling comprehensive characterization of the lipid class as well as the fatty acyl chains, we investigated the influence of the collision energy (CE) on MS^2 spectra in both ionization modes (Fig. 2.3). Lipids present in biological samples cover a wide range of masses. Thus, the NCE was used for fragmentation which represents the CE relative to *m/z* 500 and applies an adjusted actual CE depending on the *m/z* of the precursor ion, instead of applying the identical absolute CE regardless of the *m/z*. MS^2 spectra of the selected PC and PE standards were recorded in both ionization modes using NCE of 10, 20, 25, or 30, and evaluated for characteristic fragments comprising in ESI(+) the fragments of the PL' polar head group or its (partly) loss, and in ESI(-) the fragments resulting from the fatty acyl chains [30]. With an NCE of 10, only slight fragmentation was observed: MS^2 spectra were dominated by the molecular ions and only fragments of the polar head group were observed for both PL in both ionization modes (Fig. 2.3A, B, top). With a NCE of 20 and 25, the intensity of the fragments related to the polar head group increased (i.e., *m/z* 184.0733 for PC, and $[M + H - 141.0191]^+$ for PE) in ESI(+). Moreover, in ESI(-), fragments of the fatty acyl chains were detected (Fig. 2.3A, B, middle). Further increasing the NCE to 30 decreased the absolute intensity of most characteristic fragments particularly of those with a high *m/z*.

Based on these findings, a stepwise fragmentation of the precursor ions using a combination of NCE 20 and 25 for both ionization modes was applied in the final method. This is in line with previous studies using also a stepwise fragmentation of 20 and 25 in both ionization modes [39], or 20 and 25 in ESI(+) and 20, 24, and 28 in ESI(-) [8].

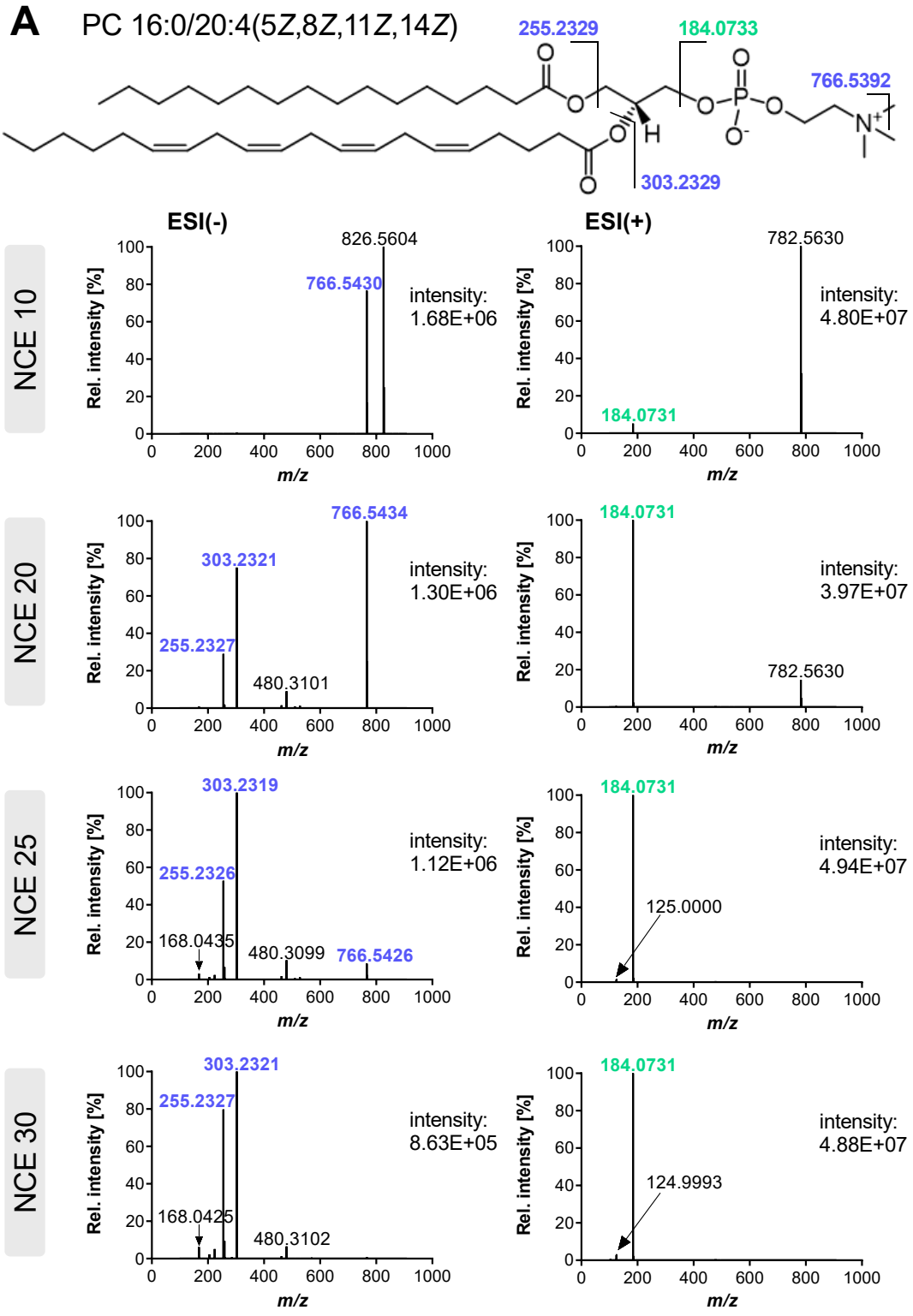

Fig. 2.3: Product ion spectra of PL with different NCE in ESI(-) and ESI(+) mode. Shown are the MS^2 spectra of **A** PC 16:0/20:4(5*Z*,8*Z*,11*Z*,14*Z*) *m/z* 826.5604 $[M + HCOO]^-$ in ESI(-) and *m/z* 782.5694 $[M + H]^+$ in ESI(+) mode, and **B** PE 18:1(9*Z*)/18:1(9*Z*) *m/z* 742.5392 $[M - H]^-$ in ESI(-)and *m/z* 744.5538 $[M + H]^+$ in ESI(+) mode. Analysis was done using untargeted LC-HRMS operating in Full MS/ddMS^2 TOP *N* mode.

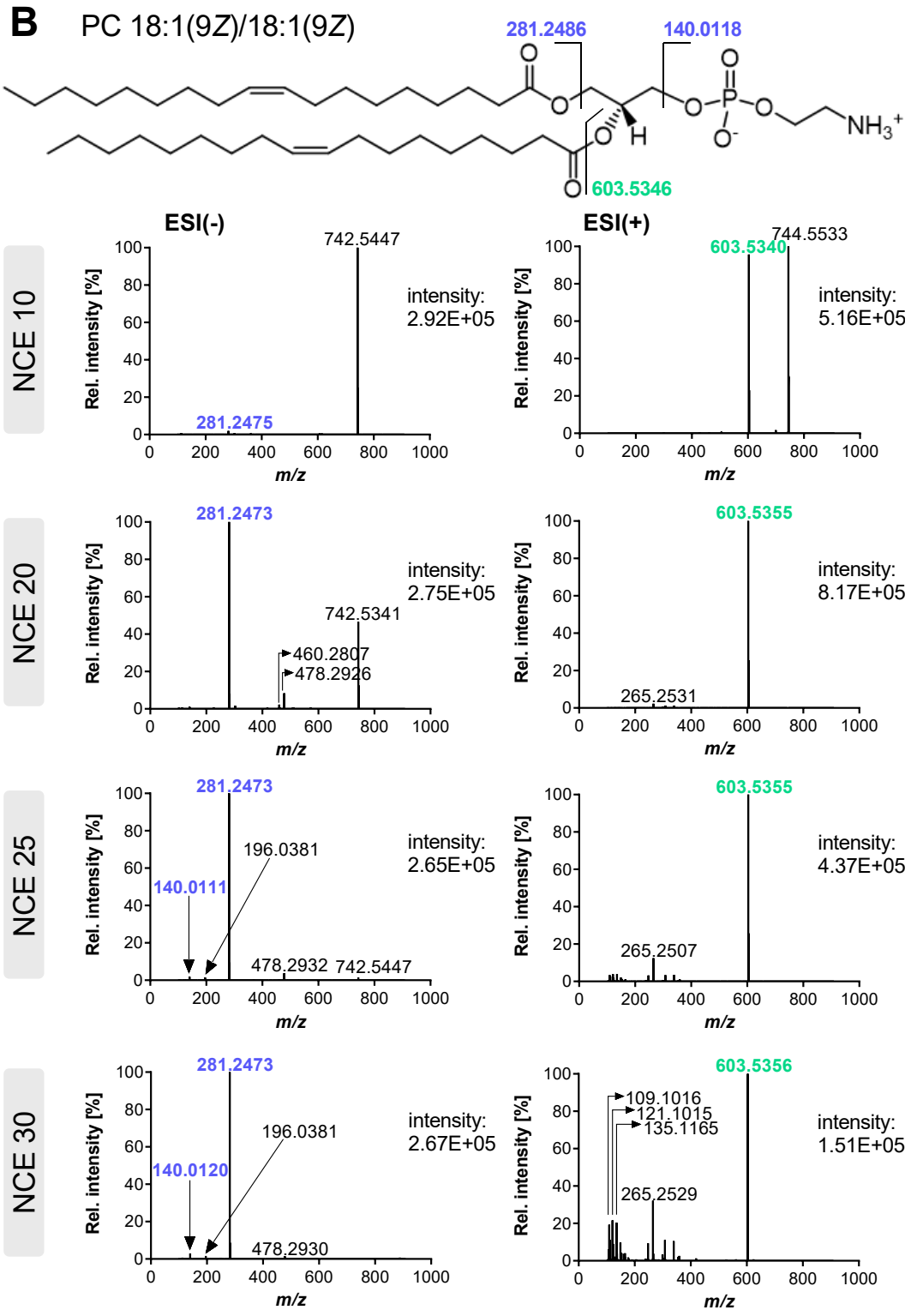

Fig. 2.3: Continued. Product ion spectra of PL with different NCE in ESI(-) and ESI(+) mode. **B** PE 18:1(9Z)/18:1(9Z) *m/z* 742.5392 $[M - H]^-$ in ESI(-) and *m/z* 744.5538 $[M + H]^+$ in ESI(+)mode.

2.3.5 Sample preparation

Selection of suitable extraction conditions for lipids from biological samples is a key prerequisite in untargeted analysis to ensure coverage of lipids with varying polarity. In the present study, individual lipid species were semi-quantified using one IS per lipid class.

Recoveries between the MeOH/MTBE [23] and the two-step extraction protocol [25] were comparable for all PL classes covered by the IS except for PS (Table 2.3). Overall, apparent extraction recoveries were good, being slightly better in ESI(-) with > 75% except for SM, while in ESI(+) it was > 70% except for lysoPC and PG. Also, reproducibility of the lipid extraction was excellent with an intra-day and inter-day variance < 100 ± 15% except for PG and SM (< 100 ± 20%). Extraction recovery of PS was considerably lower with the two-step extraction (< 13% two steps *vs.* > 80% MeOH/MTBE) and showed high variation, i.e., intra-day variance > 100 ± 47% and inter-day variance > 100 ± 97%, in both ionization modes. This poor recovery of PS with the two-step extraction is likely due to the addition of acetic acid, leading to the protonation of the serine head group, and thus the PS (partially) remains in the aqueous phase. With both processing methods, the NL, i.e., DG, TG, and Chol Ester, are also extracted. However, if also these more hydrophobic lipids are in the focus of analysis, a less polar reconstitution solvent after LLE must be chosen to ensure a better solubilization [32].

All in all, the MeOH/MTBE-based LLE is more environmentally friendly (no halogenated solvents) and the collection of the upper phase containing the lipids is easier in comparison to the extraction with $CHCl_3$, where the lipids are in the lower phase. Moreover, it showed better extraction of the PS lipid class. In consequence, the MeOH/MTBE extraction was selected and further characterized. Regarding robustness, the extraction recoveries were not impacted by the plasma pool used for LLE (Appendix Fig. 8.6).

Table 2.3: Extraction recovery of IS from human plasma. IS were spiked to three different pools of human plasma prior to extraction and samples were extracted by LLE on three different days using a one-step MeOH/MTBE extraction or a two-step extraction with IPA/*n*-hexane//$CHCl_3$/MeOH. Shown are the mean values and RSD (n = 9 for intra-day, n = 27 for inter-day).

ESI(-)	Day 1				Day 2			
	MeOH/MTBE		IPA/*n*-hexane//$CHCl_3$/MeOH		MeOH/MTBE		IPA/*n*-hexane//$CHCl_3$/MeOH	
analyte	recovery [%]	RSD [%]	recovery [%]	RSD [%]	recovery [%]	RSD [%]	recovery [%]	RSD [%]
lysoPC 18:1[D7]/0:0	87	3	85	9	82	6	75	8
lysoPE 18:1[D7]/0:0	90	4	73	8	86	6	78	5
PI 15:0/18:1[D7]	108	5	115	8	105	6	120	5
PS 15:0/18:1[D7]	93	5	4	50	89	9	12	90
PG 15:0/18:1[D7]	88	6	104	8	84	11	87	6
SM 18:1;2O/18:1[D9]	69	9	74	8	70	7	63	10
PC 15:0/18:1[D7]	79	3	93	6	78	5	85	5
PE 15:0/18:1[D7]	82	3	91	3	81	5	94	5

ESI(+)	Day 1				Day 2			
	MeOH/MTBE		IPA/*n*-hexane//$CHCl_3$/MeOH		MeOH/MTBE		IPA/*n*-hexane//$CHCl_3$/MeOH	
analyte	recovery [%]	RSD [%]	recovery [%]	RSD [%]	recovery [%]	RSD [%]	recovery [%]	RSD [%]
lysoPC 18:1[D7]/0:0	69	5	72	14	67	5	63	6
lysoPE 18:1[D7]/0:0	89	7	73	7	80	5	71	8
PI 15:0/18:1[D7]	101	7	81	9	96	4	80	6
PS 15:0/18:1[D7]	85	10	3	47	81	13	8	92
PG 15:0/18:1[D7]	65	15	75	11	57	18	76	8
SM 18:1;2O/18:1[D9]	122	7	107	11	115	4	107	6
PC 15:0/18:1[D7]	85	5	94	9	79	3	84	6
PE 15:0/18:1[D7]	126	4	117	9	115	7	129	12

Table 2.3: Continued. Extraction recovery of IS from human plasma.

ESI(-)	Day 3				Days 1 – 3	
	MeOH/MTBE		IPA/*n*-hexane//$CHCl_3$/MeOH		MeOH/MTBE	IPA/*n*-hexane//$CHCl_3$/MeOH
Analyte	recovery [%]	RSD [%]	recovery [%]	RSD [%]	$RSD_{interday}$ [%]	$RSD_{interday}$ [%]
lysoPC 18:1[D7]/0:0	80	4	76	6	6	10
lysoPE 18:1[D7]/0:0	86	5	75	7	5	7
PI 15:0/18:1[D7]	105	4	108	9	5	9
PS 15:0/18:1[D7]	91	10	22	57	8	97
PG 15:0/18:1[D7]	88	19	96	7	13	10
SM 18:1;2O/18:1[D9]	72	7	68	7	8	11
PC 15:0/18:1[D7]	82	5	84	7	5	7
PE 15:0/18:1[D7]	85	5	91	4	5	4

ESI(+)	Day 3				Days 1 – 3	
	MeOH/MTBE		IPA/*n*-hexane//$CHCl_3$/MeOH		MeOH/MTBE	IPA/*n*-hexane//$CHCl_3$/MeOH
Analyte	recovery [%]	RSD [%]	recovery [%]	RSD [%]	$RSD_{interday}$ [%]	$RSD_{interday}$ [%]
lysoPC 18:1[D7]/0:0	57	5	55	7	10	15
lysoPE 18:1[D7]/0:0	80	4	68	6	7	8
PI 15:0/18:1[D7]	91	6	80	12	7	9
PS 15:0/18:1[D7]	78	9	21	61	11	106
PG 15:0/18:1[D7]	61	15	58	9	16	15
SM 18:1;2O/18:1[D9]	78	8	84	5	20	14
PC 15:0/18:1[D7]	73	4	75	4	8	11
PE 15:0/18:1[D7]	107	9	112	8	10	12

Inter-operator variability was thus determined combining all data from three different days and plasma pools (n = 81), and was excellent (< 100 ± 12% in ESI(-) and < 100 ± 23% in ESI(+)). Only the extraction of PS was affected by the operator, showing a recovery < 56% when samples were prepared by operator 2 (Fig. 2.4), while > 80% were recovered by operators 1 and 3, which is reflected by an inter-operator variance of 100 ± 33%.

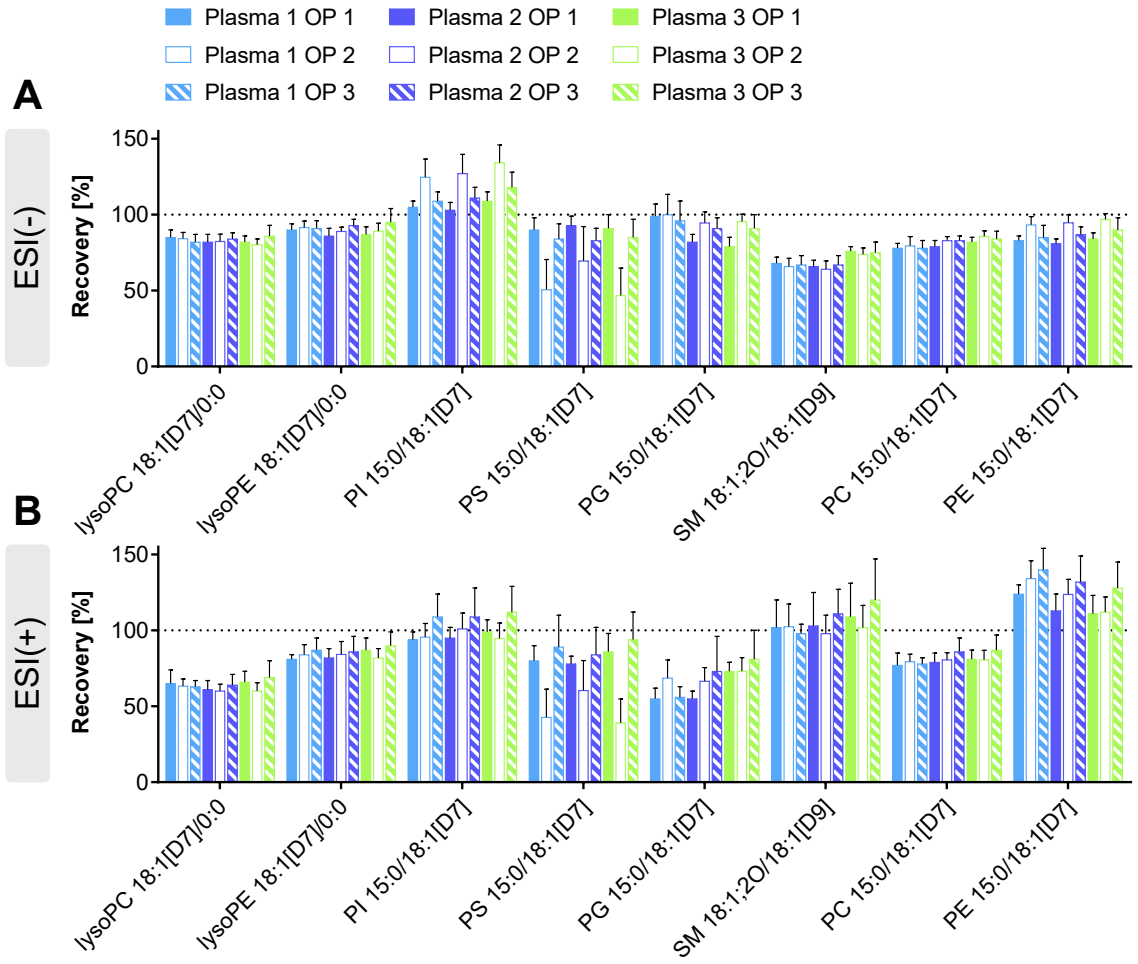

Fig. 2.4: Robustness of extraction recovery. Shown is the extraction recovery of deuterium-labeled IS from three different pools of human plasma by three different operators on three different days **A** in ESI(-) and **B** in ESI(+) mode. Shown are mean values ± SD (n = 9). Lipid extracts were analyzed by untargeted LC-HRMS operating in Full MS/ddMS^2 TOP *N* mode (orbitrap Q Exactive HF).

Comparison of extraction recoveries of IS spiked to plasma prior to or post extraction unveiled that apparent losses of IS during sample preparation are < 15% for the lysoPL and < 8% for the PL in both ionization modes (Fig. 2.5A, B). These losses during sample preparation were slightly better than those reported for a modified Matyash protocol with an average loss of 27% [43]. Low apparent recoveries were observed particularly for PG 15:0/18:1[D7] in ESI(+) (50%) when the IS was added after extraction. These losses in the signal thus occur during LC-MS analysis due to ion suppression (Fig. 2.5C, D).

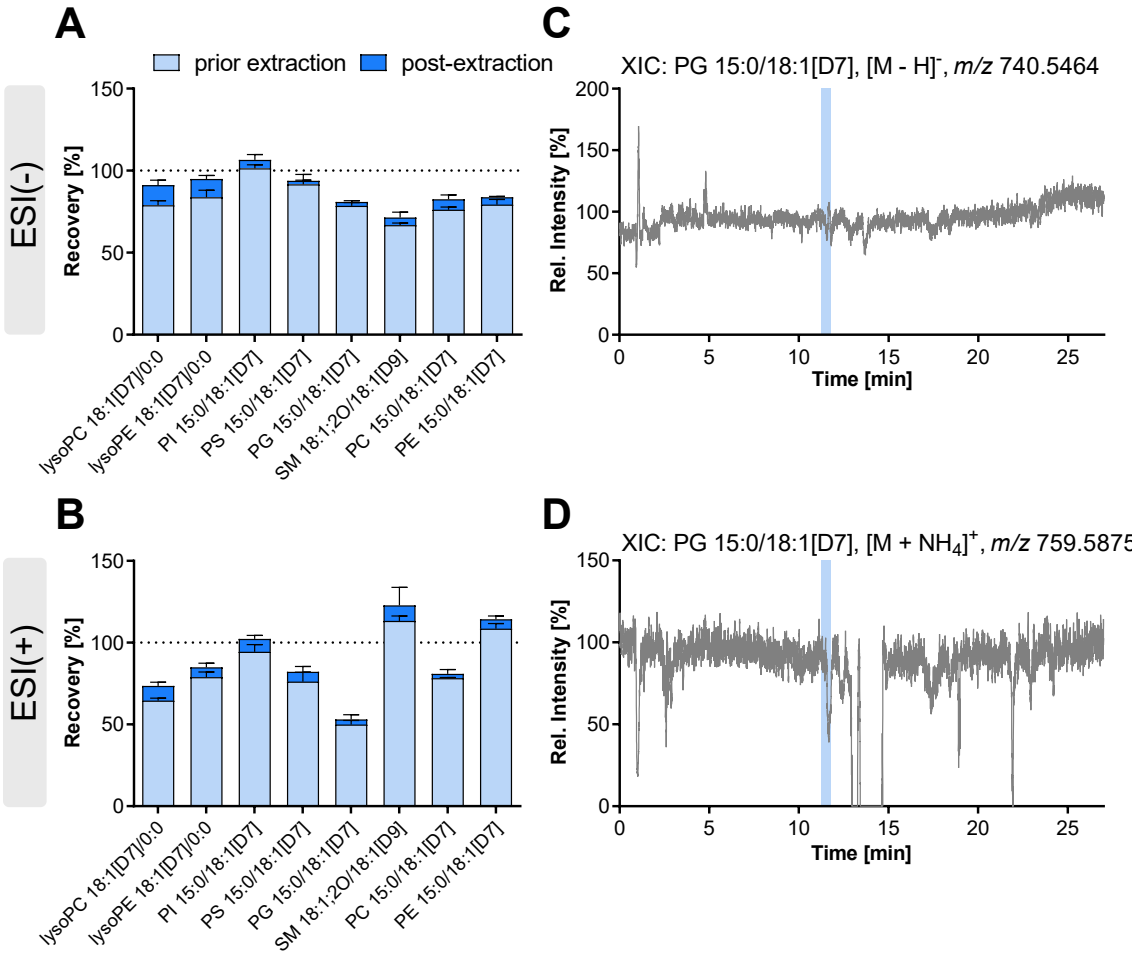

Fig. 2.5: Influence of ion suppression on the extraction recovery from plasma. Shown are the recoveries of deuterium-labeled IS from the extraction of 10 µL of human plasma **A** in ESI(-) and **B** in ESI(+) mode. IS were spiked to the plasma at the beginning of sample preparation (prior extraction) or after sample preparation, directly before measurement (post-extraction). Shown are mean values ± SD, n = 3. **C**, **D** An IS solution (1.9 µmol L^{-1}, 5 µL min^{-1}) was post-columnly mixed with the LC flow (260 µL min^{-1}) following injection of a plasma extract. Shown are the XIC of PG 15:0/18:1[D7] in **C** ESI(-) and **D** ESI(+) mode. The blue bar indicates the retention time of PG 15:0/18:1[D7].

2.3.6 Ion suppression analysis

Ion suppression analysis showed in ESI(+) a strong suppression of the signal of PG 15:0/18:1[D7] (approx. 50%) at its elution time, while in ESI(-) the signal was less affected. This confirms the results of the spiking experiments and might explain the higher variance of the recovery of PG 15:0/18:1[D7] (Fig. 2.4, Table 2.3, Fig. 2.5). Overall, ion suppression analysis revealed stronger ion suppression effects in ESI(+) compared to ESI(-), and was similar for the different investigated plasma pools. Besides ion suppression, ion enhancement effects were also observed at the corresponding elution times, e.g., for SM 18:1;2O/18:1[D9] and PE 15:0/18:1[D7] in ESI(+), and for PI 15:0/18:1[D7] in ESI(-) (not shown).

Extraction of a higher plasma volume (i.e., 20 and 50 µL) increased the ion suppression effects in ESI(+), especially for SM 18:1;O2/18:1[D9]. In ESI(-), besides ion suppression, strong ion enhancement was observed for PI 15:0/18:1[D7] and PG 15:0/18:1[D7] with higher plasma volume (Appendix Fig. 8.6). Thus, the use of 10 µL plasma is preferred as here ion suppression effects of the IS were acceptable. This sample volume is in line with previous lipidomics methods, e.g., Wang *et al.* and Chen *et al.* used 10 µL of human plasma for the extraction of lipids with a MeOH/MTBE-based LLE [44, 45] and Ottestad *et al.* extracted lipids from 10 µL of human plasma using a mixture of $CHCl_3$/MeOH [46].

Excursus: Deletion of MS signals by orbitrap MS

Ion suppression analysis unveiled in ESI(+) a complete drop of the signal of PG 15:0/18:1[D7] ($[M + NH_4]^+$ *m/z* 759.5875) to zero on two retention times between 13.24 and 15.17 min (for 116 s) (Fig. 2.5D and Fig. 2.6). Increasing the resolution setting of the Full MS scan from 60,000 to 240,000 decreased this signal drop to 32 s, but it still occurred even at the highest resolution (Fig. 2.6A). Full MS spectra indicate a distortion of the *m/z* by an interfering analyte resulting in a mass deviation > 20 ppm for the *m/z* of PG 15:0/18:1[D7] ($[M + NH_4]^+$) at both retention times (Fig. 2.6B).

Based on the *m/z* determined in the lipid extract without IS infusion, as well as its MS^2 spectra, the interference could be related to the [$^{13}C_1$] isotope of PC 16:0_18:2 ([M + H]$^+$ *m/z* 759.5728) which is present at high abundance in the plasma lipid extract (Fig. 2.6C). The elution window of this analyte from 13.30 to 15.01 min fits the deletion of the signal. The separation of this interfering *m/z* was achieved at 13.41 min with a resolution of 240,000, but this was not the case around the chromatographic apex of the peak (i.e., 14.05 min) (Fig. 2.6B, bottom).

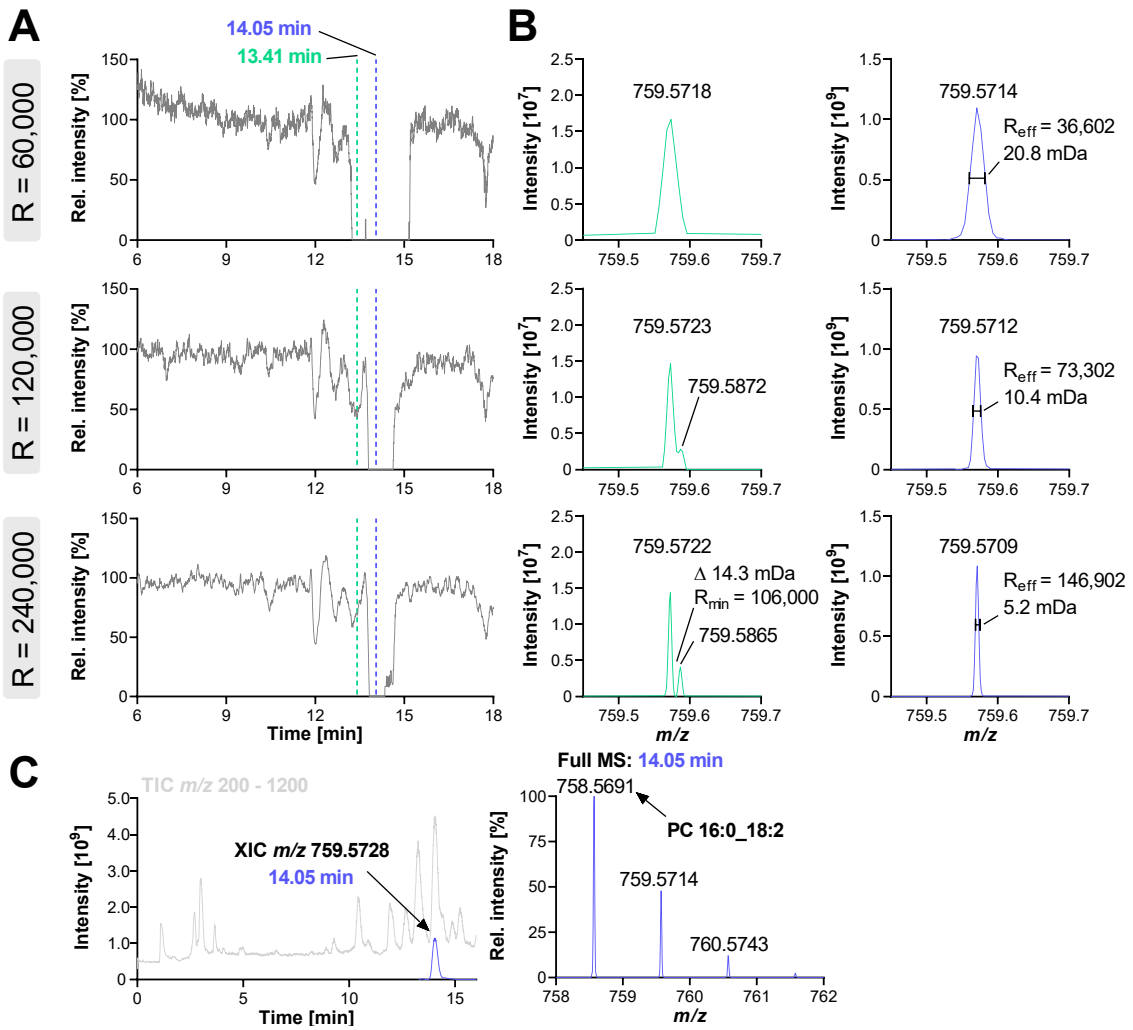

Fig. 2.6: Collapse of the signal at *m/z* 759.5875 (PG 15:0/18:1[D7], [M + NH_4]$^+$) in LC-ESI(+)-HRMS ion suppression analysis. An IS solution was post-columnly mixed with the LC flow following injection of a plasma lipid extract and Full MS spectra were recorded. **A** XIC at *m/z* 759.5875 (PG 15:0/18:1[D7], [M + NH_4]$^+$) using resolution settings of 60,000, 120,000, or 240,000. **B** Full MS spectra at 13.41 min (green) and 14.05 min (purple) showing the resolution-dependent interference of the signal. **C** LC-MS chromatogram: TIC (*m/z* 200 – 1200) and XIC at *m/z* 759.5728 showing the peak of the interference and its Full MS spectrum.

Using a standard solution of PC 16:0/18:2(9*Z*,12*Z*) instead of a lipid extract for the ion suppression analysis confirmed that the distortion of the signal of PG 15:0/18:1[D7] was caused by PC 16:0/18:2(9*Z*,12*Z*) ions at high abundance (Fig. 2.7): When 6 µmol L^{-1} of the PC 16:0/18:2(9*Z*,12*Z*) was injected, the signal of PG 15:0/18:1[D7] at 14.05 min was distorted (Fig. 2.7A, B, bottom), while decreasing the injected concentration of the PC 16:0/18:2(9*Z*,12*Z*) to a similar intensity of the ions at *m/z* 759.5728 and *m/z* 759.5875 allowed the parallel detection of both *m/z* (Fig. 2.7A, B, top).

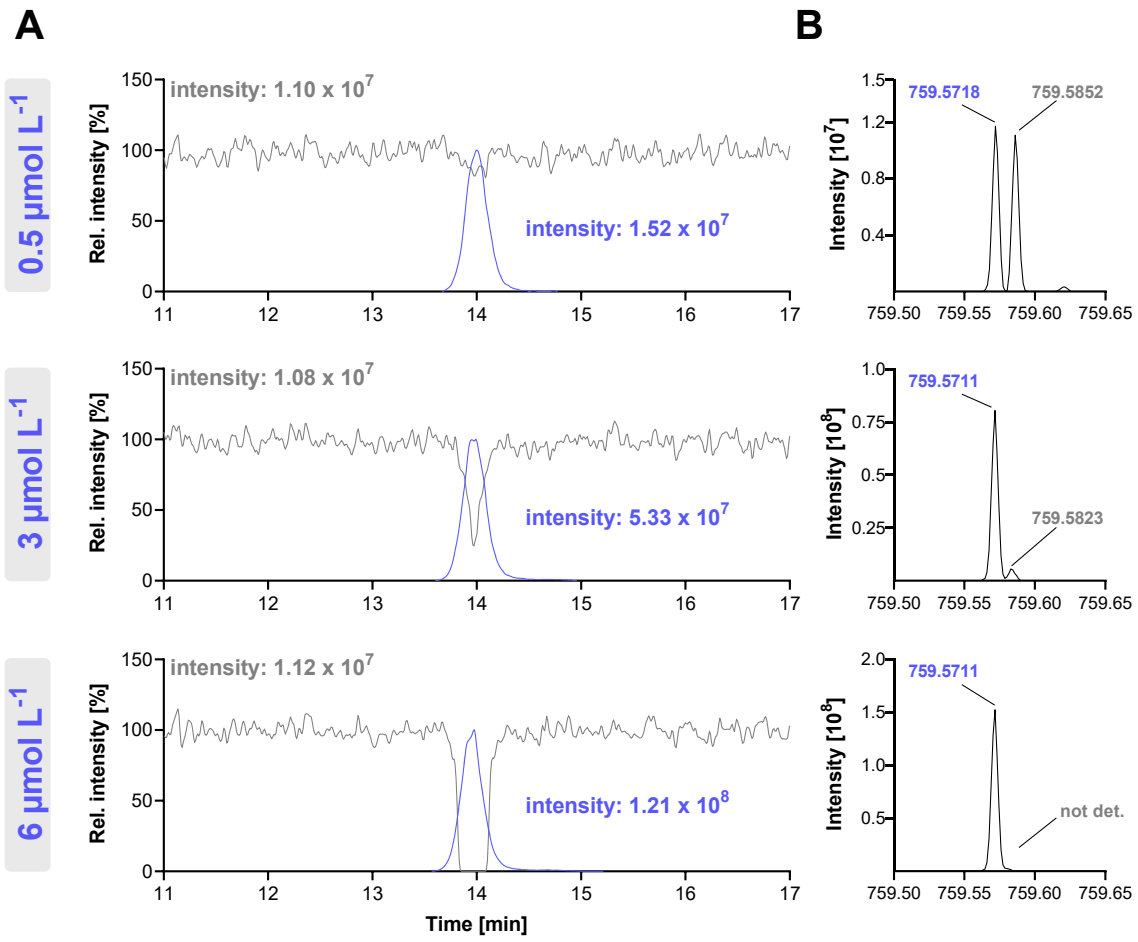

Fig. 2.7: Ion suppression analysis of PG 15:0/18:1[D7] in ESI(+). A PG 15:0/18:1[D7] solution (1.9 µmol L^{-1}, 5 µL min^{-1}) was post-columnly mixed with the LC-flow following injection (5 µL) of a standard solution of PC 16:0/18:2(9*Z*,12*Z*) ((**top**) 0.5 µmol L^{-1}, (**middle**) 3 µmol L^{-1}, and (**bottom**) 6 µmol L^{-1}) **A** XIC signal at *m/z* 759.5875 (PG 15:0/18:1[D7], $[M + NH_4]^+$) in grey and in purple the peak of ($[^{13}C_1]$ PC 16:0/18:2(9*Z*,12*Z*) $[M + H]^+$) at *m/z* 759.5728. **B** Full MS spectra at 14.05 min showing the concentration-dependent interference of the peak of PG 15:0/18:1[D7] $[M + NH_4]^+$ with the peak of $[^{13}C_1]$ PC 16:0/18:2(9*Z*,12*Z*) $[M + H]^+$ with similar *m/z*.

The distortion of the *m/z* also depended on the amount of ions and the filling of the orbitrap (defined by the AGC target): When the ratio of PC 16:0/18:2(9*Z*,12*Z*) : PG 15:0/18:1[D7] was kept constant (12 : 1), a high concentration (3 – 6 µmol L^{-1}) and a high number of ions in the trap (AGC ≥ 1 × 10^6) led again to the distortion of the signal of PG 15:0/18:1[D7]. At a lower filling of the trap (AGC target 2 × 10^4), both *m/z* were detected. In contrast, at low concentration (0.6 µmol L^{-1}) only with a higher AGC target (≥ 1 × 10^6) both *m/z* were detected (Fig. 2.8). Similar findings of distortion of the *m/z* signal by abundant almost isobaric ions (despite sufficient resolution) have already been reported in orbitrap MS and can be explained by the formation of ion clouds with almost identical *m/z* within the trap resulting in peak coalescence [47]. Overall, this shows that when using an orbitrap mass analyzer abundant lipid species influence the detection of lower abundant ones with similar *m/z* which should be considered during method development, i.e., (i) choosing the highest resolution possible for Full MS analysis, and (ii) using an efficient chromatographic separation — as described herein — to separate almost isobaric lipids.

Overall, the LLE with MeOH/MTBE yielded excellent extraction recoveries of the lysoPL and PL, and apparent losses resulted mainly from ion suppression. 10 µL of plasma was chosen for LLE to limit matrix effects and to enable semi-quantification. Intra- and inter-day variance < 100 ± 20%, as well as inter-operator variance < 100 ± 18% (except for PS and PG) using different pools of plasma demonstrate the reproducibility and robustness of the extraction method underlining its suitability for lipidomics analysis (Fig. 2.4). The observed signal erase for PG due to the [$^{13}C_1$] of PC 16:0_18:2 in ESI(+) does not impact the detection of PG 15:0/18:1[D7] because it elutes earlier at 11.43 min (Table 2.1). However, it should be kept in mind that the detection of lipid species with nearly identical *m/z* eluting at the same time might be disturbed using FT-MS instruments resulting in loss or distortion of information regarding their presence. This is particularly an issue in shotgun analysis where all ions enter the MS at the same time, but also might occur to some extent when combined with chromatographic separation.

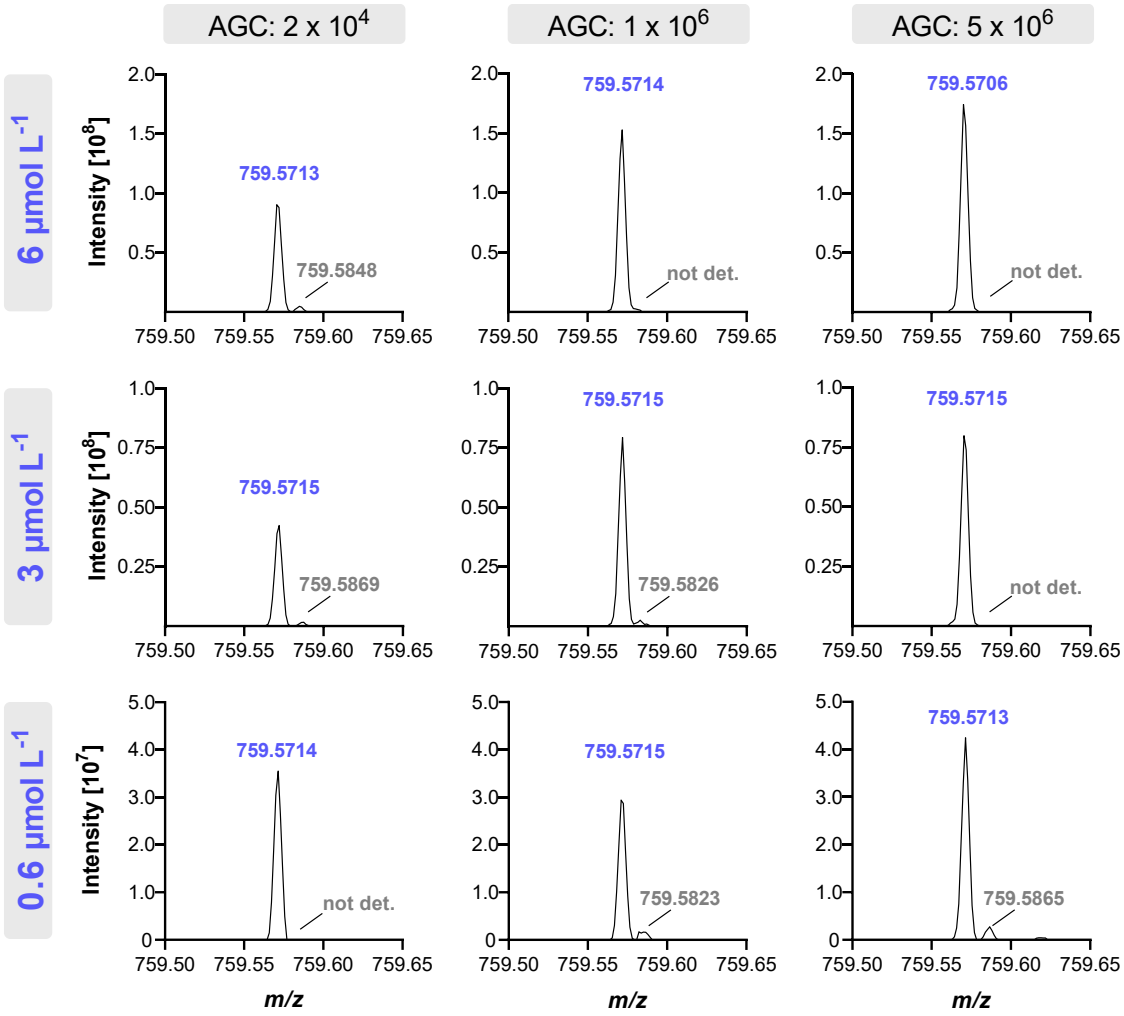

Fig. 2.8: Concentration and trap-filling dependent interference of PG 15:0/18:1[D7] and PC 16:0/18:2(9Z,12Z) in orbitrap MS. The signals of [$^{13}C_1$] PC 16:0/18:2(9Z,12Z) (*m/z* 759.5728) are highlighted in green and those of PG 15:0/18:1[D7] (*m/z* 759.5875) in grey. A mixture of the standards was analyzed by FIA-ESI(+)-HRMS at different concentrations, keeping a fixed concentration ratio of 12/1 (PC/PG). The concentrations of PC 16:0/18:2(9Z,12Z)/PG 15:0/18:1[D7] used are (**top row**) 6 µmol L^{-1}/0.5 µmol L^{-1}, (**middle row**) 3 µmol L^{-1}/0.25 µmol L^{-1}, and (**bottom row**) 0.6 µmol L^{-1}/0.05 µmol L^{-1}. Full MS spectra were recorded using different filling settings of the trap by setting the AGC to (**left column**) 2 x 10^4, (**middle column**) 1 x 10^6, and (**right column**) 5 x 10^6.

The use of a higher resolution might reduce this effect, but cannot prevent deletion of the signal of minor lipid species by dominating ions with similar *m/z.*

2.3.7 Application: Analysis of the effects of n3-PUFA supplementation on the human plasma lipidome

The effects of 12-month n3-PUFA supplementation (corresponding to 4 portions of fatty fish per week) on the plasma PL pattern in healthy subjects were investigated, aiming to characterize which PL are changing most following supplementation. After manual review of the feature assignment by MS-DIAL, 1399 features in ESI(+) and 580 in ESI(-) were found and evaluated by means of volcano plots (Fig. 2.9A). For evaluation of which lipid species showed a relevant change after n3-PUFA supplementation, only features with a – log10 (p-value) ≥ 1.303 (corresponding to – log10 ($p \leq 0.05$)) and a log2 (fold change) ≥ 0.5 or ≤ – 0.5 were further investigated (348 features in ESI(+) and 151 in ESI(-)).

From these, only the features detected in both ionization modes were semi-quantified aiming to (i) characterize the lipid class and the fatty acyl chains of the lipids, which was not done in previous lipidomics studies investigating n3-PUFA supplementation [45, 46, 48], and to (ii) provide additional confidence regarding the tentative identification of the lipid species and their modulation following n3-PUFA supplementation by comparing the results from both ionization modes. Thus, DG, TG, and Chol Ester were not further evaluated (Fig. 2.9A). Further confidence of the lipid identification was obtained utilizing retention time behavior of lipids in RP-LC, which correlates with the equivalent carbon number. Plotting the retention times of the logical series of lipid species *vs.* the carbon number of the fatty acyl chains (Appendix Fig. 8.4) or *vs.* the number of double bonds (Appendix Fig. 8.5) showed good correlation of polynomial regression for the different lipid classes [12]. A total of 98 lipid species were semi-quantified based on their peak height using the IS of the same lipid class, and concentrations obtained from the analysis in ESI(+) and ESI(-) mode were comparable (Appendix Table 8.5).

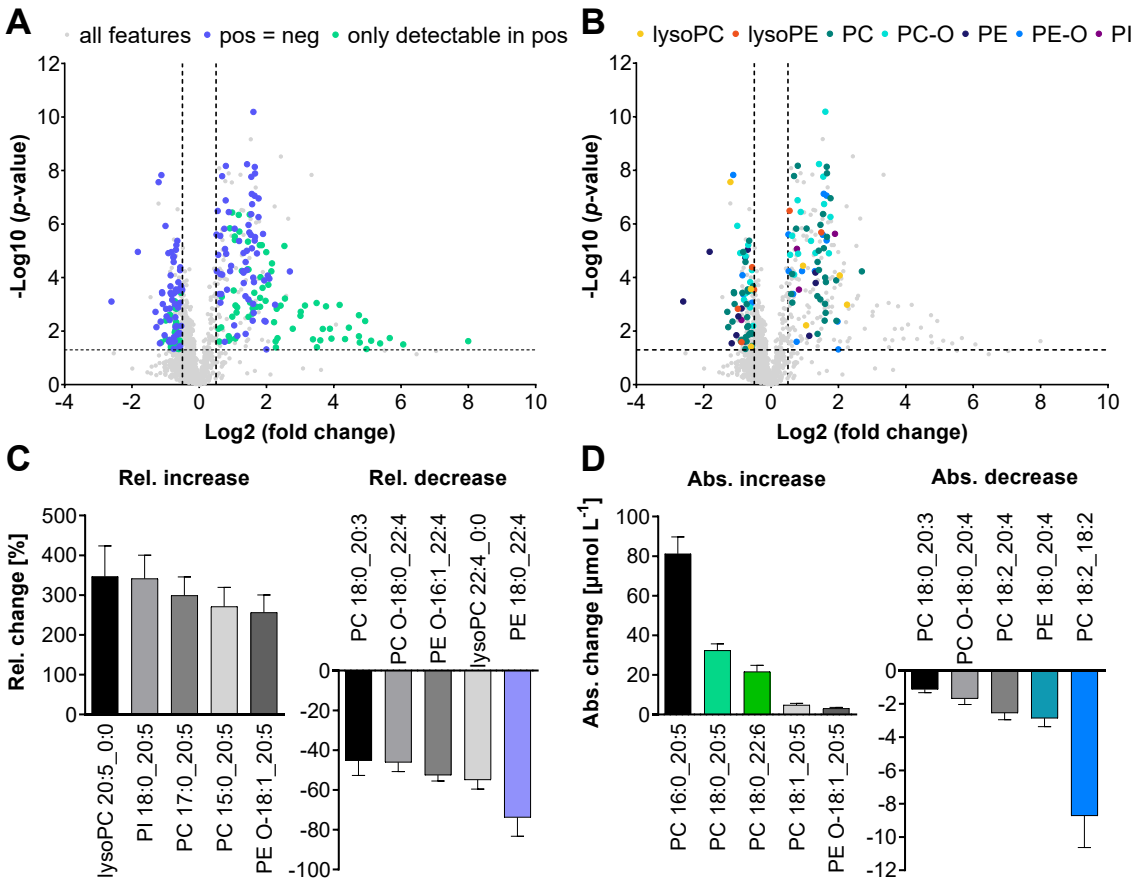

Fig. 2.9: Untargeted LC-HRMS analysis of PL in human plasma following n3-PUFA supplementation. Plasma lipid extracts at baseline and following 12 months of n3-PUFA supplementation were analyzed by untargeted LC-HRMS. **A** Shown are volcano plots highlighting significantly changing features detected in both ionization modes and those only detectable in ESI(+). **B** Significantly changing features detected in both modes are highlighted according to their lipid class. Shown are the **C** relative and **D** absolute changes observed in ESI(+) for the TOP 5 most changing tentatively identified lipids (mean ± SEM, n = 20). Highlighted lipids were further quantified by targeted LC-MS/MS.

Significant changes following n3-PUFA supplementation were observed for PC, ether PC, ether PE, PE, lysoPE, PI, and lysoPC lipid species. With 34 lipids, most changes were observed for the PC lipid class, followed by ether PC, ether PE, and PE with 24, 15, and 11 species, respectively (Fig. 2.9B). Following n3-PUFA supplementation, 8 PE species decreased, while 11 ether PE species increased. The change of a higher number of PC species is likely related to the high abundance of PC in human plasma, being the most abundant class of PL accounting for around 18% of all lipids [49, 50].

This is in line with an earlier analysis of the samples from the same study, where Browning *et al.* also found the strongest increase of DHA + EPA in the PC fraction among the different analyzed plasma lipid fractions (i.e., PC, Chol Ester, and TG). However, other PL classes were not analyzed [28].

Following n3-PUFA supplementation, the most increasing lipids bear 20:5 (Fig. 2.9C). It should be noted that the baseline concentration of lipids bearing 20:5 was lower than that of lipids bearing 22:6, which is consistent with a previous study reporting a lower total fatty acid level of 20:5(5*Z*,8*Z*,11*Z*,14*Z*,17*Z*) compared to 22:6(4*Z*,7*Z*,10*Z*,13*Z*,16*Z*,19*Z*) (40 ± 28 µmol L^{-1} and 89 ± 37 µmol L^{-1}, respectively) in plasma from healthy Canadian adults [51]. Due to their lower baseline concentration, a stronger increase was observed for lipids bearing 20:5: For example, lysoPC 20:5_0:0 was less abundant at baseline than lysoPC 22:6_0:0 (i.e., 0.25 ± 0.11 µmol L^{-1} *vs.* 0.80 ± 0.28 µmol L^{-1}) and was relatively increased by 350%, while lysoPC 22:6_0:0 showed an increase of 100%. Similar results were also observed for other PL classes, i.e., for the pairs PI 18:0_20:5/PI 18:0_22:6 (340% *vs.* 80%), PC 17:0_20:5/PC 17:0_22:6 (300% *vs.* 81%), lysoPE 20:5_0:0/lysoPE 22:6_0:0 (200% *vs.* 50%), and PC O-18:1_20:5/PC O-18:1_22:6 (180% *vs.* 82%).

These observations are in line with results from the same trial showing that the fatty acid 20:5(5*Z*,8*Z*,11*Z*,14*Z*,17*Z*) [52] and its oxylipin products (e.g., 14(15)-EpETE) [53] are relatively more affected by n3-PUFA supplementation compared to 22:6(4*Z*,7*Z*,10*Z*,13*Z*,16*Z*,19*Z*) and its oxylipin products. Our results are consistent with previous lipidomics studies showing that lysoPC 20:5_0:0 increased more than lysoPC 22:6_0:0 following n3-PUFA supplementation [45, 46]. Interestingly, also the determined relative changes for lysoPC 20:5_0:0 (i.e., 4.10 *vs.* 4.35) and lysoPC 22:6_0:0 (i.e., 1.93 *vs.* 1.89) were similar to the studies from Ottestad *et al.* where healthy subjects (n = 16) received fish oil capsules containing 0.7 g EPA + 0.9 g DHA per day for 7 weeks, indicating a steady state of modulation [46].

Table 2.4: Concentration of selected PL determined by untargeted and targeted analysis in plasma at baseline and following 12 months of n3-PUFA supplementation. Plasma lipid extracts were analyzed by untargeted LC-HRMS in both ionization modes, and lipids were semi-quantified based on normalized peak heights using one IS per lipid class. For quantification, extracts were analyzed by targeted LC-ESI(-)-MS/MS and lipids were quantified by external calibration based on analyte to corresponding IS peak area ratios. Shown are mean values ± SD, n = 20. The highlighted lipids were among the most changing species determined by untargeted LC-HRMS (see Fig. 2.9C, D).

		concentration [µmol L^{-1}]								
		baseline								
		LC-ESI(+)-HRMS			LC-ESI(-)-HRMS			LC-ESI(-)-MS/MS		
	increasing lipids									
lysoPC	lysoPC 20:5_0:0	0.25	±	0.11	0.37	±	0.15	-		
PI	PI 18:0_20:5	0.22	±	0.11	0.14	±	0.06	-		
PC	PC 15:0_20:5	0.19	±	0.08	0.37	±	0.15	-		
	PC 16:0_20:5	38	±	18	51	±	21	-		
	PC 17:0_20:5	0.34	±	0.14	0.51	±	0.21	-		
	PC 18:0/20:5(5Z,8Z,11Z,14Z,17Z)	15	±	6	20	±	8	17	±	7
	PC 18:1_20:5	2.9	±	1.3	4.4	±	1.8	-		
	PC 18:0/22:6(4Z,7Z,10Z,13Z,16Z,19Z)	32	±	12	34	±	11	51	±	17
PE-O	PE O-18:1_20:5	1.6	±	0.9	1.3	±	0.7			
	decreasing lipids									
lysoPC	lysoPC 22:4_0:0	0.06	±	0.02	0.08	±	0.03	-		
PC	PC 18:0_20:3	2.4	±	1.9	3.1	±	2.3	-		
	PC 18:2_20:4	7.0	±	2.0	11	±	2.6	-		
	PC 18:2(9Z,12Z)/18:2(9Z,12Z)	28	±	10	37	±	12	15	±	5
PE	**PE 18:0/20:4(5Z,8Z,11Z,14Z)**	6.9	±	2.6	7.4	±	2.7	11	±	4
	PE 18:0/22:4(7Z,10Z,13Z,16Z)	0.19	±	0.17	0.18	±	0.14	0.12	±	0.09
PC-O	PC O-18:0_20:4	4.8	±	1.6	5.8	±	1.5	-		
	PC O-18:0_22:4	0.61	±	0.20	0.81	±	0.20	-		
PE-O	PE O-16:1_22:4	0.47	±	0.15	0.31	±	0.09	-		

Table 2.4: Continued. Concentration of selected PL determined by untargeted and targeted analysis in plasma at baseline and following 12 months of n3-PUFA supplementation.

		concentration [µmol L^{-1}]		
		12 months		
		LC-ESI(+)-HRMS	LC-ESI(-)-HRMS	LC-ESI(-)-MS/MS
increasing lipids				
lysoPC	lysoPC 20:5_0:0	1.0 ± 0.7	1.4 ± 0.9	-
PI	PI 18:0_20:5	0.83 ± 0.42	0.42 ± 0.18	-
PC	PC 15:0_20:5	0.61 ± 0.27	1.1 ± 0.4	-
	PC 16:0_20:5	119 ± 42	134 ± 39	-
	PC 17:0_20:5	1.2 ± 0.4	1.7 ± 0.5	-
	PC 18:0/20:5(5Z,8Z,11Z,14Z,17Z)	48 ± 16	55 ± 16	56 ± 19
	PC 18:1_20:5	7.6 ± 4.4	11 ± 5	-
	PC 18:0/22:6(4Z,7Z,10Z,13Z,16Z,19Z)	54 ± 14	53 ± 15	90 ± 28
PE-O	PE O-18:1_20:5	4.7 ± 2.3	3.9 ± 1.8	-
decreasing lipids				
lysoPC	lysoPC 22:4_0:0	0.03 ± 0.01	0.03 ± 0.02	-
PC	PC 18:0_20:3	0.98 ± 0.51	1.4 ± 0.7	-
	PC 18:2_20:4	4.5 ± 1.2	6.8 ± 1.4	-
	PC 18:2(9Z,12Z)/18:2(9Z,12Z)	19 ± 7	25 ± 7.8	10 ± 3
PE	**PE 18:0/20:4(5Z,8Z,11Z,14Z)**	4.1 ± 1.1	4.8 ± 1.5	7.4 ± 2.1
	PE 18:0/22:4(7Z,10Z,13Z,16Z)	0.03 ± 0.04	0.05 ± 0.04	0.04 ± 0.03
PC-O	PC O-18:0_20:4	3.1 ± 1.1	3.7 ± 1.2	-
	PC O-18:0_22:4	0.30 ± 0.09	0.36 ± 0.13	-
PE-O	PE O-16:1_22:4	0.22 ± 0.07	0.17 ± 0.04	-

The strongest relative decrease was observed for lipids bearing 22:4 with, e.g., PE 18:0_22:4 showing a decrease of − 74% and lysoPC 22:4_0:0 of − 55% (Fig. 2.9C), and those bearing 20:3 with, e.g., PC 18:0_20:3 decreasing by − 45%. Other lipids bearing potential n6-PUFA, such as ARA (20:4(5*Z*,8*Z*,11*Z*,14*Z*)) or linoleic acid (18:2(9*Z*,12*Z*)), also decreased following n3-PUFA supplementation, e.g., PE 18:0_20:4 with − 37% and PC 18:2_18:2 with − 27%. Interestingly, the latter also showed the strongest decrease in concentration (Fig. 2.9D). These results are in line with previous studies reporting that n3-PUFA supplementation led to a decrease in the n6-PUFA content [28, 52, 54, 55]. Our results are also consistent with the study from Uhl *et al.* where a significant decrease was found for PC 16:0/22:4, PC 18:0/22:4, and PC 18:1/20:4 in plasma from subjects supplemented with 510 mg/day of DHA for 29 days by means of targeted lipidomics analysis [56]. In order to support the results determined with the untargeted approach, several of the most changing PL in the plasma were quantified using targeted LC-MS/MS.

Targeted analysis confirmed the tentative identification of the PL PC 18:0/20:5(5*Z*,8*Z*,11*Z*,14*Z*,17*Z*), PC 18:0/22:6 (4*Z*,7*Z*,10*Z*,13*Z*,16*Z*,19*Z*), PE 18:0/20:4(5*Z*,8*Z*,11*Z*,14*Z*), PE 18:0/22:4(7*Z*,10*Z*,13*Z*,16*Z*), and PC 18:2(9*Z*,12*Z*)/18:2(9*Z*,12*Z*) (Table 2.4, Appendix Fig. 8.7). Concentrations determined by quantitative targeted LC-MS/MS were in the same range as those semi-quantified by LC-HRMS, also confirming the observed increase and decrease following n3-PUFA supplementation (Fig. 2.10). Quantitative targeted analysis resulted in almost same concentration for PC 18:0/20:5(5*Z*,8*Z*,11*Z*,14*Z*,17*Z*), while < 2.5-fold difference in concentrations was found for PC 18:0/22:6(4*Z*,7*Z*,10*Z*,13*Z*,16*Z*,19*Z*), PE 18:0/20:4(5*Z*,8*Z*,11*Z*,14*Z*), PE 18:0/22:4(7*Z*,10*Z*,13*Z*,16*Z*), and PC 18:2(9*Z*,12*Z*)/18:2(9*Z*,12*Z*).

This supports the suitability of the developed untargeted LC-HRMS method to monitor changes in the PL pattern in plasma. Our results showed a significant increase in lipids bearing n3-PUFA combined with a decrease in lipids bearing n6-PUFA [28, 52, 54].

PC 18:0/20:5(5Z,8Z,11Z,14Z,17Z) and PC 18:2(9Z,12Z)/18:2(9Z,12Z) were found to be significantly modulated and might be further investigated as possible biomarkers for n3-PUFA consumption.

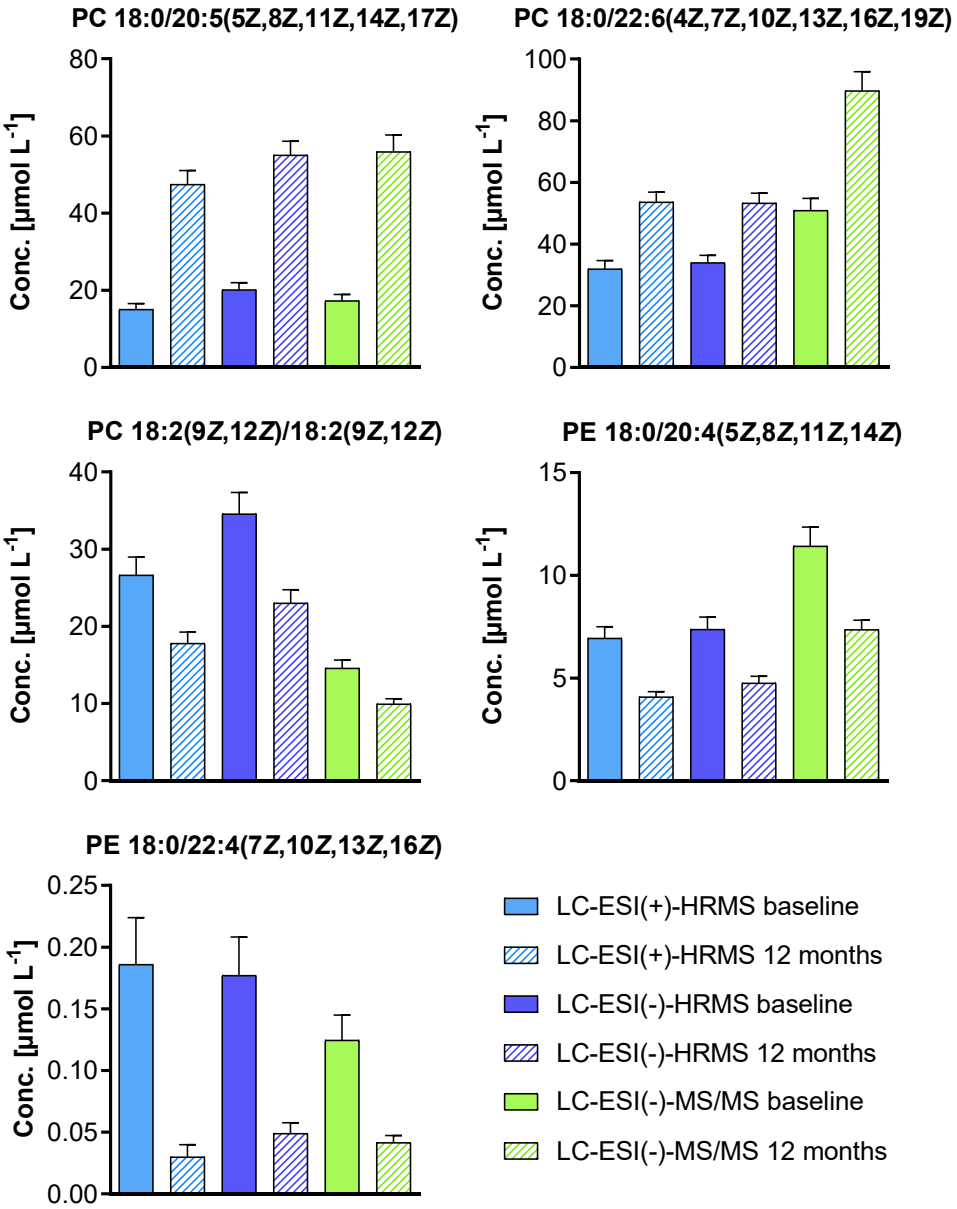

Fig. 2.10: Comparison of concentrations of selected PL determined by untargeted LC-HRMS and targeted LC-MS/MS. Plasma lipid extracts were analyzed by untargeted LC-HRMS, and lipids were semi-quantified based on peak heights using one IS per lipid class. For quantification, the extracts were analyzed by targeted LC-ESI(-)-MS/MS, and lipids were quantified by external calibration based on analyte to corresponding IS peak area ratios. Shown are the concentrations of selected PL at baseline and following 12 months of n3-PUFA supplementation (mean ± SEM, n = 20).

2.4 Conclusion

We optimized and characterized the performance of an LC-HRMS method for the semi-quantification of polar lipids in human plasma. Individual MS parameters were systematically optimized allowing a threefold gain in sensitivity. It was shown that the setting of the auxiliary gas is critical for the spray stability and the S-lens RF level has a relevant impact on the ion transmission and signal intensity. Optimization of chromatographic parameters showed that the selection of the RP C18 column has a great impact on the separation efficiency and peak shape, indicating that surface interactions play a relevant role in PL separation in RP-LC.

Data-dependent MS^2 settings were identified to be crucial and the number of TOP *N* was adjusted based on the FWHM of the chromatographic peaks over the elution time in a staggered manner. This allows the acquisition of as many meaningful MS^2 spectra as possible for lipid characterization, while recording enough data points across the peaks for semi-quantification. Of note, we found that highly abundant lipids can distort the detection of lipids with similar *m/z* in the orbitrap mass analyzer. Thus, the highest resolution possible should be selected for Full MS analysis; however, this does not resolve the problem completely.

Thorough characterization of matrix effects by pre- and post-extraction spiking as well as ion suppression analysis of plasma unveiled that apparent losses are caused by ion suppression. Thus, concentrations resulting from semi-quantification based on only one IS per lipid class might be affected by coeluting interferences in RP-LC. However, determined concentrations in plasma by untargeted LC-HRMS were comparable in ESI(-) and ESI(+), and in the same range as those obtained by targeted LC-MS/MS.

The developed LC-HRMS method was successfully used to investigate the effects of n3-PUFA supplementation on the PL pattern in human plasma. A total of 98 PL, which were significantly changed following supplementation, were semi-quantified in both ionization modes. A strong increase was found for lipids bearing 20:5, while lipids bearing 22:4, and of note PC 18:2(9*Z*,12*Z*)/18:2(9*Z*,12*Z*) were lowered.

Quantitative targeted analysis confirmed the identification of selected PL and their relative change following n3-PUFA supplementation. The concentration difference between the targeted and the untargeted approach was less than 2.5-fold, underlining the reliability of the semi-quantification using the developed untargeted LC-HRMS method.

2.5 References

1. Fahy E, Subramaniam S, Brown HA, Glass CK, Merrill AH, Murphy RC, et al. (2005) A comprehensive classification system for lipids1. *J Lipid Res*. **46**, 839–61.
2. Calder PC Functional roles of fatty acids and their effects on human health. (2015) *J Parenter Enter Nutr*. **39**, 18S-32S.
3. Li J, Wang X, Zhang T, Wang C, Huang Z, Luo X, et al. A review on phospholipids and their main applications in drug delivery systems. Asian J Pharm Sci. 2015;10(2):81–98.
4. Van Meer G, Voelker DR, Feigenson GW. (2008) Membrane lipids: where they are and how they behave. *Nat Rev Mol Cell Biol*. **9**, 112–24.
5. Bird SS, Marur VR, Stavrovskaya IG, Kristal BS (2012) Separation of cis–trans phospholipid isomers using reversed phase LC with high resolution MS detection. *Anal Chem*. **84**, 5509–17.
6. Cajka T, Fiehn O (2014) Comprehensive analysis of lipids in biological systems by liquid chromatography-mass spectrometry. TrAC, *Trends Anal Chem*. **61**, 192–206.
7. Hu C, Zhou Y, Feng J, Zhou S, Li C, Zhao S, et al. (2019) Untargeted lipidomics reveals specific lipid abnormalities in nonfunctioning human pituitary adenomas. *J Proteome Res*. **19**, 455–63.
8. Khan MJ, Codreanu SG, Goyal S, Wages PA, Gorti SK, Pearson MJ, et al. (2020) Evaluating a targeted multiple reaction monitoring approach to global untargeted lipidomic analyses of human plasma. *Rapid Commun Mass Spectrom*. **34**, e8911.
9. Shan J, Qian W, Kang A, Peng L, Xie T, Lin L, et al. (2019) Lipid profile perturbations in the plasma and lungs of mice with LPS-induced acute lung injury revealed by UHPLC-ESI-Q Exactive HF MS analysis. *J Pharm Biomed Anal*. **162**, 242–8.
10. Narváez-Rivas M, Zhang Q (2016) Comprehensive untargeted lipidomic analysis using core–shell C30 particle column and high field orbitrap mass spectrometer. *J Chromatogr A*. **1440**, 123–34.
11. Criscuolo A, Zeller M, Cook K, Angelidou G, Fedorova M (2019) Rational selection of reverse phase columns for high throughput LC–MS lipidomics. *Chem Phys Lipid*. **221**, 120–7.
12. Vaňková Z, Peterka O, Chocholoušková M, Wolrab D, Jirásko R, Holčapek M (2022) Retention dependences support highly confident identification of lipid species in human plasma by reversed-phase UHPLC/MS. *Anal Bioanal Chem*. **414**, 319–31.
13. Damen CW, Isaac G, Langridge J, Hankemeier T, Vreeken RJ (2014) Enhanced lipid isomer separation in human plasma using reversed-phase UPLC with ion-mobility/high-resolution MS detection [S]. *J Lipid Res*. **55**, 1772–83.
14. Xu T, Hu C, Xuan Q, Xu G (2020) Recent advances in analytical strategies for mass spectrometry-based lipidomics. *Anal Chim Acta*. **1137**, 156–69.
15. Züllig T, Trötzmüller M, Köfeler HC (2020) Lipidomics from sample preparation to data analysis: a primer. *Anal Bioanal Chem*. **412**, 2191–209.
16. Rund KM, Ostermann AI, Kutzner L, Galano J-M, Oger C, Vigor C, et al. (2018) Development of an LC-ESI (-)-MS/MS method for the simultaneous quantification of 35 isoprostanes and isofurans derived from the major n3-and n6-PUFAs. *Anal Chim Acta*. **1037**, 63–74.

17. Hartung NM, Mainka M, Pfaff R, Kuhn M, Biernacki S, Zinnert L, et al. (2023) Development of a quantitative proteomics approach for cyclooxygenases and lipoxygenases in parallel to quantitative oxylipin analysis allowing the comprehensive investigation of the arachidonic acid cascade. *Anal Bioanal Chem*. **415**, 913–33.
18. Zhou H, Nong Y, Zhu Y, Liang Y, Zhang J, Chen H, et al. (2022) Serum untargeted lipidomics by UHPLC-ESI-HRMS aids the biomarker discovery of colorectal adenoma. *BMC Cancer*. **22**, 1–14.
19. Gil A, Zhang W, Wolters JC, Permentier H, Boer T, Horvatovich P, et al. (2018) One-vs two-phase extraction: re-evaluation of sample preparation procedures for untargeted lipidomics in plasma samples. *Anal Bioanal Chem*. **410**, 5859–70.
20. Lee H-C, Yokomizo T (2018) Applications of mass spectrometry-based targeted and non-targeted lipidomics. *Biochem Biophys Res Commun*. **504**,576–81.
21. Wolrab D, Chocholoušková M, Jirásko R, Peterka O, Holčapek M (2020) Validation of lipidomic analysis of human plasma and serum by supercritical fluid chromatography–mass spectrometry and hydrophilic interaction liquid chromatography–mass spectrometry. *Anal Bioanal Chem*. **412**, 2375–88.
22. Koch E, Mainka M, Dalle C, Ostermann AI, Rund KM, Kutzner L, et al. (2020) Stability of oxylipins during plasma generation and longterm storage. *Talanta*. **217**, 121074.
23. Matyash V, Liebisch G, Kurzchalia TV, Shevchenko A, Schwudke D (2008) Lipid extraction by methyl-tert-butyl ether for high-throughput lipidomics. *J Lipid Res*. **49**, 1137–46.
24. Ostermann AI, Koch E, Rund KM, Kutzner L, Mainka M, Schebb NH (2020) Targeting esterified oxylipins by LC–MS-Effect of sample preparation on oxylipin pattern. *Prostaglandins Other Lipid Mediat*. **146**, 106384.
25. Meckelmann SW, Hawksworth JI, White D, Andrews R, Rodrigues P, O'Connor A, et al. (2020) Metabolic dysregulation of the lysoPL/autotaxin axis in the chromosome 9p21 gene SNP rs10757274. *Circ: Genomic and Precision Medicine*. **13**, e002806.
26. Bligh EG, Dyer WJ (1959) A rapid method of total lipid extraction and purification. *Can J Biochem Physiol*. **37**, 911–7.
27. Hara A, Radin NS (1978) Lipid extraction of tissues with a low-toxicity solvent. *Anal Biochem*. **90**, 420–6.
28. Browning LM, Walker CG, Mander AP, West AL, Madden J, Gambell JM, et al. (2012) Incorporation of eicosapentaenoic and docosahexaenoic acids into lipid pools when given as supplements providing doses equivalent to typical intakes of oily fish. *Am J Clin Nutr*. **96**, 748–58.
29. Tsugawa H, Cajka T, Kind T, Ma Y, Higgins B, Ikeda K, et al. (2015) MS-DIAL: data-independent MS/MS deconvolution for comprehensive metabolome analysis. *Nat Methods*. **12** 523–6.
30. Pi J, Wu X, Feng Y (2016) Fragmentation patterns of five types of PL by ultra-high-performance liquid chromatography electrospray ionization quadrupole time-of-flight tandem mass spectrometry. *Anal Methods*. **8**, 1319–32.
31. Liebisch G, Fahy E, Aoki J, Dennis EA, Durand T, Ejsing CS, et al. (2020) Update on LIPID MAPS classification, nomenclature, and shorthand notation for MS-derived lipid structures. *J Lipid Res*. **61**, 1539–55.
32. Bird SS, Marur VR, Sniatynski MJ, Greenberg HK, Kristal BS (2011) Serum lipidomics profiling using LC–MS and high-energy collisional dissociation fragmentation: focus on triglyceride detection and characterization. *Anal Chem*. **83**, 6648–57.

33. Kiyonami R, Peake D, Huang Y (2016) Increased identification coverage and throughput for complex lipidomes. *Thermo Fisher Scientific Application Note*. **607**, 1–8.
34. Chen W, Zeng J, Wang W, Yang B, Zhong L, Zhou J (2020) Comprehensive metabolomic and lipidomic analysis reveals metabolic changes after mindfulness training. *Mindfulness*. **11**, 1390–400.
35. Xu X, Luo Z, He Y, Shan J, Guo J, Li J (2020) Application of untargeted lipidomics based on UHPLC-high resolution tandem MS analysis to profile the lipid metabolic disturbances in the heart of diabetic cardiomyopathy mice. *J Pharm Biomed Anal*. **190**, 113525.
36. Gallart-Ayala H, Courant F, Severe S, Antignac J-P, Morio F, Abadie J, et al. (2013) Versatile lipid profiling by liquid chromatography – high resolution mass spectrometry using all ion fragmentation and polarity switching. Preliminary application for serum samples phenotyping related to canine mammary cancer. *Analytica chimica acta*. **796**, 75–83.
37. Forest A, Ruiz M, Bouchard B, Boucher G, Gingras O, Daneault C, et al. (2018) Comprehensive and reproducible untargeted lipidomic workflow using LC-QTOF validated for human plasma analysis. *J Proteome Res*. **17**, 3657–70.
38. Géhin C, Fowler SJ, Trivedi DK (2023) Chewing the fat: how lipidomics is changing our understanding of human health and disease in 2022. *Analytical Science Advances*. **4**, 104–31.
39. Hutchins PD, Russell JD, Coon JJ (2019) Accelerating lipidomic method development through in silico simulation. *Anal Chem*. **91**, 9698–706.
40. Ogiso H, Suzuki T, Taguchi R (2008) Development of a reverse-phase liquid chromatography electrospray ionization mass spectrometry method for lipidomics, improving detection of phosphatidic acid and phosphatidylserine. *Anal Biochem*. **375**, 124–31.
41. Schwaiger M, Schoeny H, El Abiead Y, Hermann G, Rampler E, Koellensperger G (2019) Merging metabolomics and lipidomics into one analytical run. *Analyst*. **144**, 220–9.
42. Zhou J, Sun L, Chen L, Liu S, Zhong L, Cui M (2019) Comprehensive metabolomic and proteomic analyses reveal candidate biomarkers and related metabolic networks in atrial fibrillation. *Metabolomics*. **15**, 1–13.
43. Wong MWK, Braidy N, Pickford R, Sachdev PS, Poljak A (2019) Comparison of single phase and biphasic extraction protocols for lipidomic studies using human plasma. *Front Neurol*. **10**, 879.
44. Wang B, Tontonoz P (2019) PL remodeling in physiology and disease. *Annu Rev Physiol*. **81**, 165–88.
45. Yan M, Cai WB, Hua T, Cheng Q, Ai D, Jiang HF, et al. (2020) Lipidomics reveals the dynamics of lipid profile altered by omega-3 polyunsaturated fatty acid supplementation in healthy people. *Clin Exp Pharmacol Physiol*. **47**, 1134–44.
46. Ottestad I, Hassani S, Borge GI, Kohler A, Vogt G, Hyötyläinen T, et al. (2012) Fish oil supplementation alters the plasma lipidomic profile and increases long-chain PUFAs of PL and triglycerides in healthy subjects. *PloS ONE*. **7**, e42550.
47. Gorshkov MV, Fornelli L, Tsybin YO (2012) Observation of ion coalescence in Orbitrap Fourier transform mass spectrometry. *Rapid Commun Mass Spectrom*. **26**, 1711–7.
48. Lankinen M, Schwab U, Erkkilä A, Seppänen-Laakso T, Hannila M-L, Mussalo H, et al. (2009) Fatty fish intake decreases lipids related to inflammation and insulin signaling—a lipidomics approach. *PLoS ONE*. **4**, e5258.

49. Bowden JA, Heckert A, Ulmer CZ, Jones CM, Koelmel JP, Abdullah L, et al. (2017) Harmonizing lipidomics: NIST interlaboratory comparison exercise for lipidomics using SRM 1950–Metabolites in Frozen Human Plasma [S]. *J Lipid Res*. **58**, 2275–88.
50. Burla B, Arita M, Arita M, Bendt AK, Cazenave-Gassiot A, Dennis EA, et al. (2018) Ms-based lipidomics of human blood plasma: A community-initiated position paper to develop accepted guidelines1. *J Lipid Res*. **59**, 2001–17.
51. Abdelmagid SA, Clarke SE, Nielsen DE, Badawi A, El-Sohemy A, Mutch DM, et al. (2015) Comprehensive profiling of plasma fatty acid concentrations in young healthy Canadian adults. *PLoS ONE*. **10**, e0116195.
52. Dawczynski C, Massey KA, Ness C, Kiehntopf M, Stepanow S, Platzer M, et al. (2013) Randomized placebo-controlled intervention with n-3 LC-PUFA-supplemented yoghurt: effects on circulating eicosanoids and cardiovascular risk factors. *Clin Nutr*. **32**, 686–96.
53. Ostermann AI, West AL, Schoenfeld K, Browning LM, Walker CG, Jebb SA, et al. (2019) Plasma oxylipins respond in a linear doseresponse manner with increased intake of EPA and DHA: results from a randomized controlled trial in healthy humans. *Am J Clin Nutr*. **109**, 1251–63.
54. Schuchardt JP, Ostermann AI, Stork L, Kutzner L, Kohrs H, Greupner T, et al. (2016) Effects of docosahexaenoic acid supplementation on PUFA levels in red blood cells and plasma. *Prostaglandins Leukot Essent Fatty Acids*. **115**, 12–23.
55. Walker CG, West AL, Browning LM, Madden J, Gambell JM, Jebb SA, et al. (2015) The pattern of fatty acids displaced by EPA and DHA following 12 months supplementation varies between blood cell and plasma fractions. *Nutrients*. **7**, 6281–93.
56. Uhl O, Demmelmair H, Klingler M, Koletzko B (2013) Changes of molecular glycerophospholipid species in plasma and red blood cells during docosahexaenoic acid supplementation. *Lipids*. **48**,1103–13.

Chapter 3

LC-HRMS analysis of phospholipids bearing oxylipins *

Several oxylipins including hydroxy- and epoxy-PUFA act as lipid mediators. In biological samples they can be present as non-esterified form, but the major part occurs esterified in PL or other lipids. Esterified oxylipins are quantified indirectly after alkaline hydrolysis as non-esterified oxylipins. However, in this indirect analysis the information in which lipid class oxylipins are bound is lost. In this work, an untargeted LC-HRMS method for the direct analysis of PL bearing oxylipins was developed. Optimized RP-LC separation achieved a sufficient separation of isobaric and isomeric PL from different lipid classes bearing oxylipin positional isomers. Individual PL species bearing oxylipins were identified based on retention time, precursor ion, and characteristic product ions. The bound oxylipin could be characterized based on product ions resulting from the α-cleavage occurring at the hydroxy/epoxy group. PL *sn*-1/*sn*-2 isomers were identified based on the neutral loss of the fatty acyl in the *sn*-2 position. A total of 422 individual oxPL species from 7 different lipid classes i.e., PI, PS, PC, PE, PC-P, PC-O, and PE-P were detected in human serum and cells. This method enabled to determine in which PL classes supplemented oxylipins are incorporated in HEK293T cells: 20:4;15OH, 20:4;14Ep, and 20:5;14Ep were mostly bound to PI. 20:4;8Ep and 20:5;8Ep were esterified to PC and PE, while other oxylipins were mainly found in PC. The developed LC-HRMS method enables the comprehensive detection as well as the semi-quantification of isobaric and isomeric PL species bearing oxylipins. With this method, we show that the position of the oxidation has a great impact and directs the incorporation of oxylipins into the different PL classes in human cells.

* modified from Carpanedo L. Rund K. M., Wende L. M., Kampschulte N., and Schebb N. H. (2024) *Anal Chim Acta*. **1326**, 343139; doi: 10.1016/j.aca.2024.343139.

Author contributions: **LC:** Writing – review & editing, Writing – original draft, Visualization, Methodology, Investigation, Formal analysis, Data curation. **KR:** Writing – review & editing, Methodology, Investigation, Conceptualization. **LMW:** Writing – review & editing, Methodology, Investigation, Formal analysis, Data curation. **NK:** Writing – review & editing, Supervision, Methodology, Investigation. **NHS:** Writing – review & editing, Writing – original draft, Supervision, Project administration, Investigation, Funding acquisition, Conceptualization.

3.1 Introduction

Eicosanoids and other oxylipins are derived from the oxidation of PUFA. The major part of oxylipins, particularly epoxy- and hydroxy-PUFA, is found esterified i.e. bound to lipids such as PL in biological samples [1-3]. Several oxylipins are potent lipid mediators [4,5], however, the biological activity and role of esterified oxylipins are not well understood. Few studies describe the effects of PL bearing oxylipins on inflammation. For example, pro-inflammatory actions such as increasing monocyte adhesion [6], platelet activation, and aggregation [7] have been described. However, other studies suggest anti-inflammatory effects in lipopolysaccharide-induced inflammation [8]. PL bearing oxylipins, i.e., oxPL can be formed (i) by the direct oxidation of the esterified PUFA via non-enzymatic lipid peroxidation or by 15-LOX accepting PL as substrate [9], or (ii) by oxidation of non-esterified PUFA followed by incorporation into lysoPL *via* the Lands' cycle pathway: Here, the PUFA is oxidized either enzymatically by COX, CYP450, or LOX, or through non-enzymatic processes [1,9–12]. In the next step, an ACSL catalyzes the activation of the oxPUFA, yielding oxPUFA-CoA. The acyl-CoA are (re)esterified into lysoPL by different enzymes such as LPLAT [9,13]. In mammalian lipids, saturated FA are usually bound at the *sn*-1 position by an ester bond or in the case of ether lipids an alkyl chain is bound *via* an ether or a vinyl-ether bond (plasmalogen) [14]. PUFA such as LA, ARA, EPA, or DHA are typically bound at the *sn*-2 position [15]. Consequently, it is also assumed that oxPL predominantly feature the oxylipin at the *sn*-2 position.

In the last decades, the quantification of esterified oxylipins was carried out indirectly by quantitative analysis of non-esterified oxylipins using targeted LC-MS/MS [16,17] following the cleavage of the ester bond by alkaline hydrolysis. However, with this analysis the information on which lipid species/classes the oxylipins are esterified is lost and thus it is impossible to study the biological roles of specific oxPL.

Only few methods directly analyzing oxPL are described [7,18–23]. However, with the exception of the study of Aoyagi *et al.* [18] characterizing about 400 PL species bearing oxylipins, these methods only cover few esterified oxylipins. The MS analysis of oxPL represents a challenge because of the large number of isomeric species giving rise to ions with the same *m/z*, which in several cases even show a similar fragmentation behavior. Therefore, chromatographic separation of oxPL is crucial enabling their identification through the acquisition of meaningful MS^2 spectra. Few studies analyzed oxPL using targeted LC-MS/MS in biological samples such as mouse peritoneal macrophages [18, 23] or mouse organs, e.g. intestine [23] or heart tissue [22]. In these studies, coeluting isobaric oxPL species are detected based on specific mass transitions, which only allows the detection of preselected PL bearing oxylipins. In contrast, untargeted LC-HRMS has been demonstrated to be an effective tool for the analysis of PC 16:0/5:0;O and PC 16:0/9:0;O in blood platelets [7], and esterified mono, double, and triple oxygenated ARA and AdA in mouse embryonic fibroblasts [19]. However, none of these studies focused on the separation and detection of isobaric and isomeric oxPL and as a consequence, only a low number of oxPL in biological samples were detected.

Here, an untargeted LC-HRMS method for the analysis of oxPL has been developed. The optimized chromatography allows the separation of a large number of isobaric and isomeric PL bearing hydroxy- or epoxy-PUFA. Individual oxPL species were identified in negative ionization mode based on the precursor ion, MS^2 spectra, and retention time. Characteristic product ions enabled to deduce the position of the hydroxy/epoxy group in the oxPUFA as well as the *sn*-1/*sn*-2 position of the fatty acyl chains. The method was applied to investigate in which PL class supplemented hydroxy-20:4 (20:4;OH), epoxy-18:2 (18:2;Ep), epoxy-20:4 (20:4;Ep), and epoxy-20:5 (20:5;Ep) positional isomers are incorporated in human cells. Semi-quantification of the oxPL unveiled a distinct incorporation pattern of individual oxylipins in specific PL classes.

3.2 Experimental

3.2.1 Chemicals and biological material

The PL standards PI 12:0/13:0, PS 12:0/13:0, PC 12:0/13:0, and PE 12:0/13:0 used as IS were purchased from Avanti Polar Lipids (local supplier: Merck KGaA, Darmstadt). The standards PC 16:0/17(18)-EpETE, PC 16:0/20:4(5*Z*,8*Z*,11*Z*,14*Z*), PC 18:0/20:4 (5*Z*,8*Z*,11*Z*,14*Z*), PE 16:0/20:4(5*Z*,8*Z*,11*Z*,14*Z*), PE 18:0/20:4(5*Z*,8*Z*,11*Z*,14*Z*), PC 18:0/20:5(5*Z*,8*Z*,11*Z*,14*Z*,17*Z*), PC 16:0/22:6(4*Z*,7*Z*,10*Z*,13*Z*,16*Z*,19*Z*), PC 18:0/22:6(4*Z*,7*Z*,10*Z*,13*Z*,16*Z*,19*Z*), PE 16:0/22:6(4*Z*,7*Z*,10*Z*,13*Z*,16*Z*,19*Z*), PC 18:0/22:4(7*Z*,10*Z*,13*Z*,16*Z*), and PE 18:0/22:4(7*Z*,10*Z*,13*Z*,16*Z*) as well as 15-HETE, 12-HETE, and 5-HETE were from Cayman Chemical (Ann Arbor, MI, USA; local supplier: Biomol, Hamburg, Germany). The PUFA standards (i.e., 18:2, 20:4, 20:5, or 22:6) were purchased from NuChek Prep, Inc. (Waterwill, MN, USA). ACN LC-MS grade, MeOH LC-MS grade, IPA LC-MS grade, as well as formic acid LC-MS grade were obtained from Fisher Scientific (Schwerte, Germany). Ultra-pure H_2O (18.2 MΩ cm) was generated using the Barnstead Genpure Pro system from Thermo Fisher Scientific (Lan genselbold, Germany). Ammonium formate was supplied by Sigma-Aldrich (Schnelldorf, Germany). Sodium deoxycholate was from Carl Roth (Karlsruhe, Germany). All other chemicals, including MTBE, were purchased from Merck KGaA (Darmstadt, Germany).

Epoxy-PUFA were synthesized in-house using *meta*-chloroperoxybenzoic acid (mCPBA) as described [24]. Briefly, 50 mg (~ 150 µmol L^{-1}) PUFA (i.e., 18:2, 20:4, 20:5, or 22:6) were dissolved in 10 mL $CHCl_3$ and mCPBA was added in an equimolar amount. After gentle stirring at room temperature overnight, the reaction was terminated by LLE with 0.5 mol L^{-1} aqueous sodium bicarbonate solution (pH = 8.0). Following drying with sodium sulfate, the organic phase was evaporated to dryness, and monoepoxy-PUFA were separated from the

remaining educt and multiple epoxidized PUFA by (semi-)preparative RP-chromatography (overall yield 50 – 70% depending on PUFA).

Soybean 15-LOX (type I – B) and the pooled human serum were purchased from Sigma-Aldrich (Schnelldorf, Germany). HEK293T cells were obtained from the German Collection of Microorganisms and Cell Cultures GmbH (DSMZ, Braunschweig, Germany).

3.2.2 Lipid extraction

Lipids in serum and HEK293T cells were extracted using a modified LLE based on Matyash *et al.* [25] described in [26] with slight modifications. Briefly, 100 µL freshly thawed human serum or 100 µL suspension of sonicated cells (in 500 µL PBS) were transferred to 3 mL glass tubes. 15 pmol of each IS (i.e., PI 12:0/13:0, PS 12:0/13:0, PC 12:0/13:0, and PE 12:0/13:0) were added, yielding a final concentration of 300 nmol L^{-1} in the lipid extract. Lipids were extracted using 225 µL MeOH and 750 µL MTBE. Phase separation was induced by the addition of 188 µL 150 mmol L^{-1} ammonium acetate. Following centrifugation and collection of the upper phase, re-extraction of the lipids was done using 300 µL MTBE. After extraction and evaporation, the dried residue was reconstituted in 50 µL of IPA/ACN (50/50, v/v). The extracts were sonicated and directly used for LC-HRMS analysis.

Extraction recovery was evaluated by adding the IS (15 pmol) and an oxPL mixture (7.5 pmol) prior to or post LLE to non-supplemented cell samples (Fig. 3.1). The recovery was calculated relative to the recovery of an IS/oxPL solution directly injected.

Inter-day variability was assessed on seven days by determining the recovery of the IS, i.e., PI, PS, PC, and PC bearing 12:0 and 13:0. Spiking experiment unveiled excellent extraction recovery > 95% for oxPL and > 85% for IS. Precision and reproducibility of the extraction were excellent with an intra-day and inter-day variance < 100 ± 10% except for PS 12:0/13:0 (< 100 ± 20%).

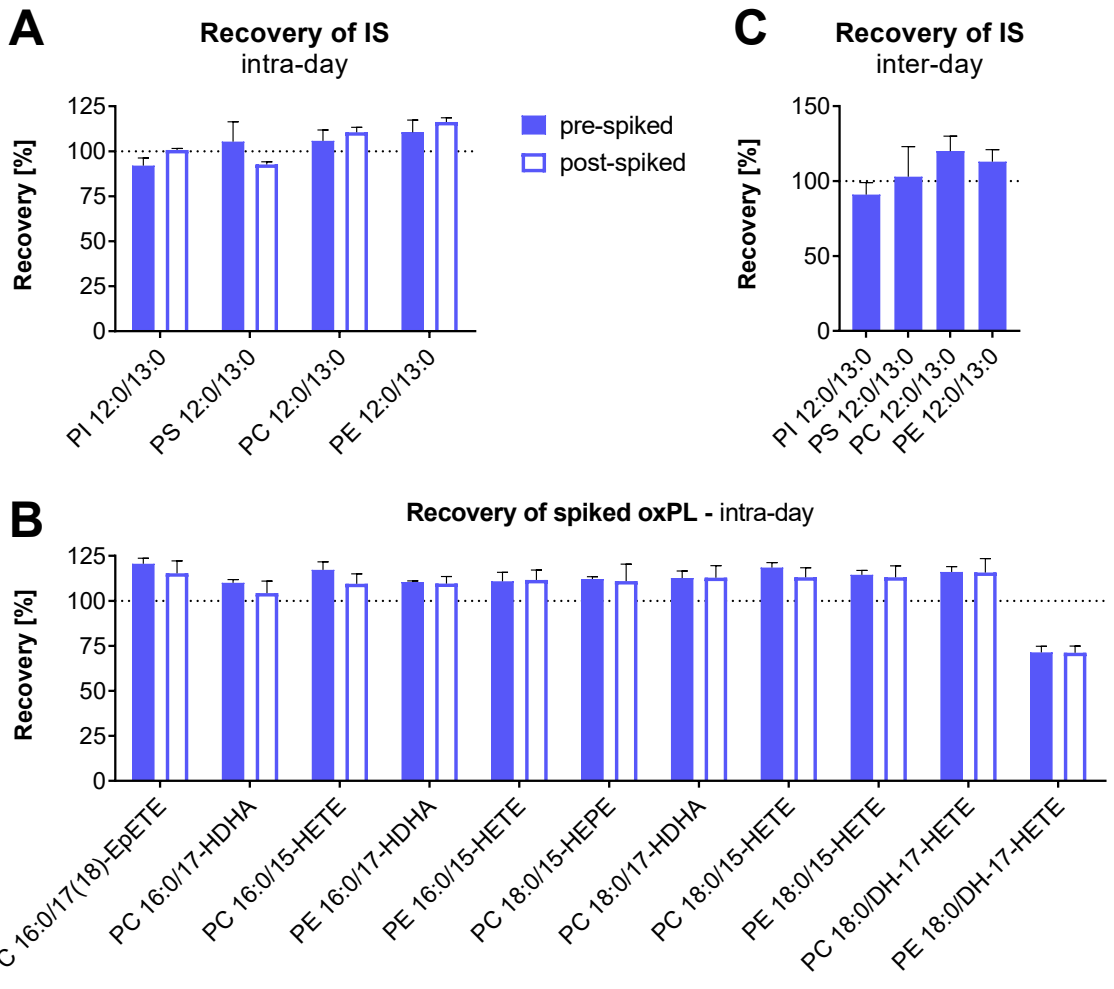

Fig. 3.1: Extraction efficiency in human cells. Shown are the recoveries of **A** IS and **B** spiked oxPL from the extraction of non-supplemented cell samples in ESI(-) mode. IS (15 pmol of each) and an oxPL mixture (7.5 pmol of each) were added to the cell sample at the beginning of sample preparation (pre-spiked) or after sample preparation, directly before untargeted LC-HRMS measurement (post-spiked). Extraction recovery was calculated relative to an IS/oxPL solution directly injected. Shown are mean values ± SD, n = 3. **C** Inter-day variability shown as mean values ± SD of IS recovery from cell extraction (7 days, each mean of n = 3).

3.2.3 Preparation of oxidized phospholipid standards by soybean 15-LOX

OxPL standards were generated based on a modified protocol from Morgan *et al.* [20]. Briefly, individual PL standards were dried using nitrogen, then resuspended in 40 mmol L^{-1} borate buffer (pH = 9.0) and 10 mmol L^{-1} deoxycholate to a final concentration of 0.1 mmol L^{-1}. The soybean 15-LOX was added (5.2 kU mL^{-1}) and samples were incubated at room temperature for 2 h. Hydroperoxides were reduced to the corresponding alcohols by adding 1.3 µmol of tin(II) chloride in H_2O, and lipids were extracted using MeOH/MTBE. The oxidized product was purified using RP-LC coupled to an ultraviolet spectroscopic detector. The concentration of the purified oxPL standards was determined by quantitative targeted LC-MS/MS analysis of hydroxy-PUFA following alkaline hydrolysis [27–30]. These oxPL were used to evaluate the sensitivity of the developed LC-HRMS method by injecting a sequential dilution of standards. A concentration of 50 nmol L^{-1} (20 pg on column) led to a clear peak.

3.2.4 Cell culture

HEK293T cells were cultivated in Dulbecco's Modified Eagle Medium (DMEM) high glucose (4.5 g L^{-1}) supplemented with 10% (v/v) fetal calf serum (FCS), 100 U mL^{-1} penicillin, 100 µg m L^{-1} streptomycin, and 1 mmol L^{-1} sodium pyruvate in a humidified atmosphere with 5 % CO_2 at 37 °C. In 6-well plates, 0.5 × 10^6 cells were seeded per well and cultivated for 24 h to allow cell adhesion. Following 24 h, the medium was replaced with 999 µL of fresh serum-free medium additionally supplemented with 1 µmol L^{-1} soluble epoxide hydrolase inhibitor (1-(1-propanoylpiperidin-4-yl)-3-[4-(trifluoromethoxy)phenyl]urea, TPPU). For supplementation, 1 µL of a mixture of oxylipins (containing hydroxy- or epoxy-PUFA regioisomers) in DMSO was directly spiked into the medium leading to a final concentration of about 2 µmol L^{-1} (0.1% DMSO) (exact concentrations are listed in Table 3.1) and incubated for 2 h. Controls were treated with 0.1% DMSO. The supplemented medium was collected and the cells were harvested by scraping in ice-cold phosphate-buffered saline (PBS).

Table 3.1: Concentration of supplemented oxylipins in the cultivation medium of HEK293T cells. Non-esterified oxylipins were quantified by targeted LC-MS/MS as described [27-30]. In 20:4;Ep-supplemented cells, 5(6)-EpETrE was excluded from further analysis due to its rapid decomposition to 6-hydroxy 1,5-lactone.

supplementation	oxylipin	concentration [µmol L^{-1}]
EpOMEs (18:2;Ep)	12(13)-EpOME (18:2;12Ep)	4.5
	9(10)-EpOME (18:2;9Ep)	5.0
HETEs (20:4;OH)	15-HETE (20:4;15OH)	2.2
	12-HETE (20:4;12OH)	2.0
	5-HETE (20:4;5OH)	2.1
EpETrEs (20:4;Ep)	14(15)-EpETrE (20:4;14Ep)	5.0
	11(12)-EpETrE (20:4;11Ep)	3.2
	8(9)-EpETrE (20:4;8Ep)	1.6
	5(6)-EpETrE (20:4;5Ep)	2.0
EpETEs (20:5;Ep)	17(18)-EpETE (20:5;17Ep)	5.1
	14(15)-EpETE (20:5;14Ep)	2.3
	11(12)-EpETE (20:5;11Ep)	2.1
	8(9)-EpETE (20:5;8Ep)	2.2
EpDPE (22:6;Ep)	19(20)-EpDPE (22:6;19Ep)	5.0
	16(17)-EpDPE (22:6;16Ep)	2.3
	13(14)-EpDPE (22:6;13Ep)	2.2
	10(11)-EpDPE (22:6;10Ep)	2.2
	7(8)-EpDPE (22:6;7Ep)	1.6

3.2.5 LC-MS analysis

Instrumental analysis was performed on a Vanquish Horizon high-performance LC system coupled to a hybrid quadrupole-orbitrap mass spectrometer (Q Exactive HF; Thermo Fisher Scientific, Dreieich, Germany). The injection volume was 5 µL. Chromatographic separation was carried out on an ACQUITY Premier CSH C18 column (2.1 × 100 mm, 1.7 µm, 130 Å; Waters, Eschborn, Germany) equipped with a guard column (2.1 × 5 mm, 1.7 µm) at 40 °C. A binary gradient was used with eluent A (H_2O/ACN, 60/40, v/v) and eluent B (IPA/ACN, 80/20, v/v, +1% H_2O), both containing 10 mmol L^{-1} ammonium formate and 0.1% formic acid. Lipids were separated using the following gradient with a flow rate of 260 µL/min: 0–0.7 min 30% B; 0.7–0.8 min 30–57.5% B; 0.8–9 min 57.5% B; 9–22 min 57.5–68% B; 22–24 min 68–99% B; 24–28 min 99% B; 28–30 min 30% B.

Lipids were analyzed following ESI(-). Few analyses were also carried out in ESI(+) mode to evaluate the elution of different lipid classes (Fig. 3.2). The Full MS scans were recorded over a mass range of *m/z* 200 – 1200 at a resolution setting of 60,000 with the AGC target set to 1×10^6 and a maximum IT of 160 ms. Optimized ion source and MS settings for PL were used [26]. NCE was optimized using PC 16:0/15-HETE, PE 16:0/15-HETE, PC 16:0/17-HDHA, and PE 16:0/17-HDHA standards (Appendix Fig. 8.8). Optimized NCE was set to 25 and 30 relative to *m/z* 500 at a resolution setting of 15,000 with an AGC target of 5×10^4 and a maximum IT of 80 ms. MS detection was carried out in Full MS/$ddMS^2$ TOP *N* mode: $ddMS^2$ scans of the 15 most intense *m/z* (TOP 15) in the Full MS scan were triggered based on an exclusion [26] and inclusion list specific for ESI(-) (Appendix Table 8.6). This led to an average duty cycle of 1.0 s. Additionally, the concentration of esterified oxylipins in samples (Appendix Tables 8.7, 8.8, 8.9) was quantified indirectly by targeted LC-MS/MS with (total oxylipins) and without (non-esterified oxylipins) alkaline hydrolysis as previously described [27–30].

3.2.6 Data processing

OxPL were tentatively identified by LC-ESI(-)-HRMS based on (i) the precursor ion within a mass tolerance ≤ 3 ppm, (ii) the product ion of the head group of the lipid class or its (partial) neutral loss, (iii) the product ion resulting from the neutral loss of the fatty acyl in the *sn*-2 position as a ketene, (iv) the product ion(s) of the (ox)FA, and (v) the product ion resulting from the α-cleavage of the oxPUFA occurring at the hydroxy/epoxy group. In case the product ion of the α-cleavage was not present in the MS^2 spectrum, only the chemical formula of the (oxidized) fatty acyl/alkyl chains is reported. In accordance with the nomenclature of PL [31], the separator "/" is used for oxPL whose *sn*-position of the fatty acyl/alkyl chains was confirmed by authentic standards or by the neutral loss of the fatty acyl in *sn*-2 position, while the separator "_" is used in case the *sn*-position is unknown. Esterified epoxy- and hydroxy-PUFA were distinguished based on different elution times, considering that PL bearing epoxy-PUFA elute later in RP chromatography (Appendix Fig. 8.9, Table 8.10).

OxPL in oxylipin-supplemented HEK293T cells were semi-quantified based on peak heights obtained in LC-ESI(-)-HRMS using one IS per lipid class: PI 12:0/13:0 was used for oxPI species, PS 12:0/13:0 for oxPS species, PC 12:0/13:0 for oxPC, oxPC-P, and oxPC-O species, and PE 12:0/13:0 for oxPE and oxPE-P species. The ionization efficiency of unoxidized bi-saturated PL used as IS was comparable (i.e., PC 12:0/13:0 and PE 12:0/13:0) to oxPC and oxPE species (Appendix Table 8.11). Thus, the concentration of the oxPL could be calculated based on their peak heights compared to that of the IS (one point calibration). For the cell culture samples the concentrations were calculated based on the amount of protein.

3.3 Results and discussion

3.3.1 Chromatographic separation of oxidized phospholipids

Oxylipins can be esterified to numerous PL classes bearing different FA resulting in a large number of oxPL including several isobaric species which can be present in biological samples. Therefore, chromatographic separation of oxPL species is crucial. Based on an established RP-LC-HRMS method for the analysis of PL [26], the chromatographic separation of PL bearing hydroxy- and epoxy-PUFA was optimized (Appendix Fig. 8.9): The oxPL elute as narrow peaks over a broad elution window from 7 to 21 min, followed by the elution of the unoxidized PL and NL (Fig. 3.2A). The elution order of the oxPL classes is identical to the RP separation of unoxidized PL, with oxPI eluting earliest, followed by oxPS, oxPC, oxPE, oxPC-P, oxPC-O, and oxPE-P (Fig. 3.3, 3.4) [26]. A constant retention time difference was found between analogue lipid species from the same lipid class differing by the fatty acyl/alkyl chain in the *sn*-1 position, e.g. analogue oxPC species bearing 16:0 *vs.* 18:0 showed a difference of 4.57 ± 0.09 min, and similarly for oxPC species bearing 16:0 *vs.* 18:1 the difference was 0.50 ± 0.06 min (Table 3.2, Appendix Table 8.12). A constant shift in retention time was also observed between PL and ether PL bearing the same (oxidized) FA, e.g., oxPC *vs.* oxPC-O (i.e., 2.4 min) and oxPC *vs.* oxPC-P (i.e., 1.7 min). The additional double bond of oxPC-P leads to an earlier elution compared to oxPC-O and is consistent with previous reports for unoxidized PL separated on a C18 column [26,32]. These distinct retention time differences enable to confidently differentiate isomeric oxPC-P and oxPC-O species such as the pair PC P-18:0/20:4;15OH and PC O-18:1/20:4;15OH.

Overall, separation of esterified hydroxy- and epoxy-PUFA positional isomers from 18:2, 20:4, 20:5, and 22:6 was achieved (Fig. 3.2B, C) as demonstrated for lipid extracts of both human serum and oxylipin-supplemented cells. The critical isobaric pairs PC 16:0/18:2;13OH and PC 16:0/18:2;9OH (R = 2.5) as well as PI 18:0/18:2;12Ep and PI 18:0/18:2;9Ep (R = 2.3) were baseline separated.

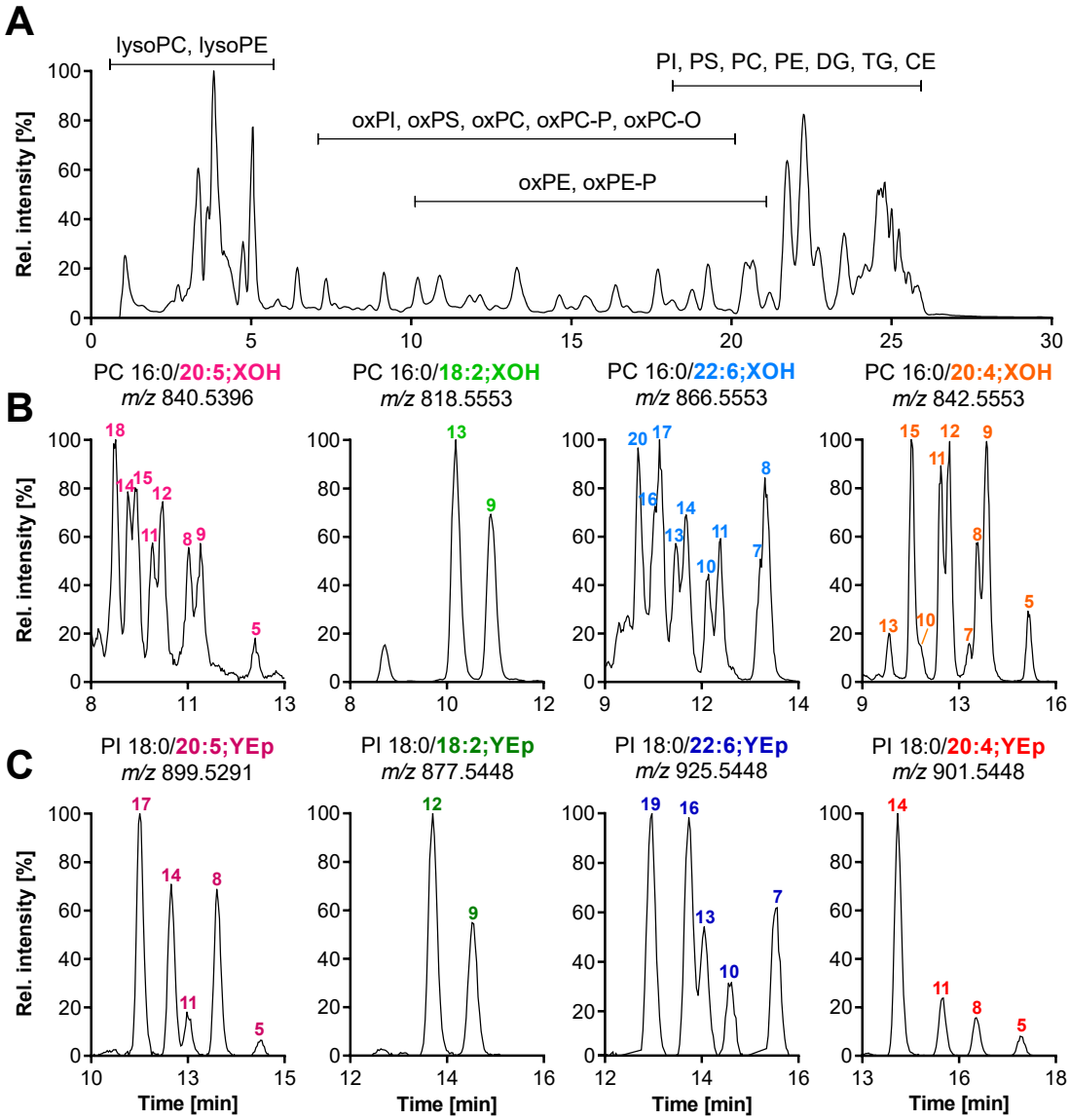

Fig. 3.2: Chromatographic separation efficiency of oxPL by means of RP-LC-HRMS. Shown is the separation of a lipid extract from human serum **A** full scan *m/z* 200 – 1200 in ESI(+) mode and **B** XIC signals of PC species bearing different hydroxy-PUFA positional isomers in ESI(-) mode (X = position of the hydroxy group). In **C**, the XIC signals of PI species bearing different epoxy-PUFA positional isomers in oxylipin-supplemented cells are shown in ESI(-) mode (Y = position of the epoxy group).

Likewise, PI bearing 20:4;14Ep, 20:4;11Ep, 20:4;8Ep, and 20:4;5Ep were separated with R > 1.5 (Fig. 3.2C). Eight PC species bearing hydroxy-20:5 (PC 16:0/20:5;OH), nine PC species bearing hydroxy-20:4 (PC 16:0/20:4;OH), and nine PC species bearing hydroxy-22:6 (PC 16:0/22:6;OH) could be at least partially separated and individually detected (Fig. 3.2B).

PL bearing oxylipins with hydroxy groups at similar position showed similar retention times, e.g., PC 16:0/20:5;14OH and PC 16:0/20:5;15OH, PC 16:0/20:4;11OH and PC 16:0/20:4;12OH, as well as PC 16:0/22:6;13OH and PC 16:0/22:6;14OH. The last eluting PC 16:0/22:6;OH, i.e., PC 16:0/22:6;7OH and PC 16:0/22:6;8OH eluted in an asymmetric and broad peak. Nonetheless, the separation was sufficient to obtain at least one meaningful MS^2 spectrum of each isomer and deduce their elution order (Appendix Fig. 8.10, 8.11, 8.12). This chromatographic separation is dramatically better than the few previous methods dedicated to the analysis of oxPL [20,21,33]. For example, Reis *et al.* described the identification of oxidized palmitoyl-linoleoyl-PC following radical peroxidation; however, no separation could be achieved for 18:2;OH positional isomers [21]. Similarly, O'Donnell and coworkers generated five 20:4;OH positional isomers esterified to PC or PE by air oxidation [20, 33], which co-eluted in the LC separation. The published method from Aoyagi *et al.* [18] led to a similar chromatographic separation of esterified 20:4;OH, however, the separation of esterified hydroxy- and epoxy-positional isomers from other PUFA such as PI 18:0/20:5;Ep and PC 16:0/22:6;OH is much better in the method described here (Appendix Table 8.14).

Table 3.2: Distinct retention time differences between lipid classes/species. Top: The differences in retention time between analogue lipids bearing the same oxylipin in *sn*-2 position and differing by the fatty acyl/alkyl chain in *sn*-1 position. **Bottom**: Differences in the retention time of analogues oxPL *vs.* oxPL-P and oxPL *vs.* oxPL-O enable the distinction of isomeric oxPL-P and oxPL-O. n.a. = not announced because the peaks of both analogues were not detected.

	Δt_R [min]		
	oxPI	**oxPC**	**oxPE**
16:0 *vs.* 18:0	4.05 ± 0.35	4.57 ± 0.09	4.61 ± 0.06
16:1 *vs.* 18:1	n.a.	4.22 ± 0.14	4.37 ± 0.04
16:0 *vs.* 18:1	0.42 ± 0.09	0.50 ± 0.06	0.51 ± 0.05
oxPL *vs.* oxPL-P	n.a.	1.76 ± 0.07	1.90 ± 0.09
oxPL *vs.* oxPL-O	n.a.	2.44 ± 0.10	n.a.

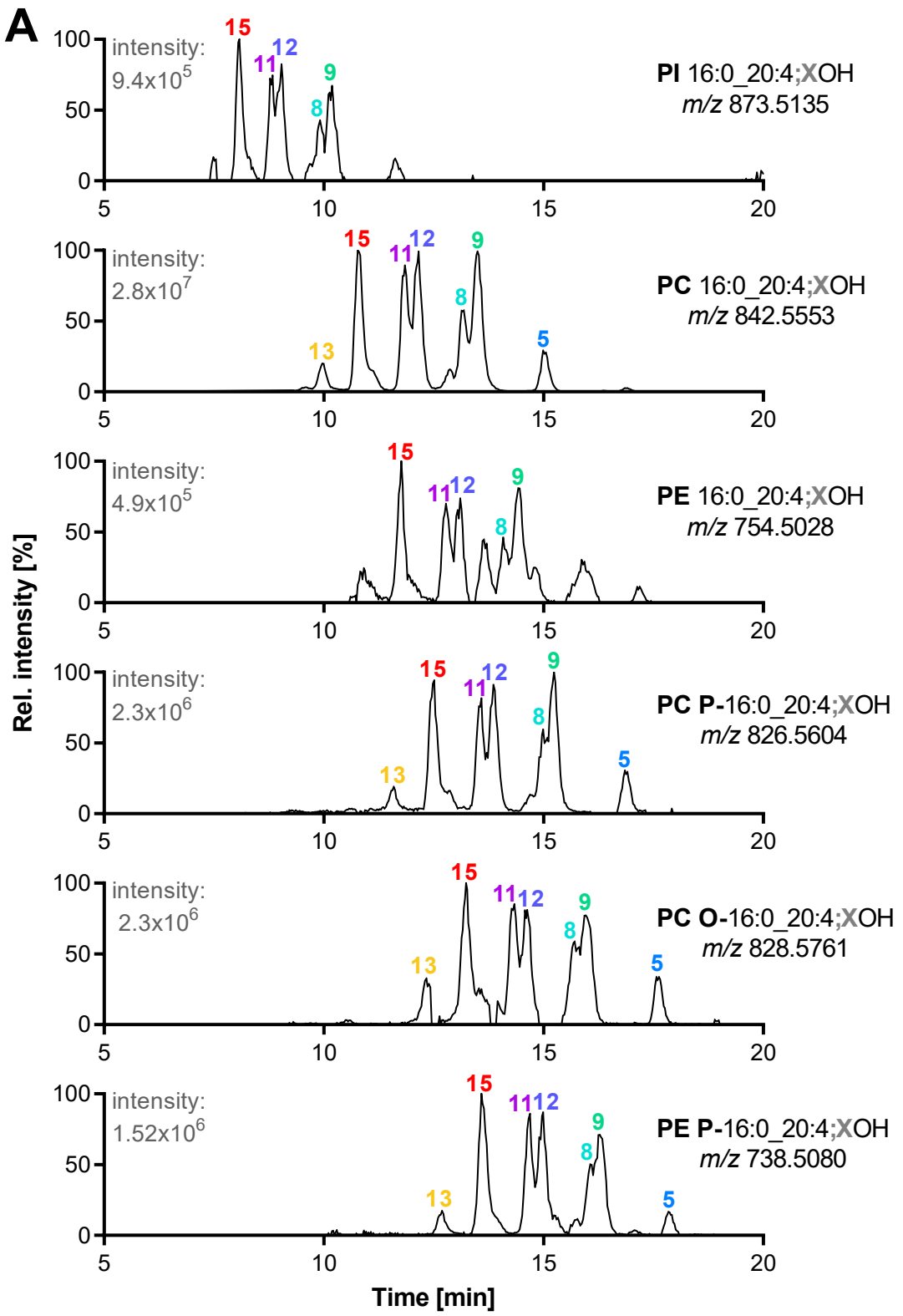

Fig. 3.3: RP-LC-ESI(-)-HRMS separation of PI, PC, PE, PC-P, PC-O, and PE-P bearing hydroxy- and epoxy-20:4. Shown is the separation of different PL classes bearing **A** 20:4;OH positional isomers in a lipid extract from human serum (X = position of the hydroxy group).

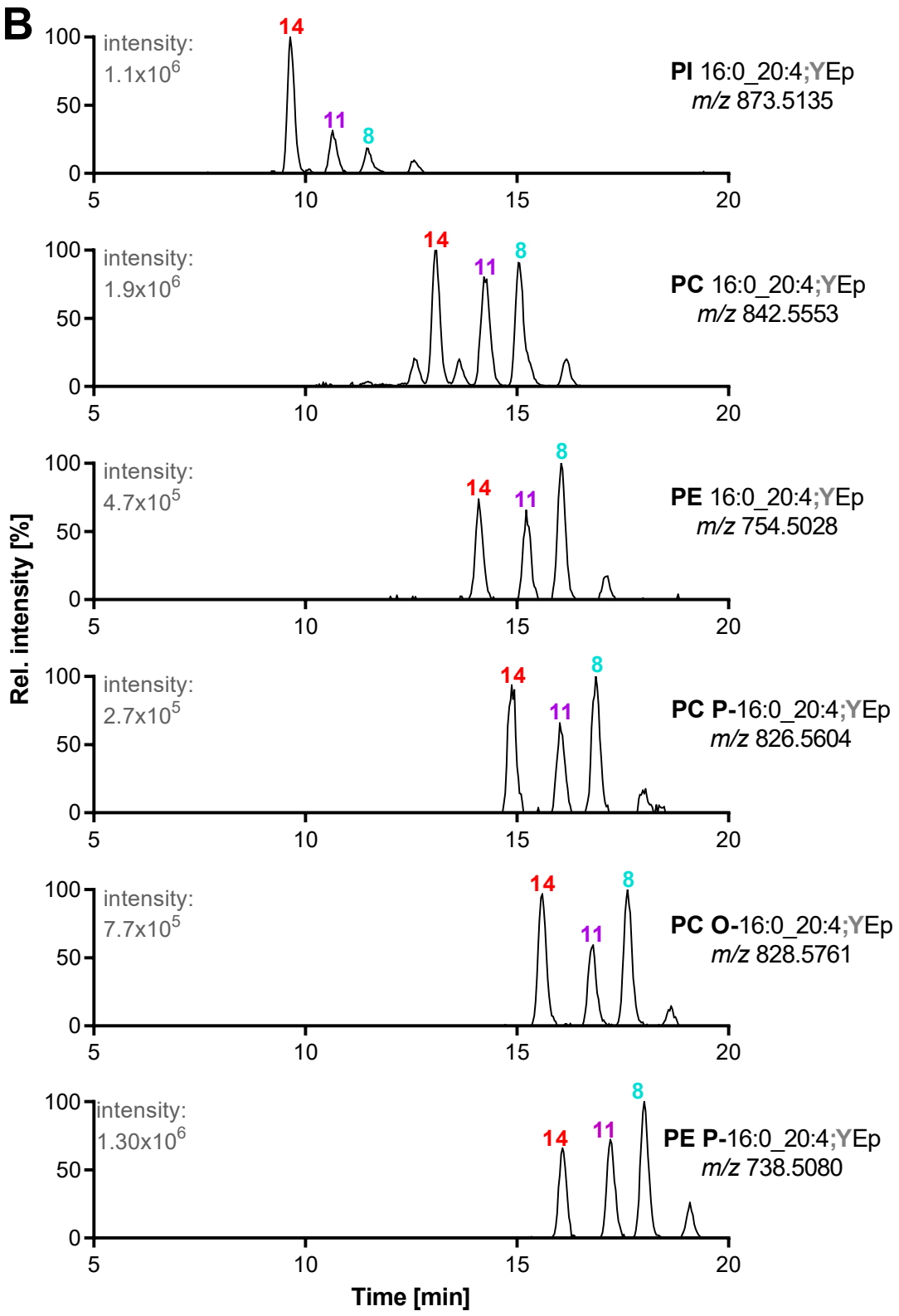

Fig. 3.3: Continued. LC-ESI(-)-HRMS separation of PI, PC, PE, PC-P, PC-O, and PE-P bearing hydroxy- and epoxy-20:4. B 20:4;Ep positional isomers in a lipid extract from 20:4;Ep-supplemented cells (Y = position of the epoxy group).

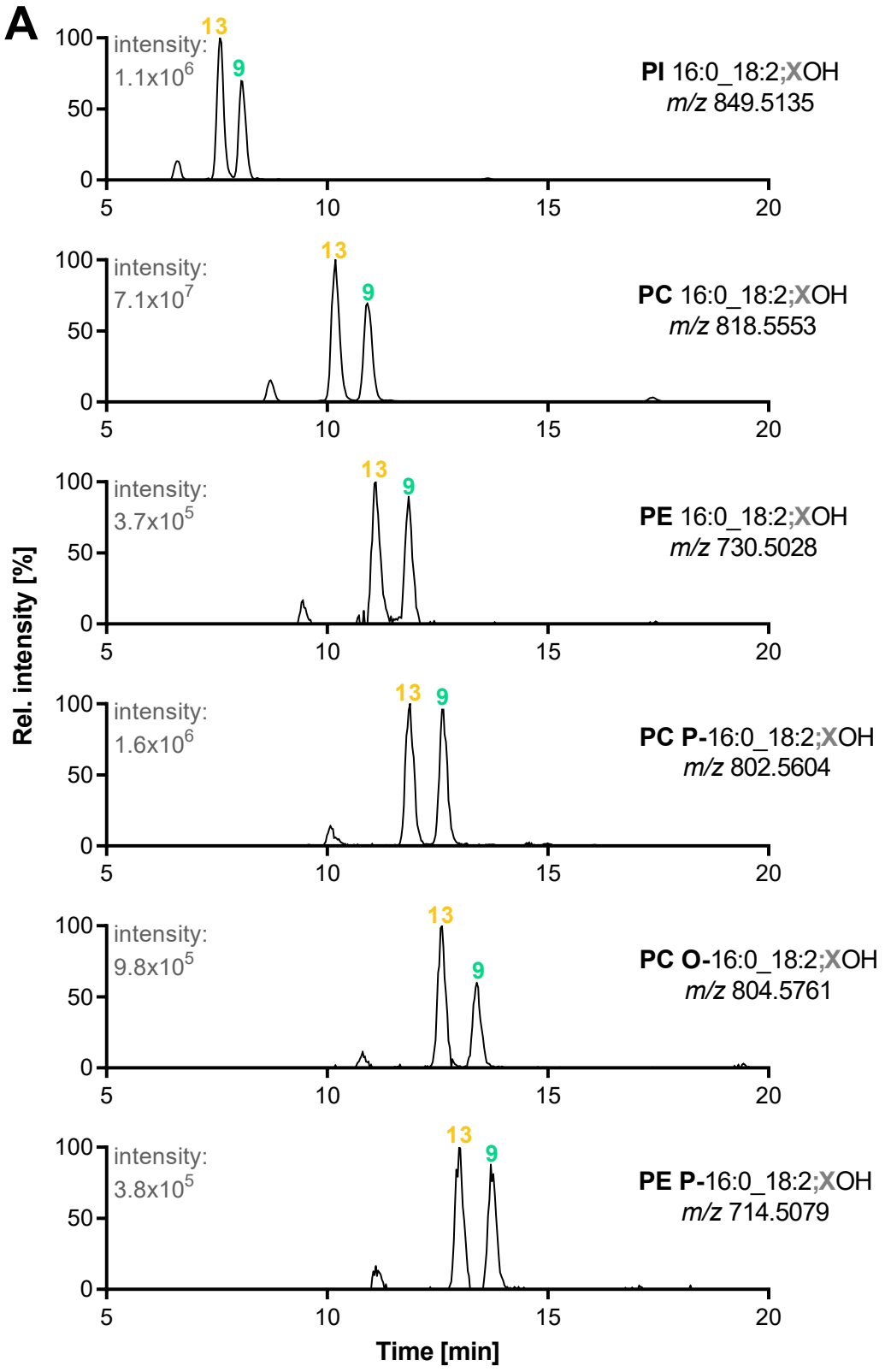

Fig. 3.4: RP-LC-ESI(-)-HRMS separation of PI, PC, PE, PC-P, PC-O, and PE-P bearing hydroxy- and epoxy-18:2. Shown is the separation of the different PL classes bearing **A** 18:2;OH positional isomers in a lipid extract from human serum (X = position of the hydroxy group).

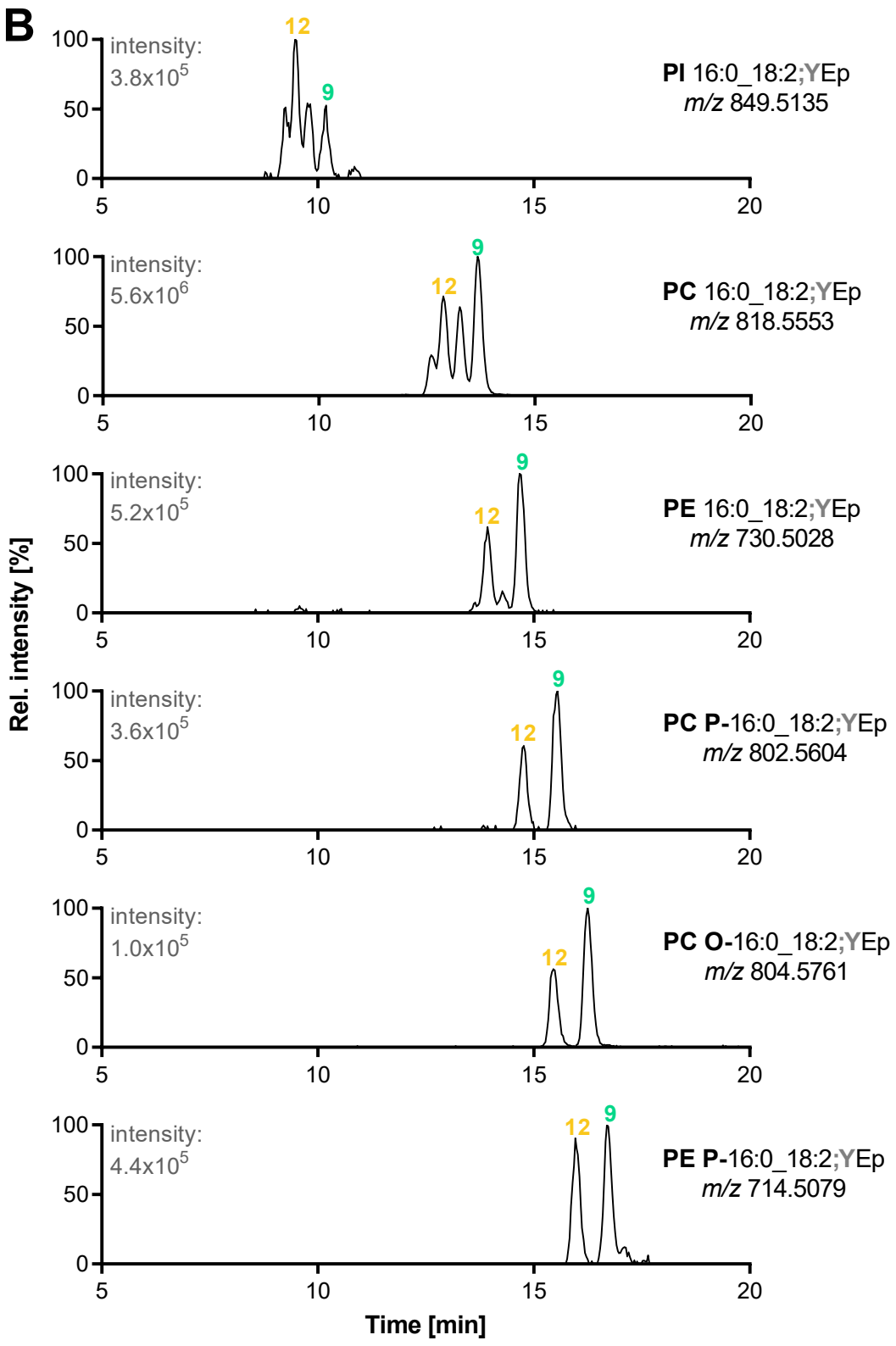

Fig. 3.4: Continued. RP-LC-ESI(-)-HRMS separation of PI, PC, PE, PC-P, PC-O, and PE-P bearing hydroxy- and epoxy-18:2. B 18:2;Ep positional isomers in a lipid extract from 18:2;Ep-supplemented cells (Y = position of the epoxy group).

The elution order of individual hydroxy- and epoxy-PUFA bound to PL is the same for the different lipid classes, i.e. PI, PC, PE, PC-P, PC-O, and PE-P (Fig. 3.3, Fig. 3.4): The shorter the distance between the ester group and the hydroxy/epoxy group, and thus the longer the aliphatic chain – causing the retention in RP chromatography – the longer is the retention time. Thus, PL bearing 20:4;15OH elute before the corresponding PL bearing 20:4;5OH (Fig. 3.3A). While in RP chromatography of non-esterified oxylipins a separation of 8- and 12-HETE, 8- and 12-HEPE as well as 10- and 14-HDHA is rarely achieved [27,34,35], their esterified analogues are well separated with the method described here. Interestingly, for 20:5;12OH and 20:5;8OH bound to PL an altered elution order compared to the analysis of non-esterified oxylipins was observed with PC 16:0/20:5;12OH eluting before PC 16:0/20:5;8OH (Fig. 3.2B). This change of elution order was already described for other oxylipin derivatives such as pentafluorophenyl esters [36]. The elution order of esterified epoxy-PUFA is identical to that of non-esterified epoxy-PUFA in RP chromatography (Fig. 3.3B, 3.4B) [27–30].

PL of different classes bearing the same fatty acyls were separated. For example, 20:4;15OH bound at *sn*-2 position to PI, PC, PE, PC-P, and PC-O (and 16:0 at *sn*-1) eluted at 8.1, 10.8, 11.8, 12.5, 13.2, and 13.6 min, respectively, with $R > 1.5$ (Fig. 3.3A). Only PC O-16:0/20:4;15OH and PE P-16:0/20:4;15OH were partially overlapping with $R = 1.0$. A similar effective separation was achieved for epoxy-PUFA bound to different PL classes, such as 20:4;Ep (Fig. 3.3B). PUFA bearing a hydroxy or an epoxy group at the same position (e.g., 20:4;15OH and 20:4;14Ep) are isobaric and yield similar MS^2 spectra [27,37]. Thus, PL bearing these hydroxy- and epoxy-PUFA have to be separated by chromatography. With respect to PL, this results in a total of 77 critical pairs bearing regioisomeric hydroxy- and epoxy-PUFA (from 18:2, 20:4, 20:5, 22:4, and 22:6) (Appendix Table 8.11): Out of those, the retention time difference of 71 critical pairs was > 1.5 min. The other critical separation pairs eluted with a retention time difference between 1.0 and 1.5 min, but were baseline separated ($R > 1.5$).

Separation of *sn*-1/*sn*-2 oxPL isomers was assessed using the generated standards and was achieved for 4 out of 9 standards with R > 1.5, while the other 5 pairs showed a resolution between 1.28 and 1.45 sufficient for qualitative analysis (Fig. 3.5).

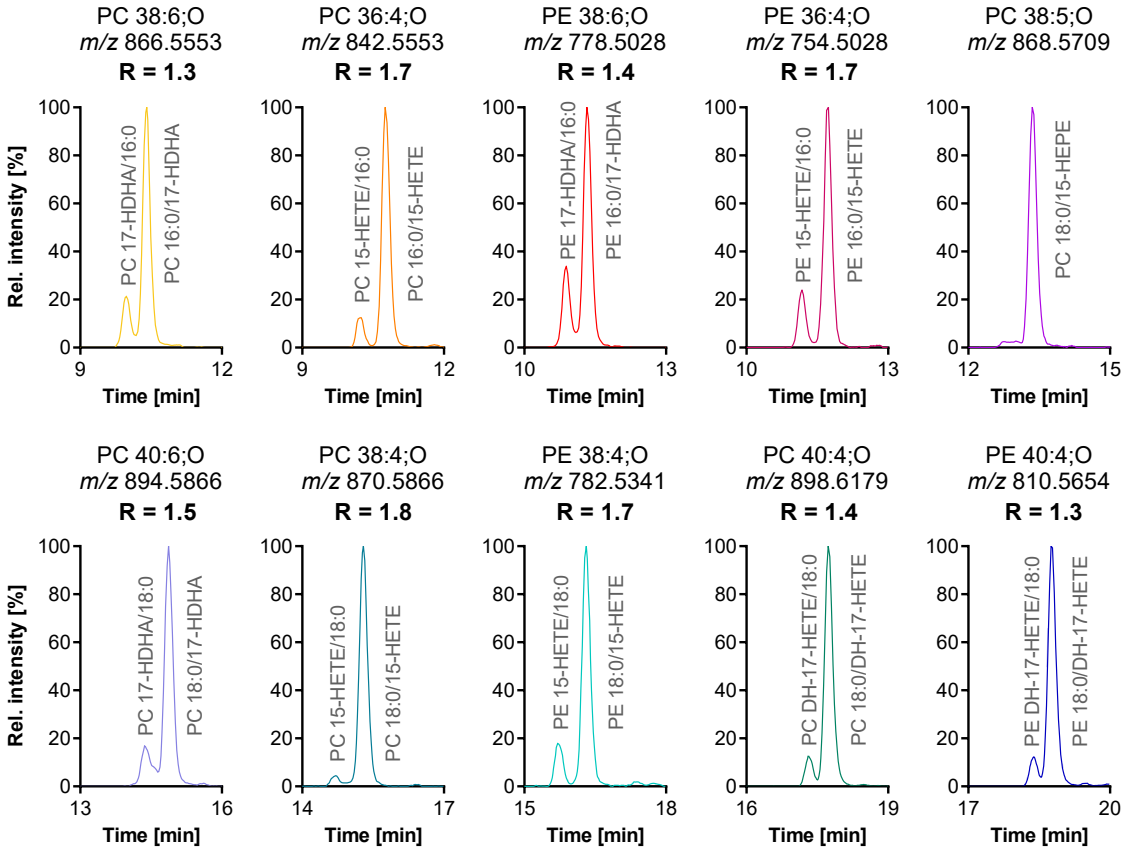

Fig. 3.5: Chromatographic separation efficiency of *sn*-1/*sn*-2 oxPL isomers. Shown are the elution order of oxPL standards generated by soybean 15-LOX (XIC, in ESI(-) mode) of PC and PE species. The oxidized standards primarily contain oxPUFA in the *sn*-2 position, with a smaller portion having the oxPUFA in the *sn*-1 position. Thus, the standards are eluting as two peaks resulting from the chromatographic separation of *sn*-1/*sn*-2 positional isomers. The *sn*-position of the fatty acyl chains of each peak was determined using characteristic product ions in the MS^2 spectra (Table 8.11).

Overall, the LC-HRMS method described herein allows the separation of PL species from different lipid classes bearing oxPUFA, by both the polar head groups as well as the hydroxy- and epoxy-PUFA positional isomers.

3.3.2 Characterization of PL bearing oxylipins by untargeted LC-HRMS

The ionization and fragmentation behavior of unoxidized PL is well described [32,38–40]. However, information about the detection and identification of PL species bearing oxylipins by LC-MS has been described only in a few studies [18,19,22,33]. We aimed to characterize/identify oxPL species in ESI(-) mode based on a mass accuracy within 3 ppm tolerance for the precursor ion, characteristic product ions in MS^2, and plausible retention time. Overall, we detected a total of 422 PL species bearing hydroxy- or epoxy-PUFA from seven different lipid classes (i.e., PI, PS, PC, PE, PC-P, PC-O, and PE-P) in human serum and oxylipin-supplemented cells. The commercial serum pool contains exceptionally high total levels of hydroxy-PUFA presumably formed by autoxidation (Appendix Table 8.7). Therefore, it was used in this study as a source of PL bearing hydroxy-PUFA, while epoxy-PUFA-supplemented cells served as a source of PL bearing epoxy-PUFA.

The detected PL bear 14:0, 16:0, 16:1, 17:1, 18:0, 18:1, and 18:2 mostly in the *sn*-1 position and an oxPUFA in the *sn*-2 position (18:2;O, 18:3;O, 20:2;O, 20:3;O, 20:4;O, 20:5;O, 22:4;O, 22:5;O, and 22:6;O). A list of all detected oxPL including their retention time, adduct ion, precursor ion, and product ions can be found in Table 8.10. In untargeted lipidomics, software tools such as MS-DIAL or mzMine are increasingly used to simplify and automate the analysis of large MS-based datasets [41,42]. Consequently, we created a database in MSP format containing precursor ion *m/z*, retention time, and MS^2 spectra of detected oxPL to facilitate its inclusion in software tools (supplementary information). Using this list in MS-DIAL (v.5.2.240218.2), we found more than 90% of the included oxPL as matching features in the analyzed samples.

158 individual oxPL species all with esterified hydroxy-PUFA were detected in the human serum with concentrations up to the micromolar range. PL bearing epoxy-PUFA were not detected, which is consistent with their lower concentration in the nanomolar range determined by targeted analysis [27–30] (Appendix Table 8.7). Nine esterified 20:4;OH positional isomers were found for example in serum in the PC class (PC 16:0/20:4;OH).

The MS^2 spectra of these oxPC in ESI(-) mode show several similarities (Fig. 3.6): Major fragment ions are the demethylated-PC 16:0/20:4;OH $[M - CH_3]^-$; an ion at *m/z* 782.5342 formed by the additional loss of HCOO, and the lysoPC 16:0/0:0 $[M - CH_3]^-$ at *m/z* 480.3090 resulting from the neutral loss of 20:4;OH as a ketene. Also, product ions of the fatty acyl chains, i.e., 16:0 at *m/z* 255.2330 and 20:4;OH at *m/z* 319.2279, were detected at high abundance. Additionally, characteristic product ions resulting from the fragmentation of the oxylipin were found, i.e., the α-cleavage occurring at the hydroxy group:
m/z 193.1234 for 13-HETE (Fig. 3.6a), *m/z* 219.1390 for 15-HETE (Fig. 3.6b), *m/z* 153.0921 for 10-HETE (Fig. 3.6c), *m/z* 167.1077 for 11-HETE (Fig. 3.6d), *m/z* 179.1077 for 12-HETE (Fig. 3.6e), *m/z* 141.0557 for 7-HETE (Fig. 3.6f), *m/z* 155.0714 for 8-HETE (Fig. 3.6g), *m/z* 167.0714 for 9-HETE (Fig. 3.6h), and *m/z* 115.0401 for 5-HETE (Fig. 3.6i). These specific ions were consistent with the MS^2 spectra of non-esterified 15-, 12-, 8-, and 5-HETE [37,43]. Also esterified hydroxy-PUFA positional isomers derived from other PUFA were characterized in the human serum e.g., 18:2;OH with three positional isomers (Appendix Fig. 8.10), 18:3;OH with three positional isomers (Appendix Table 8.10), 20:5;OH with eight positional isomers (Appendix Fig. 8.11), 22:4;OH with two positional isomers (Appendix Table 8.10), and 22:6;OH with nine positional isomers (Appendix Fig. 8.12). Likewise, product ions of esterified oxylipins were in line with the MS^2 spectra of non-esterified HODEs [44], HOTrEs [27], HEPEs [43,45], DH-HETEs [46], and HDHAs [43,47].

Based on a similar fragmentation behavior, PI and PE species bearing oxylipins were identified: The characteristic product ions of the head group of PI $[C_6H_{10}O_8P]^-$ at *m/z* 241.0119 and PE $[C_2H_7O_4NP]^-$ at *m/z* 140.0118 enabled the confident assignment of the lipid class (Appendix Table 8.10) [48].

Also, esterified oxylipins bound to PC and PE bearing an alkyl chain via an ether (i.e., PC-O) or a vinyl-ether bond (i.e., PC-P and PE-P) at *sn*-1 position were observed. Here, only the product ions of the esterified oxidized fatty acyl chain were observed in the MS^2 spectra, which is consistent with previous reports on the fragmentation of unoxidized PC-P, PC-O, and PE-P [32].

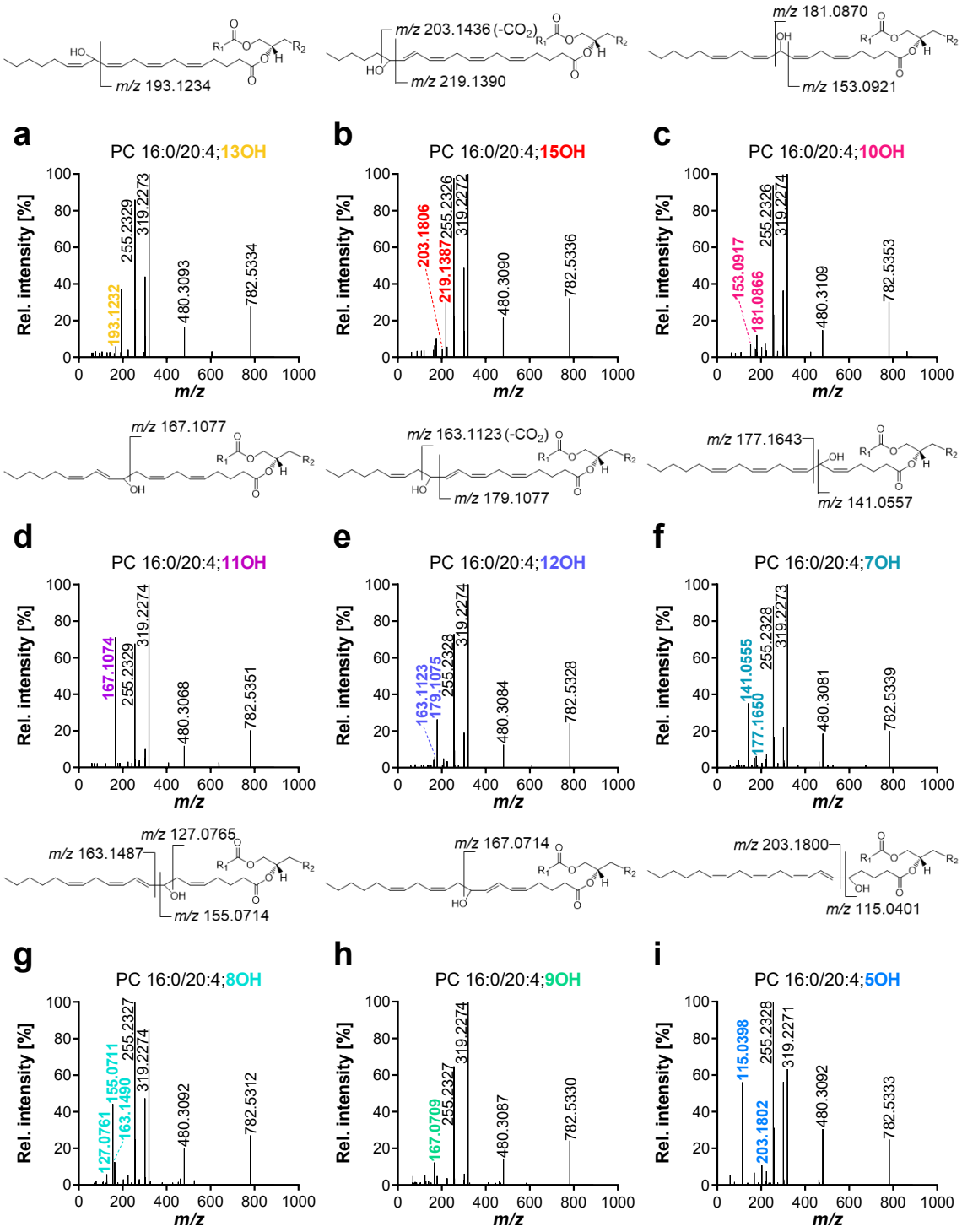

Fig. 3.6: Fragmentation spectra of PC bearing hydroxy-20:4 positional isomers: Shown are the MS^2 spectra in ESI(-) mode of PC species from human serum bearing 16:0 and 20:4;OH positional isomers recorded at **a** 9.9 min, **b** 10.8 min, **c** 11.0 min, **d** 11.8 min, **e** 12.2 min, **f** 12.8 min, **g** 13.1 min, **h** 13.5 min, and **i** 15.0 min. In the structures, suggested sites of fragmentation are indicated. $R_1 = C_{15}H_{31}$ and $R_2 = C_5H_{13}NPO_4$.

In HEK293T cells following oxylipin-supplementation levels of added epoxy-PUFA (and 20:4;OH) were ≥ 1 nmol mg^{-1} protein (Appendix Tables 8.8, 8.9). A total of 282 individual oxPL species were detected in the oxylipin-supplemented cells (Appendix Table 8.10). The elution order of the oxPL species was compared to a previous work describing about 400 oxPL in oxylipin-supplemented HEK293T cells [18] (Appendix Table 8.13): 88 individual oxPL species were detected in both studies. The difference in the detected oxPL can be explained by a supplementation with different oxylipins in the two studies. Moreover, PC-P and PE-P were not covered in the previous study [18]. Nevertheless, the 88 commonly detected oxPL species showed consistent elution order, underlining the confidence of our tentative identification. Among the 282 species detected, 256 PL bear the supplemented oxylipins (18:2;Ep, 20:4;OH, 20:4;Ep, 20:5;Ep, and 22:6;Ep) while 26 PL species bear non-supplemented oxylipins (20:2;Ep, 20:3;Ep, 22:4;Ep, or 22:5;Ep). These oxPL are presumably formed by elongation and further desaturation of the added oxylipins, e.g., 20:3;14Ep being formed from 18:2;Ep. Of note, PL species bearing e.g., 18:3;Ep resulting only from the desaturation of 18:2;Ep were not detected. For 20:4;Ep- and 20:5;Ep-supplemented cells, only esterified oxylipins derived from elongation were observed, e.g., 20:4;14Ep to 22:4;16Ep and 20:5;17Ep to 22:5;19Ep.

Again, chromatographic separation and evaluation of plausible retention time is key for the correct identification: Esterified 20:4;14Ep is not only isobaric to 20:4;15OH but also shows an identical MS^2 spectrum (Fig. 3.7a, d). Esterified 20:4;11OH and 20:4;11Ep differ in their MS^2 spectra by the additional product ion *m/z* 179.1077 resulting from the α-cleavage of 20:4;11Ep (Fig. 3.7b, e). Similarly, the product ion *m/z* 167.0707 enabled to differentiate PC 16:0/20:4;8Ep over PC 16:0/20:4;8OH (Fig. 3.7c, f).

The LC-HRMS method allows the tentative identification of individual PL species bearing hydroxy- or epoxy-PUFA. This identification was also supported by eleven authentic oxPL standards and the indirect quantification of esterified oxylipins by targeted LC-MS/MS.

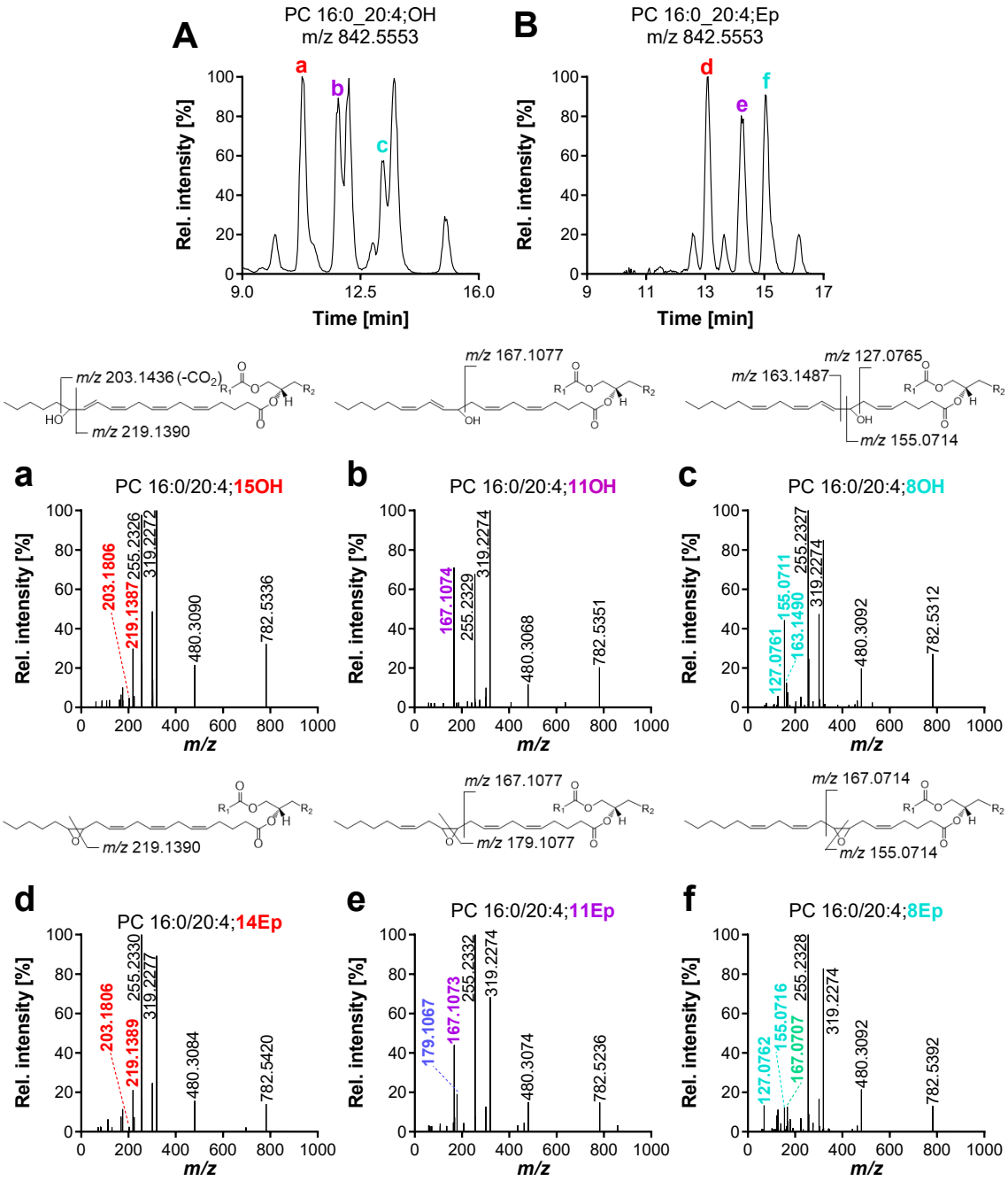

Fig. 3.7: Comparison of fragmentation of esterified position-isomeric hydroxy- and epoxy-20:4. The XIC recorded at *m/z* 842.5553 of PC 36:4;O in ESI(-) mode shows the separation of PC bearing **A** 20:4;OH positional isomers in a lipid extract from human serum and **B** 20:4;Ep positional isomers in a lipid extract from 20:4;Ep-supplemented cells. Shown are the MS^2 spectra of PC 16:0/20:4;15OH and PC 16:0/20:4;14Ep (**a** 10.8 min, **d** 13.1 min), PC 16:0/20:4;11OH and PC 16:0/20:4;11Ep (**b** 11.8 min, **e** 14.1 min) as well as PC 16:0/20:4;8OH and PC 16:0/20:4;8Ep (**c** 13.1 min, **f** 15.0 min). In the structures, suggested sites of fragmentation are indicated. $R_1 = C_{15}H_{31}$ and $R_2 = C_5H_{13}NPO_4$.

3.3.3 Differentiation of sn-1/sn-2 isomers of oxidized phospholipids

Oxylipins can be bound to both the *sn-1* or the *sn*-2 position in the PL. Here, we describe distinct fragmentation patterns following ionization in ESI(-) mode for these isomeric (oxidized) PL, allowing to assign the esterified (oxidized) FA to the *sn*-1 or the *sn*-2 position (Fig. 3.8, 3.9).

The analysis of a standard of PC 16:0/20:4 showed in addition to the expected compound a small peak (Fig. 3.8A), presumably of its *sn*-1/*sn*-2 isomer PC 20:4/16:0. Consistently, enzymatic conversion of this PL to PC 16:0_15-HETE also led to two products (Fig. 3.8B). Furthermore, analysis of 20:4;Ep-supplemented cells led to two peaks for the corresponding PC 36:4;O (Fig. 3.8C).

Fragmentation of the smaller (earlier-eluting) peak of the PC 36:4 resulted in *m/z* 528.3390 (acyl 20:4 demethylated-lysoPC), corresponding to the loss of 16:0 as a ketene (Fig. 3.8a). It is well established that the neutral loss of the fatty acyl as a ketene or as an FA is favored in the *sn*-2 position of the PL, and the one bound in the *sn*-1 position yields only minor product ions [49]. Thus, it can be concluded that the small peak is indeed caused by low levels of PC 20:4/16:0 in the PC 16:0/20:4 standard. Similarly, the earlier-eluting peak of both PC 36:4;O species (hydroxy- and epoxy-isomers) yielded *m/z* 544.3039 (acyl 20:4;O demethylated-lysoPC), resulting from the loss of 16:0 (Fig. 3.8c, e), indicating that 20:4;O is bound to the *sn*-1 position. In contrast, the main peak of the three (oxidized) PC species yielded the product ions *m/z* 480.3090 and in lower intensity *m/z* 462.2984 (Fig. 3.8b, d, f). These ions can be assigned to the acyl 16:0 demethylated-lysoPC resulting from the loss of 20:4;(O) as a ketene or the loss as FA in the *sn*-2 position, respectively. Other demethylated lysoPC-related ions resulting from the neutral loss of the fatty acyl in the *sn*-1 position were not detected, even at different collision energies (combined NCE of 20,25 or 30,35) (Appendix Fig. 8.8).

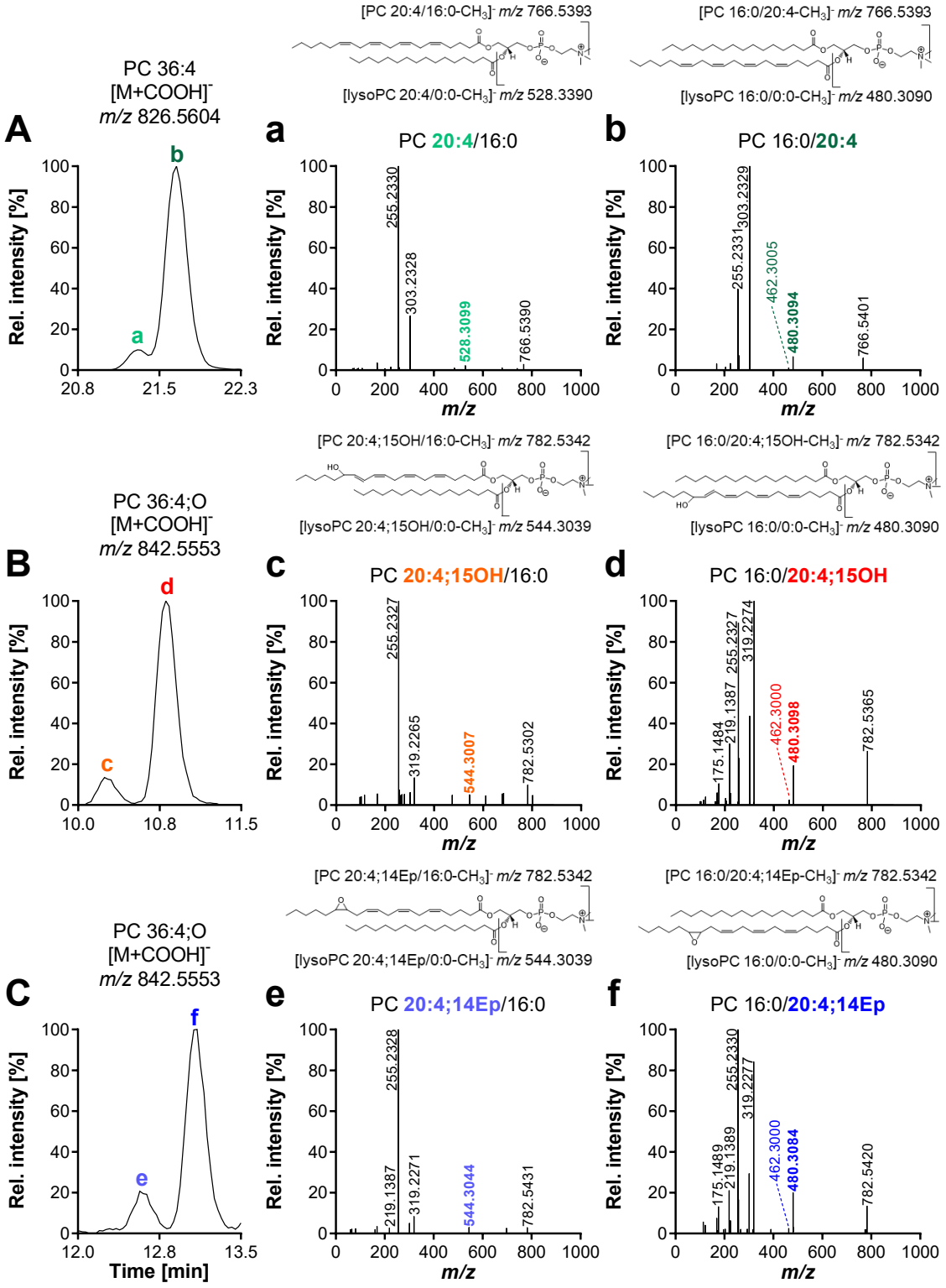

Fig. 3.8: LC-ESI(-)-HRMS characterization of *sn*-1/*sn*-2 isomers of (ox)PL. Chromatographic separation of the *sn*-1/*sn*-2 positional isomers **A** PC 36:4, **B, and C** PC 36:4;O and corresponding MS^2 spectra of the two peaks recorded at **a** 21.3 min, **b** 21.6 min, **c** 10.2 min, **d** 10.8 min, **e** 12.5 min, and **f** 13.1 min. Suggested sites of fragmentation are indicated in the structures.

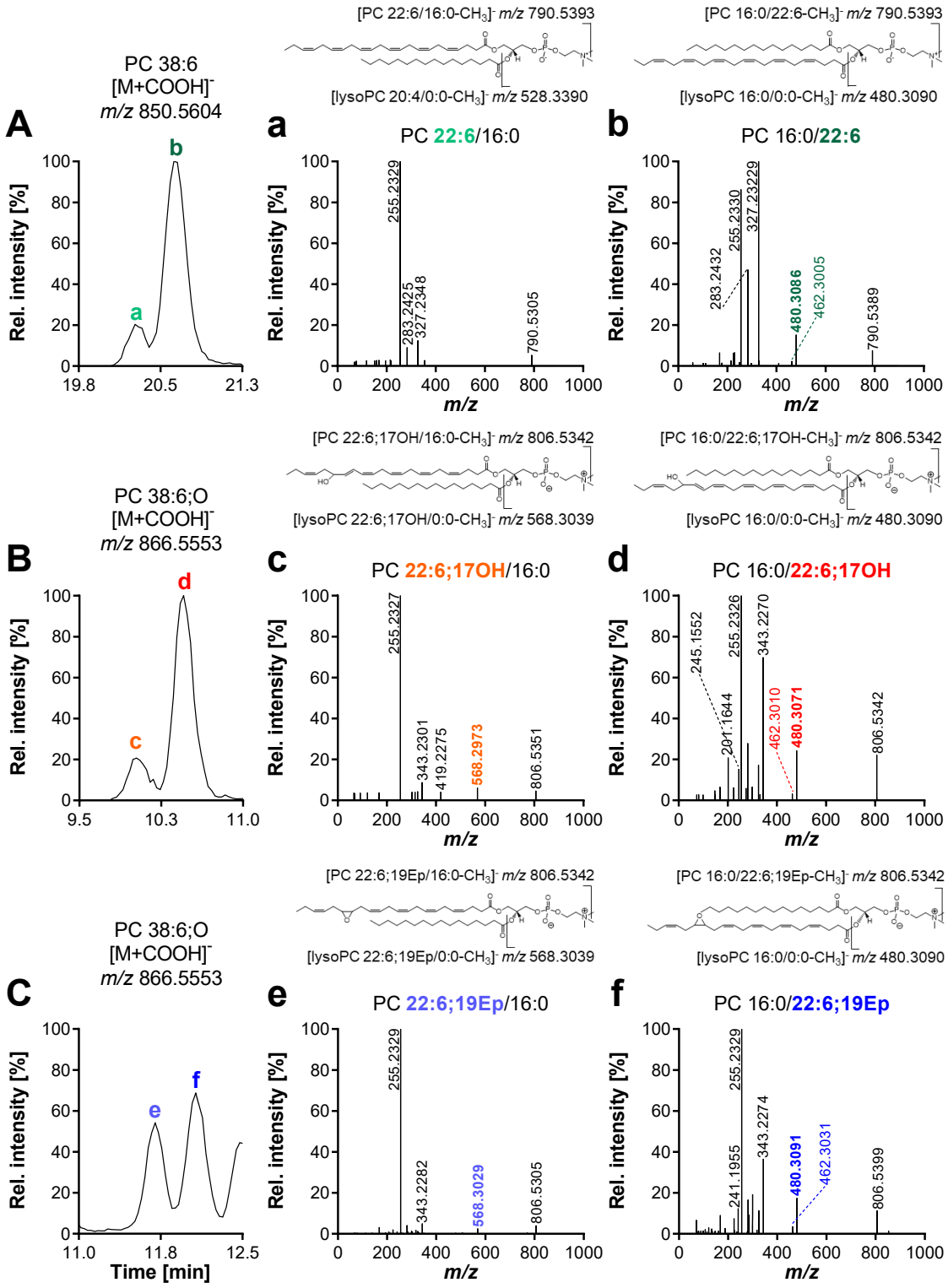

Fig. 3.9: LC-ESI(-)-HRMS characterization of *sn*-1/*sn*-2 isomers of (ox)PL. Chromatographic separation of the *sn*-1/*sn*-2 isomers **A** PC 38:6, **B, and C** PC 38:6;O and corresponding MS^2 spectra of the two peaks recorded at **a** 20.3 min, and **b** 20.6 min, **c** 10.0 min, **e** 10.5 min, **e** 11.7 min, and **f** 12.1 min. Suggested sites of fragmentation are indicated in the structures.

Regarding the characterization of the oxPL it is important to note that the *sn*-position of the (oxidized) fatty acyl chains impacts the intensity of the detected product ions (Fig. 3.8): If the 20:4(;O) is bound in the *sn*-1 position, the abundance of its product ion (*m/z* 319.2279 and *m/z* 303.2328 for the oxidized or unoxidized 20:4, respectively) is lower compared to the product ion of the acyl bound at *sn*-2 position, i.e., 16:0 *m/z* 255.2330 and *vice versa* (Fig. 3.8, 3.9). Similarly, the product ion resulting from the α-cleavage in the carbon chain of the oxylipin (*m/z* 219.1390) is low abundant when the 20:4;O is esterified in the *sn*-1 position, but is clearly detected when the oxPUFA is bound in the *sn*-2 position (Fig. 3.8B, C, Fig. 3. 9B, C).

With this data, we could show that the specific fragmentation pattern of PC (and also other PL) allows to characterize in which *sn*-position an oxylipin is bound in the PL. Of note, the low intensity for characteristic product ions resulting from the fragmentation of the oxPUFA at the *sn*-1 position may hinder structural characterization. However, the oxidized fatty acyl esterified in the *sn*-2 position can clearly be distinguished from the species with the same fatty acyl in the *sn*-1 position. In our study, oxylipins were dominantly found in the *sn*-2 position in human serum and cells. However, several oxPL species bearing the oxylipin in *sn*-1 position were detected. In the human serum four PC species all bearing 18:2;OH; and in supplemented cells with twenty oxPL bearing different epoxy-PUFA (Appendix Table 8.10).

3.3.4 Incorporation of hydroxy- and epoxy-PUFA in human cells

The uptake and the esterification of oxylipins into PL in human cells were investigated by applying the developed LC-HRMS method. The sum of esterified oxylipins in these samples was indirectly quantified by an established targeted LC-MS/MS method [27–30]. Specifically, we aimed to characterize in which PL class 18:2;Ep, 20:4;OH, 20:4;Ep, and 20:5;Ep positional isomers are incorporated.

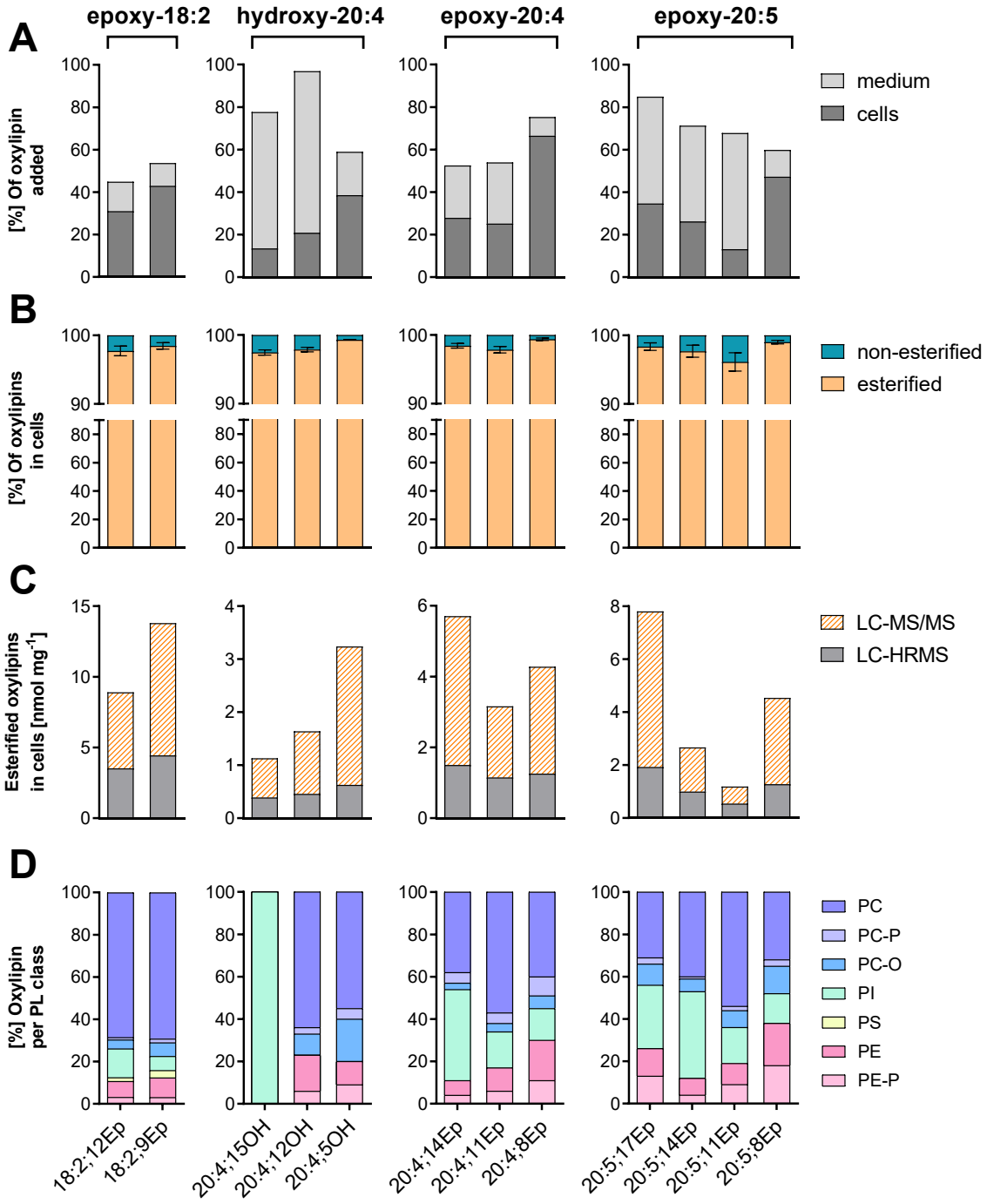

Fig. 3.10: Incorporation of oxylipins in the PL of cells. 0.5 × 10^6 cells were used per experiment. HEK293T cells were supplemented with either a mixture of 18:2;Ep, 20:4;OH, 20:4;Ep, or 20:5;Ep positional isomers (Table 3.1). Shown are **A** the recovery of the added oxylipins in the medium and the cells, and **B** the esterification rate (%) in the cells determined by quantitative targeted LC-MS/MS [27–30]. **C** The concentration of esterified oxylipins in the cells quantified following alkaline hydrolysis by targeted LC-MS/MS is compared to the sum of oxPL semi-quantified by untargeted LC-ESI(-)-HRMS. **D** Relative amount of oxylipins found in the different PL classes by untargeted LC-ESI(-)-HRMS.

Quantitative targeted analysis unveiled distinct incorporation rates for hydroxy- and epoxy-PUFA positional isomers (Fig. 3.10A): e.g. for epoxy-18:2 (18:2;12Ep: 31% *vs.* 18:2;9Ep: 43%), hydroxy-20:4 (20:4;15OH: 14% *vs*. 20:4;5OH: 39%), epoxy-20:4 (20:4;14Ep: 28% *vs*. 20:4;8Ep: 67%), epoxy-20:5 (20:5;14Ep: 26% *vs*. 20:5;8Ep: 47%), and epoxy-22:6 (22:6;16Ep: 27% *vs.* 22:6;7Ep: 41%). For both 20:4-derived epoxy- and hydroxy-PUFA, a trend can be identified that the closer the functional group is to the carboxyl end – thus the longer the non-polar (FA-like) acyl chain – the higher the incorporation rate. This is also the case for the two investigated 18:2-derived epoxy-PUFA, while epoxy-20:5 regioisomers show inconstant incorporation rates (Fig. 3.10A).

Almost all oxylipins in the cells were esterified (> 96%, Fig. 3.10B). The highest esterification rate was found for 20:4;8Ep with > 99% and the lowest for 20:5;11Ep with 96%, whose uptake in the cells is also among the lowest (i.e., 14%) (Fig. 3.10A). Thus, oxylipins which are taken up from the medium in the cells are rapidly incorporated into lipids. This is consistent with our previous work demonstrating that hydroxy-PUFA are mainly found esterified in HEK293T cells transfected with 15-LOX-1/-2 enzymes [50]. Nevertheless, kinetic experiments analyzing incorporation and remodeling at different incubation times are required to investigate how the position of the oxidation impacts the esterification rate.

Using the developed untargeted LC-ESI(-)-HRMS method, a total of 153 oxPL were semi-quantified (Table 3.3). The resulting concentrations (sum of individual oxPL species) were in the same order of magnitude as the (indirect) quantification of esterified oxylipins by targeted LC-MS/MS following alkaline hydrolysis (Fig. 3.10C). At least 20% and up to 46% of oxylipins were found bound to PL species covered by the LC-HRMS method, e.g., with 36% for 20:4;11Ep with 1.2 nmol mg^{-1} *vs.* 3.2 nmol mg^{-1} for the indirect quantification. Oxylipins were found esterified in PI, PS, PC, PE, PC-P, PC-O, and PE-P lipid classes bearing 16:0, 18:0, or 18:1, but could not be detected in PG, PA, or SM (Table 3.3). Except for 20:4;15OH, each oxylipin was found esterified in the *sn*-2 position to PC-P, PC-O, and PE-P bearing 16:0 (and also 18:1 for PC-O), and to PC and PE species bearing either 16:0, 18:0, or 18:1. 20:4;15OH could only be detected in PI bearing either 16:0, 18:0, or 18:1.

Epoxy-PUFA could be detected in relevant amounts in PI bearing either 16:0, 18:0, or 18:1. Only epoxy-18:2 were found in PS species. Additionally, several oxylipins such as 18:2;12Ep, 20:4;14Ep, or 20:5;17Ep were found esterified both in the *sn*-1 position or in the *sn*-2 position to PC or PI (only epoxy-18:2).

Both hydroxy- and epoxy-PUFA positional isomers were distinctly incorporated into PL classes (Fig. 3.10D): While almost 70% of 18:2;12Ep and 18:2;9Ep were found in PC, incorporation in PI was 14% *vs.* 6.7% and in PS 1.8% *vs.* 3.5% for 18:2;12Ep and 18:2;9Ep, respectively. Similarly, > 50% of 20:4;5OH and 20:4;12OH were found in PC, while 20% of 20:4;5OH and only 10% of 20:4;12OH were detected in PC-O and none of them in PI. In contrast, 20:4;15OH was found esterified exclusively to PI species. Also, other oxylipins bearing a hydroxy or epoxy functionality at the C15-position, namely 20:4;15OH, 20:4;14Ep, and 20:5;14Ep were preferentially incorporated into PI. A characteristic pattern was observed for epoxy-20:4 positional isomers: The closer the epoxy functionality to the ester group – and thus the longer the non-substituted acyl chain – the larger is the fraction of the oxylipin bound in PE and PE-P (10%, 17%, and 30% for 20:4;14Ep, 20:4;11Ep, and 20:4;8Ep, respectively). Positional analogues of epoxy-20:4 and epoxy-20:5 showed an almost identical distribution in the lipid classes: e.g. for 20:4;14Ep and 20:5;14Ep 43% and 41% in PI, 38% and 39% in PC, 6.7% and 8.2% in PE, 6.4% and 6.3% in PC-O, 3.6% and 3.7% in PE-P, and 1.7% and 1.4% in PC-P. All in all, this indicates that the position of the oxidation has a great impact on the incorporation of the oxylipins into the PL class. These results are consistent with a previous study in which a large percentage of [$^{14}C_1$]14(15)-EpETrE was found in PI while only [$^{14}C_1$]11(12)-EpETrE and [$^{14}C_1$]8(9)-EpETrE were detected in PE following the incubation of endothelial cells with different regioisomers of [$^{14}C_1$]EpETrE [51]. Stenson *et al*. also found that [$^{14}C_1$]12-HETE was mostly incorporated in PC among all PL in neutrophils supplemented with [$^{14}C_1$]12-HETE [52]. The same study reported that the major part of [$^{14}C_1$]12-HETE was found in TG, which is line with our results showing that 71% of 12-HETE is not esterified to PL (Fig. 3.10C).

Table 3.3: Concentration of oxPL species detected in oxylipin-supplemented cells. 0.5×10^6 cells were used per experiment. HEK293T cells were supplemented either with a mixture of 18:2;Ep, 20:4;OH, 20:4;Ep, or 20:5;Ep positional isomers (Table 3.1). OxPL were semi-quantified by LC-ESI(-)-HRMS based on peak heights, using one IS per lipid class. Shown is the mean ± SD (n = 3) of the concentration per mg of cell protein. n.d = not detected.

concentration of oxPL in oxylipin-supplemented HEK293T cells [pmol mg^{-1} protein]				
analyte	**+18:2;Ep**	**+20:4;OH**	**+20:4;Ep**	**+20:5;Ep**
		oxPI		
PI 18:2;12Ep_16:0	26 ± 9	n.d.	n.d.	n.d.
PI 16:0_18:2;12Ep	54 ± 12	n.d.	n.d.	n.d.
PI 18:2;9Ep_16:0	32 ± 8	n.d.	n.d.	n.d.
PI 16:0_18:2;9Ep	27 ± 6	n.d.	n.d.	n.d.
PI 18:0/18:2;12Ep	320 ± 74	n.d.	n.d.	n.d.
PI 18:0/18:2;9Ep	170 ± 23	n.d.	n.d.	n.d.
PI 18:1_18:2;12Ep	80 ± 19	n.d.	n.d.	n.d.
PI 18:1_18:2;Ep	65 ± 16	n.d.	n.d.	n.d.
PI 16:0_20:4;15OH	n.d.	53 ± 3	n.d.	n.d.
PI 16:0/20:4;14Ep	n.d.	n.d.	85 ± 7	n.d.
PI 16:0/20:4;11Ep	n.d.	n.d.	33 ± 6	n.d.
PI 16:0/20:4;8Ep	n.d.	n.d.	25 ± 5	n.d.
PI 16:0/20:5;17Ep	n.d.	n.d.	n.d.	75 ± 4
PI 16:0/20:5;14Ep	n.d.	n.d.	n.d.	61 ± 4
PI 16:0/20:5;11Ep	n.d.	n.d.	n.d.	28 ± 2
PI 16:0/20:5;8Ep	n.d.	n.d.	n.d.	26 ± 3
PI 18:0/20:4;15OH	n.d.	240 ± 11	n.d.	n.d.
PI 18:0/20:4;14Ep	n.d.	n.d.	430 ± 33	n.d.
PI 18:0/20:4;11Ep	n.d.	n.d.	130 ± 20	n.d.
PI 18:0/20:4;8Ep	n.d.	n.d.	130 ± 27	n.d.
PI 18:1/20:4;15OH	n.d.	100 ± 5	n.d.	n.d.
PI 18:1/20:4;14Ep	n.d.	n.d.	130 ± 11	n.d.
PI 18:1/20:4;11Ep	n.d.	n.d.	39 ± 5	n.d.
PI 18:1/20:4;8Ep	n.d.	n.d.	34 ± 6	n.d.
PI 18:0/20:5;17Ep	n.d.	n.d.	n.d.	390 ± 25
PI 18:0/20:5;14Ep	n.d.	n.d.	n.d.	260 ± 9
PI 18:0/20:5;11Ep	n.d.	n.d.	n.d.	49 ± 3
PI 18:0/20:5;8Ep	n.d.	n.d.	n.d.	120 ± 10
PI 18:1_20:5;17Ep	n.d.	n.d.	n.d.	110 ± 4
PI 18:1_20:5;14Ep	n.d.	n.d.	n.d.	88 ± 3
PI 18:1_20:5;11Ep	n.d.	n.d.	n.d.	17 ± 1
PI 18:1_20:5;8Ep	n.d.	n.d.	n.d.	33 ± 3
		oxPS		
PS 18:0/18:2;12Ep	62 ± 9	n.d.	n.d.	n.d.
PS 18:0/18:2;9Ep	150 ± 32	n.d.	n.d.	n.d.
		oxPC		
PC 18:2;12Ep/16:0	330 ± 51	n.d.	n.d.	n.d.
PC 16:0/18:2;12Ep	800 ± 120	n.d.	n.d.	n.d.
PC 18:2;9Ep/16:0	700 ± 120	n.d.	n.d.	n.d.
PC 16:0/18:2;9Ep	1200 ± 210	n.d.	n.d.	n.d.
PC 18:2;12Ep/16:0	330 ± 51	n.d.	n.d.	n.d.

Table 3.3: Continued 1/3. Concentration of oxPL detected in oxylipin-supplemented cells.

concentration of oxPL in oxylipin-supplemented HEK293T cells [pmol mg^{-1} protein]				
analyte	**+18:2;Ep**	**+20:4;OH**	**+20:4;Ep**	**+20:5;Ep**
		oxPC		
PC 16:1/18:2;12Ep	320 ± 46	n.d.	n.d.	n.d.
PC 18:2;9Ep/16:1	210 ± 34	n.d.	n.d.	n.d.
PC 16:1/18:2;9Ep	240 ± 53	n.d.	n.d.	n.d.
PC 18:0/18:2;12Ep	210 ± 39	n.d.	n.d.	n.d.
PC 18:0/18:2;9Ep	160 ± 30	n.d.	n.d.	n.d.
PC 18:1/18:2;12Ep	760 ± 120	n.d.	n.d.	n.d.
PC 18:1/18:2;9Ep	550 ± 82	n.d.	n.d.	n.d.
PC 16:0/20:4;12OH	n.d.	150 ± 4	n.d.	n.d.
PC 20:4;5OH_16:0	n.d.	76 ± 9	n.d.	n.d.
PC 16:0/20:4;5OH	n.d.	170 ± 17	n.d.	n.d.
PC 20:4;14Ep/16:0	n.d.	n.d.	190 ± 40	n.d.
PC 16:0/20:4;14Ep	n.d.	n.d.	220 ± 9	n.d.
PC 20:4;11Ep/16:0	n.d.	n.d.	160 ± 41	n.d.
PC 16:0/20:4;11Ep	n.d.	n.d.	370 ± 59	n.d.
PC 16:0/20:4;8Ep	n.d.	n.d.	300 ± 34	n.d.
PC 20:5;17Ep/16:0	n.d.	n.d.	n.d.	46 ± 6
PC 16:0/20:5;17Ep	n.d.	n.d.	n.d.	360 ± 27
PC 20:5;14Ep/16:0	n.d.	n.d.	n.d.	76 ± 10
PC 16:0/20:5;14Ep	n.d.	n.d.	n.d.	150 ± 6
PC 16:0/20:5;11Ep	n.d.	n.d.	n.d.	230 ± 17
PC 16:0/20:5;8Ep	n.d.	n.d.	n.d.	266 ± 13
PC 18:0/20:4;12OH	n.d.	36 ± 5	n.d.	n.d.
PC 18:0/20:4;5OH	n.d.	26 ± 4	n.d.	n.d.
PC 18:0/20:4;14Ep	n.d.	n.d.	45 ± 2	n.d.
PC 18:0_20:4;11Ep	n.d.	n.d.	18 ± 1	n.d.
PC 18:0/20:4;8Ep	n.d.	n.d.	57 ± 4	n.d.
PC 18:1/20:4;12OH	n.d.	110 ± 7	n.d.	n.d.
PC 18:1/20:4;5OH	n.d.	83 ± 7	n.d.	n.d.
PC 18:1/20:4;14Ep	n.d.	n.d.	120 ± 7	n.d.
PC 18:1/20:4;11Ep	n.d.	n.d.	100 ± 4	n.d.
PC 18:1/20:4;8Ep	n.d.	n.d.	150 ± 12	n.d.
PC 18:0/20:5;17Ep	n.d.	n.d.	n.d.	190 ± 8
PC 20:5;14Ep/18:0	n.d.	n.d.	n.d.	67 ± 4
PC 18:0/20:5;14Ep	n.d.	n.d.	n.d.	99 ± 8
PC 18:0_20:5;11Ep	n.d.	n.d.	n.d.	69 ± 6
PC 18:0/20:5;8Ep	n.d.	n.d.	n.d.	140 ± 5
		oxPC-P		
PC P-16:0/18:2;12Ep	41 ± 10	n.d.	n.d.	n.d.
PC P-16:0/18:2;9Ep	78 ± 13	n.d.	n.d.	n.d.
PC P-16:0/20:4;12OH	n.d.	13 ± 2	n.d.	n.d.
PC P-16:0/20:4;5OH	n.d.	30 ± 4	n.d.	n.d.
PC P-16:0/20:4;14Ep	n.d.	n.d.	26 ± 2	n.d.
PC P-16:0/20:4;11Ep	n.d.	n.d.	21 ± 1	n.d.
PC P-16:0/20:4;8Ep	n.d.	n.d.	39 ± 4	n.d.
PC P-16:0/20:5;17Ep	n.d.	n.d.	n.d.	54 ± 3
PC P-16:0/20:5;14Ep	n.d.	n.d.	n.d.	14.0 ± 0.1
PC P-16:0_20:5;11Ep	n.d.	n.d.	n.d.	9 ± 1
PC P-16:0/20:5;8Ep	n.d.	n.d.	n.d.	43 ± 2

Table 3.3: Continued 2/3. Concentration of oxPL detected in oxylipin-supplemented cells.

concentration of oxPL in oxylipin-supplemented HEK293T cells [pmol mg^{-1} protein]				
analyte	**+18:2;Ep**	**+20:4;OH**	**+20:4;Ep**	**+20:5;Ep**
		oxPC-O		
PC O-16:0/18:2;12Ep	130 ± 21	n.d.	n.d.	n.d.
PC O-16:0/18:2;9Ep	220 ± 39	n.d.	n.d.	n.d.
PC O-18:1/18:2;12Ep	28 ± 5	n.d.	n.d.	n.d.
PC O-18:1/18:2;9Ep	66 ± 10	n.d.	n.d.	n.d.
PC O-16:0/20:4;12OH	n.d.	35 ± 1	n.d.	n.d.
PC O-16:0/20:4;5OH	n.d.	100 ± 5	n.d.	n.d.
PC O-16:0/20:4;14Ep	n.d.	n.d.	72 ± 4	n.d.
PC O-16:0/20:4;11Ep	n.d.	n.d.	57 ± 5	n.d.
PC O-16:0/20:4;8Ep	n.d.	n.d.	110 ± 5	n.d.
PC O-16:0/20:5;17Ep	n.d.	n.d.	n.d.	140 ± 4
PC O-16:0/20:5;14Ep	n.d.	n.d.	n.d.	47 ± 4
PC O-16:0/20:5;11Ep	n.d.	n.d.	n.d.	33.3 ± 0.9
PC O-16:0/20:5;8Ep	n.d.	n.d.	n.d.	120 ± 14
PC O-18:1/20:4;12OH	n.d.	11 ± 1	n.d.	n.d.
PC O-18:1/20:4;5OH	n.d.	26 ± 1	n.d.	n.d.
PC O-18:1/20:4;14Ep	n.d.	n.d.	24 ± 1	n.d.
PC O-18:1/20:4;11Ep	n.d.	n.d.	20.4 ± 0.4	n.d.
PC O-18:1/20:4;11Ep	n.d.	n.d.	43 ± 3	n.d.
PC O-18:1/20:5;17Ep	n.d.	n.d.	n.d.	59 ± 3
PC O-18:1/20:5;14Ep	n.d.	n.d.	n.d.	16.3 ± 0.3
PC O-18:1/20:5;11Ep	n.d.	n.d.	n.d.	10 ± 1
PC O-18:1/20:5;8Ep	n.d.	n.d.	n.d.	50 ± 2
		oxPE		
PE 16:0/18:2;12Ep	66 ± 5	n.d.	n.d.	n.d.
PE 16:0/18:2;9Ep	115 ± 11	n.d.	n.d.	n.d.
PE 18:0/18:2;12Ep	75 ± 7	n.d.	n.d.	n.d.
PE 18:0/18:2;9Ep	110 ± 14	n.d.	n.d.	n.d.
PE 18:1/18:2;12Ep	120 ± 8	n.d.	n.d.	n.d.
PE 18:1/18:2;9Ep	180 ± 23	n.d.	n.d.	n.d.
PE 16:0/20:4;12OH	n.d.	19 ± 2	n.d.	n.d.
PE 16:0/20:4;5OH	n.d.	22 ± 2	n.d.	n.d.
PE 16:0/20:4;14Ep	n.d.	n.d.	28 ± 2	n.d.
PE 16:0/20:4;11Ep	n.d.	n.d.	35 ± 2	n.d.
PE 16:0/20:4;8Ep	n.d.	n.d.	61 ± 8	n.d.
PE 16:0/20:5;17Ep	n.d.	n.d.	n.d.	71 ± 3
PE 16:0/20:5;14Ep	n.d.	n.d.	n.d.	22 ± 2
PE 16:0_20:5;11Ep	n.d.	n.d.	n.d.	16 ± 1
PE 16:0/20:5;8Ep	n.d.	n.d.	n.d.	68 ± 4
PE 18:0/20:4;12OH	n.d.	28 ± 1	n.d.	n.d.
PE 18:0_20:4;5OH	n.d.	18 ± 3	n.d.	n.d.
PE 18:0/20:4;14Ep	n.d.	n.d.	31 ± 3	n.d.
PE 18:0/20:4;11Ep	n.d.	n.d.	49 ± 2	n.d.
PE 18:0/20:4;8Ep	n.d.	n.d.	92 ± 10	n.d.
PE 18:1_20:4;12OH	n.d.	32 ± 2	n.d.	n.d.
PE 18:1_20:4;5OH	n.d.	27 ± 2	n.d.	n.d.
PE 18:1/20:4;14Ep	n.d.	n.d.	41 ± 3	n.d.
PE 18:1/20:4;11Ep	n.d.	n.d.	41 ± 2	n.d.
PE 18:1/20:4;8Ep	n.d.	n.d.	84 ± 6	n.d.

Table 3.3: Continued 3/3. Concentration of oxPL detected in oxylipin-supplemented cells.

concentration of oxPL in oxylipin-supplemented HEK293T cells [pmol mg^{-1} protein]				
analyte	**+18:2;Ep**	**+20:4;OH**	**+20:4;Ep**	**+20:5;Ep**
oxPE				
PE 18:0/20:5;17Ep	n.d.	n.d.	n.d.	97 ± 6
PE 18:0/20:5;14Ep	n.d.	n.d.	n.d.	28 ± 2
PE 18:0_20:5;11Ep	n.d.	n.d.	n.d.	19.9 ± 0.7
PE 18:0/20:5;8Ep	n.d.	n.d.	n.d.	95 ± 2
PE 18:1/20:5;17Ep	n.d.	n.d.	n.d.	93 ± 2
PE 18:1_20:5;14Ep	n.d.	n.d.	n.d.	31 ± 2
PE 18:1_20:5;11Ep	n.d.	n.d.	n.d.	19.7 ± 0.8
PE 18:1/20:5;8Ep	n.d.	n.d.	n.d.	88 ± 4
oxPE-P				
PE P-16:0/18:2;12Ep	85 ± 7	n.d.	n.d.	n.d.
PE P-16:0/18:2;9Ep	100 ± 15	n.d.	n.d.	n.d.
PE P-18:1/18:2;12Ep	26 ± 3	n.d.	n.d.	n.d.
PE P-18:1/18:2;9Ep	30 ± 5	n.d.	n.d.	n.d.
PE P-16:0/20:4;12OH	n.d.	30.2 ± 0.6	n.d.	n.d.
PE P-16:0/20:4;5OH	n.d.	58 ± 9	n.d.	n.d.
PE P-16:0/20:4;14Ep	n.d.	n.d.	55 ± 6	n.d.
PE P-16:0/20:4;11Ep	n.d.	n.d.	75 ± 6	n.d.
PE P-16:0/20:4;8Ep	n.d.	n.d.	140 ± 12	n.d.
PE P-16:0/20:5;17Ep	n.d.	n.d.	n.d.	240 ± 25
PE P-16:0/20:5;14Ep	n.d.	n.d.	n.d.	36.7 ± 0.9
PE P-16:0/20:5;11Ep	n.d.	n.d.	n.d.	48 ± 1
PE P-16:0/20:5;8Ep	n.d.	n.d.	n.d.	230 ± 3

The observed distinct incorporation of hydroxy- and epoxy-PUFA positional isomers into the PL classes could depend on the substrate specificity of the enzymes involved in the formation of PL and integration of FA during the Lands' remodeling cycle [9,13], i.e. ACSL and LPLAT. Klett *et al.* demonstrated that all five human ACSL isoforms (i.e. ACSL1, -3, -4, -5, and -6) accept both EpETrEs (20:4;Ep) and HETEs (20:4;OH) positional isomers as substrate [53]. This suggests that the observed unique incorporation pattern depends not on ACSL but on the specificity of LPLAT isoforms towards the positional isomers. LPLAT11 was reported to incorporate PUFA-CoAs into lysoPI [54,55]. Furthermore, in humans four isoforms of lysoPC acyl transferase (LPCAT) are described, i.e., LPCAT1, -2, -3, and -4 [13], which exhibit differences regarding both the acyl-CoA and the LPLAT activity. LPLAT8 (LPCAT1) transfers 16:0-, 18:2-, and 18:3-CoA to lysoPG and LPLAT10 (LPCAT4) only transfers 18:1-CoA into lysoPC and lysoPE. LPLAT9 (LPCAT2) and LPLAT12 (LPCAT3) use preferentially 18:2- and

20:4-CoAs as substrates [56,57]. While LPLAT9 only incorporates PUFA-CoAs into lysoPC, LPLAT12 additionally transfers them to lysoPS and lysoPE. Based on these specificities, our results would suggest that LPLAT11 preferentially uses 20:4;15OH-, 20:4;14Ep-, and 20:5;14Ep-CoAs as a substrate while the other oxylipins might be preferentially transferred by LPLAT9 and/or LPLAT12. The distinct incorporation of oxylipins into lysoPL warrants further investigation including a detailed analysis of the role of LPLAT9, LPLAT11, and LPLAT12.

3.4 Conclusion

A RP-LC separation method covering a large number of isobaric and isomeric PL species bearing different biologically relevant oxylipin positional isomers such as 18:2;O, 20:4;O, 20:5;O, and 22:6;O was developed. In combination with ESI(-)HRMS analysis, the position of the hydroxy/epoxy groups and the *sn*-1/*sn*-2 position of the (oxidized) fatty acyl chains could be deduced, and esterified hydroxy-PUFA are differentiated from epoxy-PUFA. This enables for the first time a comprehensive analysis of oxylipins being bound to PL. Untargeted semiquantification of oxPL in oxylipin-supplemented HEK293T cells using one IS per lipid class unveiled that 20% and up to 46% of the esterified oxylipins are bound to different PL classes. Each oxylipin showed a distinct incorporation pattern: 20:4;15OH, 20:4;14Ep, and 20:5;14Ep are mostly esterified into PI. 20:4;8Ep and 20:5;8Ep are found in PC and PE while 20:5;17Ep is mainly found in PC and PI. The other oxylipins are mainly found in PC accounting for example from > 50% for 20:4;12OH to > 65% for 18:2;12Ep. Overall, the developed and optimized LC-HRMS method enabled us to get a first insight in which PL class oxylipins are bound. We conclude that the position of the oxidation has a great impact and directs the incorporation of oxylipins into the different PL classes.

3.5 References

1. J.D. Morrow, J.A. Awad, H.J. Boss, I.A. Blair, 2nd L Roberts (1992) Non-cyclooxygenasederived prostanoids (F2-isoprostanes) are formed in situ on phospholipids, *Proc. Natl. Acad. Sci. USA*. **89**, 10721–10725.
2. N.H. Schebb, A.I. Ostermann, J. Yang, B.D. Hammock, A. Hahn, J.P. Schuchardt (2014) Comparison of the effects of long-chain omega-3 fatty acid supplementation on plasma levels of free and esterified oxylipins, *Prostag. Other Lipid Mediat*. **113**, 21–29.
3. G.C. Shearer, J.W. Newman (2009) Impact of circulating esterified eicosanoids and other oxylipins on endothelial function, Curr. *Atherosclerosis Rep*. **11**, 403–410.
4. W.W. Christie, J.L. Harwood. (2020) Oxidation of polyunsaturated fatty acids to produce lipid mediators, *Essays Biochem*. **64**, 401–421.
5. S.C. Dyall, L. Balas, N.G. Bazan, J.T. Brenna, N. Chiang, F. da Costa Souza, et al. (2022) Polyunsaturated fatty acids and fatty acid-derived lipid mediators: recent advances in the understanding of their biosynthesis, structures, and functions, *Prog. Lipid Res*. **86**, 101165.
6. Soňa Čejková, Ivana Králová Lesná, R. Poledne (2016) Monocyte adhesion to the endothelium is an initial stage of atherosclerosis development, *Cor Vasa*. **58**, e419–e425.
7. M. Chatterjee, D. Rath, J. Schlotterbeck, J. Rheinlaender, B. Walker-Allgaier, N. Alnaggar, et al. (2017) Regulation of oxidized platelet lipidome: implications for coronary artery disease, *Eur. Heart J*. **38**, 1993–2005.
8. V.N. Bochkov, A. Kadl, J. Huber, F. Gruber, B.R. Binder, N. Leitinger (2002) Protective role of phospholipid oxidation products in endotoxin-induced tissue damage, *Nature*. **419**, 77–81.
9. V.B. O'Donnell, M. Aldrovandi, R.C. Murphy, G. Kronke (2019) Enzymatically oxidized phospholipids assume center stage as essential regulators of innate immunity and cell death, *Sci. Signal*. **12**, eaau2293.
10. J.Z. Haeggstrom, C.D. Funk. (2011) Lipoxygenase and leukotriene pathways: biochemistry, biology, and roles in disease, *Chem. Rev*. **111**, 5866–5898.
11. H. Yin, Y. Zhou, M. Zhu, S. Hou, Z. Li, H. Zhong, et al. (2013) Role of mitochondria in programmed cell death mediated by arachidonic acid-derived eicosanoids, *Mitochondrion*. **13**, 209–224.
12. C.D. Funk (2001) Prostaglandins and leukotrienes: advances in eicosanoid biology, *Science*. **294**, 1871–1875.
13. B. Wang, P. Tontonoz (2019) Phospholipid remodeling in physiology and disease, *Annu. Rev. Physiol*. **81**, 165–188.
14. J.I. MacDonald, H. Sprecher (1991) Phospholipid fatty acid remodeling in mammalian cells, *Biochim. Biophys. Acta***. 1084**, 105–121.
15. V.B. O'Donnell, J. Rossjohn, M.J. Wakelam (2019) Phospholipid signaling in innate immune cells, J. *Clin. Investig*. **128**, 2670–2679.
16. C.E. Annevelink, R.E. Walker, G.C. Shearer (2022) Esterified oxylipins: do they matter? *Metabolites*. **12**, 1007.
17. I. Liakh, A. Pakiet, T. Sledzinski, A. Mika. (2020) Methods of the analysis of oxylipins in biological samples, *Molecules*. **25**, 349.
18. R. Aoyagi, K. Ikeda, Y. Isobe, M. Arita (2017) Comprehensive analyses of oxidized phospholipids using a measured MS/MS spectra library, *J. Lipid Res*. **58**, 2229–2237.

19. V.E. Kagan, G. Mao, F. Qu, J.P.F. Angeli, S. Doll, C.S. Croix, et al. (2017) Oxidized arachidonic and adrenic PEs navigate cells to ferroptosis, *Nat. Chem. Biol*. **13**, 81–90.
20. A.H. Morgan, V.J. Hammond, L. Morgan, C.P. Thomas, K.A. Tallman, Y.R. GarciaDiaz, et al. (2010) Quantitative assays for esterified oxylipins generated by immune cells, *Nat. Protoc*. **5**, 1919–1931.
21. Reis, M. Domingues, F. Amado, A. Ferrer-Correia, P. Domingues (2007) Radical peroxidation of palmitoyl-lineloyl-glycerophosphocholine liposomes: identification of long-chain oxidised products by liquid chromatography–tandem mass spectrometry, *J. Chromatogr. B*. **855**, 186–199.
22. H. Nakanishi, Y. Iida, T. Shimizu, R. Taguchi (2009) Analysis of oxidized phosphatidylcholines as markers for oxidative stress, using multiple reaction monitoring with theoretically expanded data sets with reversed-phase liquid chromatography/tandem mass spectrometry, *J. Chromatogr. B*. **877**, 1366–1374.
23. A.H. Morgan, V. Dioszeghy, B.H. Maskrey, C.P. Thomas, S.R. Clark, S.A. Mathie, et al. (2009) Phosphatidylethanolamine-esterified eicosanoids in the mouse: tissue localization and inflammation-dependent formation in Th-2 disease, *J. Biol. Chem*. **284**, 21185–21191.
24. J. Falck, L.M. Reddy, Y.K. Reddy, M. Bondlela, U.M. Krishna, Y. Ji, et al. (2003) 11, 12-epoxyeicosatrienoic acid (11, 12-EET): structural determinants for inhibition of TNF-α-induced VCAM-1 expression, *Bioorgan. Med.Chem. Lett*. **13**, 4011–4014.
25. V. Matyash, G. Liebisch, T.V. Kurzchalia, A. Shevchenko, D. Schwudke (2008) Lipid extraction by methyl-tert-butyl ether for high-throughput lipidomics, *J. Lipid Res*. **49**, 1137–1146.
26. K.M. Rund, L. Carpanedo, R. Lauterbach, T. Wermund, A.L. West, L.M. Wende, et al. (2024) LC-ESI-HRMS—lipidomics of phospholipids: characterization of extraction, chromatography and detection parameters, *Anal. Bioanal. Chem*. **406**, 925–944.
27. N.M. Hartung, M. Mainka, R. Pfaff, M. Kuhn, S. Biernacki, L. Zinnert, et al. (2023) Development of a quantitative proteomics approach for cyclooxygenases and lipoxygenases in parallel to quantitative oxylipin analysis allowing the comprehensive investigation of the arachidonic acid cascade, *Anal. Bioanal. Chem*. **415**, 913–933.
28. L. Kutzner, K. Rund, A. Ostermann, N. Hartung, J. Galano, L. Balas, et al. (2019) Development of an optimized LC-MS method for the detection of specialized proresolving mediators in biological samples, Front. Pharmacol. **10**, 169.
29. A.I. Ostermann, E. Koch, K.M. Rund, L. Kutzner, M. Mainka, N.H. Schebb (2020) Targeting esterified oxylipins by LC–MS-Effect of sample preparation on oxylipin pattern, *Prostag. Other Lipid Mediat*. **146**, 106384.
30. K.M. Rund, A.I. Ostermann, L. Kutzner, J.-M. Galano, C. Oger, C. Vigor, et al. (2018) Development of an LC-ESI (-)-MS/MS method for the simultaneous quantification of 35 isoprostanes and isofurans derived from the major n3-and n6-PUFAs, *Anal. Chim. Acta*. **1037**, 63–74.
31. G. Liebisch, E. Fahy, J. Aoki, E.A. Dennis, T. Durand, C.S. Ejsing, et al. (2020) Update on LIPID MAPS classification, nomenclature, and shorthand notation for MS-derived lipid structures, *J. Lipid Res*. **61**, 1539–1555.
32. Zuzana Vaňková, Ondřej Peterka, Michaela Chocholoušková, Denise Wolrab, Robert Jirásko, Michal Holčapek (2022) Retention dependences support highly confident identification of lipid species in human plasma by reversed-phase UHPLC/MS, *Anal. Bioanal. Chem*. **414**, 319–331.

33. V.B. O'Donnell (2011) Mass spectrometry analysis of oxidized phosphatidylcholine and phosphatidylethanolamine, *Biochim. Biophys. Acta*. **1811**, 818–826.
34. K.A. Massey, A. Nicolaou (2013) Lipidomics of oxidized polyunsaturated fatty acids, *Free Radic. Biol. Med*. **59**, 45–55.
35. K. Strassburg, A.M. Huijbrechts, K.A. Kortekaas, J.H. Lindeman, T.L. Pedersen, A. Dane, et al. (2012) Quantitative profiling of oxylipins through comprehensive LC-MS/ MS analysis: application in cardiac surgery, *Anal. Bioanal. Chem*. **404**, 1413–1426.
36. S.W. Meckelmann, S. Hellhake, M. Steuck, M. Krohn, N.H. Schebb (2017) Comparison of derivatization/ionization techniques for liquid chromatography tandem mass spectrometry analysis of oxylipins, *Prostag. Other Lipid Mediat*. **130**, 8–15.
37. R. Harkewicz, E. Fahy, A. Andreyev, E.A. Dennis (2007) Arachidonate-derived dihomoprostaglandin production observed in endotoxin-stimulated macrophagelike cells, *J. Biol. Chem*. **282**, 2899–2910.
38. S.S. Bird, V.R. Marur, I.G. Stavrovskaya, B.S. Kristal (2013) Qualitative characterization of the rat liver mitochondrial lipidome using LC–MS profiling and high energy collisional dissociation (HCD) all ion fragmentation, *Metabolomics*. **9**, 67–83.
39. P.T. Ivanova, S.B. Milne, M.O. Byrne, Y. Xiang, H.A. Brown (2007) Glycerophospholipid identification and quantitation by electrospray ionization mass spectrometry, *Methods Enzymol*. **432**, 21–57.
40. Miroslav Lísa, Eva Cífková, Michal Holčapek (2011) Lipidomic profiling of biological tissues using offline two-dimensional high-performance liquid chromatography–mass spectrometry, *J. Chromatogr. A*. **1218**, 5146–5156.
41. H. Tsugawa, K. Ikeda, M. Takahashi, A. Satoh, Y. Mori, H. Uchino, et al. (2020) A lipidome atlas in MS-DIAL 4, *Nat. Biotechnol*. **38**, 1159–1163.
42. C.Z. Ulmer, R.E. Patterson, J.P. Koelmel, T.J. Garrett, R.A. Yost (2017) A robust lipidomics workflow for mammalian cells, plasma, and tissue using liquidchromatography high-resolution tandem mass spectrometry, *Lipidom: Methods Protocols*. **1609**, 91–106.
43. I. Vlasakov, P. Norris, J. Winkler, J. Dalli, C. Serhan (2016) Lipid Mediator Metabololipidomics LC-MS-MS Spectra Book, *Brigh Women's Hosp Harv Med Sch*, Boston, MA, 1–122.
44. H. Song, H. Wu, Z. Geng, C. Sun, S. Ren, D. Wang, et al. (2016) Simultaneous determination of 13-HODE, 9, 10-DHODE, and 9, 10, 13-THODE in cured meat products by LC-MS/MS, *Food Anal. Methods*. **9**, 2832–2841.
45. Y. Lu, S. Hong, R. Yang, J. Uddin, K.H. Gotlinger, N.A. Petasis, et al. (2007) Identification of endogenous resolvin E1 and other lipid mediators derived from eicosapentaenoic acid via electrospray low-energy tandem mass spectrometry: spectra and fragmentation mechanisms, *Rapid Commun. Mass Spectrom*. **21**, 7–22.
46. P.G. Kopf, D.X. Zhang, K.M. Gauthier, K. Nithipatikom, X.-Y. Yi, J.R. Falck, et al. (2010) Adrenic acid metabolites as endogenous endothelium-derived and zona glomerulosa-derived hyperpolarizing factors, *Hypertension*. **55**, 547–554.
47. S. Hong, Y. Lu, R. Yang, K.H. Gotlinger, N.A. Petasis, C.N. Serhan (2007) Resolvin D1, protectin D1, and related docosahexaenoic acid-derived products: analysis via electrospray/low energy tandem mass spectrometry based on spectra and fragmentation mechanisms, *J. Am. Soc. Mass Spectrom*. **18**, 128–144.
48. J. Pi, X. Wu, Y. Feng (2016) Fragmentation patterns of five types of phospholipids by ultra-high-performance liquid chromatography electrospray ionization quadrupole time-of-flight tandem mass spectrometry, *Anal. Methods*. **8**, 1319–1332.

49. H. Nakanishi, Y. Iida, T. Shimizu, R. Taguchi (2010) Separation and quantification of sn-1 and sn-2 fatty acid positional isomers in phosphatidylcholine by RPLC-ESIMS/MS, *J. Biochem*. **147**, 245–256.
50. B. Goebel, L. Carpanedo, S. Reif, T. Gobel, N.H. Schebb, D. Steinhilber, et al. (2023) Development of a cell-based model system for the investigation of ferroptosis, *Front Cell Death*. **2**, 1182239.
51. M. VanRollins, T. Kaduce, H. Knapp, A. Spector (1993) 14, 15-Epoxyeicosatrienoic acid metabolism in endothelial cells, *J. Lipid Res*. **34**, 1931–1942.
52. W.F. Stenson, C.W. Parker (1979) 12-L-hydroxy-5, 8, 10, 14-eicosatetraenoic acid, a chemotactic fatty acid, is incorporated into neutrophil phospholipids and triglyceride, *Prostaglandins*. **18**, 285–292.
53. E.L. Klett, S. Chen, A. Yechoor, F.B. Lih, R.A. Coleman (2017) Long-chain acyl-CoA synthetase isoforms differ in preferences for eicosanoid species and long-chain fatty acids, *J. Lipid Res*. **58**, 884–894.
54. A. Caddeo, K. Hedfalk, S. Romeo, P. Pingitore (2021) LPIAT1/MBOAT7 contains a catalytic dyad transferring polyunsaturated fatty acids to lysophosphatidylinositol, *Biochim. Biophys. Acta*. **1866**, 158891.
55. S. Matsuda, T. Inoue, H.C. Lee, N. Kono, F. Tanaka, K. Gengyo-Ando, et al., (2008) Member of the membrane-bound O-acyltransferase (MBOAT) family encodes a lysophospholipid acyltransferase with broad substrate specificity, *Gene Cell*. **13**, 879–888.
56. D. Hishikawa, H. Shindou, S. Kobayashi, H. Nakanishi, R. Taguchi, T. Shimizu (2008) Discovery of a lysophospholipid acyltransferase family essential for membrane asymmetry and diversity, *Proc. Natl. Acad. Sci. USA*. **105**, 2830–2835.
57. H. Shindou, D. Hishikawa, H. Nakanishi, T. Harayama, S. Ishii, R. Taguchi, et al. (2007) A single enzyme catalyzes both platelet-activating factor production and membrane biogenesis of inflammatory cells: cloning and characterization of acetylCoA: LYSO-PAF acetyltransferase, *J. Biol. Chem*. **282**, 6532–6539.

Chapter 4

Substrate-dependent incorporation of 15-lipoxygenase products in phospholipids: 15-HETE and 15-HEPE in PI, 17-HDHA in plasmalogen PE, and 13-HODE in PC *

Several oxylipins including hydroxy-PUFA act as lipid mediators. In biological samples the major part occurs esterified in PL or other lipids. In this work, the incorporation into PL of 15(*S*)-HETE, 15(*S*)-HEPE, 17(*S*)-HDHA, and 13(*S*)-HODE was investigated in oxylipin-supplemented HEK293T cells and cells overexpressing 15-LOX-2 (ALOX15B). Indirect quantification of esterified oxylipins in lipid fractions showed that > 97% of each supplemented 15-LOX-2 product is esterified and that < 25% are bound to NL, while > 75% are bound to distinct PL classes, depending on the hydroxy-PUFA. 15-HETE and 15-HEPE were found in PI/PS, while 17-HDHA was in PE and 13-HODE in PC. The same pattern was found for oxylipins endogenously formed by overexpression of 15-LOX-2. A new targeted method for the analysis of oxPL enabled to pinpoint the specific molecular species of the oxylipins. 15-HETE and 15-HEPE are dominantly found as PI 18:0/20:4;15OH (70%) and PI 18:0/20:5;15OH (80%), respectively. This preferential incorporation of 20:4;15OH and 20:5;15OH into PI may be biologically relevant for PI signaling pathways. In contrast, > 50% of 17-HDHA was found in PE P-16:0/22:6;17OH, PE P-18:0/22:6;17OH, and PE P-18:1/22:6;17OH. At least 40% of 13-HODE was incorporated into PC 16:0/18:2;13OH and relevant amounts were found in PI 18:0/18;13OH, PC 18:1/18;13OH, and PC-O 16:0/18;13OH. The distinct incorporation of 15-LOX-2 products from different PUFA into PL might contribute to the biological effect of these oxylipins and their precursor FA.

* modified from Carpanedo L. Wende L. M., Goebel B, Häfner AK, Chromik M. A., Kampschulte N., Steinhilber D., and Schebb N. H. (2025) *J Lipid Res*. Accepted for publication.

Author contributions: **LC:** Writing – review & editing, Writing – original draft, Visualization, Methodology, Investigation, Formal analysis, Data curation, and Conceptualization. **LMW:** Writing – review & editing, Methodology, Visualization, Investigation, Formal analysis. **BG:** Writing – review & editing, Resources. **AKH:** Writing – review & editing, Resources. **MAC:** Writing – review & editing, Investigation. **NK:** Writing – review & editing, Methodology. **DS:** Writing – review & editing, Resources, Supervision, Funding acquisition. **NHS:** Writing – review & editing, Writing – original draft, Methodology, Supervision, Project administration, Investigation, Funding acquisition, Conceptualization.

4.1 Introduction

Eicosanoids and other oxylipins are formed by oxidation of PUFA [1, 2]. Hydroxy-PUFA can be obtained by the reduction of hydroperoxy-PUFA which are generated non-enzymatically via reactive oxygen species, or enzymatically by COX, CYP450, and LOX enzymes such as 15-LOX-1, 15-LOX-2, 5-LOX, and 12-LOX [2-4]. 15-LOX can oxidize both, non-esterified PUFA as well as PUFA esterified to PL [3, 5]. ARA oxidation by 15-LOX-1 leads to the two products 15(*S*)-H(p)ETE and 12(*S*)-H(p)ETE, with pronounced species differences [6, 7]. 15-LOX-2 converts ARA only to 15(*S*)-H(p)ETE [8]. 15(*S*)-hydroxyeicosapentaenoic acid (HEPE), 17(*S*)-hydroxydocosahexaenoic acid (HDHA), and 13(*S*)-HODE are generated by 15-LOX-2 from EPA, DHA, and LA, respectively [7]. Moreover, both 15-HETE and 13-HODE can be formed in minor amounts by COX-2 [9-11] and CYP450 enzymes [12]. 15(*S*)-HETE and in part 13(*S*)-HODE are discussed to act predominantly anti-inflammatory [1, 13] and were found for example to have antitumor roles in smokers with non-small cell lung carcinoma [14]. However, increased levels were also observed in inflammation, and higher levels of 15-HETE and 13-HODE were found in atherosclerotic plaques [15, 16]. 15-HEPE may exhibit inflammatory effects and was found to protect wild-type mice against chemically induced colitis [17]. Also, 17(*S*)-HDHA prevented hyperhomocysteinemia-induced formation of the nucleotide-binding oligomerization domain-like receptor containing pyrin domain 3 inflammasome in podocytes of mice, and inhibited the formation of the pro-inflammatory cytokine interleukin-1β [18].

The major part of hydroxy-PUFA occurs in biological samples as esterified in lipids such as PL or NL [13, 19-22]. In the last decades, the quantification of esterified oxylipins was carried out indirectly by quantitative analysis of non-esterified oxylipins using targeted LC coupled to MS/MS following the cleavage of the ester bond by alkaline hydrolysis [23, 24]. This analysis does not provide the information in which lipid classes/species, and at which *sn*-position oxylipins are esterified. Thus, it is not possible to study the biological roles of

oxPL, including PL bearing 15-HETE (20:4;15OH), 15-HEPE (20:5;15OH), 17-HDHA (22:6;17OH), and 13-HODE (18:2;13OH).

In the 1990s, incorporation of 15-HETE and 13-HODE was investigated into lipids using TLC following supplementation of cells with radioactively labeled oxylipins, e.g. [^{3}H]15-HETE or [^{14}C]15-HETE [25-32]. This approach provided a first insight in which lipid classes these oxylipins are incorporated following supplementation, but could not provide information in which molecular species they are esterified. Moreover non-labeled oxylipins, and thus endogenous formation could not be investigated. In the 2010s, the main LOX products from ARA, i.e., 15-HETE, 12-HETE, and 5-HETE, have been detected in different PL species by LC-MS in human monocytes [33], in murine peritoneal macrophages from naïve lavage [34], human platelets [33, 35], and human neutrophils [36] by O'Donnell and coworkers.

In this study, we aimed to characterize for the first time in which PL classes dominating 15-LOX products from the main PUFA are esterified. For this purpose, we investigated the pattern of oxylipins in HEK293T cells following either exogenous oxylipin supplementation or endogenous oxylipin formation by 15-LOX-2 using a genetically modified cell line. The vast majority of oxylipins were found esterified in HEK293T cells, predominantly in PL. Hydroxy-PUFA exhibited distinct incorporation patterns across PL classes. Using a newly developed targeted LC-MS/MS method, each hydroxy-PUFA was found to be specifically esterified into distinct molecular PL species. Supplemented and 15-LOX-2 overexpressing HEK293T cells showed a similar incorporation pattern of 15-LOX products into PL classes and species. The dramatic differences between the incorporation pattern of the 15-LOX products of different PUFA might be relevant for PI signaling pathways.

4.2 Materials and methods

4.2.1 Chemicals and biological material

PI 12:0/13:0, PG 12:0/13:0, PC 12:0/13:0, and PE 12:0/13:0 were purchased from Avanti Polar Lipids (local supplier: Merck, Darmstadt, Germany). PL standards as well as 15(*S*)-HETE, 15(*S*)-HEPE, 17(*S*)-HDHA, and 13(*S*)-HODE were from Cayman Chemical (Ann Arbor, MI, USA; local supplier: Biomol, Hamburg, Germany). Ultra-pure H_2O (18.2 MΩ cm) was generated using the Barnstead Genpure Pro system from Thermo Fisher Scientific (Langenselbold, Germany). Ammonium formate was supplied by Sigma-Aldrich (Schnelldorf, Germany). Soybean 15-LOX (type I-B) and all other chemicals were purchased from Merck (Darmstadt, Germany).

HEK293T cells were obtained from the German Collection of Microorganisms and Cell Cultures GmbH (DSMZ, Braunschweig, Germany). Transfected HEK293T cells with doxycycline-inducible 15-LOX-2 expression using a sleeping beauty system characterized in [19] were used.

4.2.2 Preparation of oxidized phospholipid standards by soybean 15-LOX-1

OxPL standards were generated based on a protocol from Morgan *et al.* [37]. Briefly, individual PL standards were dried using nitrogen, then resuspended in 40 mmol L^{-1} borate buffer (pH = 9.0) and 10 mmol L^{-1} deoxycholate to a final concentration of 0.1 mmol L^{-1}. Soybean 15-LOX was added (5.2 kU mL^{-1}) and samples were incubated at room temperature for 2 h. Hydroperoxy-PUFA were reduced to the corresponding hydroxy-PUFA by adding 1.3 µmol of tin(II) chloride in H_2O and lipids were extracted using a mixture of MeOH and MTBE. The oxidized product was separated from its unoxidized precursor using RP-LC coupled to an ultraviolet spectroscopic detector. Chromatographic separation was achieved on a LiChrospher 100 C18 column (4.6 × 250 mm, 5 µm, 95 Å;

Bischoff) with a flow rate of 1 mL min^{-1}. A binary gradient (68% B to 100% B over 15 min, hold 100% B for 20 min) was used with eluent A (H_2O/MeOH, 95/5, v/v) and eluent B (MeOH/H_2O, 99/1, v/v), both containing 10 mmol L^{-1} ammonium formate. Elution of oxPL was monitored at 235 nm and the PL precursor at 205 nm. The concentration of the purified oxPL standards was determined by quantitative targeted LC-MS/MS analysis of oxylipins following alkaline hydrolysis [24, 38-40].

4.2.3 Extraction

A single cell pellet was used for the parallel analysis of total and non-esterified oxylipins, esterified oxylipins in lipid fractions, intact oxPL (Fig. 4.1), as well as peptides. Dry pellets were resuspended in 290 µL MeOH/H_2O (50/50, v/v), followed by the addition of 10 µL antioxidant/inhibitor mixture (10 µL 0.2 mg mL^{-1} BHT, 100 µmol L^{-1} indomethacin and 100 µmol L^{-1} t-AUCB) [24, 38-40]. Samples were vortexed and sonicated for 10 s. Protein content was determined from the cell homogenate by bicinchoninic acid assay [41, 42]. The concentrations of oxylipins and oxPL were calculated based on the amount of cellular protein.

Non-polar solid-phase extraction. Non-esterified and total oxylipins were extracted using an established procedure [24, 38-40], using 50 µL and 100 µL of cell suspension, respectively (Fig. 4.1A, B). Deuterium-labeled oxylipins (Cayman Chemicals, local supplier: Biomol, Hamburg, Germany) were added as IS. Protein precipitation was performed using 280 µL MeOH for non-esterified oxylipins and 400 µL IPA for total oxylipins. After centrifugation (4 °C, 10 min, 20,000 × g), the supernatant from the total oxylipin samples was hydrolyzed for 30 min at 60 °C with 100 µL 0.6 M KOH (H_2O/MeOH, 25/75, v/v) (Fig. 4.1B) [24]. Following alkaline hydrolysis, oxylipins were extracted using mixed-mode solid-phase extraction (SPE) with Bond Elut Certify II cartridges (C8 and anion exchange, 40 µm, 3 mL/200 mg; Agilent, Waldbronn, Germany) [24, 39]. For the extraction of non-esterified oxylipins (Fig. 4.1), the supernatant was directly applied to the SPE cartridges. After evaporation, the residues were reconstituted, sonicated, and analyzed by targeted metabolomics LC-MS/MS [24, 38-40].

Peptide digestion and extraction. Sample preparation was carried out as described [38]. In brief, the cell pellet obtained after the protein precipitation was re-dissolved in 5% w/v sodium deoxycholate containing 1% protease inhibitor mix (39102.02, SERVA Electrophoresis GmbH, Heidelberg, Germany), sonicated, and centrifuged (4 °C, 10 min, 15,000 × *g*). A solution containing 500 µg total protein was used for analysis. Proteins were precipitated and washed with four volumes of ice-cold acetone. Dried pellets were reconstituted in 6 mol L^{-1} urea to a final concentration of 5 mg mL^{-1}. The disulfide bridges were reduced for 1 h with 200 mmol L^{-1} dithiothreitol (in 50 mmol L^{-1} NH_4HCO_3), and the resulting free sulfhydryl groups were alkylated for 1 h with 200 mmol L^{-1} iodoacetamide (in 50 mmol L^{-1} NH_4HCO_3). Tryptic digestion using > 6.000 U g^{-1} trypsin from porcine pancreas (Merck 37286.03) was performed for 15 h at 37°C (pH ≈ 7.8). The digestion was stopped by the addition of concentrated acetic acid reducing the pH to 3 – 4. Heavy labeled peptides (lys: U-$^{13}C_6$; U-$^{15}N_2$; arg: U-$^{13}C_6$; U-$^{15}N_4$) serving as IS were added. Following centrifugation, peptides were extracted by SPE (Strata-X 33 µm polymeric reversed phase material, Phenomenex LTD, Aschaffenburg, Germany). After evaporation, the residues were reconstituted, sonicated, and analyzed by targeted proteomics LC-MS/MS (Fig. 4.2) [38].

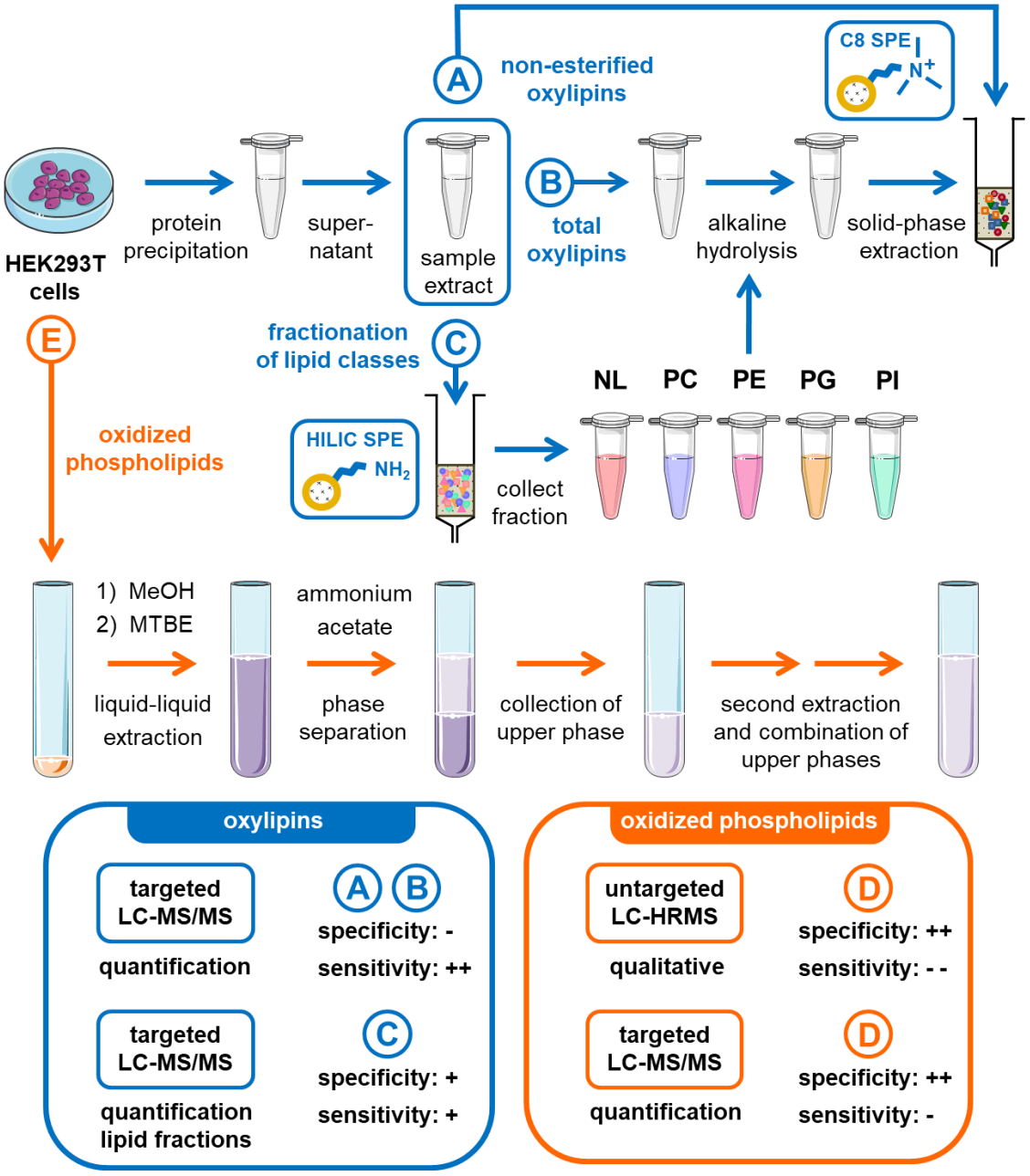

Fig. 4.1: Workflow of comprehensive oxylipin analysis. In **A** non-esterified oxylipins are analyzed directly. In **B** total oxylipins are analyzed and quantified as non-esterified oxylipins following hydrolysis. **C** To quantify oxylipins bound in different PL, the lipids were fractionated by HILIC-SPE prior to hydrolysis, followed by the quantification of esterified oxylipins in each fraction. In **D** PL bearing oxylipins are analyzed directly.

HILIC-based solid-phase extraction. Lipids were fractionated into distinct lipid classes using HILIC-based SPE with CHROMABOND cartridges (aminopropyl-modified silica, 45 µm, 3 mL/500 mg; Machery-Nagel, Düren, Germany) (Fig. 4.1C) [43-45]. Briefly, 400 µL of ice-cold IPA was added to 50 µL suspension of sonicated cells. Samples were vortexed and frozen at – 80 °C for at least 30 min. Cartridges were preconditioned with 6 mL of H_2O/ACN (5/95, v/v). Following centrifugation (4 °C, 10 min, 20,000 × g), the supernatant of the sample was diluted on the cartridge with 1 mL of ACN. NL fraction including monoacylglycerides, DG, TG, Chol Ester, and ceramides was eluted with 4.5 mL of H_2O/ACN (5/95, v/v). The second fraction containing all choline-bearing PL (i.e., lysoPC, PC, and SM) was collected with 5.5 mL of H_2O/ACN (11/89, v/v). The fraction comprising lysoPE and PE was isolated using 12 mL of MeOH with 0.1% acetic acid. Non-esterified FA and oxylipins were washed off with 18 mL MeOH containing 0.1% acetic acid. PG were isolated with 12 mL of H_2O/ACN/IPA (6/18/76, v/v/v), and PI/PS were simultaneously eluted using 12 mL of H_2O/ACN/IPA (20/35/45, v/v/v). Elution of the individual lipid fractions was conducted under slight vacuum (~ 900 mbar) in glass tubes containing 8 µL of 30% glycerol in MeOH. Following evaporation to dryness, residues of each fraction were reconstituted in IPA. Esterified oxylipins in each lipid fraction – PI/PS, PE, PC, PG, and NL – were quantified following alkaline hydrolysis as described above.

Liquid-liquid extraction. Lipids were extracted from the HEK293T cells using a modified LLE based on Matyash *et al.* [46] with slight modifications described in [47] (Fig. 4.1D). Briefly, 50 µL suspension of sonicated cells (i.e., 0.38 mg protein) was transferred to 3 mL glass tubes. 2.5 pmol of each IS (i.e., PI 12:0/13:0, PC 12:0/13:0, and PE 12:0/13:0) were added, yielding a final concentration of 50 nmol L^{-1} in the lipid extract. Lipids were extracted using a mixture of MeOH and MTBE. After extraction and evaporation, the dried residue was reconstituted in 50 µL of IPA/ACN (50/50, v/v) containing 50 nmol L^{-1} PG 12:0/13:0 as IS2 used to calculate the extraction recovery of IS. The extracts were sonicated and directly used for oxPL LC-MS measurement.

4.2.4 LC-MS/MS analysis

Targeted analysis of oxylipins. Targeted LC-MS/MS analysis of oxylipins was carried out using a 1290 Infinity II (Agilent, Waldbronn, Germany) LC system coupled to a QTRAP 5500 mass spectrometer (Sciex, Darmstadt, Germany) as described [24, 38-40]. The injection volume was 5 µL. Chromatographic separation was carried out on a ZORBAX Eclipse Plus C18 column (2.1 × 150 mm, 1.8 µm, 95 Å; Agilent) equipped with a guard column (2.1 × 2 mm, 1.8 µm) at 40 °C. A binary gradient was used with eluent A (0.1% acetic acid in H_2O/eluent B, 95/5, v/v*)* and eluent B (ACN/MeOH/acetic acid, 800/150/1, v/v/v). Oxylipins were separated using the following gradient with a flow rate of 300 µL min^{-1}: 0–1.0 min 21% B; 1.0–1.5 min 21–26% B; 1.5–10 min 26–51% B; 10–19 min 51–66% B; 19–25.1 min 66–98% B; 25.1–27.6 min 98% B; 27.6–27.7 min 21% B; 27.7–31.5 min 21% B. MS detection of oxylipins was performed in scheduled selected reaction monitoring mode following ESI(-). Oxylipins were quantified using external calibrations with IS (Fig. 4.3).

Targeted analysis of peptides. Analysis of peptides was carried out using a 1290 Infinity II (Agilent, Waldbronn, Germany) LC system coupled to a QTRAP 6500+ mass spectrometer (Sciex, Darmstadt, Germany) as described [1]. Chromatographic separation was carried out on a ZORBAX Eclipse Plus C18 column (2.1 × 150 mm, 1.8 µm, 95 Å; Agilent) equipped with a guard column (2.1 × 2 mm, 1.8 µm) at 40 °C. A binary gradient was used with eluent A (H_2O/ACN, 95/5, v/v) and eluent B (H_2O/ACN, 5/95, v/v), both containing 0.1% acetic acid. Peptides were separated using the following gradient with a flow rate of 300 µL min^{-1}: 0–1.0 min 0% B; 1.0–30.5 min 0–35% B; 30.5–30.6 min 35–100% B; 30.6–33.5 min 100% B; 33.5–33.7 min 100–0% B; 33.7–36 min 0% B. MS detection of peptides was performed in scheduled MRM mode following positive ESI. Peptides were quantified using external calibrations with IS, and concentrations were normalized on the amount of cellular protein (Fig. 4.2).

Untargeted analysis of oxPL. Untargeted LC-HRMS analysis of oxPL was carried out as described [47] on a Vanquish Horizon high-performance LC system coupled to a hybrid quadrupole-orbitrap mass spectrometer (Q Exactive HF; Thermo Fisher Scientific, Dreieich, Germany). The injection volume was 5 µL. Chromatographic separation was carried out on an ACQUITY Premier CSH C18 column (2.1 × 100 mm, 1.7 µm, 130 Å; Waters, Eschborn, Germany) equipped with a guard column (2.1 × 5 mm, 1.7 µm) at 40 °C. A binary gradient was used with eluent A (H_2O/ACN, 60/40, v/v) and eluent B (IPA/ACN, 80/20, v/v, + 1% H_2O), both containing 10 mmol L^{-1} ammonium formate and 0.1% formic acid. Lipids were separated using the following gradient with a flow rate of 260 µL min^{-1}: 0–0.7 min 30% B; 0.7–0.8 min 30–57.5% B; 0.8–9 min 57.5% B; 9–22 min 57.5–68% B; 22–24 min 68–99% B; 24–28 min 99% B; 28–30 min 30% B. Lipids were analyzed in Full MS Full MS/$ddMS^2$ TOP 15 mode following ESI(-) mode. The Full MS scans were recorded over a mass range of *m/z* 200 – 1200 at a resolution setting of 120,000 and $ddMS^2$ spectra were acquired at a resolution setting of 15,000. For data acquisition and instrument control Chromeleon software (version 7.2.11, Thermo Fisher Scientific) was used. OxPL species were characterized as described in [47] based on precursor ion, product ions, and retention time using Freestyle software (version 1.8, Thermo Fisher Scientific) (Fig. 4.4).

Targeted analysis of oxPL. Targeted LC-MS/MS analysis of oxPL was carried out using a 1290 Infinity II (Agilent, Waldbronn, Germany) LC system coupled to a QTRAP 6500+ mass spectrometer (Sciex, Darmstadt, Germany). The injection volume was 5 µL. Lipids were separated using the ACQUITY Premier CSH C18 column with the same eluents and gradient conditions as the untargeted LC-HRMS method, see above. MS detection was performed in negative ESI mode with the following settings: ion spray voltage − 4500 V, source temperature 650 °C, nebulizer gas (gas 1, compressed air purified with RAMS05Z; CMC instruments, Eschborn, Germany) 60 psi and drying gas (gas 2, purified compressed air) 60 psi, curtain gas (nitrogen, generated with the nitrogen generator Eco Inert-ESP4; DWT, Bottrop, Germany) 35 psi, collision gas (nitrogen) 6 psi.

MS detection was carried out in scheduled MRM mode acquiring three transitions per oxPL: two for qualification and one for quantification resulting from the specific cleavage of the oxidized fatty acyl chains. The detection window was set to 120 s around the retention time and the (maximum) cycle time to 1 s. The CE was optimized for each of the oxPL. The declustering potential, entrance potential, and collision cell exit potential were – 50 volts, – 2 volts, and – 10 volts, respectively, as these parameters have a minor impact on the signal intensity. MS parameters for targeted oxPL analysis can be found in Table 4.1 and Table 8.14. Analyst (Sciex, version 1.7) was used for instrument control and data acquisition, and Multiquant (Sciex, version 2.1.1) for data evaluation.

For calibration, individual oxPL standards were mixed and diluted in ACN/IPA (50/50, v/v) at 11 concentration levels. Each calibration level contained the same amount of the IS (PI 12:0/13:0, PC 12:0/13:0, and PE 12:0/13:0; 50 nmol L^{-1} for each). Linear calibration was carried out using linear least square regression (weighting: $1/x^2$). Analyte quantification was done based on the analyte to corresponding IS peak area ratio using the obtained linear calibrations. All standards are listed in Table 4.2 and Table 8.15, and the concentration of oxPL in oxylipin-supplemented cells and in 15-LOX-2 overexpressing cells can be found in Table 8.16.

4.2.5 Method characterization of targeted analysis of oxPL

The LC-MS/MS method was characterized and validated regarding sensitivity (LOD and LLOQ), linearity, extraction recovery, intra- and inter-day accuracy and precision, and dilution integrity (Fig. 4.5, 4.6, 4.7, 4.8, 4.9 and Tables 4.2, 4.3, 8.17, 8.18) based on criteria of the Guideline on bioanalytical method validation of the International Council for Harmonization [48]. Resulting concentrations of oxPL obtained by the targeted LC-MS/MS method were compared to an established oxylipin LC-MS/MS method (Fig. 4.10).

4.2.6 Cell culture

HEK293T cells were cultivated in DMEM high glucose (4.5 g L^{-1}) supplemented with 10% (v/v) FCS, 100 U mL^{-1} penicillin, 100 µg mL^{-1} streptomycin, and 1 mmol L^{-1} sodium pyruvate in a humidified atmosphere with 5% CO_2 at 37 °C. In 10 cm^2 dishes, 5 × 10^6 cells were seeded and cultivated for 24 h to allow cell adhesion. Following 24 h, the medium was replaced with 10 mL of fresh serum-free medium. For supplementation, 10 µL of either 15(*S*)-HETE, 15(*S*)-HEPE, 17(*S*)-HDHA, or 13(*S*)-HODE in DMSO was directly spiked into the medium leading to a final concentration of 300 nmol L^{-1} (0.1% DMSO) and incubated for 2 h [47]. Cells were harvested by scraping in ice-cold PBS.

HEK293T cells were transfected with 15-LOX-2 using the sleeping beauty system [49] described in [19] using the pSBtetmChP_15-LOX-2 plasmid for construct. This plasmid results in a silenced gene expression until doxycycline treatment and also contains the mCherry gene as a fluorescent marker and a puromycin resistance gene for positive selection. In a 6-well plate, 1 × 10^5 HEK293T cells were seeded and allowed to adhere for 24 h. The medium was replaced with 2 mL of fresh medium followed by the addition of the transfection mixture containing the plasmid (2.5 µg), a second plasmid carrying the SB100X transposase gene (0.25 µg), and polyethylenemine (12.5 µg). Stable transfection of cells was performed for 16 h. The medium was exchanged with fresh medium containing 2.5 µg mL^{-1} puromycin and homogenous mCherry expression was checked by fluorescence.

To induce 15-LOX-2 overexpression in transfected HEK293T_15-LOX-2 cells, 5 × 10^6 cells were seeded and cultivated for 24 h to allow cell adhesion. The medium was replaced after 24 h with 10 mL of fresh medium containing 200 ng mL^{-1} doxycycline for 24 h (0.1% DMSO). Cells were harvested by scraping in ice-cold PBS. Overexpression of 15-LOX-2 in HEK293T_15-LOX-2 cells was characterized by quantification of the enzyme level of 15-LOX-2 and concentration levels of 15-LOX-2 oxylipin products using combined targeted LC-MS/MS proteomics [38, 50] and oxylipin metabolomics [24, 38-40] (Fig. 4.2).

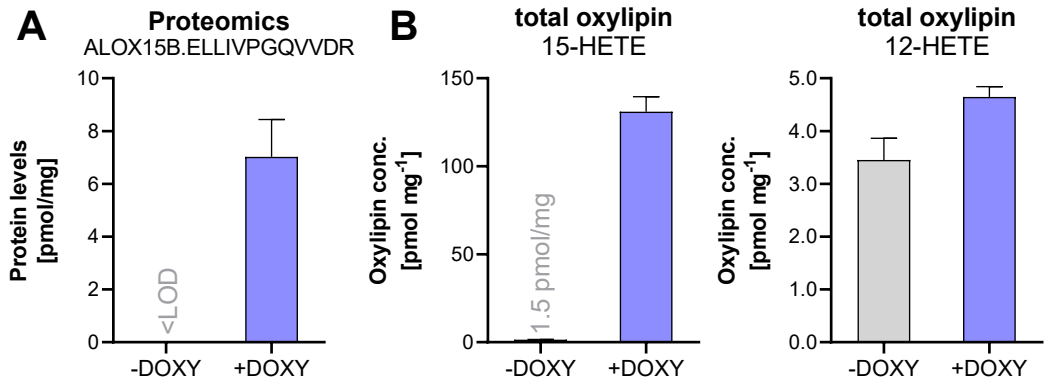

Fig. 4.2: Characterization of 15-LOX-2 overexpression induced by doxycycline in HEK293T cells transfected with 15-LOX-2 using combined targeted proteomics and oxylipin metabolomics. Shown are **A** protein level of expressed 15-LOX-2 and **B** total oxylipin concentration of (left) 15-HETE and (right) 12-HETE of the HEK293T cells inducible transfected with 15-LOX-2 with and without incubation of doxycycline (DOXY) (200 ng mL^{-1}, 24 h). ALOX15B peptides were measured following tryptic digestion by targeted LC-MS/MS proteomics [38, 50]. Total oxylipins were analyzed following alkaline hydrolysis by targeted LC-MS/MS [24, 38-40]. Shown is the mean concentration ± SD per mg cellular protein (n = 3).

4.2.7 Lipid notation

Oxylipins in human HEK293T cells were analyzed using a combination of indirect and direct LC-MS approaches (Fig. 4.1). The terms “indirect quantification” or “indirect analysis” refer to the measurement of esterified oxylipins as non-esterified by targeted LC-MS/MS following alkaline hydrolysis (Fig. 4.1B, C). The terms “direct quantification” or “direct analysis” refer to the measurement of esterified oxylipins as oxPL using untargeted LC-HRMS [47] or the targeted LC-MS/MS method developed in this work (Fig. 4.1D).

The notations 15-HETE, 15-HEPE, 17-HDHA, and 13-HODE are used when identification was confirmed using authentic standards (i.e., oxylipin or oxPL), whereas the notations 20:4;15OH, 20:5;15OH, 22:6;17OH, and 18:2;13OH are used when authentic standards of the oxylipin-containing species were not available. Furthermore, the notations 15(*S*)-HETE, 15(*S*)-HEPE, 17(*S*)-HDHA, and 13(*S*)-HODE are used only to describe the supplemented (enantiopure) oxylipins.

4.3 Results and discussion

4.3.1 Incorporation of oxylipins into phospholipid classes

Oxylipins − especially hydroxy-PUFA − are mainly found esterified to lipids in biological samples [19-21, 51]. However, information in which lipid class hydroxy-PUFA are bound is scarce and has been described only in studies following oxylipin-supplementation [25-32, 47]. We aimed to investigate in which PL classes of the HEK293T cell line the 15-LOX products 15(*S*)-HETE, 15(*S*)-HEPE, 17(*S*)-HDHA, and 13(*S*)-HODE are incorporated (Fig. 4.3).

Quantitative targeted analysis unveiled that the baseline concentration of total 15-HETE, 15-HEPE, 17-HDHA, and 13-HODE is ≤ 4.0 pmol mg^{-1} protein, with non-esterified concentrations below 0.48 pmol mg^{-1} (Fig. 4.3A). Following supplementation (300 nmol L^{-1}, 2 h), levels of the added hydroxy-PUFA increased to 40 – 270 pmol mg^{-1}. 97% of 15-HETE and 15-HEPE occurred esterified and showed similar incorporation rates of 20 ± 2% and 21.4 ± 0.3% of the added amount, respectively. While 17-HDHA and 13-HODE were also only detected esterified (> 97%) but were incorporated with lower amounts (12.8 ± 0.7% and 3.4 ± 0.3%, respectively). Alpert *et al.* [29] also found by TLC a comparable incorporation rate of 29 ± 5% in human tracheal epithelial cells following a 2 h incubation with 1 µmol L^{-1} of [^{3}H]15(*S*)-HETE. Concentrations of hydroxy-PUFA formed endogenously via 15-LOX-2 using a genetically modified HEK293T cell line were in the same order of magnitude. Most oxylipins (> 97%) in the cells were esterified, which is consistent with our previous works showing that 15-HETE and other hydroxy-PUFA such as 12-HETE and 5-HETE occur in cells esterified at baseline, following supplementation, and endogenous formation by 15-LOX [19, 47].

Using HILIC fractionation [43-45], we found that > 75% of the hydroxy-PUFA were bound to polar lipids i.e. lysoPL and PL and less than 25% were esterified into NL such as DG, TG, and Chol Ester (Fig. 4.3B). Following supplementation (300 nmol L^{-1}, 2 h), incorporation of hydroxy-PUFA in NL was higher compared to oxylipins endogenously formed by 15-LOX-2, especially for 15-HEPE with 25% in NL *vs.* 2.8% in cells overexpressing 15-LOX-2. For 15-HETE, 17-HDHA, and 13-HODE smaller differences (< 10%) were found between supplementation and endogenous formation. This is consistent with earlier reports showing that 15-HETE incorporation in both PL and PI is saturable in human tracheal epithelial and that increased amounts of [H^3]15-HETE were found in NL above 1 µmol L^{-1} supplementation [29]. In our study, the concentrations of 15-HETE and 15-HEPE following supplementation were higher compared to 15-LOX-2 endogenous formation, e.g., for 15-HEPE with 270 pmol mg^{-1} *vs.* 55 pmol mg^{-1} in 15-LOX-2 overexpressing cells (Fig. 4.3A). When a lower concentration was used for supplementation (i.e., ~ 50 nmol L^{-1}, 2 h), fewer hydroxy-PUFA were incorporated in NL and the proportion was similar to the one in 15-LOX-2 expressing cells (Appendix Table 8.19). These results indicate the incorporation of 15-HETE and 15-HEPE into PL via specific mechanisms that can be saturated.

Oxylipins were distinctly incorporated into PL classes, i.e. PI/PS, PE, and PC. Only very low amounts were bound to PG. Despite minor differences, the incorporation patterns of hydroxy-PUFA into PL classes were comparable at baseline concentration, following supplementation, and in cells overexpressing 15-LOX-2 (Fig. 4.3B): The majority of 15-HETE and 15-HEPE were found in PI/PS, while more than half of 17-HDHA was detected in PE and over half of 13-HODE was found in PC. Following supplementation, 178 ± 8 pmol mg^{-1} (95%) of 15-HETE was found in PI/PS, and 90 ± 10 pmol mg^{-1} (84%) of endogenously formed 15-HETE was incorporated into PI/PS. Incorporation of 15-HETE into other PL classes was minor in both supplemented cells and 15-LOX-2 overexpressing cells, with 8.4 ± 0.9 pmol mg^{-1} *vs.* 15 ± 1 pmol mg^{-1}, respectively, in the sum of PC and PE.

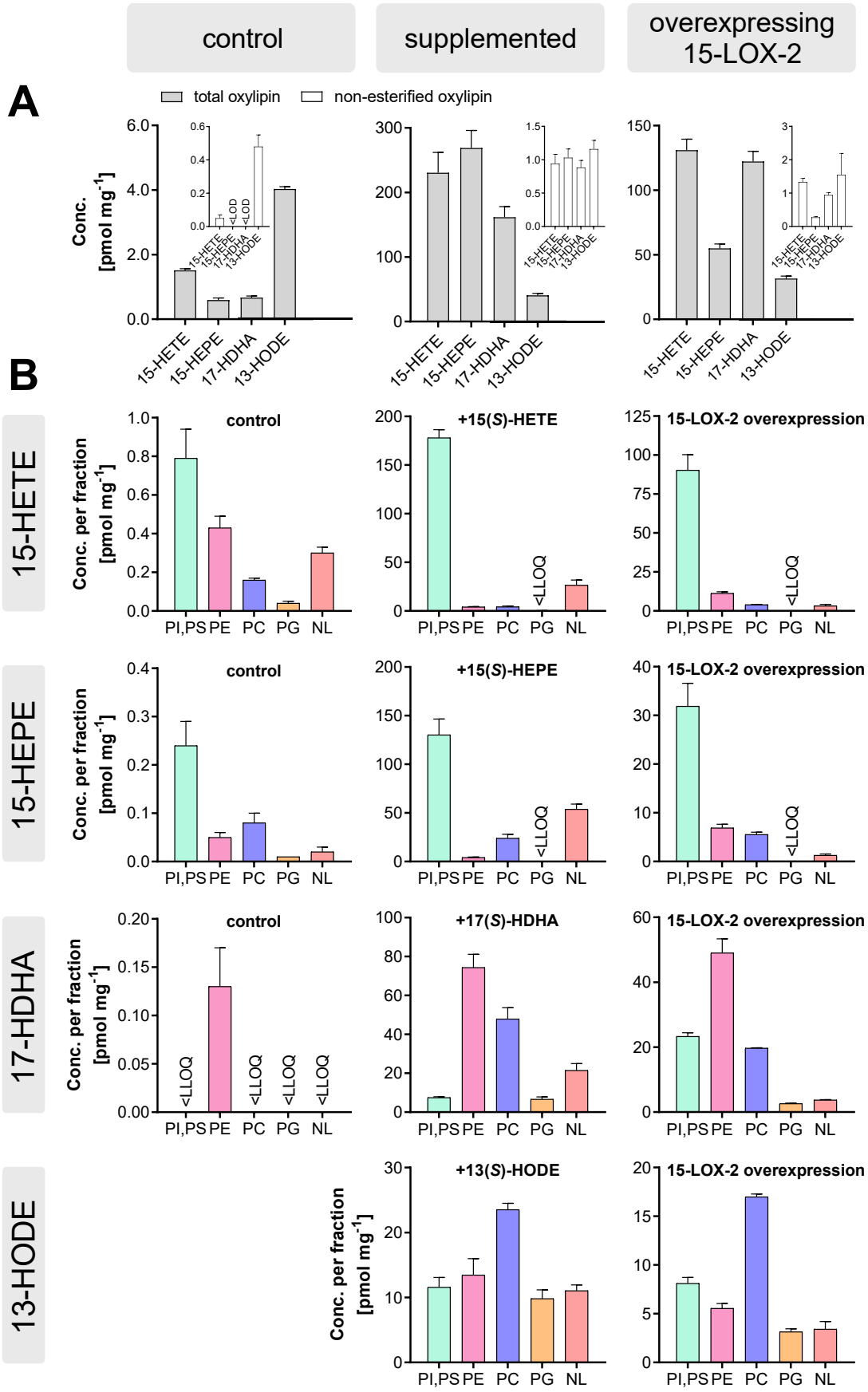
control
supplemented
overexpressing 15-LOX-2
A
total oxylipin
non-esterified oxylipin
Conc. [pmol mg-1]
<LOD
15-HETE
15-HEPE
17-HDHA
13-HODE
B
15-HETE
15-HEPE
17-HDHA
13-HODE
Conc. per fraction [pmol mg-1]
control
+15(S)-HETE
15-LOX-2 overexpression
+15(S)-HEPE
+17(S)-HDHA
+13(S)-HODE
<LLOQ
PI,PS
PE
PC
PG
NL

Fig. 4.3: (Previous page) Incorporation of oxylipins in distinct lipid classes at baseline, following supplementation, and following overexpression of 15-LOX-2 in HEK293T cells. 5×10^6 HEK293T cells were used per experiment. (**left column**) HEK293T cells treated with 0.1% DMSO as controls. (**middle column**) HEK293T cells supplemented with either 15(*S*)-HETE, 15(*S*)-HEPE, 17(*S*)-HDHA, or 13(*S*)-HODE (300 nmol L^{-1}, 2 h). (**right column**) Endogenous formation of oxPL elicited by overexpression of 15-LOX-2 in HEK293T_15-LOX-2 cells (200 ng mL^{-1} doxycycline, 24 h). Oxylipins were analyzed as non-esterified following alkaline hydrolysis by targeted LC-MS/MS method. Shown are the concentrations per mg cellular protein of **A** non-esterified and total oxylipins and **B** esterified oxylipins in each HILIC-separated lipid fraction (mean ± SD (n = 3)). At baseline concentration, 13-HODE is not shown due to interferences caused by a contamination occurring in the HILIC-based cartridges.

15-HEPE presented a similar distribution between the PL classes (Fig. 4.3B): 32 ± 5 pmol mg^{-1} (72%) of 15-HEPE was in PI/PS, 6.9 ± 0.7 pmol mg^{-1} in PE, and 5.5 ± 0.5 pmol mg^{-1} in PC in cells overexpressing 15-LOX-2. For both 15-HETE and 15-HEPE, incorporation into PE was higher in 15-LOX-2 overexpressing cells compared to cells supplemented with oxylipins: 11% and 16%, respectively, of endogenously formed 15-HETE and 15-HEPE was found in PE *vs.* 2.0% and 1.6% following supplementation. At baseline concentration, 17-HDHA was only detected in PE, likely due to its low concentration i.e. 0.13 pmol mg^{-1} close to the LLOQ. Following supplementation and endogenous formation by 15-LOX-2, most 17-HDHA was also found in PE, 74 ± 7 pmol mg^{-1} (55%) and 49 ± 4 pmol mg^{-1} (52%), respectively. One noticeable difference was observed in the incorporation pattern of 17-HDHA: endogenously formed 17-HDHA was more incorporated into PI/PS with 23 ± 1 pmol mg^{-1} (25%) *vs.* 7.5 ± 0.4 pmol mg^{-1} (5.5%) following supplementation. PI/PS were also the second most abundant PL classes for 13-HODE incorporation, with 8.1 ± 0.6 pmol mg^{-1}, but the major part of 13-HODE was detected in PC with 17.0 ± 0.3 pmol mg^{-1} (50%) in 15-LOX-2 overexpressing cells. In 13(*S*)-HODE-supplemented cells, 23 ± 1 pmol mg^{-1} (40%) and 12 ± 2 pmol mg^{-1}, were found in PC and PI, respectively.

In this work, we demonstrate for the first time that 15-LOX products show a distinct incorporation pattern into PL, and we also show the incorporation of 17-HDHA and 15-HEPE into lipids which was not previously described. Importantly, we demonstrate this pattern not only following supplementation, as carried out for labeled 15-HETE and 13-HODE in the 1990s [25-32], but also for oxylipins endogenously formed by 15-LOX-2. Because our method also allows us to detect unlabeled lipids, we demonstrate that endogenously formed hydroxy-PUFA, at baseline or upon 15-LOX-2 activity show a comparable incorporation pattern, highlighting the biological relevance of these findings.

4.3.2 Direct analysis of oxidized phospholipids

Indirect analysis of oxPL in lipid fractions in HEK293T cells unveiled that 15-HETE, 15-HEPE, 17-HDHA, and 13-HODE are incorporated into specific polar lipid classes. Based on this finding, we aimed to characterize and quantify the PL molecular species into which the oxylipins are incorporated.

Therefore, we developed a targeted LC-MS/MS method for the direct analysis of PL bearing hydroxy-PUFA in HEK293T cells based on an established untargeted LC-HRMS method [47] (Fig. 4.4): OxPL were screened in Full MS/ddMS^2 mode in lipid cell extracts and characterized based on MS^2 spectra and retention time as described in [47] (Fig. 4.4A, C). Notably, no oxylipins were found esterified in PL with a sphingosine backbone, i.e., SM. Untargeted LC-HRMS detected the hydroxy-PUFA bound to PI, PC, PE, PC-P, PC-O, and PE-P lipid classes but none in lysoPL, PS, or PG (Fig. 4.4A). The detected PL bear 16:0, 16:1, 18:0, and 18:1 in the *sn*-1 position and 18:2;13OH, 20:4;15OH, 20:5;15OH, 22:4;17OH, 22:5;17OH, and 22:6;17OH in the *sn*-2 position. The most relevant oxPL species were included in the targeted LC-MS/MS method.

Three mass transitions were selected to monitor product ions corresponding to (i) the saturated FA, (ii) the oxPUFA, and (iii) the characteristic product ion resulting from the α-cleavage of the oxPUFA at the hydroxy group (Fig. 4.4D): For example, PI 18:0/20:4;15OH was detected with the mass transitions *m/z* 901.5 → 319.2, *m/z* 901.5 → 283.2, and *m/z* 901.5 → 219.2. In total, 67 oxPL species from six different PL classes (i.e., PI, PC, PE, PC-P, PC-O, and PE-P) were included in the targeted MRM method (Table 4.1, Table 8.14).

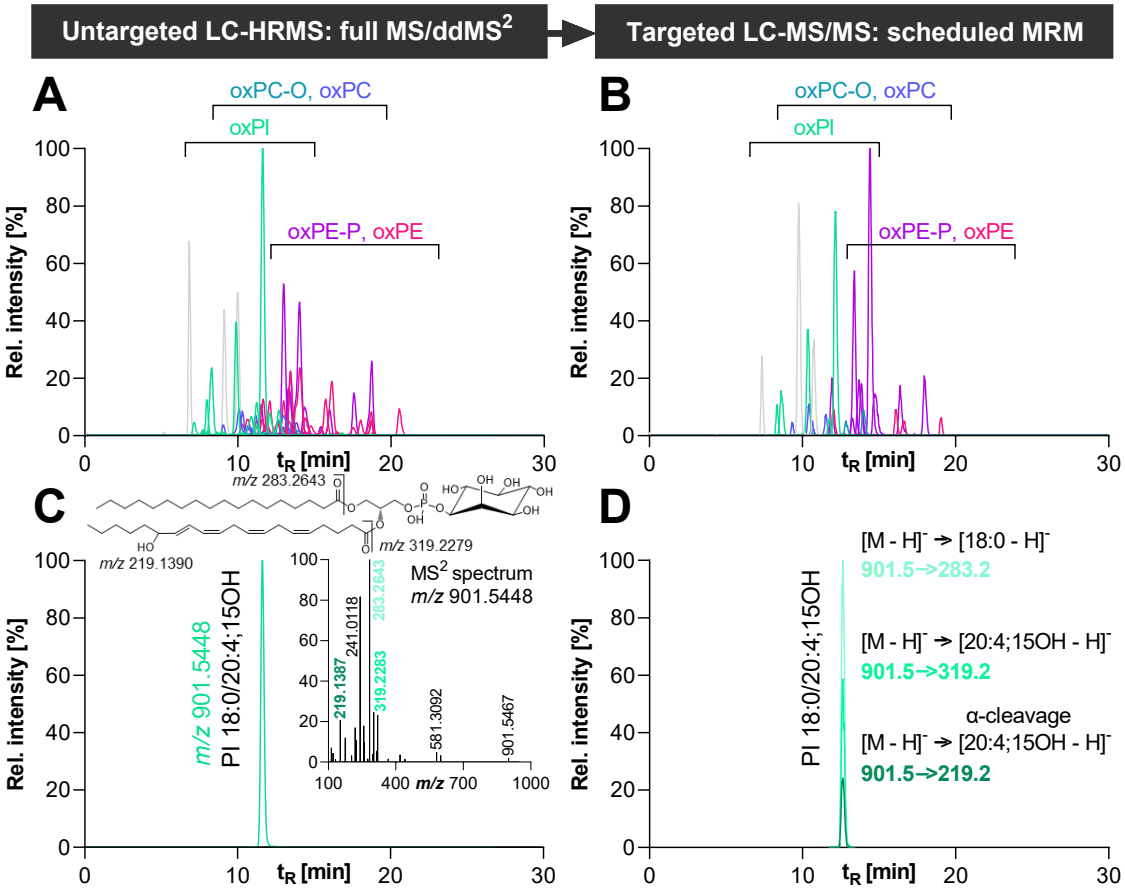

Fig. 4.4: Development of a targeted LC-MS/MS method based on an untargeted LC-HRMS method. Shown is the detection in ESI(-) mode of PL bearing hydroxy-PUFA in 15-LOX-2 overexpressing HEK293T_15-LOX-2 cells (200 ng mL^{-1} doxycycline, 24 h): **A** untargeted LC-HRMS in full MS/ddMS^2 mode (Q Exactive HF) **B** by targeted LC-MS/MS in scheduled MRM (QTRAP 6500+). **C** HRMS-extracted ion chromatogram as well as MS^2 spectrum and **D** MS/MS MRM chromatograms of PI 18:0/20:4;15OH.

Table 4.1: Parameters of the targeted LC-ESI(-)-MS/MS method. Shown are the mass transitions used for quantification in scheduled MRM method, CE, and t_R. Transitions used for qualification are depicted in Table 8.14.

Analyte	Mass transition		CE	t_R
	Q1	Q3		[min]
PI 16:0/18:2;13OH	849.5	195.2	-65	8.39
PI 18:0/18:2;13OH	877.6	195.2	-65	12.60
PI 16:0/20:4;15OH	873.5	219.2	-55	8.77
PI 16:0/20:5;15OH	871.5	219.2	-55	7.79
PI 18:0/20:4;15OH	901.5	219.2	-55	12.60
PI 18:1/20:4;15OH	899.5	219.2	-55	9.08
PI 18:0/20:5;15OH	899.5	219.2	-55	10.81
PI 16:0/22:5;17OH	899.5	247.2	-55	9.34
PI 18:1/20:5;15OH	897.5	219.2	-55	8.04
PI 16:0/22:6;17OH	897.5	201.3	-55	8.50
PI 18:0/22:5;17OH	927.6	247.2	-60	13.00
PI 18:0/22:6;17OH	925.5	201.3	-60	12.16
PI 18:1/22:6;17OH	923.5	201.3	-55	8.80
PC 16:0/18:2;13OH	818.5	195.1	-60	10.87
PC 16:1/18:2;13OH	816.5	195.2	-60	7.96
PC 18:0/18:2;13OH	846.6	195.1	-60	15.31
PC 18:1/18:2;13OH	844.6	195.1	-60	11.20
PC 16:0/15-HETE	842.4	219.2	-50	11.80
PC 16:0/20:5;15OH	840.5	219.2	-50	9.79
PC 18:0/15-HETE	870.6	219.2	-55	16.36
PC 16:0/22:5;17OH	868.5	247.2	-50	11.95
PC 18:0/15-HETE	868.5	219.2	-50	14.07
PC 18:1/20:5;15OH	866.4	219.2	-50	10.37
PC 16:0/17-HDHA	866.4	201.3	-50	11.08
PC 18:0/DH-17-HETE	898.5	247.3	-55	18.70
PC 18:1/22:5;17OH	894.5	247.2	-55	12.64
PC 18:0/17-HDHA	894.5	201.3	-55	15.53
PC 18:1/22:6;17OH	892.6	201.3	-50	11.74
PC P-16:0/18:2;13OH	802.6	195.1	-60	12.55
PC P-16:0/20:4;15OH	826.6	219.2	-50	13.16
PC P-16:0/22:5;17OH	852.6	247.2	-55	14.20
PC O-16:0/18:2;13OH	804.6	195.1	-60	13.30
PC O-16:0/20:4;15OH	828.6	219.2	-50	13.92
PC O-18:1/20:4;15OH	854.6	219.2	-55	14.22
PC O-16:0/22:5;17OH	854.6	247.2	-55	14.44
PC O-16:0/22:6;17OH	852.6	201.3	-50	13.44
PC O-18:1/22:5;17OH	880.6	247.2	-55	14.70

Table 4.1: Continued. Parameters of the targeted LC-ESI(-)-MS/MS method.

Analyte	Mass transition		CE	t_R
	Q1	Q3		[min]
PC O-18:1/22:6;17OH	878.6	201.3	-60	13.75
PE 16:0/18:2;13OH	730.5	195.2	-50	11.81
PE 18:0/18:2;13OH	758.5	195.2	-55	16.32
PE 16:0/20:4;15OH	754.4	219.2	-45	12.40
PE 16:0/20:5;15OH	752.4	219.2	-40	10.85
PE 18:0/15-HETE	782.5	219.2	-45	17.10
PE 18:1/20:4;15OH	780.5	219.2	-45	12.86
PE 18:0/20:5;15OH	780.5	219.2	-45	15.32
PE 18:1/20:5;15OH	778.4	219.2	-45	11.27
PE 16:0/17-HDHA	778.4	201.3	-45	12.02
PE 18:0/DH-17-HETE	810.7	247.1	-48	19.50
PE 18:0/22:5;17OH	808.5	247.2	-45	17.83
PE 18:0/22:6;17OH	806.5	201.3	-45	16.51
PE 18:1/22:5;17OH	806.5	247.2	-50	13.41
PE 18:1/22:6;17OH	804.5	201.3	-45	12.45
PE P-16:0/18:2;13OH	714.5	195.2	-50	13.70
PE P-16:0/20:4;15OH	738.5	219.2	-45	14.29
PE P-16:0/20:5;15OH	736.5	219.2	-40	12.36
PE P-18:0/20:4;15OH	766.5	219.2	-45	19.27
PE P-16:0/DH-17-HETE	766.5	247.2	-45	16.84
PE P-18:1/20:4;15OH	764.5	219.2	-45	14.92
PE P-18:0/20:5;15OH	764.5	219.2	-40	17.25
PE P-16:0/22:5;17OH	764.5	247.2	-45	14.86
PE P-18:1/20:5;15OH	762.5	219.2	-45	12.98
PE P-16:0/22:6;17OH	762.5	201.5	-45	13.82
PE P-18:0/DH-17-HETE	794.6	247.2	-45	19.81
PE P-18:0/22:5;17OH	792.5	247.2	-45	19.50
PE P-18:1/22:5;17OH	790.5	247.2	-45	15.20
PE P-18:0/22:6;17OH	790.5	201.3	-45	18.44
PE P-18:1/22:6;17OH	788.5	201.3	-45	14.11
PI 12:0/13:0 (IS)	711.4	241.0	-48	7.56
PC 12:0/13:0 (IS)	680.4	213.0	-42	9.89
PE 12:0/13:0 (IS)	592.0	213.0	-38	10.84
PG 12:0/13:0 (IS)	623.2	213.0	-42	8.30

4.3.3 Method characterization and validation of the oxPL targeted analysis

Method performance

Quantification of the oxPL was carried out based on the analyte to corresponding IS area ratio using linear calibration. OxPC and oxPE species were quantified using identical standards or when not available, standards of the same lipid class and similar fatty acyl chain composition (Appendix Table 8.15). OxPI species were quantified using OxPC species standards with similar fatty acyl chain composition. PL bearing 18:2;13OH were quantified using PL standard containing 20:4;15OH, while PL bearing 22:5;17OH were quantified using PL standard containing 22:6;17OH. For oxPL species whose standard was not available, the relative concentration was determined using selected ion monitoring (SIM)/MRM measurements of both the lipid extracts and standard solutions, assuming similar ionization efficiency [52]. Based on that, a factor of the MRM signal was calculated for each analyte and corresponding compound used as standard (Appendix Table 8.15). IS was assigned for each oxPL species based on the polar head group: PI 12:0/13:0 for oxPI species, PC 12:0/13:0 for oxPC species, and PE 12:0/13:0 for oxPE species. For oxPI quantification, PI 12:0/13:0 was used as IS to calculate the area ratio for the calibration (Table 4.2).

The sensitivity of the method was evaluated by determining LOD and LLOQ based on S/N. The concentration yielding an S/N ≥ 3 was defined as LOD. Analytes showed an LOD ranging from 7.5 to 30 fmol (0.59 to 4.8 pg) on column, i.e. 1.5 to 12 nmol L^{-1} (Table 4.2). The concentration with an S/N ≥ 5 and an accuracy of 80 – 120% within the linear calibration was defined as LLOQ and set as the lowest concentration of the linear calibration. All oxPL were detected with an LLOQ in the same order of magnitude from 30 to 125 fmol (2.36 to 10 pg) on column, i.e. 6 to 25 nmol L^{-1} in the injected solution. Few studies have reported information about the LOD, LLOQ, and linear range of oxPL species. Linearity was assessed using standard solutions covering a concentration range from 0.75 to 1000 nmol L^{-1} (30 – 5000 fmol on column).

Table 4.2: Method characterization of the targeted LC-ESI(-)-MS/MS method. Shown are the t_R, the FWHM, the LOD (nmol L^{-1} in solution and fmol on column), the calibration range, the assigned IS, the R^2, and the slope of the linear calibration for standard oxPL.

analyte	t_R[a]	FWHM[a]	LOD[b]		calibration range	IS	R^2[e]	slope
					LLOQ[c] – [d]			
	[min]	[s]	[nmol L^{-1}]	[fmol]	[nmol L^{-1}]			
PC 16:0/17-HDHA	11.02 ± 0.03	12.9 ± 0.2	6.0	30	25 – 800	PC 12:0/13:0 PI 12:0/13:0	0.997 0.996	3.4E-04 1.1E-03
PC 16:0/15-HETE	11.42 ± 0.03	13.4 ± 0.5	6.0	30	12 – 800	PC 12:0/13:0 PI 12:0/13:0	0.997 0.996	6.1E-04 2.0E-03
PE 16:0/17-HDHA	11.97 ± 0.03	13.2 ± 0.3	6.0	30	12 – 800	PE 12:0/13:0	0.995	5.1E-03
PC 18:0/15-HEPE	14.04 ± 0.03	13.3 ± 0.2	6.0	30	12 – 800	PC 12:0/13:0 PI 12:0/13:0	0.995 0.997	6.6E-04 2.3E-03
PC 18:0/17-HDHA	15.54 ± 0.03	13.1 ± 0.5	6.0	30	12 – 800	PC 12:0/13:0 PI 12:0/13:0	0.997 0.996	3.3E-04 1.1E-03
PC 18:0/15-HETE	15.99 ± 0.03	12.9 ± 0.4	1.5	7.5	6 – 800	PC 12:0/13:0 PI 12:0/13:0	0.997 0.997	8.2E-04 2.7E-03
PE 18:0/15-HETE	17.01 ± 0.03	14.2 ± 0.1	1.5	7.5	6 – 800	PE 12:0/13:0	0.997	9.6E-03
PC 18:0/DH-17-HETE	18.43 ± 0.03	14.1 ± 0.5	6.0	30	12 – 800	PC 12:0/13:0	0.999	9.5E-04
PE 18:0/DH-17-HETE	19.49 ± 0.03	14.6 ± 0.2	1.5	7.5	6 – 800	PE 12:0/13:0	0.997	1.6E-02

[a] FWHM were determined as mean from standards with the concentration 125 nmol L^{-1} (n = 3)

[b] LOD was set to the lowest concentration yielding a S/N ratio ≥ 3.

[c] LLOQ was set to the lowest calibration standard injected yielding a S/N ratio ≥ 5 and an accuracy in the calibration curve within 100% ± 20%.

[d] concentration does not represent the end of the dynamic range, but is the highest calibration standard injected.

[e] Calibration was performed as linear weighted least square regression using 1/x2 weighting.

Few methods also investigated oxPL using a triple quadrupole mass spectrometer: Slatter *et al.* established a targeted method for 111 oxPL species in human platelets [35], Aoyagi *et al.* quantified 20 oxPL species in mouse peritoneal macrophages [53], and Nakanishi *et al*. analyzed 44 PC species bearing hydroxy-PUFA, hydroperoxy-PUFA, aldehyde-bearing PUFA, and carboxylated PUFA [54]. If provided, these methods had a similar sensitivity and linearity as the method developed here, but none of them includes all the important PL bearing hydroxy-PUFA as in the present study. Aoyagi *et al.* found a LOD of 10 fmol for oxPC and oxPE using a QTRAP6500 mass spectrometer and a linear range of 10 – 500 fmol on column [53]. Using a QTRAP4000 mass spectrometer, Nakanishi *et al.* reported a linear range of 50 – 100,000 fmol on column [54].

Choice of internal standards

IS are key for accurate quantification as they compensate for sample losses during extraction, ion suppression, correct for instrumental variability, and enhance the reproducibility. In untargeted lipidomics, at least one isotopically labeled IS is employed per lipid class. However, no deuterium (^{2}H, D)- or ^{13}C-labeled oxPL are commercially available. Therefore, unoxidized PL – either deuterium-labeled or containing odd-carbon fatty acyl chains – were evaluated regarding their suitability as IS (Fig. 4.5).

Comparison of recoveries of IS spiked to cell samples added prior or after post extraction showed acceptable losses of less than 20% during extraction for all IS tested (Fig. 4.5B, C, D). Adding the IS after sample preparation revealed relevant ion suppression effects for those potential IS (i.e., deuterium-labeled PL as well as PC 17:0/14:1 and PE 17:0/14:1) eluting after the elution window of oxPL (i.e., 20 min), with over 50% signal suppression (Fig. 4.5A, C, D). Therefore, these compounds are not suitable as IS. Within the early elution window of oxPL, from 7 to 11 min, ion suppression effects were minor (Fig. 4.5A, B): Using 0.76 mg of protein for LLE, the signals of PI, PC and PE

bearing 12:0 and 13:0 were partially suppressed (less than 20%) while no matrix effects were observed using 0.38 mg of protein. Thus, the three unoxidized PL i.e. PI, PC, and PE bearing 12:0 and 13:0, were chosen as IS. Moreover, the amount of sample was set to 0.38 mg protein for extraction because no apparent ion suppression effects were observed (Fig. 4.5B).

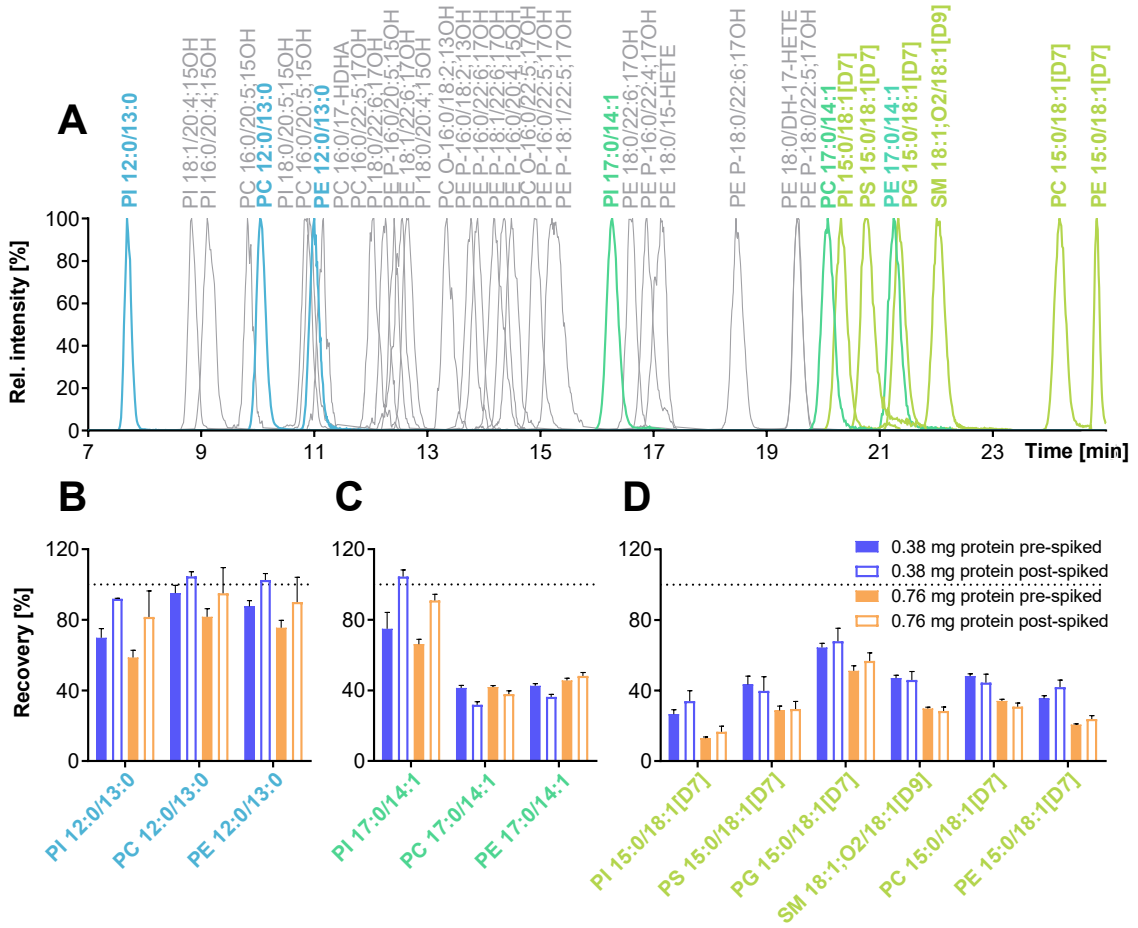

Fig. 4.5: Choice of IS. A Elution order of possible IS compared to PL bearing hydroxy-PUFA detected in HEK293T_15-LOX-2 cells overexpressing 15-LOX-2. In **B, C,** and **D,** the recoveries of the IS (2.5 pmol of each) added before or after sample preparation (pre- or post-spiked) were evaluated using different amounts of sample (0.38 mg protein or 0.76 mg protein). Shown is the mean ± SD (n = 3).

Our results showed that strong ion suppression effects occur after the elution window of oxPL, while minor matrix effects are observed in the early elution window of oxPL. This indicates that PL with short fatty acyl chains are suitable IS for oxPL. This is in line with previous studies where PE 14:0/14:0 was used as IS for the quantification of oxPL in human platelets [35] and mice organs

[34]. Also, PC 14:0/14:0 was used for the quantification of oxPC in human serum [55]. Aoyagi *et al.* used PI, PS, PG, PC, and PE all bearing 17:0 and 14:1 as IS for the analysis of oxPL in primary mouse peritoneal macrophages [53], but did not provide information about extraction recovery. In our hands, the signal of both PC 17:0/14:1 and PE 17:0/14:1 is partially suppressed by the HEK293T cell matrix (Fig. 4.5C) and thus are not suitable for the tested matrix. Because no isotopically labeled oxPL are available, the selection of PL as IS requires caution and their extraction recovery should be evaluated in the matrix using prior- and post-spiking experiments as described here.

Effect of sample amount on the concentration of endogenous oxPL

Investigation of recoveries of IS added at the end of the sample preparation allowed the selection of suitable IS for the analysis of oxPL (see above). Here we found no or minimal interference at a sample amount of 0.38 mg protein (Fig. 4.5B). In the next step, the effect of the sample amount was further characterized based on the determined apparent concentration of endogenous oxPL (Fig. 4.6A).

Analysis of samples containing 0.38 mg protein allowed a sensitive detection of oxPL in 15-LOX-2 overexpressing cells: A total of 40 oxPL species were quantified, while 0.76 mg protein led to the additional detection of 6 oxPL species. However, considerably fewer oxPL were detected when lower amounts of protein were used, with 30 oxPL species quantified at 0.19 mg protein and 20 oxPL species at 0.076 mg protein. Using different cellular protein amounts for LLE, consistent concentrations were obtained for 16 of the 20 detected oxPL, with less than 18% difference compared to the value obtained with 0.38 mg protein (Fig. 4.6A). For PE 18:0/22:6;17OH and PE 18:0/15-HETE, the use of 0.57 mg protein or more leads to deviations by ion suppression/enhancement effects, indicating that 0.38 mg protein or less should be analyzed. An unacceptable variation in concentrations was found for the last-eluting analyte, i.e., PE P-18:0/22:5;17OH, probably caused by ion enhancement effects.

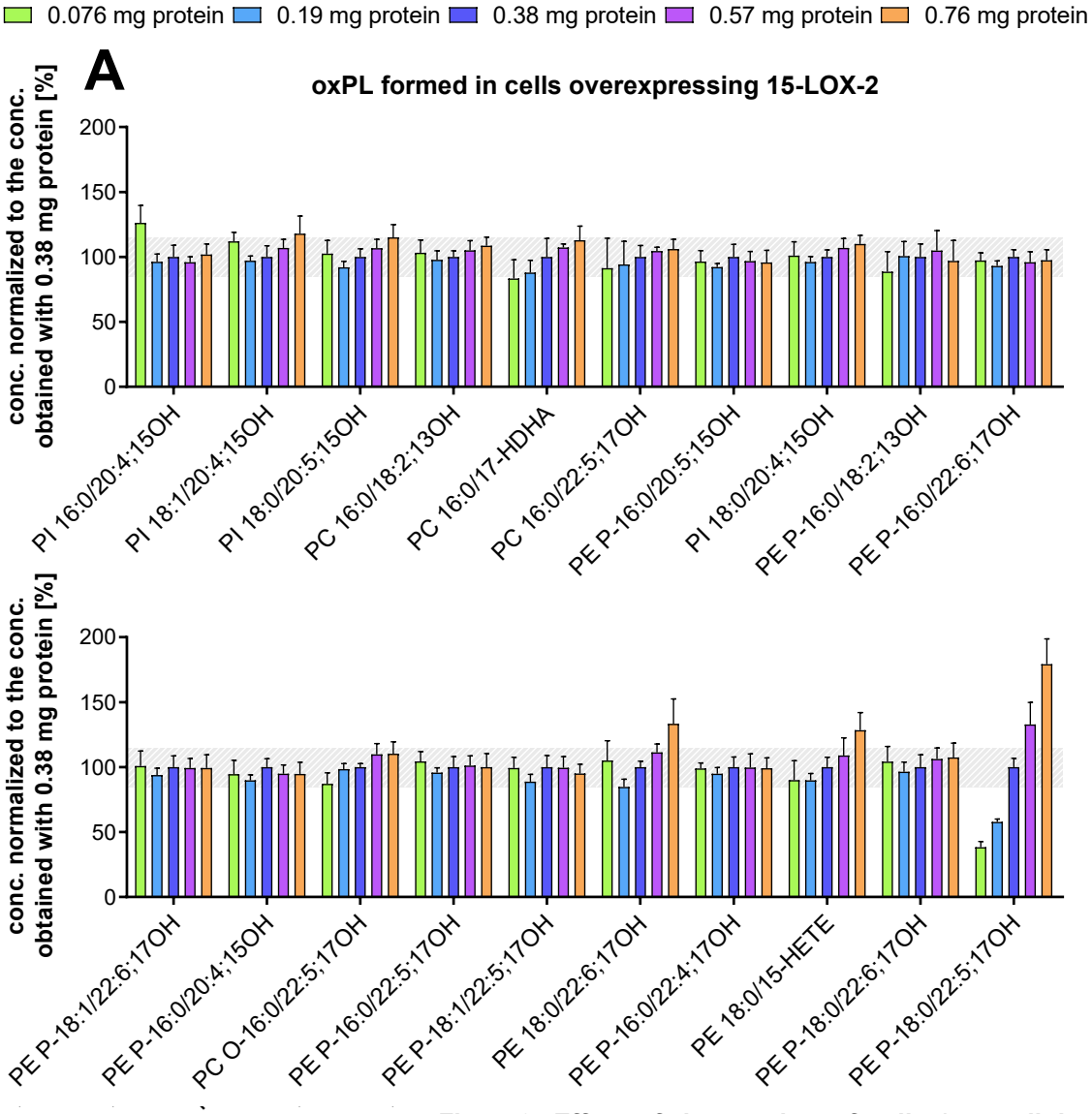

Fig. 4.6: Effect of the number of cells (mg cellular protein) on the apparent concentration and the recovery of IS. Endogenous formation of oxPL elicited by overexpression of 15-LOX-2 in 5×10^6 HEK293T_15-LOX-2 cells. LLE was performed using different volumes of cell homogenate — 10 µL (0.076 mg protein), 25 µL (0.19 mg protein), 50 µL (0.38 mg protein), 75 µL (0.57 mg protein), and 100 µL (0.76 mg protein) — while maintaining identical extraction solvent volumes. Analytes are sorted by retention time. Shown is the mean ± SD (n = 3) of **A** the concentrations normalized to the one obtained with 0.38 mg protein and **B** the recovery of the IS. The concentration of each oxPL species can be found in Table 8.17.

The signals of IS were partially suppressed when 0.57 mg and 0.76 mg protein were used for extraction (Fig. 4.6B): Apparent recoveries of PI 12:0/13:0, PC 12:0/13:0, and PE 12:0/13:0 were 37%, 61%, and 76%, respectively, when 0.76 mg protein was used for LLE. However, good recoveries of 62%, 90%, and 104% were achieved when 0.38 mg protein was used for LLE, as previously shown (Fig. 4.5B).

Overall, varying protein amounts used for extraction yielded consistent concentrations for almost all oxPL (Fig. 4.6A), with a few exceptions, emphasizing the robustness of the developed LC-MS/MS method. Good recoveries of IS and no apparent matrix effects were observed within the elution window of 7 to 18 min when 0.38 mg protein or less was used for LLE (Fig. 4.6). Extraction using 0.38 mg protein also enabled the detection of more oxPL species compared to lower protein amounts. Therefore, a sample amount of 0.38 mg cellular protein was selected for extraction, as it minimized matrix interferences while enabling the sensitive detection of oxPL.

Extraction efficiency of oxidized phospholipids

OxPL are present in much lower concentrations compared to unoxidized PL in biological samples and thus their detection can be challenging. Selection of a suitable extraction procedure from biological samples is a key prerequisite to ensure good extraction recovery and coverage of oxPL with varying polarity.

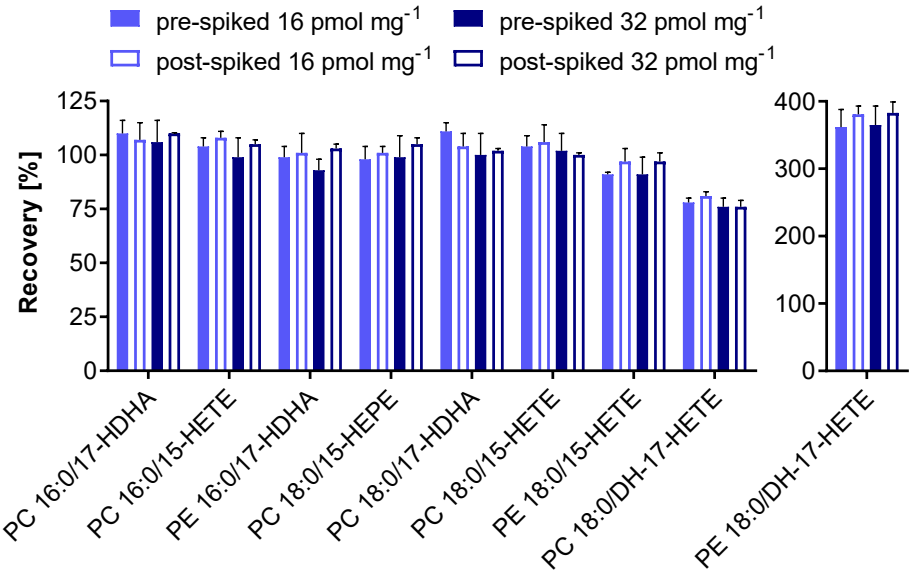

Fig. 4.7: (Previous page) Extraction efficiency of spiked oxPL in HEK293T cells. Shown are the recoveries of spiked oxPL from HEK293T cell homogenates (0.38 mg protein). A mixture of oxPL was added to the cell sample (6.25 or 12.5 pmol of each) before or after sample preparation (pre- or post-spiked). OxPL are sorted by retention time. Shown are mean values ± SD, (n = 3).

MTBE-based LLE effectively extracts both unoxidized PL (Fig. 4.5) and oxPL species (Fig. 4.7) differing in polar head groups and fatty acyl chain composition. Comparison of recoveries of oxPL spiked to cell samples prior or post extraction showed losses of less than 10% during extraction for all oxPC and oxPE tested (Fig. 4.7). The addition of oxPL before LC-MS/MS analysis unveiled ion suppression/enhancement effects for the two last eluting PL bearing dihomo-17-hydroxyeicosatetraenoic acid (DH-17-HETE): while only 20% of the signal of PC 18:0/DH-17-HETE was suppressed, PE 18:0/DH-17-HETE was subjected to a strong enhancement effect of almost 400%, probably caused by coelution with abundant PE P-18:0/22:5;17OH (Fig. 4.6A). Thus, these two-lipid species can be analyzed by the LC-MS/MS method after dilution (see below). Other analytes eluting from 11 to 17 min were not affected by matrix effects. Intra- and inter-day variability were excellent with < 100 ± 14% for almost all analytes and slightly lower for PC 18:0/17-HDHA with ≤ 100 ± 19% (Appendix Table 8.18).

All in all, these results indicate that MTBE-based LLE is well suited for the extraction of oxPL species in HEK293T cells. Previous studies extracted oxPL using a solvent mixture of acetic acid/IPA/*n*-hexane [34, 35] or using SPE with C18 cartridges [53, 54], but did not present data about extraction recovery. In this study, the sample preparation used for oxPL is simple, environmentally friendly, and efficiently extracts lipids without discrimination of lipid species, enabling the investigation of both PL and oxPL by a single extraction procedure.

Intra- and inter-day accuracy and precision

Intra- and inter-day accuracy and precision of the analytical procedure were characterized based on the Guideline on bioanalytical method validation of the International Council for Harmonization [48]. In order to evaluate the accuracy and precision, HEK293T cell samples spiked at four concentration levels were analyzed in three replicates on three different days (Table 4.3).

Table 4.3: Intra- and inter-day accuracy (acc.) as well as precision (prec.) of the extraction of oxPL from human cells. For the determination of accuracy and precision, oxPL were spiked in four concentration levels (1.25, 2.50, 6.25, and 12.5 pmol of each) to the HEK293T cell samples (0.38 mg protein) at the beginning of the sample preparation. Accuracy was determined from the calculated concentration following extraction using an external calibration and precision was calculated as the relative standard deviation of the sample sets (n = 3 for intra- and n = 3 for inter-day). Analytes are sorted by t_R.

Analyte	t_R	conc.	INTRA-DAY		INTER-DAY	
			day 1		3 days	
	[min]	[pmol mg^{-1}]	acc. [%]	prec. [%]	acc. [%]	prec. [%]
PC 16:0/17-HDHA	11.00	3.2	94	± 3	99	± 4
		6.4	105	± 9	102	± 6
		16.1	108	± 2	104	± 4
		32.1	112	± 5	108	± 4
PC 16:0/15-HETE	11.40	3.2	108	± 13	102	± 5
		6.4	103	± 9	104	± 1
		16.1	106	± 6	100	± 7
		32.1	111	± 4	105	± 5
PE 16:0/17-HDHA	11.90	3.2	90	± 9	85	± 7
		6.4	95	± 11	98	± 5
		16.1	101	± 1	99	± 3
		32.1	105	± 7	104	± 1
PC 18:0/15-HEPE	14.00	3.2	86	± 13	82	± 8
		6.4	94	± 9	97	± 3
		16.1	101	± 5	96	± 6
		32.1	101	± 6	100	± 1
PC 18:0/17-HDHA	15.50	3.2	99	± 10	98	± 3
		6.4	110	± 2	100	± 9
		16.1	107	± 4	97	± 8
		32.1	105	± 10	101	± 8
PC 18:0/15-HETE	16.00	3.2	90	± 7	92	± 6
		6.4	101	± 7	98	± 3
		16.1	102	± 2	98	± 4
		32.1	102	± 6	101	± 3
PE 18:0/15-HETE	17.00	3.2	87	± 5	88	± 2
		6.4	95	± 3	98	± 5
		16.1	103	± 6	99	± 3
		32.1	101	± 5	101	± 1
PC 18:0/DH-17-HETE	18.40	3.2	73	± 9	69	± 5
		6.4	78	± 2	75	± 4
		16.1	78	± 2	73	± 8
		32.1	84	± 8	80	± 5
PE 18:0/DH-17-HETE	19.50	3.2	348	± 3	345	± 1
		6.4	391	± 4	387	± 9
		16.1	411	± 6	389	± 5
		32.1	380	± 4	387	± 3

Excellent intra- and inter-day accuracy and precision were obtained for analytes eluting from 11 min to 17 min, while later-eluting analytes i.e. PC/PE bearing 18:0 and DH-17-HETE, were detected with lower accuracy (Table 4.3). Indeed, except for PC/PE bearing DH-17-HETE, the intra-day accuracy ranged from 75% to 112%, indicating low interference of cell matrix in the elution window from 11 to 17 min.

For PC 18:0/DH-17-HETE (t_R = 18.3 min), inter- and intra-day accuracy was lower but still acceptable ranging from 66% to 80%, indicating moderate ion suppression effects. For all analytes, intra-day precision calculated as RSD was < 15% at all spiked levels with two exceptions (18% and 21%) over 108 data points calculated. Inter-day precision was better, below 9% indicating a stable method enabling the analysis of large sample batches.

Our results show that most oxPL can be analyzed with excellent accuracy. Only the signal of oxPL eluting after 17 min could be disturbed by severe matrix effects as shown for PE 18:0/DH-17-HETE. Lipidomics analysis typically relies on a single IS to cover multiple analytes [34, 35, 53-55], which does not correct for possible matrix effects in reversed-phase chromatography. Also, in our approach only few, non-oxidized PL are used as IS (see above). Thus, matrix effects cannot be fully compensated by the IS, which emphasizes the importance of assessing oxPL accuracy as shown here.

Dilution integrity of the determined concentration for oxidized phospholipids

Extraction recoveries and accuracy evaluations showed a strong enhancement effect on PE 18:0/DH-17-HETE (Fig. 4.6A, Fig. 4.7), while other analytes exhibited excellent accuracy and recoveries. To further characterize and support the absence of matrix effects, we evaluated accuracy and extraction recoveries of oxPL and IS added at the beginning of the sample preparation in non-diluted and diluted lipid extracts (Fig. 4.8).

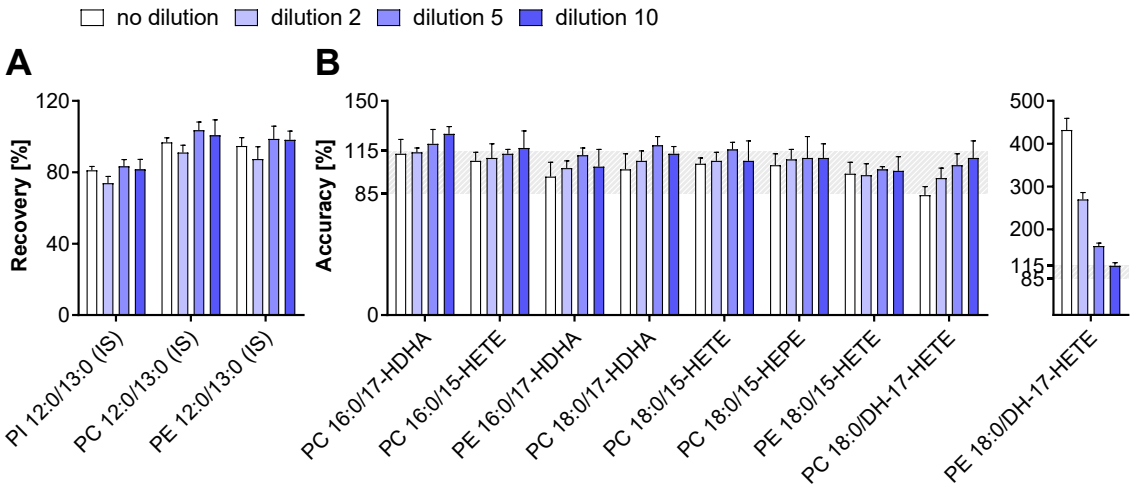

Fig. 4.8: Dilution integrity of IS and spiked oxPL in HEK293T cells. Cell homogenates (0.38 mg protein) were spiked with a mixture of oxPL (12.5 pmol of each) and IS (2.5 pmol of each) prior to LLE. Lipid extracts were diluted by factor 2, 5, or 10 prior to targeted LC-MS/MS analysis. Shown are in non-diluted and diluted cell extracts **A** the recovery of the spiked IS, and **B** the accuracy of oxPL determined from the calculated concentration (mean ± SD (n = 3)). Analytes are sorted by retention time.

No ion suppression effects are present for analytes eluting from 7.4 to 17 min (Fig. 4.8). However, ion suppression or ion enhancement effects were observed for analytes eluting after 18 min (Fig. 4.8B). Calculated extraction recoveries of IS were nearly identical in non-diluted and diluted lipid extracts (Fig. 4.8A). Also, remarkable constant concentrations were observed across different dilutions of the lipid extract with an accuracy ranging from 97% and 120% (Fig. 4.8B), except for PC 16:0/17-HDHA with an accuracy of 127% in the 1:10 diluted extract close to the LLOQ. This supports the data of the accuracy and precision (Table 4.3). Increasing dilution improved the accuracy of the two late-eluting PL bearing DH-17-HETE (Fig. 4.8B), indicating a reduction of ion matrix effects: For PC 18:0/DH-17-HETE, the accuracy increased from 84% in the non-diluted extract to 110% in the 1:10 diluted extract. Similarly, the accuracy of PE 18:0/DH-17-HETE was dramatically improved by dilution: Starting from 432%, to 270%, 161%, and finally 115% in the 1:10 diluted extract. Thus, a 1:10 dilution also enabled accurate quantification for these two-lipid species.

The 1:10 dilution of the oxPL extract (Fig. 4.9) reduced the matrix effects on PE P-18:0/22:5;17OH formed via 15-LOX-2 in HEK293T_15-LOX-2 cells.

The calculated concentration of PE P-18:0/22:5;17OH dropped from 61 pmol mg^{-1} in non-diluted extract (Fig. 4.9A) to 15 pmol mg^{-1} in the 1:10 diluted extract (Fig. 4.9B). After dilution, the resulting concentration of (the sum of) PL bearing 22:5;17OH was nearly identical compared to the targeted oxylipin method, with only a 15% difference (Fig. 4.9B). This demonstrates the accuracy of the quantification of PE P-18:0/22:5;17OH by targeted LC-MS/MS using an extraction volume of 50 µL (0.38 mg protein) and a 1:10 dilution.

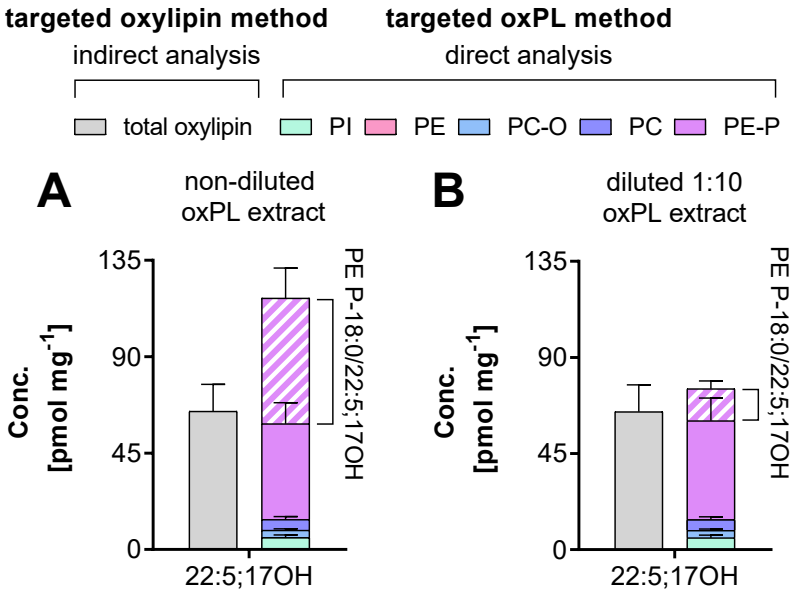

Fig. 4.9: Dilution of oxPL extract improves quantification accuracy by reducing ion suppression of PE P-18:0/22:5;17OH. Esterified oxylipins were quantified in 15-LOX-2 overexpressing HEK293T_15-LOX-2 cells (0.38 mg protein) either following alkaline hydrolysis or as intact oxPL by targeted LC-MS/MS methods. Shown is the comparison of the concentration of 22:5;17OH in **A** non-diluted oxPL extract and **B** 1:10 diluted oxPL extract. (**Light Grey bar**) Total 22:5;17OH quantified following alkaline hydrolysis. (**Colored bar**) sum of individual oxPL species of each lipid class. Shown is the mean ± SD per mg cellular protein (n = 3).

All in all, these results support the occurrence of ion suppression/enhancement effects after 18 min but also demonstrate that a factor 10 dilution of the oxPL extract can resolve these matrix effects, consistent with the literature [56]. Additionally, the consistent concentrations observed for all other analytes across different dilutions of the oxPL extract underline the robustness of the developed method and the absence of matrix interferences.

Comparison of direct oxPL analysis with indirect analysis

The developed targeted LC-MS/MS method was compared to orthogonal approaches using an indirect analysis following alkaline hydrolysis as shown in Fig. 4.1.

The developed targeted oxPL LC-MS/MS method resulted in remarkably consistent concentrations with the indirect quantification of esterified oxylipins following alkaline hydrolysis (with and without HILIC-based SPE fractionation). This is shown in Figure 4.10 exemplarily for 15-LOX-2 overexpressing cells: The differences between (the sum of) concentrations determined by targeted quantification of oxPL were < 14% compared to the targeted oxylipin method, the current gold standard for esterified oxylipin analyses. This underlines that the new targeted oxPL method covers all relevant oxylipin-bearing species, and this also further demonstrates the accuracy of the method. Thus, esterified 15-LOX-2 products bound in PL can be accurately quantified as individual oxPL species by the developed targeted method.

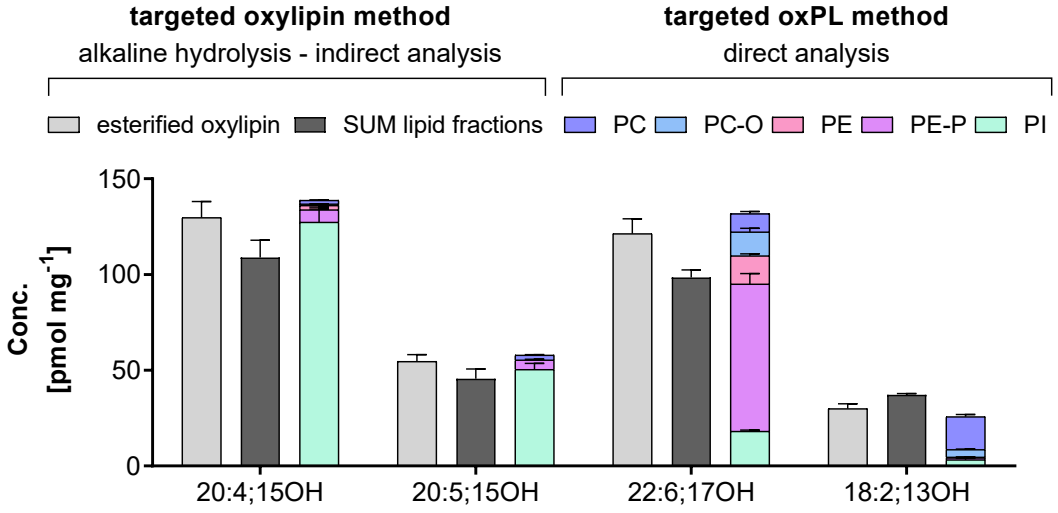

Fig. 4.10: Targeted analysis of PL bearing hydroxy-PUFA leads to similar concentrations as targeted esterified oxylipin analysis. Esterified oxylipins were quantified in 15-LOX-2 overexpressing 5×10^6 HEK293T_15-LOX-2 cells (200 ng mL^{-1} doxycycline, 24 h), either indirectly following alkaline hydrolysis or directly as intact oxPL by targeted LC-MS/MS methods. Shown is the comparison of the results. (**Light grey bar**) esterified oxylipins determined as total – non-esterified oxylipins. (**Dark grey bar**) sum of esterified oxylipins in the HILIC-separated lipid fractions. (**Colored bars**) sums of individual oxPL species of each lipid class. Shown is the mean concentration ± SD per mg cellular protein (n = 3).

4.3.4 Incorporation of oxylipins into distinct phospholipid species

Using the developed targeted LC-MS/MS method, we could show that esterified 15-LOX-2 products occur in a few PL species (Fig. 4.11): The oxylipins were always found in the *sn*-2 position of the PL species (Fig. 4.11B, D). The fatty acyls at *sn*-1 were dominantly 16:0 (PC, PE-P, and PC-O) and 18:0 (PI and PE). Analysis of oxPL in HEK293T cells following supplementation or overexpression of 15-LOX-2 showed a comparable distribution of oxylipins both in the PL classes (Fig. 4.11A, C) and across PL species (Fig.11B, D), except for PE as shown for 15-HETE and 15-HEPE (Fig. 4.3B): In 15-LOX-2 overexpressing cells, 5.7% of 20:4;15OH and 12% of 20:5;15OH were incorporated into PE-P bearing 16:0 at the *sn*-1 position, while less than 1% of supplemented 20:4;15OH and 20:5;15OH were found in these lipids. 15-LOX-2 can oxidize both non-esterified PUFA but also PUFA esterified in PL [3, 5]. Following incubation of cell homogenates with exogenous 15-LOX-2 (Fig. 4.12), 61% of 20:4;15OH was bound to PI species compared to at least 90% for 20:4;15OH in supplemented and 15-LOX-2 overexpressing cells. Almost half of the 20:5;15OH formed by PL oxidation by 15-LOX-2 was incorporated into PE-P species, while at least 80% of supplemented and endogenously formed 20:5;15OH was esterified into PI.

A notable specificity of oxylipin incorporation towards certain PL species was observed (Fig. 4.11B, D), both in supplemented and 15-LOX-2 overexpressing cells: While 20:4;15OH (15-HETE) and 20:5;15OH (15-HEPE) showed a narrow distribution between few PI species, 22:6;17OH (17-HDHA) and 18:2;13OH (13-HODE) were more evenly distributed across the PL classes and species. 20:4;15OH was predominantly bound to the species PI 18:0/20:4;15OH with 71 ± 1% in 15-LOX-2 overexpressing cells (Fig. 4.11D). 20:4;15OH was detected in notable amounts in PI 18:1/20:4;15OH and PI 16:0/20:4;15OH, with 12.4 ± 0.6% and 7.1 ± 0.4%, respectively. A minor part of 20:4;15OH was detected in PE-P 16:0/20:4;15OH with 5.7 ± 0.3%, while the six remaining PC and PE species detected represented each less than 1.5%.

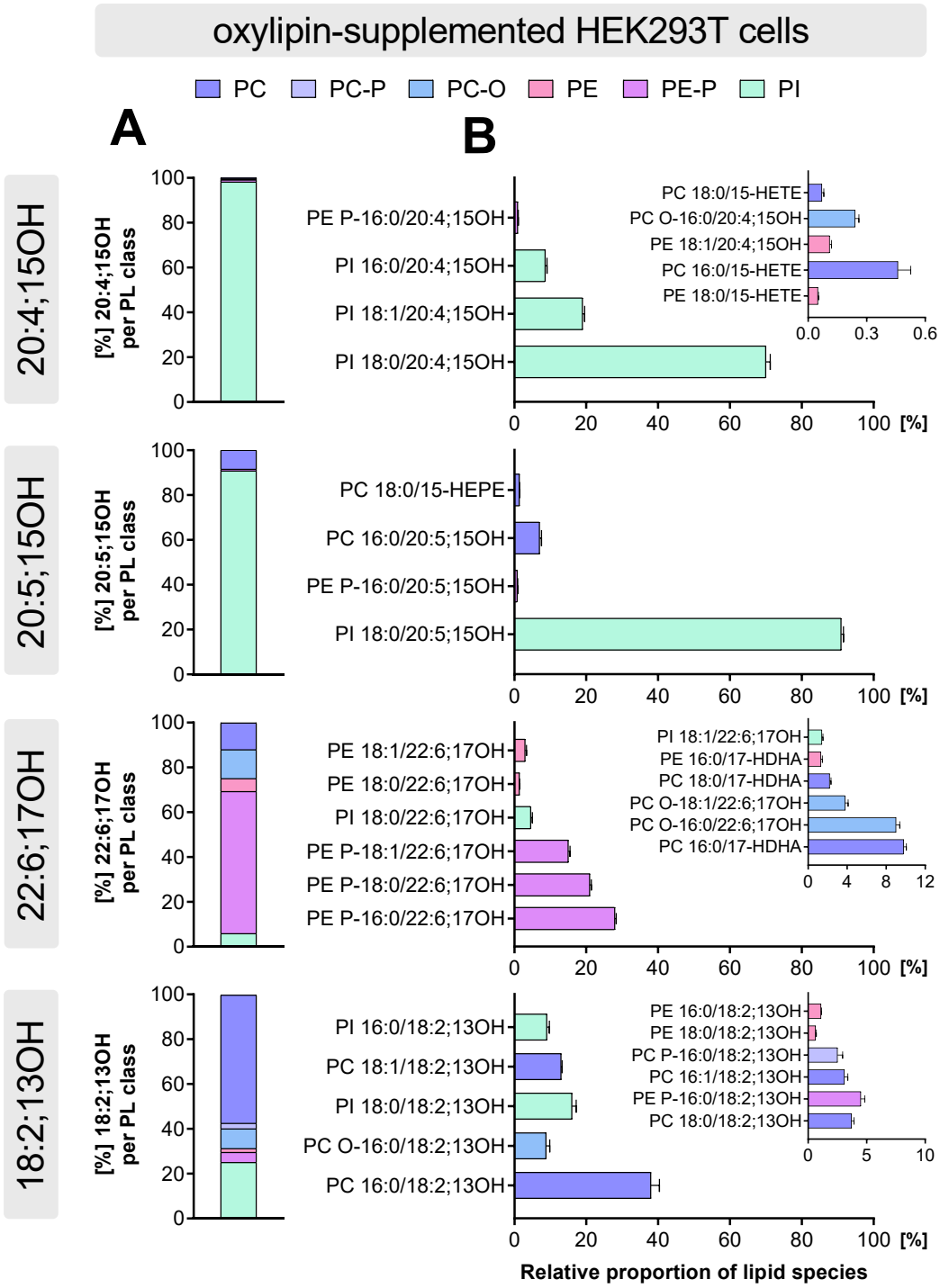

Fig. 4.11: 15-LOX-2 products of PUFA are esterified to distinct PL classes and specific molecular PL species following supplementation and in 15-LOX-2 overexpressing cells. 5×10^6 cells were used per experiment. **A and B** HEK293T cells supplemented with either 15(*S*)-HETE, 15(*S*)-HEPE, 17(*S*)-HDHA, or 13(*S*)-HODE (300 nmol L^{-1}, 2 h). Shown is the relative distribution of 20:4;15OH, 20:5;15OH, 22:6;17OH, and 18:2;13OH **A** in PL classes and **B** for the PL molecular species. For each oxylipin, the percentage of the sum of all oxPL quantified by targeted LC-MS/MS was calculated. Mean concentration ± SD per mg cellular protein (n = 3) can be found in Table 8.16.

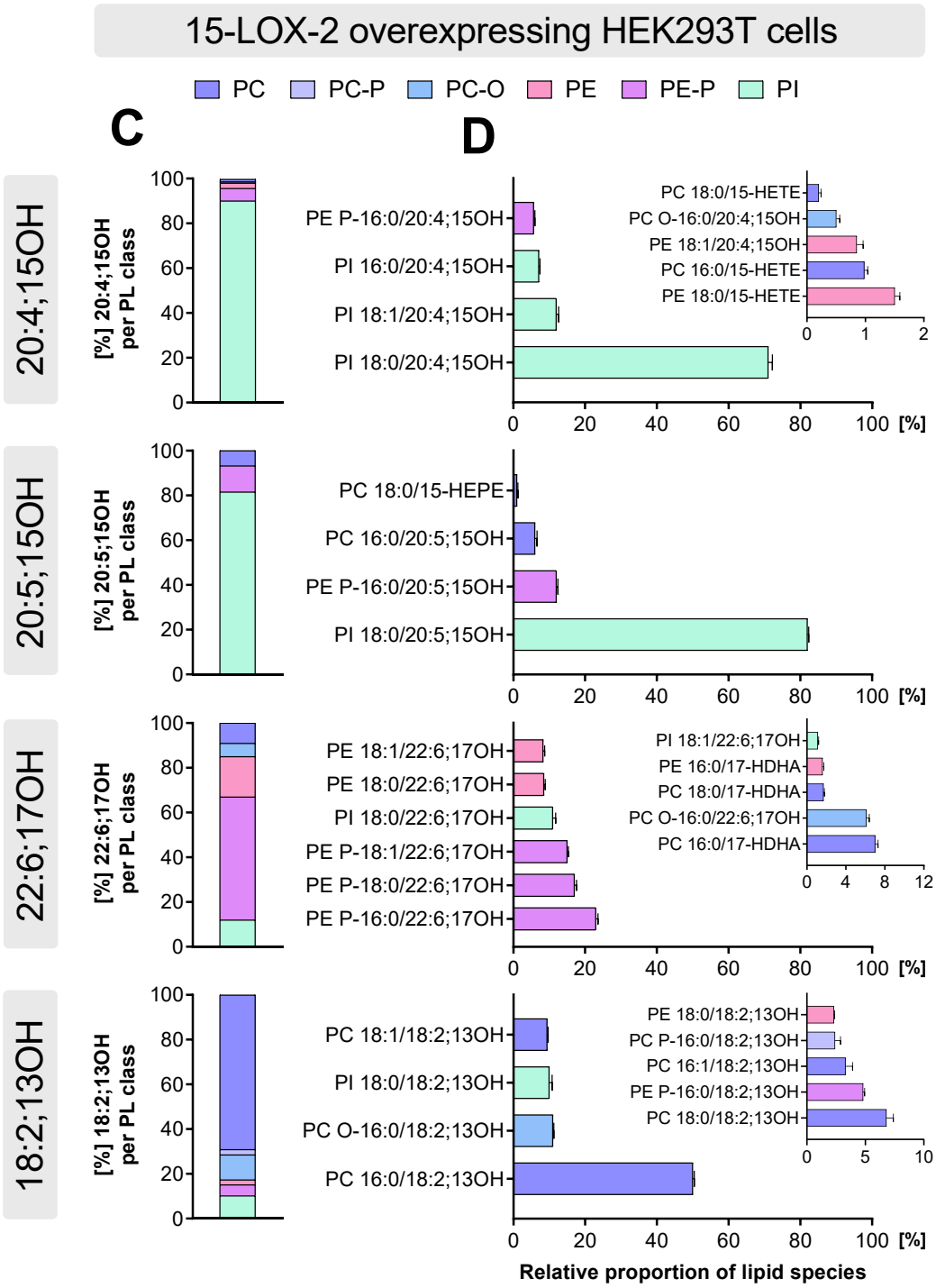

Fig. 4.11: Continued. 15-LOX-2 products of PUFA are esterified to distinct PL classes and specific molecular PL species following supplementation and in 15-LOX-2 overexpressing cells. 5 × 10^6 cells were used per experiment. **C and D** Endogenous formation of oxPL elicited by overexpression of 15-LOX-2 in HEK293T_15-LOX-2 cells (200 ng mL^{-1} doxycycline, 24 h). Shown is the relative distribution of 20:4;15OH, 20:5;15OH, 22:6;17OH, and 18:2;13OH **C** in PL classes and **D** for the PL molecular species. For each oxylipin, the percentage of the sum of all oxPL quantified by targeted LC-MS/MS was calculated. Mean concentration ± SD per mg cellular protein (n = 3) can be found in Table 8.16.

Similar to 20:4;15OH, the vast majority of 20:5;15OH was found in PI 18:0/20:5;15OH accounting for 81.6 ± 0.4%. At lower amount, 20:5;15OH was found in PE P-16:0/20:4;15OH and PC 16:0/20:5;15OH species, with 11.7 ± 0.4% and 5.9 ± 0.6%, respectively. Direct oxPL analysis showed that 22:6;17OH is predominantly esterified to PE-P: More than 50% was detected among the three species PE P-16:0/22:6;17OH (23%), PE P-18:0/22:6;17OH (17%), and PE P-18:1/22:6;17OH (15%) in cells overexpressing 15-LOX-2. The second most abundant PL class was PI, with the species PI 18:0/22:6;17OH accounting for 11 ± 1%. 30% of 22:6;17OH was distributed quasi-equally between four lipid species i.e. PE bearing 18:0 and 18:1, and PC(-O) bearing 16:0. 18:2;13OH was detected in four PC species bearing 16:0, 16:1, 18:0, and 18:1 in the *sn*-1 position, but was predominantly bound to PC 16:0/18:2;13OH with 49.6 ± 0.4%. Each of the three species PC O-16:0/18;13OH, PI 18:0/18;13OH, and PC 18:1/18;13OH accounted for ~ 10% of esterified 18:2;13OH. The last 20% of 18:2;13OH was distributed between the six lowest-concentration PC(-O) and PE(-P) species. The differences observed in oxylipin distribution across PL species seem not to depend on the concentration: Among the analyzed oxylipins in cells overexpressing 15-LOX-2 (Fig. 4.10), 18:2;13OH is the least abundant with 29.9 ± 2.5 pmol mg^{-1} while 20:5;15OH is nearly twice as abundant at 54.6 ± 3.5 pmol mg^{-1} and exhibits a restricted distribution between only four oxPL species (Fig. 4.11D).

4.3.5 Biological relevance of oxylpins' distinct incorporation

Oxylipins were found to be distinctly incorporated into both PL classes and molecular species (Fig. 4.3B, Fig. 4.11). Supplementation and endogenous formation of oxylipins led to a comparable incorporation pattern, while direct oxidation of cell PL by exogenously added 15-LOX-2 was different (Fig. 4.12). These results indicate that for the formation of oxPL in the 15-LOX-2 overexpressing cells, FA are first released, the non-esterified FA is oxidized, and then incorporated into lysoPL and not formed by direct oxidation of intact PL by the LOX enzyme.

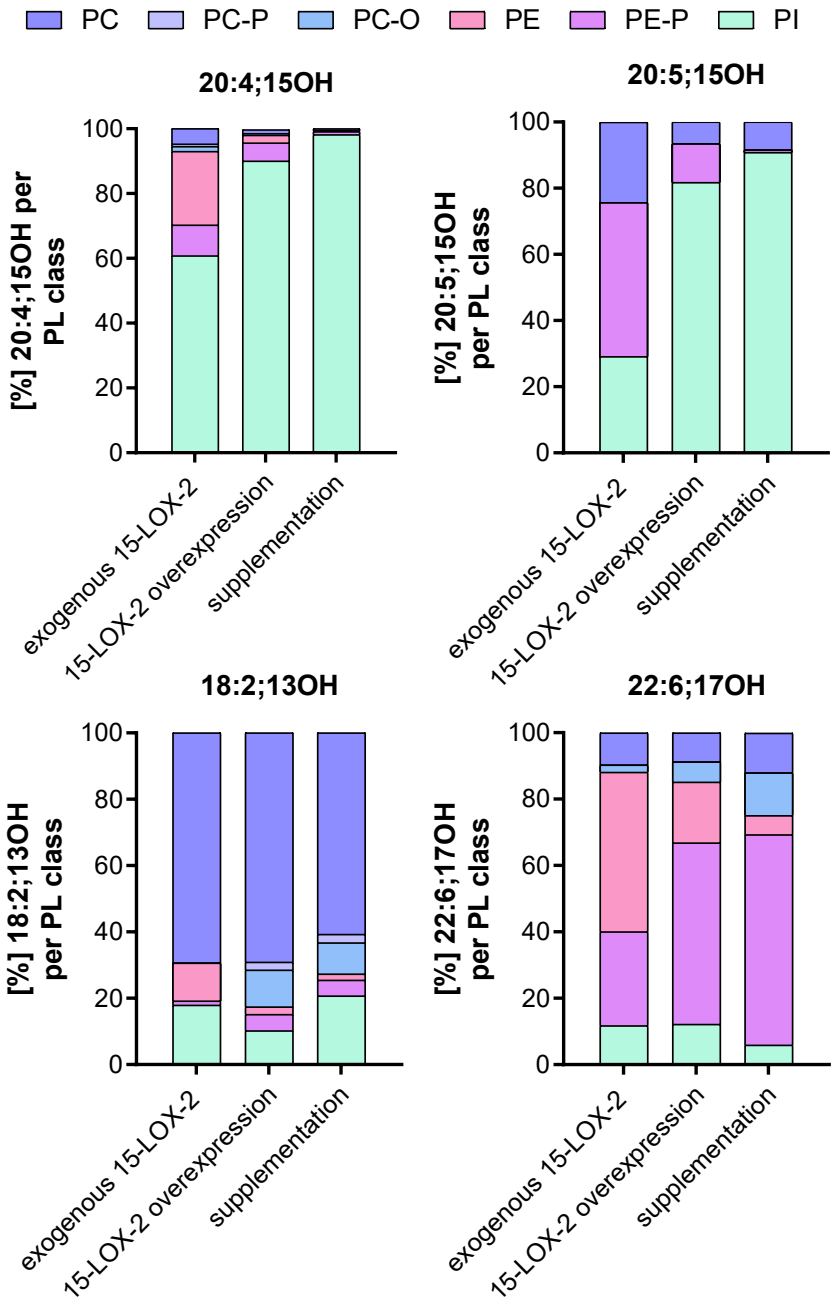

Fig. 4.12: Investigation of the oxPL pattern formed by exogenous 15-LOX-2 added to the cell homogenate *vs.* endogenous formation by 15-LOX-2 or incorporation following supplementation. Shown is the relative distribution of 20:4;15OH, 20:5;15OH, 22:6;17OH, and 18:2;13OH per PL class in HEK293T cells (mean ± SD (n = 3)). (**Left bar**) 15-LOX-2 human enzyme added to cell homogenate of HEK293T cells and incubated (6.9×10^{-3} U mL^{-1} in assay, 2 h at 37 °C). (**Middle bar**) Endogenous formation of oxPL elicited by overexpression of 15-LOX-2 in HEK293T_15-LOX-2 (200 ng mL^{-1} doxycycline, 24 h). (**Right bar**) HEK293T cells supplemented with either 15(*S*)-HETE, 15(*S*)-HEPE, 17(*S*)-HDHA, or 13(*S*)-HODE (300 nmol L^{-1}, 2 h). For each oxylipin, data were normalized on the sum of all oxPL quantified by targeted oxPL LC-MS/MS. The concentrations of each oxPL species can be found in Table 8.16.

The observed distinct incorporation of oxylipins into the membranes (Fig. 4.3B, Fig. 4.11) thus depends on the specificity of the enzymes generating the PL during the Lands' remodeling cycle. This involves the different ACSL and LPLAT enzymes [57, 58]. Different ACSL isoforms (i.e., ACSL-1, -3, -4, -5, and -6) accept 15-HETE, 12-HETE, and 5-HETE as substrates [59]. Thus, the LPLAT-catalyzed transfer of activated acyl-CoA into lysoPL seems to cause this distinct incorporation. 14 LPLAT have been identified exhibiting pronounced differences in substrate preferences and lysoPL enzymatic activities [57, 60-64]. For example, while LPLAT12 (LPCAT3) incorporates 18:2- and 20:4-CoAs into lysoPC, lysoPE, and lysoPS [62], LPLAT13 (MBOAT2) and LPLAT14 (MBOAT1) both transfer 22:6-CoA into lysoPE (and lysoPC for LPLAT13) [64]. Moreover, LPLAT11 (MBOAT7) transfers 20:4- and 20:5-CoAs predominantly into lysoPI [60]. Inhibition of LPLAT12 using 10 µM (*R*)-HTS-3 reduced the formation of PC and PE species bearing 12-HETE, but not those containing 11- or 15-HETE, in thrombin-activated platelets [65]. These results would indicate that LPLAT12 exhibits selectivity toward oxylipin positional isomers. The almost exclusive incorporation of 20:4;15OH and 20:4;15OH into PI observed in this study thus might result from LPLAT11. In contrast, the esterification of 22:6;17OH into lysoPE is likely catalyzed by other LPLAT, e.g., LPLAT13 or LPLAT14. Similarly, incorporation of 18:2;13OH into lysoPC might be catalyzed by LPLAT12.

Preferred incorporation of 15-HETE into PI has been previously described following supplementation of labeled [^{3}H]/[$^{14}C_1$]15-HETE (0.1 – 1 µmol L^{-1}, 20 – 120 min) in bovine pulmonary arterial endothelial cells [30], human primary neutrophils [31], mouse macrophage-like RAW 5774.2 cell line [32], human tracheal epithelial cells [29], and Madin-Darby canine kidney cells [27]. Using radioactively labeled oxylipins, these studies showed by TLC that between 69% and 86% of labeled 15-HETE was incorporated into PI, and in smaller amounts into PC and PE, ranging from 4.9% to 21% for PC plus PE. Similarly, favored incorporation of [^{14}C]13-HODE into PC was shown: Cho *et al.* reported by TLC that 58% of [^{14}C]13-HODE was incorporated into PC, 23% into PI, 12% into PS, and 6.8% into PE following supplementation in the epidermis (1.6 µmol L^{-1}, 6 h) [28]. In this study, consistent incorporation patterns of 20:4;15OH and 18:3;13OH

into PL classes were found following supplementation in HEK293T cells (Fig. 4.3B, Fig. 4.11A). Specific incorporation of 15-HETE into PI bearing 18:0 at the *sn*-1 position was reported in two studies. Legrand *et al.* identified [^{3}H]15(*S*)-HETE in PI bearing 18:0 or 18:1 by GC-MS following separation by TLC in supplemented endothelial cells (1 µmol L^{-1}, 2 h) [30]. In our previous work, non-labeled 20:4;15OH was identified exclusively into PI species containing 18:0, 18:1, or 16:0 in 15-HETE-supplemented HEK293T cells (2 µmol L^{-1}, 2 h) [47]. Here, targeted LC-MS/MS not only supported this distinct incorporation of 20:4;15OH into these three PI species (Fig. 4.11B, D), but also enabled the detection of low concentrated PC and PE species bearing 20:4;15OH. Moreover, we could also show a similar specific incorporation of 20:5;15OH into PI bearing 18:0. 22:6;17OH and 18:2;13OH were found to be more evenly distributed into PE-P and PC species, respectively, but 10% of these oxylipins were also bound to PI bearing 18:0 (Fig. 4.11D).

Overall, these findings could be of high importance as PI species are involved in two main regulatory pathways, which impact cell growth and signaling [66-69]. In the PI-cycle pathway, PI is converted to PIP_2 by a two-step reaction. Binding of an agonist to a Gq-coupled receptor leads to the activation of phospholipase C (PLC), which cleaves PIP_2 into DG and inositol 1,4,5-trisphosphate (IP_3) [66, 67]. Both act as second messengers. IP_3 activates protein kinase C regulating e.g. the production of pro-inflammatory cytokines [70]. In the protein kinase B (Akt/PKB) signaling pathway, PIP_2 is phosphorylated to PIP_3 via phosphoinositide 3-kinases. PIP_3 then recruits Akt/PKB to the plasma membrane enabling its phosphorylation by phosphoinositide-dependent kinase-1, controlling e.g. cell proliferation via Akt/PKB and mTOR [68]. In this context, specific incorporation into PI of 15-HETE and 15-HEPE could play a key role in the regulation of these pathways. Indeed, previous studies described that [^{3}H]/[^{14}C]15-HETE caused an elevation of labeled 15-HETE-DG in bovine pulmonary endothelial cells exposed to bradykinin [30], and in epithelial cells treatment with platelet activated factor was associated with a selective decrease in [^{3}H]15-HETE-PI [26]. In the same study, [^{14}C]15-HETE-DG was able to stimulate protein kinase C-α [26]. Setty *et al.* reported that 15-HETE caused an

elevation of cellular DG and as well as a stimulation of endothelial cells' DNA synthesis and cell growth [71]. Here, we show that the 15-LOX products of DHA and LA are not incorporated into PI. Thus, a shift in the fatty acid pattern could alter PI signaling. It is well known that intake of long-chain n3-PUFA leads to a shift in the FA composition, thereby increasing n3-PUFA (largely DHA) and decreasing n6-PUFA (largely ARA) [72-74]. The formation and occurrence of hydroxy-PUFA correlate with the concentration of the substrate [75, 76], and 15-LOX even prefers DHA as substrate compared to ARA [7].

As we show here, hydroxy-PUFA occur exclusively esterified and dominantly in PL (Fig. 4.3B), the diet directly seems to also modify the oxylipin pattern and thus the PL membrane composition. Therefore, a diet rich in long-chain n3-PUFA increasing 17-HDHA via 15-LOX while decreasing 15-HETE might influence PI signaling pathway(s), which could contribute to the biological effects of a n3-PUFA-rich diet [77-79]. Additionally, several studies demonstrate that 15-HETE and 15-HEPE have anti-inflammatory effects [17]. Importantly, the preferential incorporation of 15-HETE into PI is not limited to the supplemented or 15-LOX-2 overexpressing HEK293T cells used in this study, but has also been consistently observed in a variety of other cell types following supplementation [26, 27, 30-32] – highlighting the physiological relevance of this incorporation. With the modification of PI-based signaling, we suggest here a new pathway that may explain the effects of n3-PUFA and 15-LOX products, warranting further investigation.

4.4 Conclusion

Combined analysis of esterified oxylipins enabled the characterization in which PL classes and molecular PL species 15-LOX-2 oxylipin products are located in HEK293T cells. Indirect quantification of esterified oxylipins in lipid fractions identified the specific PL classes in which 15-LOX-2 oxylipin products are located at baseline, following supplementation, and in 15-LOX-2 overexpressing cells. Targeted LC-MS/MS quantification of PL bearing hydroxy-PUFA enabled to pinpoint in which molecular species and *sn*-1/*sn*-2 position oxylipins are esterified following supplementation and endogenous formation. The vast majority of 15-HETE and 15-HEPE was incorporated into distinct PI species with more than 70% of 20:4;15OH and 80% of 20:5;15OH esterified in the *sn*-2 position of PI bearing 18:0. On the opposite, 17-HDHA and 13-HODE were more evenly distributed into PL classes and species. 17-HDHA was predominantly found in PE, particularly PE-P species bearing 16:0, 18:0, and 18:1 in the *sn*-1 position. Most of 13-HODE was found in PC with a marked abundance of PC 16:0/18:2;13OH at 50%, while the other half was distributed mainly between PC(-O) and PI species. For these two oxylipins the second most abundant PL class was PI, specifically PI bearing 18:0. Based on this accurate quantification using two orthogonal approaches, a distinct incorporation of 15-LOX formed oxylipins both into PL classes/species was shown. The associated biological effects remain to be uncovered and may explain the anti-inflammatory effects of n3-PUFA and 15-LOX by altering PI-based signaling pathways.

4.5 References

1. Gabbs M, Leng S, Devassy JG, Monirujjaman M, Aukema HM (2015) Advances in our understanding of oxylipins derived from dietary PUFAs. *Advances in nutrition*. **6**, 513-40.
2. Buczynski M, Dumlao D, Dennis E (2009) An integrated omics analysis of eicosanoid biology. Thematic review series: proteomics. *J Lipid Res*. **50**, 1015-38.
3. Brash AR (1999) Lipoxygenases: occurrence, functions, catalysis, and acquisition of substrate. *Journal of Biological Chemistry*. **274**, 23679-82.
4. Kuhn H, Belkner J, Wiesner R, Brash A (1990) Oxygenation of biological membranes by the pure reticulocyte lipoxygenase. *Journal of Biological Chemistry*. **265**, 18351-61.
5. O'Donnell VB, Murphy RC (2012) New families of bioactive oxidized phospholipids generated by immune cells: identification and signaling actions. *Blood, The Journal of the American Society of Hematology*. **120**, 1985-92.
6. Bryant RW, Bailey JM, Schewe T, Rapoport S (1982) Positional specificity of a reticulocyte lipoxygenase. *J biol Chem*. **257**, 6050-5.
7. Kutzner L, Goloshchapova K, Heydeck D, Stehling S, Kuhn H, Schebb NH (2017) Mammalian ALOX15 orthologs exhibit pronounced dual positional specificity with docosahexaenoic acid. *Biochimica et Biophysica Acta (BBA)-Molecular and Cell Biology of Lipids*. **1862**, 666-75.
8. Brash AR, Boeglin WE, Chang MS (1997) Discovery of a second 15 S-lipoxygenase in humans. *Proceedings of the National Academy of Sciences*. **94**, 6148-52.
9. Hwa Lee S, Rangiah K, Williams MV, Wehr AY, DuBois RN, Blair IA (2007) Cyclooxygenase-2-mediated metabolism of arachidonic acid to 15-oxo-eicosatetraenoic acid by rat intestinal epithelial cells. *Chemical Research in Toxicology*. **20**, 1665-75.
10. Kampschulte N, Kirchhoff R, Löwen A, Schebb NH (2024) Deducing formation routes of oxylipins by quantitative multiple heart-cutting achiral-chiral 2D-LC-MS. *Journal of Lipid Research*. **65**, 100694.
11. Gottschall H, Schmöcker C, Hartmann D, Rohwer N, Rund K, Kutzner L, et al. (2018) Aspirin alone and combined with a statin suppresses eicosanoid formation in human colon tissue. *Journal of lipid research*. **59**, 864-71.
12. Kampschulte N, Alasmer A, Empl MT, Krohn M, Steinberg P, Schebb NH (2020) Dietary polyphenols inhibit the cytochrome P450 monooxygenase branch of the arachidonic acid cascade with remarkable structure-dependent selectivity and potency. *Journal of agricultural and food chemistry*. **68**, 9235-44.
13. Gladine C, Ostermann AI, Newman JW, Schebb NH (2019) MS-based targeted metabolomics of eicosanoids and other oxylipins: Analytical and inter-individual variabilities. *Free Radical Biology and Medicine*. **144**, 72-89.
14. Li MY, Yuan H-L, Ko FW, Wu B, Long X, Du J, et al. (2015) Antineoplastic effects of 15 (S)-hydroxyeicosatetraenoic acid and 13-S-hydroxyoctadecadienoic acid in non–small cell lung cancer. *Cancer*. **121**, 3130-45.
15. Shibata N, Toi S, Shibata T, Uchida K, Itabe H, Sawada T, et al. (2009) Immunohistochemical detection of 13 (R)-hydroxyoctadecadienoic acid in atherosclerotic plaques of human carotid arteries using a novel specific antibody. *Acta histochemica et cytochemica*. **42**, 197-203.

16. Simon TC, Makheja AN, Bailey JM (1989) Formation of 15-hydroxyeicosatetraenoic acid (15-HETE) as the predominant eicosanoid in aortas from Watanabe Heritable Hyperlipidemic and cholesterol-fed rabbits. *Atherosclerosis*. **75**, 31-8.
17. Rohwer N, Chiu CY, Huang D, Smyl C, Rothe M, Rund KM, et al. (2021) Omega-3 fatty acids protect from colitis via an Alox15-derived eicosanoid. *The FASEB Journal*. **35**, e21491.
18. Li G, Chen Z, Bhat OM, Zhang Q, Abais-Battad JM, Conley SM, et al. (2017) NLRP3 inflammasome as a novel target for docosahexaenoic acid metabolites to abrogate glomerular injury [S]. *Journal of lipid research*. **58**, 1080-90.
19. Goebel B, Carpanedo L, Reif S, Göbel T, Schebb NH, Steinhilber D, et al. (2023) Development of a cell-based model system for the investigation of ferroptosis. *Front Cell Death*. **2**, 1182239.
20. Morrow JD, Awad JA, Boss HJ, Blair IA, Roberts 2nd L (1992) Non-cyclooxygenase-derived prostanoids (F2-isoprostanes) are formed in situ on phospholipids. *Proc Natl Academy Sci*. **89**, 10721-5.
21. Schebb NH, Ostermann AI, Yang J, Hammock BD, Hahn A, Schuchardt JP (2014) Comparison of the effects of long-chain omega-3 fatty acid supplementation on plasma levels of free and esterified oxylipins. *Prostaglandins & other lipid mediators*. **113**, 21-9.
22. Shearer GC, Newman JW (2008) Lipoprotein lipase releases esterified oxylipins from very low-density lipoproteins. *Prostaglandins, leukotrienes and essential fatty acids*. **79**, 215-22.
23. Quehenberger O, Dahlberg-Wright S, Jiang J, Armando AM, Dennis EA (2018) Quantitative determination of esterified eicosanoids and related oxygenated metabolites after base hydrolysis. *Journal of lipid research*. **59**, 2436-45.
24. Ostermann AI, Koch E, Rund KM, Kutzner L, Mainka M, Schebb NH (2020) Targeting esterified oxylipins by LC–MS-Effect of sample preparation on oxylipin pattern. *Prostaglandins & Other Lipid Mediators*. **146**, 106384.
25. Fang X, Kaduce TL, Spector AA (1999) 13-(S)-Hydroxyoctadecadienoic acid (13-HODE) incorporation and conversion to novel products by endothelial cells 1. *Journal of lipid research*. **40**, 699-707.
26. Alpert SE, Walenga RW, Mandal A, Bourbon N, Kester M (1999) 15-HETE-substituted diglycerides selectively regulate PKC isotypes in human tracheal epithelial cells. *American Journal of Physiology-Lung Cellular and Molecular Physiology*. **277**, L457-L64.
27. Girton RA, Spector AA, Gordon JA (1994) 15-HETE: selective incorporation into inositol phospholipids of MDCK cells. *Kidney international*. **45**, 972-80.
28. Cho Y, Ziboh VA (1994) Incorporation of 13-hydroxyoctadecadienoic acid (13-HODE) into epidermal ceramides and phospholipids: phospholipase C-catalyzed release of novel 13-HODE-containing diacylglycerol. *Journal of lipid research*. **35**, 255-62.
29. Alpert SE, Walenga RW (1993) Human tracheal epithelial cells selectively incorporate 15-hydroxyeicosatetraenoic acid into phosphatidylinositol. *American journal of respiratory cell and molecular biology*. **8**, 273-.
30. Legrand A, Lawson J, Meyrick B, Blair I, Oates J (1991) Substitution of 15-hydroxyeicosatetraenoic acid in the phosphoinositide signaling pathway. *Journal of Biological Chemistry*. **266**, 7570-7.
31. Brezinski ME, Serhan CN (1990) Selective incorporation of (15S)-hydroxyeicosatetraenoic acid in phosphatidylinositol of human neutrophils: agonist-induced deacylation and transformation of stored hydroxyeicosanoids. *Proceedings of the National Academy of Sciences*. **87**, 6248-52.

32. Stenson W, Nickells M, Atkinson J (1983) Esterification of monohydroxyfatty acids into the lipids of a macrophage cell line. *Prostaglandins*. **26**, 253-64.
33. Maskrey, B. H., Bermudez-Fajardo, A., Morgan, A. H., StewartJones, E, Dioszeghy, V., Taylor, G. W., et al. (2007) Activated platelets and monocytes generate four hydroxyphosphatidylethanolamines via lipoxygenase. *J. Biol. Chem.* **282**, 20151–20163
34. Morgan, A. H., Dioszeghy, V., Maskrey, B. H., Thomas, C. P., Clark, S. R., Mathie, S. A., et al. (2009) Phosphatidylethanolamineesterified eicosanoids in the mouse: tissue localization and inflammation-dependent formation in Th-2 disease. *J. Biolog. Chem.* **284**, 21185–21191
35. Slatter, D. A., Aldrovandi, M., O'Connor, A., Allen, S. M., Brasher, C. J., Murphy, R. C., et al. (2016) Mapping the human platelet lipidome reveals cytosolic phospholipase A2 as a regulator of mitochondrial bioenergetics during activation. *Cell. Metab.* **23**, 930–944
36. Clark, S. R., Guy, C. J., Scurr, M. J., Taylor, P. R., Kift-Morgan, A. P., Hammond, V. J., et al. (2011) Esterified eicosanoids are acutely generated by 5-lipoxygenase in primary human neutrophils and in human and murine infection. *Blood.* **117**, 2033–2043
37. Morgan, A. H., Hammond, V. J., Morgan, L., Thomas, C. P., Tallman, K. A., Garcia-Diaz, Y. R., et al. (2010) Quantitative assays for esterified oxylipins generated by immune cells. *Nat. Protoc.* **5**, 1919–1931
38. Hartung, N. M., Mainka, M., Pfaff, R., Kuhn, M., Biernacki, S., Zinnert, L., et al. (2023) Development of a quantitative proteomics approach for cyclooxygenases and lipoxygenases in parallel to quantitative oxylipin analysis allowing the comprehensive investigation of the arachidonic acid cascade. *Anal. Bioanal. Chem.* **415**, 913–933
39. Rund, K. M., Ostermann, A. I., Kutzner, L., Galano, J-M., Oger, C., Vigor, C., et al. (2018) Development of an LC-ESI(-)-MS/MS method for the simultaneous quantification of 35 isoprostanes and isofurans derived from the major n3-and n6-PUFAs. *Anal. Chim. Acta.* **1037**, 63–74
40. Kutzner, L., Rund, K., Ostermann, A., Hartung, N., Galano, J., Balas, L., et al. (2019) Development of an optimized LC-MS method for the detection of specialized pro-resolving mediators in biological samples. *Front. Pharma.* **10**, 169
41. Rund, K. M., and Schebb, N. H. (2024), Chapter 13. Quantitative analysis of eicosanoids and other oxylipins. (2024) A practical guide to metabolomics applications in health and disease: from samples to insights into metabolism, Julijana Ivanisevic & Martin Giera. Springer, Cham, Switzerland, 343–369
42. Smith, P., Krohn, R. I., Hermanson, G., Mallia, A., Gartner, F., Provenzano, M., et al. (1985) Measurement of protein using bicinchoninic acid. *Anal. Biochem.* **150**, 76–85
43. Fauland, A., Trö tzmüller, M., Eber, A., Afiuni-Zadeh, S., Köfeler, H., Guo, X. H., et al. (2013) An improved SPE method for fractionation and identification of phospholipids. *J. Sep. Sci.* **36**, 744–751
44. Pinkart, H. C., Devereux, R., and Chapman, P. J. (1998) Rapid separation of microbial lipids using solid phase extraction columns. *J. Microbiol. Methods.* **34**, 9–15
45. Kaluzny, M., Duncan, L., Merritt, M., and Epps, D. (1985) Rapid separation of lipid classes in high yield and purity using bonded phase columns. *J. Lipid. Res.* **26**, 135–140
46. Matyash V, Liebisch G, Kurzchalia TV, Shevchenko A, Schwudke D (2008) Lipid extraction by methyl-tert-butyl ether for high-throughput lipidomics. *Journal of lipid research*. **49**, 1137-46.
47. Carpanedo L, Rund KM, Wende LM, Kampschulte N, Schebb NH (2024) LC-HRMS analysis of phospholipids bearing oxylipins. *Analytica Chimica Acta*. **1326**, 343139.

48. Ojha A, Bhargava S. (2022) International council for harmonisation (ICH) guidelines. Regulatory affairs in the pharmaceutical industry: Elsevier. p. 47-74.
49. Kowarz E, Löscher D, Marschalek R (2015) Optimized Sleeping Beauty transposons rapidly generate stable transgenic cell lines. *Biotechnology journal*. **10**, 647-53.
50. Hartung NM, Ostermann AI, Immenschuh S, Schebb NH (2021) Combined Targeted Proteomics and Oxylipin Metabolomics for Monitoring of the COX-2 Pathway. *Proteomics*. **21**, 1900058.
51. Shearer GC, Newman JW (2009) Impact of circulating esterified eicosanoids and other oxylipins on endothelial function. *Curr Atherosclerosis Rep*. **11**, 403-10.
52. Hartung NM, Mainka M, Kampschulte N, Ostermann AI, Schebb NH (2019) A strategy for validating concentrations of oxylipin standards for external calibration. *Prostaglandins & Other Lipid Mediators*. **141**, 22-4.
53. Aoyagi R, Ikeda K, Isobe Y, Arita M (2017) Comprehensive analyses of oxidized phospholipids using a measured MS/MS spectra library. *J Lipid Res*. **58**, 2229-37.
54. Nakanishi H, Iida Y, Shimizu T, Taguchi R (2009) Analysis of oxidized phosphatidylcholines as markers for oxidative stress, using multiple reaction monitoring with theoretically expanded data sets with reversed-phase liquid chromatography/tandem mass spectrometry. *J Chromatography B*. **877**, 1366-74.
55. Hammad LA, Wu G, Saleh MM, Klouckova I, Dobrolecki LE, Hickey RJ, et al. (2009) Elevated levels of hydroxylated phosphocholine lipids in the blood serum of breast cancer patients. *Rapid Communications in Mass Spectrometry: An International Journal Devoted to the Rapid Dissemination of Up-to-the-Minute Research in Mass Spectrometry*. **23**, 863-76.
56. Stahnke H, Reemtsma T, Alder L (2009) Compensation of matrix effects by postcolumn infusion of a monitor substance in multiresidue analysis with LC− MS/MS. *Analytical chemistry*. **81**, 2185-92.
57. Wang B, Tontonoz P (2019) Phospholipid remodeling in physiology and disease. *Annu Rev Physiol*. **81**, 165-88.
58. O'Donnell VB, Aldrovandi M, Murphy RC, Krönke G (2019) Enzymatically oxidized phospholipids assume center stage as essential regulators of innate immunity and cell death. *Sci Signal*. **12**, eaau2293.
59. Klett EL, Chen S, Yechoor A, Lih FB, Coleman RA (2017) Long-chain acyl-CoA synthetase isoforms differ in preferences for eicosanoid species and long-chain fatty acids. *J Lipid Res*. **58**, 884-94.
60. Caddeo A, Hedfalk K, Romeo S, Pingitore P (2021) LPIAT1/MBOAT7 contains a catalytic dyad transferring polyunsaturated fatty acids to lysophosphatidylinositol. *Biochimica et Biophysica Acta (BBA)-Molecular and Cell Biology of Lipids*. **1866**, 158891.
61. Matsuda S, Inoue T, Lee HC, Kono N, Tanaka F, Gengyo-Ando K, et al. (2008) Member of the membrane-bound O-acyltransferase (MBOAT) family encodes a lysophospholipid acyltransferase with broad substrate specificity. *Genes to Cells*. **13**, 879-88.
62. Hishikawa D, Shindou H, Kobayashi S, Nakanishi H, Taguchi R, Shimizu T (2008) Discovery of a lysophospholipid acyltransferase family essential for membrane asymmetry and diversity. *Proc Natl Academy Sci*. **105**, 2830-5.
63. Shindou H, Hishikawa D, Nakanishi H, Harayama T, Ishii S, Taguchi R, et al. (2007) A single enzyme catalyzes both platelet-activating factor production and membrane biogenesis of inflammatory cells: cloning and characterization of acetyl-CoA: LYSO-PAF acetyltransferase. *J Biolog Chem*. **282**, 6532-9.

64. Valentine WJ, Yanagida K, Kawana H, Kono N, Noda NN, Aoki J, et al. (2022) Update and nomenclature proposal for mammalian lysophospholipid acyltransferases, which create membrane phospholipid diversity. *Journal of Biological Chemistry*. **298**, 101470.
65. Protty, M. B., Tyrrell, V. J., Hajeyah, A. A., Morgan, B., Costa, D., Li, Y., et al. (2025) Aspirin modulates generation of procoagulant phospholipids in cardiovascular disease, by regulating LPCAT3. *J. Lipid Res.* **66**, 100727
66. Epand RM (2017) Features of the phosphatidylinositol cycle and its role in signal transduction. *The Journal of membrane biology*. **250**, 353-66.
67. Huang YH, Sauer K (2010) Lipid signaling in T-cell development and function. *Cold Spring Harbor perspectives in biology*. **2**, a002428.
68. Song G, Ouyang G, Bao S (2005) The activation of Akt/PKB signaling pathway and cell survival. *Journal of cellular and molecular medicine*. **9**, 59-71.
69. Wang X (2004) Lipid signaling. *Current opinion in plant biology*. **7**, 329-36.
70. Kontny E, ZiÓŁKowska M, Ryżewska A, Maśliński W (1999) Protein kinase C-dependent pathway is critical for the production of pro-inflammatory cytokines (TNF-α, IL-1β, IL-6). *Cytokine*. **11**, 839-48.
71. Setty B, Graeber J, Stuart M (1987) The mitogenic effect of 15-and 12-hydroxyeicosatetraenoic acid on endothelial cells may be mediated via diacylglycerol kinase inhibition. *Journal of Biological Chemistry*. **262**, 17613-22.
72. Browning LM, Walker CG, Mander AP, West AL, Madden J, Gambell JM, et al. (2012) Incorporation of eicosapentaenoic and docosahexaenoic acids into lipid pools when given as supplements providing doses equivalent to typical intakes of oily fish. *The American journal of clinical nutrition*. **96**, 748-58.
73. Schuchardt JP, Ostermann AI, Stork L, Kutzner L, Kohrs H, Greupner T, et al. (2016) Effects of docosahexaenoic acid supplementation on PUFA levels in red blood cells and plasma. *Prostaglandins, Leukotrienes and Essential Fatty Acids*. **115**, 12-23.
74. Dawczynski C, Massey KA, Ness C, Kiehntopf M, Stepanow S, Platzer M, et al. (2013) Randomized placebo-controlled intervention with n-3 LC-PUFA-supplemented yoghurt: effects on circulating eicosanoids and cardiovascular risk factors. *Clinical nutrition*. **32**, 686-96.
75. Ostermann AI, West AL, Schoenfeld K, Browning LM, Walker CG, Jebb SA, et al. (2019) Plasma oxylipins respond in a linear dose-response manner with increased intake of EPA and DHA: results from a randomized controlled trial in healthy humans. *The American journal of clinical nutrition*. **109**, 1251-63.
76. Kirchhoff R, Kampschulte N, Rothweiler C, Rohwer N, Weylandt KH, Schebb NH (2025) An Optimized Ex Vivo n–3 PUFA Supplementation Strategy for Primary Human Macrophages Shows That DHA Suppresses Prostaglandin E2 Formation. *Molecular Nutrition & Food Research*. **69**, e202400716.
77. Calder PC (2015) Functional roles of fatty acids and their effects on human health. *Journal of parenteral and enteral nutrition*. **39**, 18S-32S.
78. Calder PC (2012) Mechanisms of action of (n-3) fatty acids. *The Journal of nutrition*. **142**, 592S-9S.
79. Calder PC (2008) Session 3: Joint nutrition society and Irish nutrition and dietetic institute symposium on 'Nutrition and autoimmune disease'PUFA, inflammatory processes and rheumatoid arthritis: Symposium on 'the challenge of translating nutrition research into public health nutrition'. *Proceedings of the Nutrition Society*. **67**, 409-18.

Chapter 5

Concluding Remarks and Future Perspectives

Oxylipins are potent lipid mediators derived from PUFA and are predominantly found esterified to complex lipids, such as PL, in biological samples. Within this thesis, the analytical and pre-analytical basis for a comprehensive analysis of unoxidized and oxidized PL in biological samples has been established. The presented untargeted LC-HRMS methods enable a comprehensive and unbiased analysis of isobaric and isomeric (ox)PL from different lipid classes. Full MS detection settings – the auxiliary gas and the S-lens RF level – were found to be crucial for reducing noise and enhancing the sensitivity of the analysis. Sufficient chromatographic separation of isobaric and positional isomeric (ox)PL species was achieved over an extended elution window using an RP C18 column, enabling the acquisition of meaningful MS^2 spectra for each (ox)PL species. Characterization of (ox)PL species – including the polar head group, (oxidized) fatty acyl chains, their *sn*-positions, and the position of the oxidation in the oxPUFA – was performed using precursor ions, characteristic product ions, and retention times. Isobaric PL species with different fatty acyl chain compositions could be distinguished based on the characteristic product ions of their fatty acyl chains. Likewise, isomeric PL species containing positional isomeric oxylipins could be distinguished by characteristic α-cleavage occurring at the oxidation site on the oxylipin. The retention time dependence of unoxidized PL on carbon number or degree of unsaturation, along with the consistent shifts observed between corresponding oxPL analogues, provides strong support for highly confident characterization. Notably, retention time shifts are crucial to distinguish isomeric plasmalogen and ether PL species with identical fragmentation behavior. All in all, reliable characterization of thousands of (ox)PL species is achievable by untargeted LC-HRMS even in the absence of authentic standards.

In lipidomics, quantification typically relies on a single IS per lipid class due to the limited availability of standards and the presence of thousands of distinct lipid species. Evaluation of the extraction recovery as well as the ion matrix is essential, as one IS cannot compensate for potential loss during extraction and matrix effects affecting analytes. In the developed methods, the sample volume for the extraction of PL and oxPL in human plasma and cells was carefully selected to ensure the sensitive detection of analytes while minimizing ion suppression effects. The addition of standards prior to or post-extraction showed excellent extraction recovery for unoxidized and oxidized PL tested. Semi-quantification of (ox)PL based on peak heights, using a single IS per lipid class, offered a straightforward and effective approach that produced meaningful results. PL species that changed significantly following n-3 PUFA supplementation in human plasma were successfully characterized and semi-quantified. Lipids containing 20:5 were the most elevated, whereas those bearing 22:4 showed the greatest decrease. For identification and accurate quantification of selected (ox)PL, targeted LC-MS/MS methods were developed based on the established untargeted methods. Targeted quantitative analysis of selected PL in human plasma from subjects supplemented with n3-PUFA confirmed their tentative identification and yielded comparable concentrations compared to those obtained by untargeted LC-HRMS. Similarly, resulting concentrations of the sum of individual oxPL species were remarkably consistent compared to those obtained via indirect quantification of esterified oxylipins following alkaline hydrolysis. Of note, the synthesis of authentic standards for additional analytes would be valuable to confirm their identification and achieve accurate quantification.

Combined untargeted and targeted oxPL LC-MS analyses, along with indirect quantification in lipid fractions, showed distinct incorporation patterns of regioisomer oxylipins into both PL classes and species in human cells. Indirect quantification of esterified oxylipins in lipid fractions revealed that over 90% of hydroxy-PUFA are incorporated into PL while less than 10% are present in NL from cells overexpressing the 15-LOX-2 enzyme. In oxylipin-supplemented cells, the proportion detected in NL is higher (25%) due to saturation of the mechanism

for the esterification into both PI and PL. The incorporation of oxylipins into specific NL species, i.e. TG, Chol Ester, and DG, is not considered within the scope of this thesis. Extending the presented LC-MS methods to their analysis could be valuable for the comprehensive evaluation of oxylipin incorporation into both polar and non-polar lipid species.

Oxylipins formed endogenously via 15-LOX-2 and supplemented oxylipins showed comparable incorporation into PL, with a few exceptions observed in PE species. The observed distinct incorporation of oxylipins into PL classes is influenced by the carbon chain length and degree of unsaturation but is primarily determined by the position of the oxidation of the oxylipin. Positional analogues exhibited nearly identical incorporation patterns – for example, the pairs 20:4;14Ep/20:4;15Ep, 20:4;11Ep/20:4;12Ep, and 20:4;8Ep/20:4;9Ep – following supplementation with a mixture of epoxy-PUFA regioisomers. Similarly, the pair 22:6;17OH and 22:5;17OH exhibited comparable incorporation into PL classes from cells overexpressing 15-LOX-2, with predominant incorporation into PE-P species. Oxylipins with a hydroxy or epoxy functionality at the C12-position, namely 20:4;12OH, 20:4;11Ep, and 20:5;11Ep, were mostly detected to PC, specifically at the *sn*-2 position of PC bearing 16:0. In contrast, oxylipins with a hydroxy or epoxy functionality at the C15-position, namely 20:4;15OH, 20:5;15OH, 20:4;14Ep, and 20:5;14Ep, were preferentially incorporated into PI, particularly at the *sn*-2 position of PI bearing 18:0. Notably, 20:4;15OH and 20:5;15OH were esterified almost exclusively into PI species, representing more than 70% of their total lipid incorporation. Therefore, the development of LC-MS methods for the analysis of the phosphorylated derivatives of PI is of great interest for evaluating the relation between the incorporation of 20:4;15OH (and 20:5;15OH) and the two distinct PI-based signaling pathways. Specifically, the characterization of PIP, PIP_2, and PIP_3 species bearing oxylipins is particularly relevant to the Akt/PKB signaling pathway, while the analysis of PIP and PIP_2 bearing oxylipins is crucial in the context of the PI-cycle pathway. For the latter pathway, the analysis of the hydrophobic DG species would also be valuable, as they are second messengers generated through the cleavage of PIP_2 by PLC. The distinct incorporation patterns of oxylipins are likely driven by the substrate

specificity of LPLAT enzymes. Indeed, different LPLAT isoforms have been shown to exhibit specificity toward both their acyl-CoA substrates and lysoPL acceptors. While several studies have investigated the preference of LPLAT enzymes for unoxidized FA substrates, no experiments to date have specifically examined their activity toward oxylipins. Exploring the substrate specificity of LPLAT enzymes for oxylipins thus represents a promising and valuable area of research.

Overall, this thesis advances our understanding of oxylipin incorporation into PL classes and molecular species through a combined analytical approach. New untargeted LC-HRMS methods enabled a comprehensive detection of lipids, while targeted LC-MS/MS allowed the accurate quantification of selected lipids.

Summary

Phospholipids (PL) are the main components of the cellular membranes and play a key role in cell signaling. They consist of a glycerol backbone with two fatty acid chains attached at the *sn*-1 and *sn*-2 position, while the *sn*-3 position contains a phosphate group linked to an organic moiety. Saturated fatty acids are usually bound at the sn-1 position, whereas the *sn*-2 position is typically occupied by polyunsaturated fatty acids (PUFA). Diet can modulate the proportion of n6-PUFA and n3-PUFA in the organism. In Western diets, n6-PUFA contained in soybean and sunflower oils are largely consumed, while the intake of n3-PUFA from flaxseed oils or fatty fish remains low. This results in a high n6- to n3-PUFA ratio. However, n6-PUFA are prone to pro-inflammation, whereas n3-PUFA are associated with anti-inflammatory and beneficial health effects.

In **Chapter 2**, an untargeted LC-high resolution (HR)MS method operating in Full MS/data-dependent (dd) MS^2 TOP *N* mode was developed for the semi-quantification of polar lipids in plasma to investigate the effect of n3-PUFA supplementation on the PL pattern. The settings of the Full MS and MS^2 detection were thoroughly characterized and optimized. The heated auxiliary gas facilitating the ionization of the lipids had the greatest impact on spray stability. In contrast, the S-lens RF level focusing the ion beam to the quadrupole had the strongest influence on signal intensity. Optimized MS settings improved peak shape and increased signal intensity of lipids by a factor 3 compared to default parameters. The TOP *N* setting, which determines the acquisition of MS^2 spectra for a *N* number of precursor ions, was adjusted across chromatographic runs based on peak width: narrower peaks required a lower TOP *N* value, while broader peaks allowed for a higher TOP *N*. This ensured sufficient data points across chromatographic peaks and enabled ddMS^2 acquisition to be triggered for as many lipids as possible.

Chromatographic separation of critical isobaric pairs was successfully achieved over a long elution window on a reversed-phase C18 column with charged hydrid particles. Fragmentation of PL in positive and negative electrospray mode yielded characteristic product ions of the fatty acyl chains and the polar head group. This combined analysis in both ionization modes ensured a comprehensive detection of lipids as well as a confident characterization of lipid species.

Good extraction recovery as well as minimized ion suppression effects are key to ensure accurate quantification as lipidomics analysis typically relies on one internal standard per lipid class. Two liquid-liquid extraction (LLE) protocols were evaluated: one using MeOH/MTBE, and the other involving a two-step procedure with IPA/*n*-hexane followed by $CHCl_3$/MeOH. The MeOH/MTBE-based LLE was selected as it resulted in good extraction > 85% for all lipid classes with a low inter- and intra-day variability < 15%. Ion suppression analysis using post-column infusion of a standard revealed a complete signal drop (at *m/z* 759.5875) attributed to an interfering PL with a nearly identical *m/z* and high concentration in the plasma. The addition of standard prior or post-extraction revealed excellent extraction recovery and acceptable ion suppression effects for all analytes tested, with a few exceptions.

The developed method was successfully applied to evaluate the change in the plasma PL pattern following 12 months of n3-PUFA supplementation. Evaluation using MS-DIAL software resulted in 1399 features and 580 features, respectively, in ESI(+) and ESI(-) modes. Statistical evaluation of the significant changes yielded 348 features in ESI(+) mode and 151 features in ESI(-) mode, respectively. From these, a total of 101 polar lipids were semi-quantified using one internal standard per lipid class. Following n3-PUFA supplementation, the most pronounced increasing lipids bear 20:5, while lipids containing 22:4 were the most decreased. Quantitative targeted analysis of selected PL using corresponding standards resulted in comparable concentrations to those semi-quantified by untargeted LC-HRMS. Specifically, LPC 20:5_0:0 and PC 16:0_20:5 were found to be the strongest elevated, while PE 18:0_22:4 and PC 18:2_18:2 were decreased after n3-PUFA supplementation.

PUFA bound in the *sn*-2 position of PL can undergo oxidation through two distinct pathways (i) the oxidation of non-esterified PUFA or (ii) the direct oxidation of PUFA esterified to PL. Oxidation of PUFA can occur through enzymatic or non-enzymatic processes and leads to the formation of structurally distinct products known as oxylipins. These are potent lipid mediators involved in the regulation of physiological functions, and alterations in the oxylipin profiles have been associated with the pathogenesis of several diseases. Oxylipins can be present in non-esterified form in biological samples, but the major part is bound to lipids such as PL. Research on the biological effects of esterified oxylipins remains scarce as the direct analysis of oxPL is challenging due to (i) the presence of many isobaric and isomeric oxPL, (ii) the lack of commercially available standards for identification and quantification, and (iii) their low concentrations in biological samples.

In **Chapter 3** of this thesis, an untargeted LC-ESI(-)-HRMS method was developed for the semi-quantitative analysis of PL bearing oxylipins, specifically hydroxy- and epoxy-PUFA. This method was developed based on the LC-HRMS method established in Chapter 2. Due to the extremely limited availability of commercial standards, oxidized standards were generated from non-oxidized ones using 15-LOX-1, and biological samples also served as sources of esterified oxylipins. A human serum with an exceptionally high concentration of esterified hydroxy-PUFA was used. Non-esterified epoxy-PUFA were supplemented to human cells, leading to their incorporation into lipid membranes as PL bearing epoxy-PUFA. Generated standards and biological samples were used for the method development.

Chromatographic separation of isobaric and isomeric oxPL species was optimized on a reversed-phase C18 column over a long isocratic elution window. Baseline separation for several PL species bearing positional isomer oxylipins could be achieved, for example the critical pair PI 18:0/18:2;12Ep and PI 18:0/18:2;9Ep. For isomeric oxPL species that could not be baseline-separated, the resolution was sufficient to acquire at least one meaningful MS^2 spectrum per isomer and to deduce their elution order. The elution order of the oxPL classes is identical to the RP separation of unoxidized PL, with oxPI eluting

earliest, followed by oxPS, oxPC, oxPE, oxPC-P, oxPC-O, and oxPE-P. Isomeric plasmalogen PL and ether PL exhibiting identical fragmentation behavior could be confidently differentiated based on their elution, with PL-P eluting earlier than its isomeric PL-O. The elution order of individual hydroxy- and epoxy-PUFA bound to PL is the same for the different lipid classes. Notably, PL of different classes bearing the same fatty acyl chains were baseline separated with a few exceptions. Separation of *sn*-1/*sn*-2 isomeric oxPL was assessed using the oxidized standard and was achieved for 5 out of 9 standards with R > 1.5, while the others were partially overlapping. Corresponding PL bearing position-isomeric oxylipins, e.g., PC 16:0/20:4;15OH and PC 16:0/20:4;14Ep, presenting identical MS^2 spectra, were differentiated based on their retention times with epoxy-PUFA eluting later than the corresponding hydroxy-PUFA.

A total of 422 oxPL were detected in the human serum and the oxylipin-supplemented cells. The detected oxPL typically bear 16:0, 18:0, or 18:1 at the *sn*-1 position, and an oxPUFA at the *sn*-2 position, such as 18:2;O, 20:4;O, 20:5;O, or 22:6;O. OxPL species were thoroughly characterized based on retention time, precursor ion within a mass tolerance ≤ 3 ppm, and characteristic product ions acquired in ESI(-) mode. The fatty acyl chain composition of each oxPL species was deduced based on the product ions of the (ox)FA. The position of the oxidation of the oxPUFA was determined based on the characteristic α-cleavage occurring at the epoxy or hydroxy group. Moreover, the *sn*-position of the fatty acyl chain was assessed using the preferential neutral loss of the (ox)FA in the *sn*-2 position as a ketene. This distinct fragmentation behavior could be shown using (oxidized) PL standards, which contained a mixture of isomeric *sn*-1/*sn*-2 (ox)PL. Notably, the *sn*-position also influences the intensity of the fatty acyl chain product ions, with a higher abundance observed for the (ox)FA bound at the *sn*-2 position compared to that at *sn*-1.

The developed LC-HRMS method was employed to investigate the incorporation of hydroxy-20:4, epoxy-18:2, -20:4, and -20:5 regioisomers into PL of human cells. Parallel analysis of non-esterified and total oxylipins by targeted LC-MS/MS following alkaline hydrolysis (total analysis) showed that almost all oxylipins in the cells are esterified (> 96 %). Using untargeted LC-HRMS, a total

of 153 oxPL species were semi-quantified in oxylipin-supplemented cells using one internal standard per lipid class. Oxylipins were found esterified in PI, PS, PC, PE, PC-P, PC-O, and PE-P lipid classes. A distinct incorporation of regiosiomers into PL classes was observed. While 20:4;15OH was exclusively detected in PI, 20:4;12OH and 20:4;5OH were mostly found in PC, and to a lesser extent in PE. Positional analogues of epoxy-20:4 and epoxy-20:5 showed an almost identical distribution in the lipid classes. For example, 43% of 20:4;14Ep and 41% of 20:5;14Ep were incorporated in PI, and 38% *vs.* 39%, respectively, were detected in PC.

Addition of exogenous oxylipins resulted in distinct incorporation into specific PL classes and species. However, this may not accurately reflect the "*in vivo*" incorporation behavior within the cells. In **Chapter 4** of this thesis, the incorporation of endogenously formed oxylipins was investigated using a genetically modified HEK293T cell line overexpressing the 15-LOX-2 enzyme, and the results were compared to those obtained from exogenous supplementation. As a first approach, esterified oxylipins formed via 15-LOX-2 were indirectly quantified in lipid fractions separated using hydrophilic interaction liquid chromatography (HILIC)-based cartridges. Indirect quantification of esterified hydroxy-PUFA revealed that over 75% are bound to PL, while less than 25% are found in neutral lipids. A comparable incorporation pattern into PL classes was observed between endogenously formed 15-LOX-derived oxylipins and those incorporated following supplementation. Of note, 15-HETE and 15-HEPE endogenously formed were found to be more incorporated into PE compared to exogenous addition.

To further characterize the molecular PL species, a targeted LC-ESI(-)-MS/MS method for the analysis of oxPL was developed based on the untargeted LC-HRMS established in Chapter 3. MS detection was performed using multiple reaction monitoring (MRM), recording three mass transitions for each oxPL species and two for oxPL-P and oxPC-O species. For quantification, the mass transition involving the specific product ion resulting from the α-cleavage of the oxPUFA moiety was used, while the product ions corresponding to the fatty acyl chains served as qualifiers. The new targeted

LC-MS/MS method covered the analysis of 67 PL bearing hydroxy-PUFA and was validated in terms of sensitivity, linearity, extraction recovery, accuracy, precision, and dilution integrity. Quantitative targeted analysis of oxPL in 15-LOX-2 overexpressing led to nearly identical concentrations when compared to indirect quantification of esterified oxylipins following hydrolysis.

Targeted analysis of oxPL showed a distinct incorporation of hydroxy-PUFA into both PL classes and species in 15-LOX-2 overexpressing and oxylipin-supplemented cells. 20:4;15OH (15-HETE) and 20:5;15OH (15-HEPE) showed a restricted distributed into PI species bearing 18:0, 18:1, and 16:0. Specifically, 70% of 20:4;15OH and 80% of 20:5;15OH were esterified in the *sn*-2 position of PI bearing 18:0. These oxylipins were also detected in minor amounts in PC and PE species. In contrast, 22:6;17OH (17-HDHA) and 18:2;13OH (13-HODE) were more evenly distributed across the PL classes and species. Half of 22:6;17OH was incorporated in the *sn*-2 position of PE-P species bearing 16:0, 18:0, and 18:1. Most of 18:2;13OH was found in PC with a marked abundance of PC 16:0/18:2;13OH at 50%, while the other half was distributed mainly between PC(-O) and PI species. For 22:6;17OH and 18:2;13OH the second most abundant PL class was PI, specifically PI bearing 18:0. The associated biological effects of esterified oxylipins remain to be uncovered, but this preferential incorporation of 20:4;15OH and 20:5;15OH into PI may be biologically relevant in the context of PI-based signaling pathways.

Appendix

Chapter 2

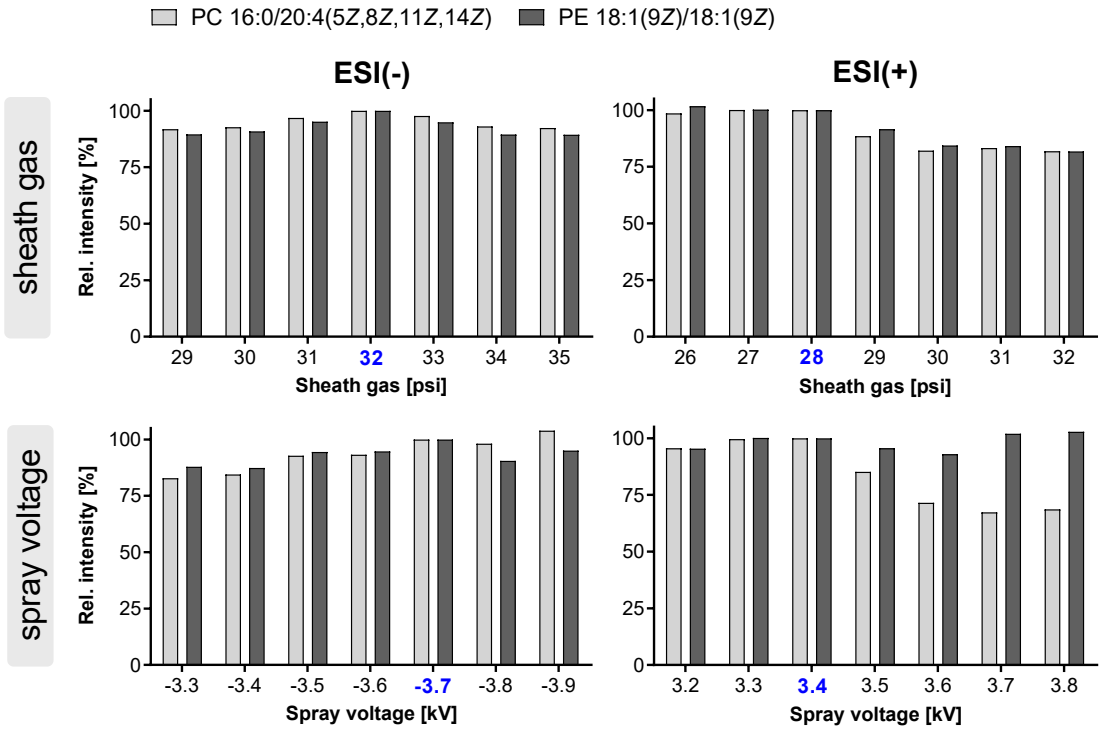

Fig. 8.1: Effect of selected source parameters on the intensity of the ESI-MS signal (orbitrap Q Exactive HF). Shown is the influence of **(top)** the sheath gas and **(bottom)** spray voltage on the signal intensity in ESI(-) and in ESI(+) mode for PC 16:0/20:4(5*Z*,8*Z*,11*Z*,14*Z*) and PE 18:1(9*Z*)/18:1(9*Z*), while other parameters were set to default (Fig. 2.1). Intensities are depicted relative to the signal intensity at the optimized values highlighted in blue.

ESI-spray voltage and sheath gas showed only little effect on the signal intensity around the optimal range (Fig. 8.1). Increasing the spray voltage from |2| to |4| kV increased the signal, but higher values led to a less stable spray. In the optimal range (|3.3| – |3.8| kV), the applied voltage showed only marginal effects on the signal intensity of PE 18:1(9*Z*)/18:1(9*Z*) in both ionization modes (≤ 12%), while for PC 16:0/20:4(5*Z*,9*Z*,11*Z*,14*Z*) the signal intensity was increased by 33% in ESI(+) and 17% in ESI(-). The selected optimized values, i.e., 3.4 and – 3.7 kV, are lower compared to the spray voltage used in the application note (i.e. |4.2| kV) and higher compared to the default settings in negative mode (i.e., 2.5 kV). However, our results are in line with previous methods using a Q Exactive HF for the analysis of lipids in rat plasma and liver [1] and in pituitary adenoma tissues [2] with a spray voltage between |3| and |4| kV. Variation of the sheath gas flow (range 10 – 50 psi) showed for both lipids the same change in signal intensity, having a greater effect in ESI(+). 32 and 28 psi were chosen in ESI(-) and ESI(+), respectively. Using the same flow rate (i.e. 260 µL min^{-1}), Hu *et al.* used a higher sheath gas flow of 45 psi in both ionization modes for lipidomics analysis, which is similar to the default settings. However, they did not show if and how this value was optimized [2].

The sweep gas flows towards the entrance of the heated ion transfer tube at the sweep cone thus acting as a barrier for non-charged molecules and non-volatiles preventing contamination of the source. Increasing the sweep gas flow (i.e. from 2 to 8 psi) led to a slight increase in signal intensity. However, this resulted also in elevated noise of the signal. The selected sweep gas flow of 2 psi was consistent with previously described methods using a sweep gas flow of 1 psi for lipidomics analysis [1, 3, 4]. No noticeable effect on the signal could be observed when varying the capillary temperature (i.e. 200 °C – 350 °C). Thus 250 °C was selected, which is consistent with the range (230 °C – 350 °C) used in other lipidomics methods [1, 3-7].

1. Narváez-Rivas M, Zhang Q (2016) Comprehensive untargeted lipidomic analysis using core–shell C30 particle column and high field orbitrap mass spectrometer. Journal of Chromatography A. **1440**, 123-34.
2. Hu C, Zhou Y, Feng J, Zhou S, Li C, Zhao S, et al. (2019) Untargeted lipidomics reveals specific lipid abnormalities in nonfunctioning human pituitary adenomas. Journal of proteome research. **19**, 455-63.
3. Criscuolo A, Zeller M, Cook K, Angelidou G, Fedorova M (2019) Rational selection of reverse phase columns for high throughput LC–MS lipidomics. Chemistry and physics of lipids. **221**, 120-7.
4. Khan MJ, Codreanu SG, Goyal S, Wages PA, Gorti SK, Pearson MJ, et al. (2020) Evaluating a targeted multiple reaction monitoring approach to global untargeted lipidomic analyses of human plasma. Rapid Communications in Mass Spectrometry. **34**, e8911.
5. Shan J, Qian W, Kang A, Peng L, Xie T, Lin L, et al. (2019) Lipid profile perturbations in the plasma and lungs of mice with LPS-induced acute lung injury revealed by UHPLC-ESI-Q Exactive HF MS analysis. Journal of pharmaceutical and biomedical analysis. **162**, 242-8.
6. Chen W, Zeng J, Wang W, Yang B, Zhong L, Zhou J (2020) Comprehensive metabolomic and lipidomic analysis reveals metabolic changes after mindfulness training. Mindfulness. **11**, 1390-400.
7. Schwaiger M, Schoeny H, El Abiead Y, Hermann G, Rampler E, Koellensperger G (2019) Merging metabolomics and lipidomics into one analytical run. Analyst. **144**, 220-9.

Table 8.1: Exclusion list for ESI(+) and ESI(-) mode used for the Full MS/ddMS^2 TOP *N* acquisition. Shown are the *m/z* of common contaminants found in solvents and extraction blanks to exclude from MS^2 data acquisition.

ESI(+)		ESI(-)	
462.1463		665.1593	
508.1886		666.0596	
536.1653		729.1785	
554.1757		803.1971	Polysiloxanes
582.2070		877.2155	
610.1838		951.2345	
628.1946	Polysiloxanes	1025.2535	
656.2259		1173.2897	
702.2131			
730.2444			
776.2322			
804.2635			
663.4532			
684.2029			
708.5112	Alkane polymers		
363.2630			
419.3156	Phtalates		
447.3469			

Table 8.2: Inclusion list in ESI(+) and ESI(-) mode used for the Full MS/ddMS^2 TOP *N* acquisition. Shown are the m/z of ions of PC and PE bearing biologically relevant PUFA included in the inclusion list.

PC							
ESI(+)				ESI(-)			
analyte	[M + H]$^+$	analyte	[M + H]$^+$	analyte	[M + COOH]$^-$	analyte	[M + COOH]$^-$
PC 18:0_18:2	786.6007	PC 16:0_18:2	758.5694	PC 18:0_18:2	830.5917	PC 16:0_18:2	802.5604
PC 18:0_18:3	784.5851	PC 16:0_18:3	756.5538	PC 18:0_18:3	828.5760	PC 16:0_18:3	800.5447
PC 18:0_20:4	810.6007	PC 16:0_20:4	782.5694	PC 18:0_20:4	854.5917	PC 16:0_20:4	826.5604
PC 18:0_20:5	808.5851	PC 16:0_20:5	780.5538	PC 18:0_20:5	852.5760	PC 16:0_20:5	824.5447
PC 18:0_22:6	834.6007	PC 16:0_22:6	806.5694	PC 18:0_22:6	878.5917	PC 16:0_22:6	850.5604
PC 18:0_22:4	838.6320	PC 16:0_22:4	810.6007	PC 18:0_22:4	882.6230	PC 16:0_22:4	854.5917
PE							
ESI(+)				ESI(-)			
analyte	[M + H]$^+$	analyte	[M + H]$^+$	analyte	[M – H]$^-$	analyte	[M – H]$^-$
PE 18:0_18:2	744.5538	PE 16:0_18:2	716.5225	PE 18:0_18:2	742.5329	PE 16:0_18:2	714.5079
PE 18:0_18:3	742.5381	PE 16:0_18:3	714.5068	PE 18:0_18:3	740.5236	PE 16:0_18:3	712.4923
PE 18:0_20:4	768.5538	PE 16:0_20:4	740.5225	PE 18:0_20:4	766.5392	PE 16:0_20:4	738.5079
PE 18:0_20:5	766.5381	PE 16:0_20:5	738.5068	PE 18:0_20:5	764.5236	PE 16:0_20:5	736.4923
PE 18:0_22:6	792.5538	PE 16:0_22:6	764.5225	PE 18:0_22:6	790.5392	PE 16:0_22:6	762.5079
PE 18:0_22:4	796.5851	PE 16:0_22:4	768.5538	PE 18:0_22:4	794.5705	PE 16:0_22:4	766.5392

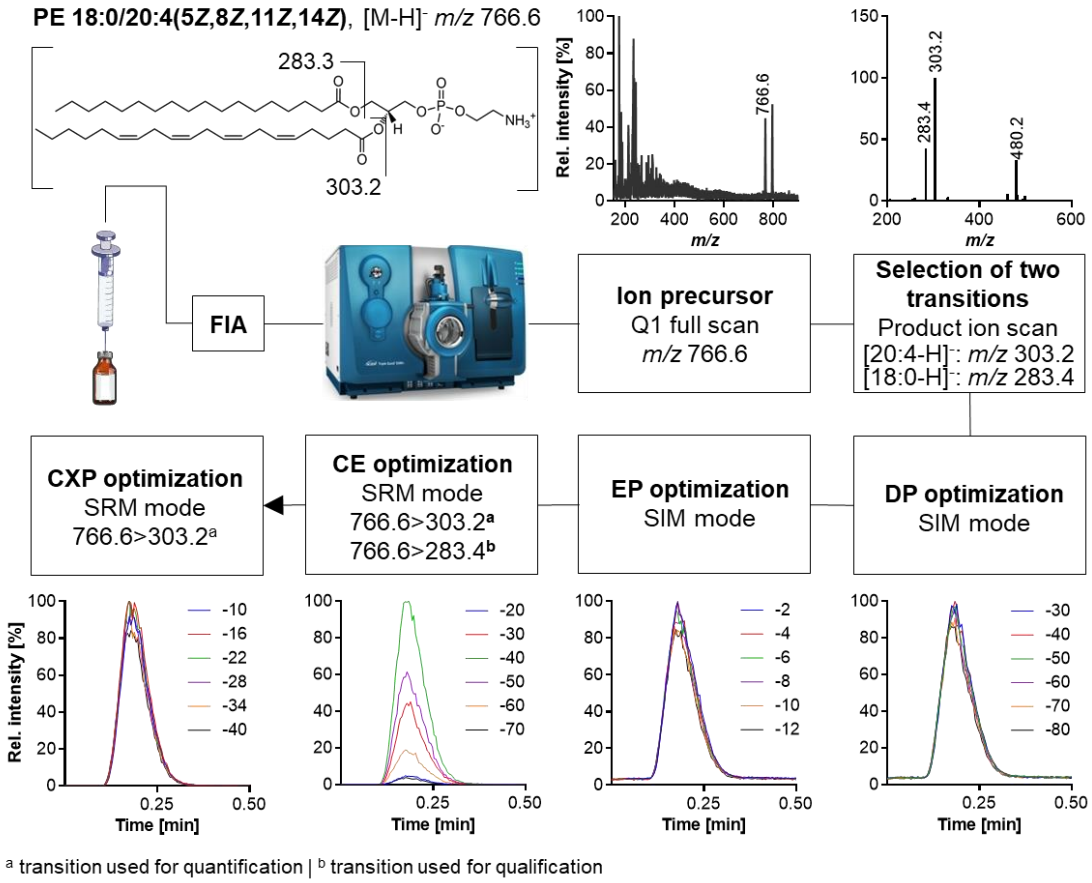

Fig. 8.2: Method development of the targeted LC-ESI(-)-MS/MS method. Shown is a scheme illustrating the individual steps of optimization including selection of transitions, as well as optimization of electronic parameters, i.e., DP, EP, CE, and CXP. Optimization was carried out by FIA from repeated injections of 5 µL of a standard solution. Data is shown exemplary for PE 18:0/20:4(5Z,8Z,11Z,14Z).

Table 8.3: Parameters and method performance of the targeted LC-ESI(-)-MS/MS method. Shown are the mass transitions in scheduled MRM mode, electronic MS parameters (DP, EP, CE, CXP), the t_R, the FWHM, the LOD, the calibration range, and the correlation coefficient (R^2) of the linear calibration. PC 15:0/18:1[D7] IS was assigned to PC species and PE 15:0/18:1[D7] to PE species.

Analyte		mass transition		MS parameters				t_R[c]	FWHM[c]	LOD[d]	calibration range LLOQ[e]	[f]	R^2[g]
		Q1	Q3	DP	EP	CE	CXP	[min]	[s]	[nmol L^{-1}]	[nmol L^{-1}]		
PC 18:2(9Z,12Z) /18:2(9Z,12Z)	[a]	826.6	279.3	-11	-3	-46	-22	11.11 ± 0.07	14.37 ± 0.30	0.24	0.49	1004	0.998
PC 18:0/20:5 (5Z,8Z,11Z,14Z,17Z)	[a]	852.7	301.1	-10	-2	-46	-17	15.20 ± 0.09	15.97 ± 0.25	0.77	1.5	1060	0.998
	[b]	852.7	283.4	-10	-2	-53	-17	15.19 ± 0.09	15.14 ± 0.56				
PC 18:0/22:6 (4Z,7Z,10Z,13Z,16Z,19Z)	[a]	878.7	327.3	-30	-7	-45	-11	17.01 ± 0.09	16.04 ± 0.35	1.8	3.6	920	0.998
	[b]	878.7	283.3	-30	-7	-53	-11	17.01 ± 0.10	17.21 ± 0.62				
PE 18:0/20:4 (5Z,8Z,11Z,14Z)	[a]	766.6	303.2	-50	-2	-40	-15	19.53 ± 0.10	14.89 ± 0.19	0.22	0.45	925	0.998
	[b]	766.6	283.4	-50	-2	-49	-15	19.53 ± 0.10	15.58 ± 0.54				
PE 18:0/22:4 (7Z,10Z,13Z,16Z)	[a]	794.6	331.3	-35	-2	-43	-16	22.24 ± 0.03	6.97 ± 0.20	0.23	0.46	956	0.998
	[b]	794.6	283.3	-35	-2	-53	-16	22.23 ± 0.03	7.93 ± 0.13				
PC 15:0/18:1[D7] (IS)	[a]	797.5	288.4	-40	-2	-51	-16	15.59 ± 0.09	16.99 ± 0.26				
	[b]	797.5	241.4	-40	-2	-55	-16	15.58 ± 0.10	16.95 ± 0.53				
PE 15:0/18:1[D7] (IS)	[a]	709.5	288.4	-40	-2	-45	-16	16.79 ± 0.10	14.91 ± 0.20				
	[b]	709.5	241.3	-40	-2	-40	-16	16.78 ± 0.10	15.31 ± 0.24				

[a] mass transition used for quantification.
[b] mass transition used for qualification.
[c] t_R and FWHM were determined as mean from standards with the concentration 100 nmol L^{-1} (n = 3).
[d] LOD was set to the lowest concentration yielding a S/N ratio ≥ 3.
[e] LLOQ was set to the lowest calibration standard injected yielding a S/N ratio ≥ 5 and an accuracy in the calibration curve within 100 ± 20%.
[f] concentration does not represent the end of the dynamic range, but is the highest calibration standard injected.
[g] Calibration was performed as linear weighted least square regression using $1/x^2$ weighting.

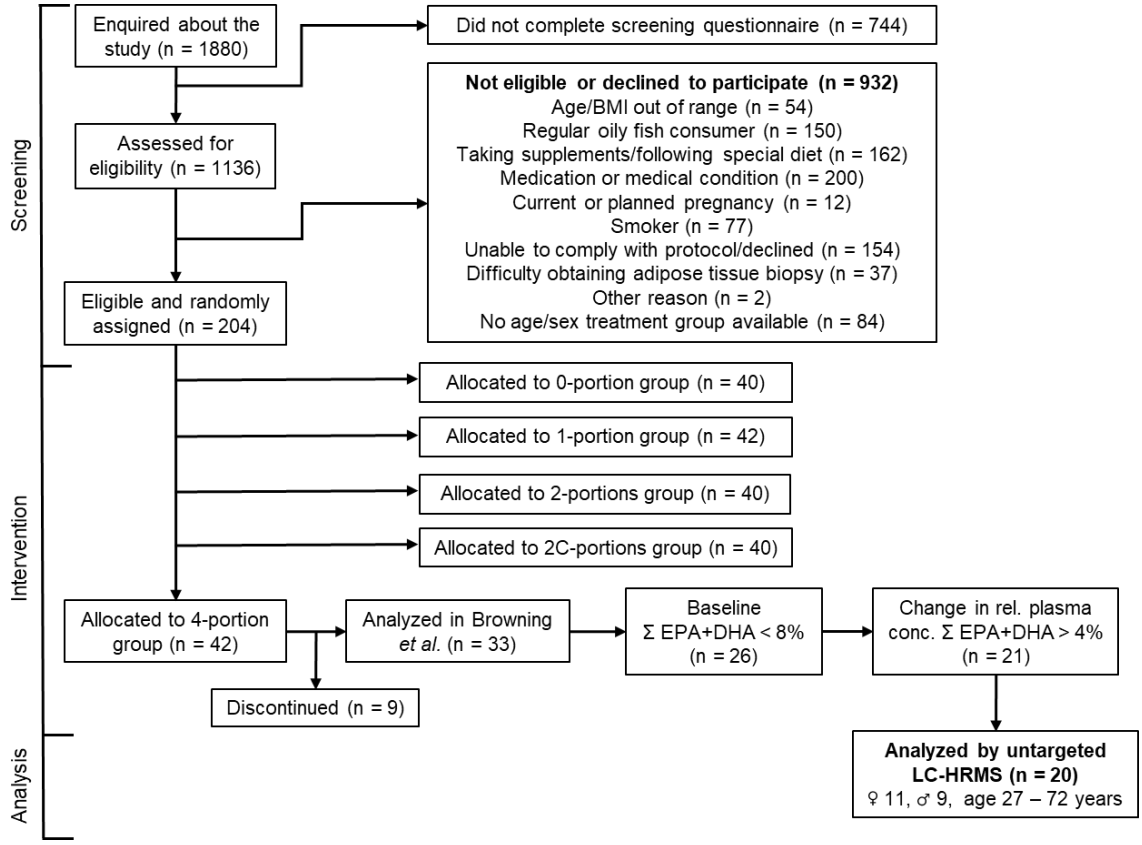

Fig. 8.3: Study design and selection of the human n3-PUFA intervention study (adapted from [1]). Effects of n3-PUFA supplementation on the plasma PL pattern were investigated in a subset of subjects from a supplementation study (28). Only subjects fulfilling the following criteria were included: individuals received n3-PUFA capsules corresponding to 4 portions of fatty fish per week (1.5 g EPA and 1.8 g DHA as TG per portion), the relative level of EPA + DHA in human plasma was < 8% at baseline, and the change in the relative level in human plasma of EPA + DHA was > 4% after 12 months of intervention. Plasma samples were analyzed at baseline and after 12 months of supplementation (n = 20, ♀ 11, ♂ 9, age 27 – 72 years).

1. Browning LM, Walker CG, Mander AP, West AL, Madden J, Gambell JM, et al. (2012) Incorporation of eicosapentaenoic and docosahexaenoic acids into lipid pools when given as supplements providing doses equivalent to typical intakes of oily fish. *Am J Clin Nutr.* **96**, 748–58.

Table 8.4: Parameters used for data processing by MS-DIAL. Shown are the parameters used for the data processing in ESI(+) and ESI(-) mode, sorted according to the tabs in the MS-DIAL software, i.e., data collection from the acquired data, peak detection, identification, and alignment.

MS-DIAL parameters		
Data collection	MS1 tolerance	0.01 Da
	MS2 tolerance	0.015 Da
	retention time begin	1 min
	retention time end	28 min
	MS1 mass range begin	200 Da
	MS1 mass range end	1200 Da
	MS/MS mass range begin	0 Da
	MS/MS mass range end	1200 Da
	Max changed number	2
Peak detection	Minimum Peak height	10000
	Mass slice width	0.02 Da
Identification	MSP file/solvent type	$HCOONH_4$
	Retention time tolerance	100 min
	Accurate mass tolerance (MS1)	0.006 Da
	Accurate mass tolerance (MS2)	0.01 Da
	Identification score cut off	75%
	Retention time tolerance	0.3 min
	Accurate mass tolerance	0.006 Da
	Identification score cut off	85%
Alignement parameter setting	Retention time tolerance	0.3 min
	MS1 tolerance	0.004 Da
	Retention time factor	0.5
	MS1 factor	0.5
	Peak count filter	0%
	N% detected in at leat one grou	50%
	Remove features based on blank information	true
	Sample max/blank average	5
	Keep 'reference matched'	true
	Keep 'suggested' (w/o MS2)	false
	Keep removable features	true
	Gap filling by compulsion	true

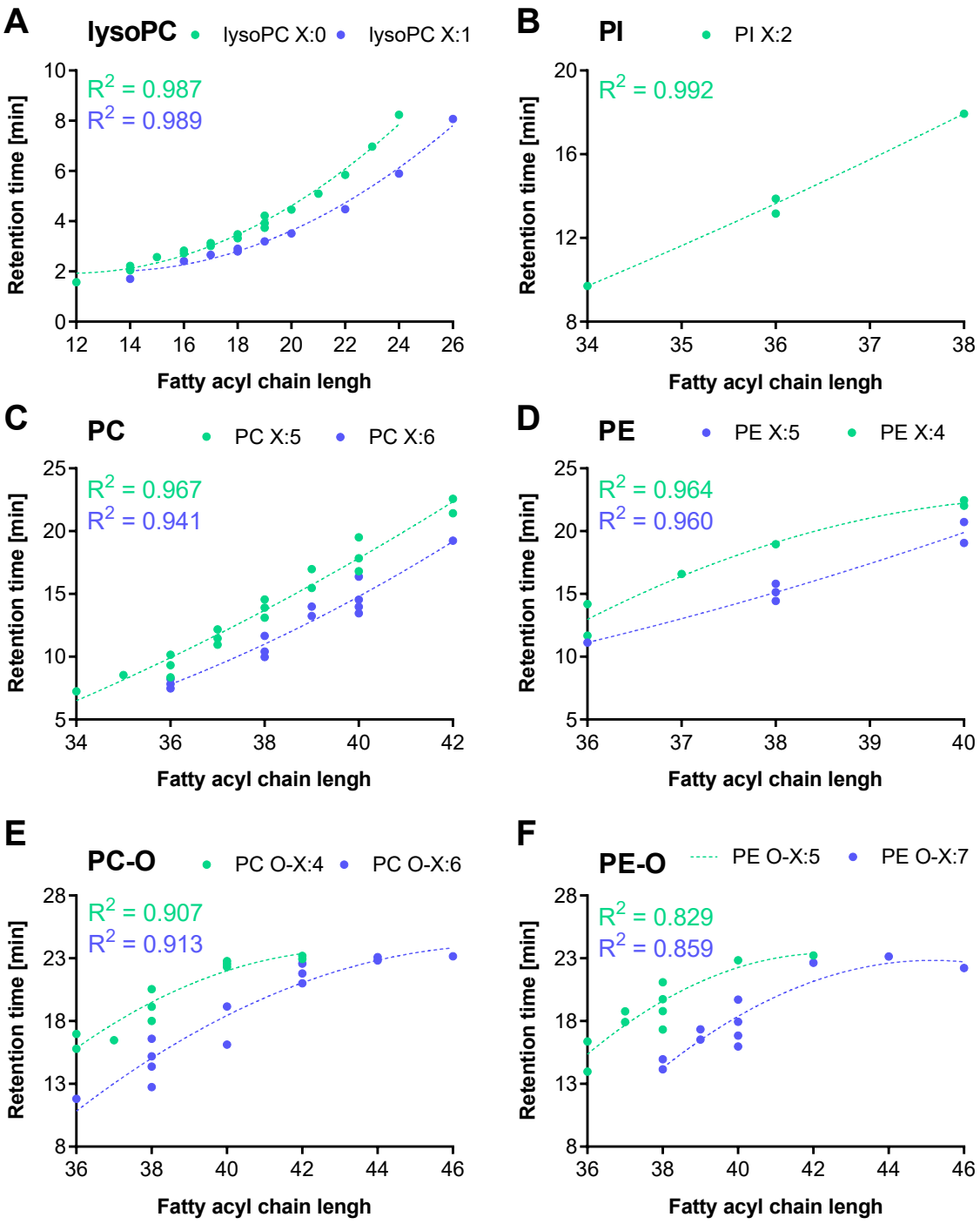

Fig. 8.4: Polynomial dependences of the retention times on the length of the fatty acyl chains (X = carbon number sum). Shown are **A** lysoPC X:0 and lysoPC X:1, **B** PI X:2, **C** PC X:5 and PC X:6, **D** PE X:5 and PE X:4, **E** PC O-X:4 and PC O-X:6, and **F** PE O-X:5 and PE O-X:7. Lipid extracts were analyzed by untargeted LC-HRMS operating in Full MS/ddMS^2 TOP *N* mode (orbitrap Q Exactive HF).

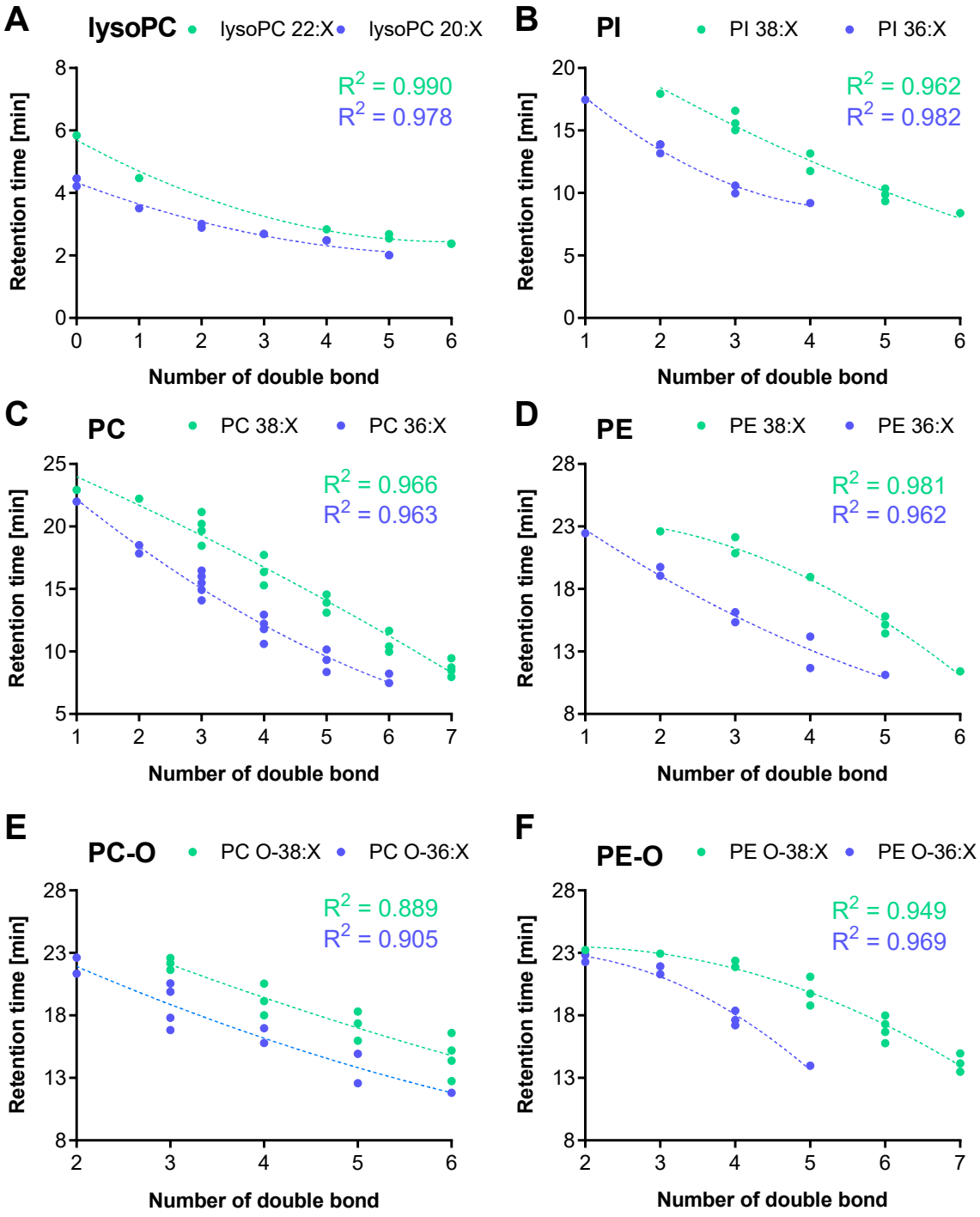

Fig. 8.5: Polynomial dependences of the retention times on the number of double bonds (X = double bond number). Shown are **A** lysoPC 20:X and lysoPC 22:X, **B** PI 36:X and PI 38:X, **C** PC 36:X and PC 38:X, **D** PE 36:X and PE 38:X, **E** PC O-36:X and PC O-38:X, and **F** PE O-36:X and PE O-38:X. Lipid extracts were analyzed by untargeted LC-HRMS operating in Full MS/ddMS^2 TOP *N* mode (orbitrap Q Exactive HF).

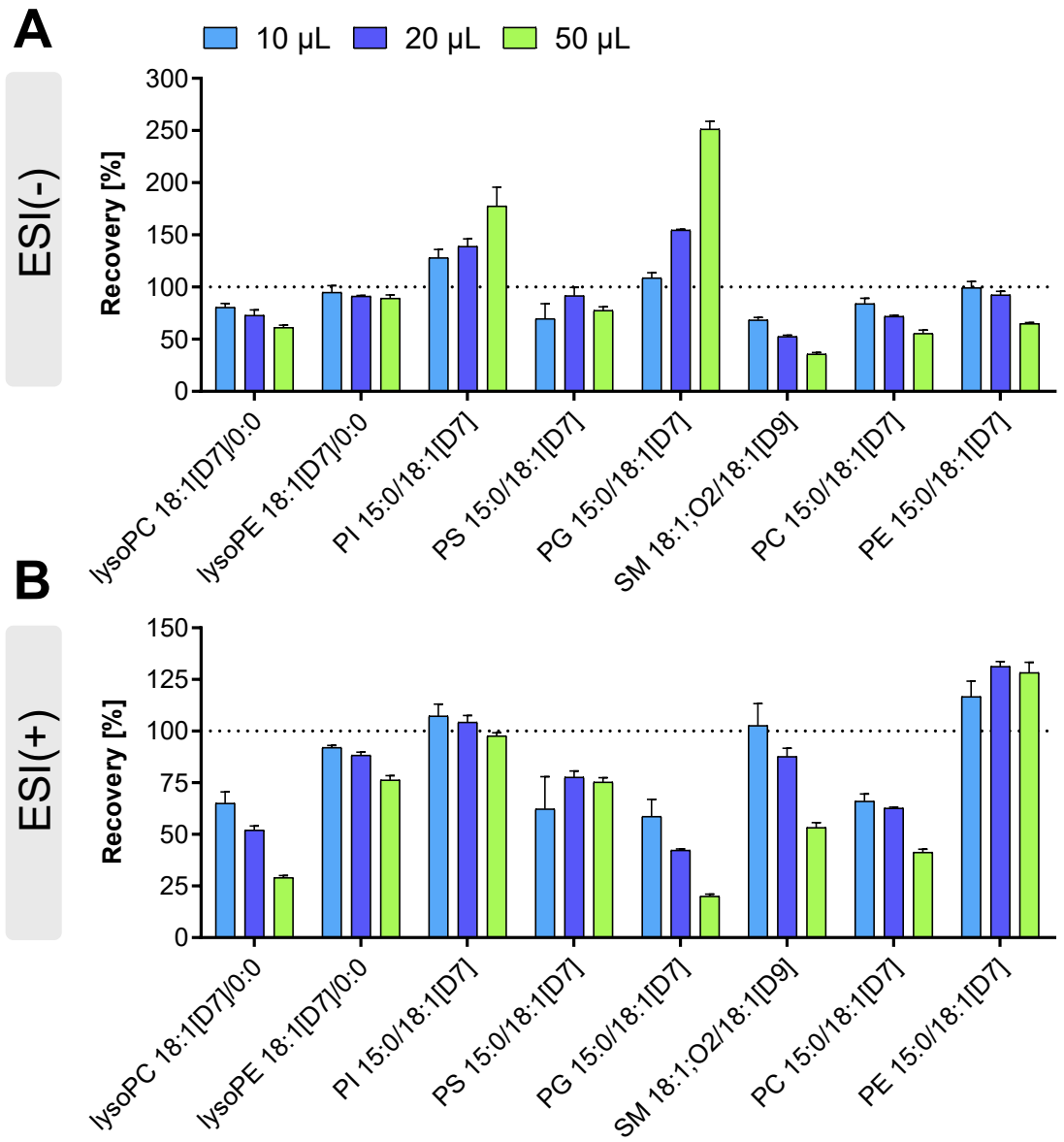

Fig. 8.6: Influence of the plasma volume on the extraction recovery. Shown is the extraction recovery of deuterium-labeled IS from the extraction of different volumes of human plasma **A** in ESI(-) and **B** in ESI(+) mode. Extraction recovery was calculated relative to an IS solution directly injected. Shown are mean values ± SD (n = 3). Lipid extracts were analyzed by untargeted LC-HRMS operating in Full MS/ddMS^2 TOP *N* mode (orbitrap Q Exactive HF).

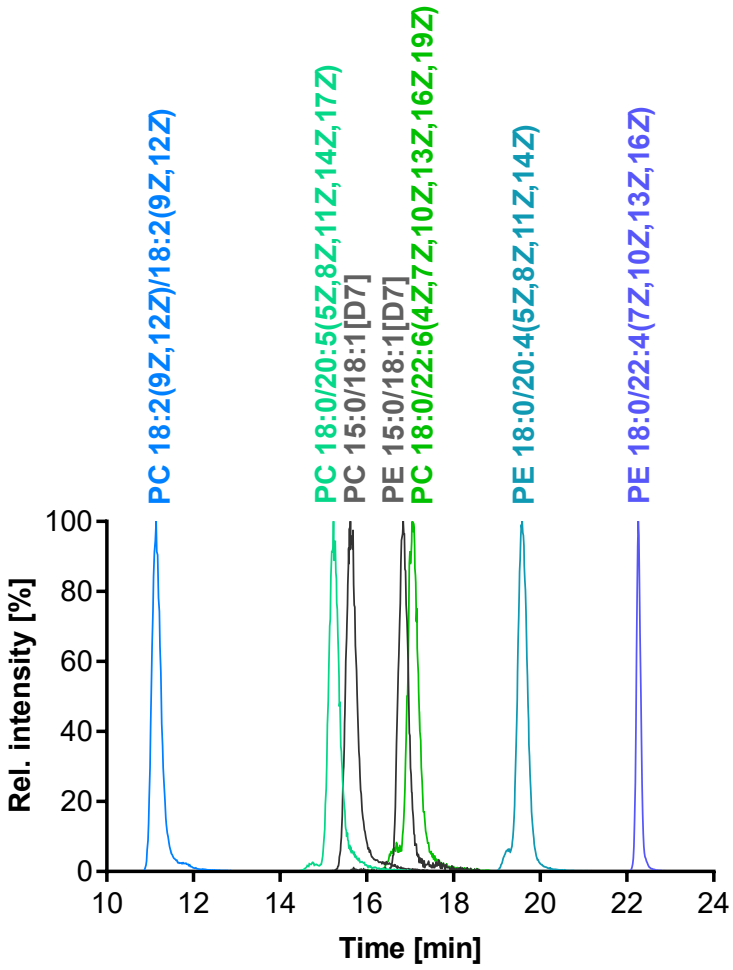

Fig. 8.7: Chromatographic separation of PL by targeted LC-ESI(-)-MS/MS. Shown are the MRM signals of the quantifier transitions of selected PL, as well as the IS for the analysis of a multi-analyte standard solution (400 nmol L^{-1}).

Table 8.5: List of PL semi-quantified in ESI(-) and ESI(+) modes by MS-DIAL. Shown are the t_R, the measured *m/z*, and the concentrations in µmol L^{-1}. Concentrations at baseline and following 12 months of n3-PUFA supplementation are shown as mean ± SD, n = 20.

LC-ESI(-)-HRMS						LC-ESI(+)-HRMS			
Analyte	**t_R [min]**	***m/z***	**baseline**	**12 months**		**t_R [min]**	***m/z***	**baseline**	**12 months**
lysoPC 20:3_0:0	2.69	590.3455	2.1 ± 0.6	1.3 ± 0.4		2.69	546.3547	2.2 ± 0.7	1.5 ± 0.6
lysoPC 20:5_0:0	2.01	586.3148	0.37 ± 0.15	1.4 ± 0.9		2.01	542.3254	0.25 ± 0.11	1.0 ± 0.7
lysoPC 22:4_0:0	2.84	616.3628	0.08 ± 0.03	0.03 ± 0.02		2.84	572.3708	0.06 ± 0.02	0.03 ± 0.01
lysoPC 22:6_0:0	2.37	612.3284	1.1 ± 0.3	2.0 ± 0.7		2.38	568.3398	0.80 ± 0.28	1.5 ± 0.7
lysoPE 16:1_0:0	2.48	450.2626	0.08 ± 0.06	0.05 ± 0.03		2.48	452.2757	0.09 ± 0.06	0.05 ± 0.03
lysoPE 18:2_0:0	2.61	476.2770	2.3 ± 0.7	1.6 ± 0.5		2.61	478.2921	2.4 ± 0.8	1.7 ± 0.6
lysoPE 20:3_0:0	2.75	502.2933	0.20 ± 0.10	0.10 ± 0.05		2.75	504.3075	0.21 ± 0.11	0.11 ± 0.05
lysoPE 20:4_0:0	2.54	500.2782	1.6 ± 0.5	1.0 ± 0.3		2.54	502.2924	1.8 ± 0.6	1.3 ± 0.3
lysoPE 20:5_0:0	2.11	498.2620	0.07 ± 0.03	0.20 ± 0.09		2.11	500.2763	0.06 ± 0.02	0.18 ± 0.08
lysoPE 22:6_0:0	2.45	524.2779	1.2 ± 0.3	1.7 ± 0.4		2.45	526.2934	1.2 ± 0.3	1.76 ± 0.37
PI 18:0_20:3	16.57	887.5645	0.49 ± 0.36	0.29 ± 0.14		16.52	906.6076	1.1 ± 0.8	0.58 ± 0.35
PI 18:0_20:5	10.36	883.5320	0.14 ± 0.06	0.42 ± 0.18		10.33	902.5752	0.22 ± 0.11	0.83 ± 0.42
PI 16:0_22:6	8.40	881.5189	0.44 ± 0.15	0.86 ± 0.33		8.38	900.5638	0.60 ± 0.27	1.1 ± 0.4
PI 18:0_22:6	11.90	909.5498	0.65 ± 0.18	1.3 ± 0.4		11.87	928.5931	6.7 ± 2.0	11 ± 4
PC 15:0_16:1	10.66	762.5293	0.34 ± 0.16	0.24 ± 0.11		10.67	718.5369	0.27 ± 0.14	0.18 ± 0.07
PC 16:1_16:1	9.26	774.5278	0.59 ± 0.38	0.36 ± 0.21		9.26	730.5397	0.37 ± 0.27	0.22 ± 0.13
PC 16:1_18:1	13.15	802.5598	6.7 ± 2.8	4.4 ± 1.5		13.17	758.5690	7.5 ± 3.8	4.90 ± 1.77
PC 16:1_18:2	9.91	800.5426	10 ± 3	6.5 ± 1.7		9.92	756.5540	6.9 ± 2.6	4.32 ± 1.49
PC 16:0_18:3	11.33	800.5433	7.1 ± 4.5	4.0 ± 2.3		11.36	756.5541	5.6 ± 4.2	3.0 ± 1.69
PC 14:0_20:5	7.24	796.5153	0.50 ± 0.22	1.3 ± 0.6		7.25	752.5212	0.21 ± 0.09	0.65 ± 0.42
PC 15:0_20:3	12.56	814.5634	1.1 ± 0.4	0.59 ± 0.23		12.57	770.5704	0.88 ± 0.36	0.49 ± 0.17
PC 15:0_20:5	8.54	810.5273	0.37 ± 0.15	1.1 ± 0.4		8.55	766.5378	0.19 ± 0.08	0.61 ± 0.27
PC 16:0_20:3	14.93	828.5764	93 ± 32	57 ± 20		14.95	784.5847	96 ± 34	58 ± 21
PC 18:2_18:2	10.61	826.5574	37 ± 12	25 ± 8		10.62	782.5709	28 ± 10	19 ± 7
PC 16:1_20:4	9.33	824.5459	3.0 ± 1.5	1.8 ± 0.6		9.33	780.5535	1.7 ± 0.9	1.0 ± 0.5
PC 16:0_20:5	10.16	824.5454	51 ± 21	134 ± 39		10.17	780.5534	38 ± 18	119 ± 42

Table 8.5: Continued 1/3. List of PL semi-quantified in ESI(-) and ESI(+) modes by MS-DIAL. Shown are the t_R, the measured *m/z*, and the concentrations in µmol L^{-1}.

	LC-ESI(-)-HRMS				LC-ESI(+)-HRMS			
Analyte	**t_R [min]**	***m/z***	**baseline**	**12 months**	**t_R [min]**	***m/z***	**baseline**	**12 months**
PC 16:1_20:5	7.47	822.5270	0.48 ± 0.26	1.1 ± 0.5	7.48	778.5378	0.22 ± 0.12	0.57 ± 0.41
PC 16:1_20:5	7.82	822.5269	0.14 ± 0.07	0.37 ± 0.16	7.84	778.5378	0.07 ± 0.03	0.20 ± 0.10
PC 17:0_20:3	16.59	842.5938	1.1 ± 0.4	0.61 ± 0.26	16.58	798.6 030	0.84 ± 0.29	0.48 ± 0.19
PC 17:0_20:3	17.30	842.5931	1.3 ± 0.6	0.77 ± 0.27	17.32	798.6027	1.2 ± 0.6	0.75 ± 0.24
PC 37:5	11.46	838.5624	0.33 ± 0.17	0.92 ± 0.41	11.51	794.5714	0.61 ± 0.29	1.6 ± 0.8
PC 17:0_20:5	12.18	838.5629	0.51 ± 0.21	1.7 ± 0.5	12.21	794.5712	0.34 ± 0.1	1.2 ± 0.4
PC 18:0_20:3	20.20	856.6068	3.9 ± 1.4	2.3 ± 0.9	20.22	812.6146	2.8 ± 1.2	1.6 ± 0.7
PC 18:0_20:3	21.15	856.6066	3.1 ± 2.3	1.4 ± 0.7	21.16	812.6146	2.4 ± 1.9	0.98 ± 0.51
PC 18:1_20:3	15.29	854.5902	9.1 ± 4.3	4.3 ± 1.6	15.29	810.6038	6.8 ± 3.3	3.1 ± 1.1
PC 16:0_22:4	16.36	854.5906	7.6 ± 3.8	4.3 ± 2.7	16.39	810.5973	6.7 ± 3.7	4.1 ± 2.3
PC 18:0_20:5	14.56	852.5769	20 ± 8	55 ± 16	14.58	808.5818	15 ± 6	48 ± 16
PC 18:2_20:4	9.97	850.5620	10.6 ± 2.6	6.8 ± 1.4	9.98	806.5674	7.0 ± 1.9	4.5 ± 1.2
PC 18:1_20:5	10.41	850.5610	4.4 ± 1.8	10.5 ± 4.7	10.42	806.5672	2.9 ± 1.3	7.6 ± 4.3
PC 18:2_20:5	7.95	848.5464	1.6 ± 0.6	4.2 ± 2.3	7.96	804.5532	0.76 ± 0.29	2.4 ± 1.6
PC 39:5	16.98	866.5927	0.07 ± 0.02	0.19 ± 0.06	17.01	822.5974	0.05 ± 0.02	0.13 ± 0.06
PC 17:0_22:6	14.00	864.5747	0.97 ± 0.35	1.7 ± 0.5	14.00	820.5830	0.88 ± 0.30	1.5 ± 0.45
PC 20:0_20:3	22.67	884.6395	0.79 ± 0.25	0.49 ± 0.15	22.64	840.6467	0.48 ± 0.16	0.29 ± 0.10
PC 18:0_22:4	20.96	882.6228	3.2 ± 1.4	1.6 ± 0.6	20.98	838.6346	2.4 ± 1.4	1.1 ± 0.4
PC 18:0_22:6	16.38	878.5904	34 ± 11	53 ± 14	16.39	834.6016	32 ± 12	54 ± 14
PC 18:1_22:6	12.55	876.5727	1.3 ± 0.9	1.9 ± 1.2	12.55	832.5861	1.1 ± 0.7	1.6 ± 0.9
PC 20:4_20:5	7.38	872.5454	0.17 ± 0.09	0.40 ± 0.24	7.39	828.5505	0.07 ± 0.04	0.2 ± 0.16
PC 20:5_22:6	6.75	896.5460	0.05 ± 0.03	0.31 ± 0.19	6.76	852.5536	0.03 ± 0.01	0.16 ± 0.12
PE 18:1_18:2	15.34	740.5258	1.1 ± 0.7	0.67 ± 0.42	15.35	742.5383	1.1 ± 0.7	0.59 ± 0.33
PE 16:0_20:3	16.14	740.5217	0.37 ± 0.3	0.19 ± 0.13	16.24	742.5367	0.37 ± 0.27	0.18 ± 0.14
PE 18:2_18:2	11.67	738.5071	0.08 ± 0.07	0.03 ± 0.03	11.65	740.5277	0.19 ± 0.14	0.05 ± 0.05

Table 8.5: Continued 2/3. List of PL semi-quantified in ESI(-) and ESI(+) modes by MS-DIAL.
Shown are the t_R, the measured *m/z*, and the concentrations in µmol L^{-1}.

LC-ESI(-)-HRMS								LC-ESI(+)-HRMS							
Analyte	**t_R [min]**	***m/z***	**baseline**			**12 months**		**t_R [min]**	***m/z***	**baseline**			**12 months**		
PE 16:0_20:4	14.20	738.5084	3.1	±	1.5	2.0	± 0.8	14.19	740.5206	4.4	±	2.0	2.4	±	1.0
PE 16:0_20:5	11.13	736.4921	0.36	±	0.24	0.90	± 0.53	11.14	738.5071	0.25	±	0.15	0.63	±	0.36
PE 18:0_20:3	20.87	768.5557	0.87	±	0.75	0.43	± 0.36	20.90	770.5703	0.67	±	0.63	0.30	±	0.24
PE 18:0_20:4	18.96	766.5416	7.4	±	2.7	4.8	± 1.5	18.97	768.5537	6.9	±	2.5	4.1	±	1.1
PE 18:0_20:5	15.80	764.5236	0.67	±	0.36	1.7	± 0.92	15.82	766.5384	0.64	±	0.35	1.6	±	0.8
PE 18:1_20:5	11.40	762.5068	0.09	±	0.06	0.18	± 0.11	11.48	764.5199	0.13	±	0.03	0.29	±	0.26
PE 18:0_22:4	22.03	794.5687	0.18	±	0.14	0.05	± 0.04	22.05	796.5823	0.19	±	0.17	0.03	±	0.04
PE 18:0_22:5	20.73	792.5527	0.16	±	0.11	0.10	± 0.06	20.75	794.5714	0.12	±	0.08	0.07	±	0.04
PC O-18:0_18:2	21.34	816.6143	1.5	±	0.4	1.0	± 0.4	21.36	772.6243	1.2	±	0.3	0.83	±	0.3
PC O-16:0_20:3	17.81	814.5945	1.6	±	0.5	0.91	± 0.23	17.82	770.6055	1.8	±	0.5	1.1	±	0.2
PC O-18:1_20:3	18.01	840.6143	1.2	±	0.4	0.66	± 0.19	18.02	796.6196	1.1	±	0.5	0.65	±	0.16
PC O-16:0_22:4	19.14	840.6144	1.1	±	0.3	0.58	± 0.15	19.15	796.6193	0.95	±	0.36	0.50	±	0.16
PC O-18:0_20:4	20.54	840.6143	5.8	±	1.5	3.7	± 1.2	20.55	796.6197	4.8	±	1.6	3.2	±	1.1
PC O-18:1_20:3	21.64	840.6143	0.34	±	0.15	0.23	± 0.09	21.68	796.6194	0.28	±	0.13	0.19	±	0.07
PC O-18:0_20:5	17.36	838.5952	0.57	±	0.20	1.2	± 0.5	17.38	794.6078	0.61	±	0.23	1.4	±	0.6
PC O-16:1_22:4	18.30	838.5966	0.79	±	0.26	0.48	± 0.15	18.33	794.6072	0.69	±	0.26	0.43	±	0.15
PC O-16:0_22:6	14.37	836.5801	2.7	±	0.8	3.9	± 1.1	14.39	792.5926	2.2	±	0.76	3.2	±	0.9
PC O-18:1_20:5	16.60	836.5808	0.35	±	0.15	0.87	± 0.44	16.59	792.5925	0.30	±	0.15	0.75	±	0.39
PC O-18:2_20:5	12.09	834.5643	0.17	±	0.08	0.49	± 0.22	12.09	790.5781	0.12	±	0.07	0.36	±	0.17
PC O-16:1_22:6	13.53	834.5634	2.2	±	0.9	3.7	± 1.2	13.54	790.5765	1.8	±	0.7	3.0	±	1.0
PC O-18:0_22:4	22.54	868.6449	0.81	±	0.20	0.36	± 0.13	22.55	824.6534	0.61	±	0.20	0.30	±	0.09
PC O-18:1_22:4	19.29	866.6269	0.46	±	0.11	0.32	± 0.08	19.30	822.6364	0.38	±	0.13	0.24	±	0.06
PC O-18:1_22:4	22.33	866.6265	0.25	±	0.09	0.15	± 0.05	22.33	822.6360	0.20	±	0.09	0.12	±	0.05
PC O-20:0_20:5	22.01	866.6252	0.25	±	0.07	0.41	± 0.16	22.01	822.6377	0.23	±	0.08	0.40	±	0.13
PC O-18:1_22:6	18.28	862.5991	0.64	±	0.34	1.1	± 0.5	18.32	818.6054	0.57	±	0.30	0.91	±	0.41

Table 8.5: Continued 3/3. List of PL semi-quantified in ESI(-) and ESI(+) modes by MS-DIAL. Shown are the t_R, the measured *m/z*, and the concentrations in µmol L^{-1}.

	LC-ESI(-)-HRMS						LC-ESI(+)-HRMS					
Analyte	**t_R [min]**	***m/z***	**baseline**		**12 months**		**t_R [min]**	***m/z***	**baseline**		**12 months**	
PC O-18:2_22:6	13.89	860.5825	0.26 ±	0.11	0.44 ±	0.17	13.90	816.5915	0.26 ±	0.10	0.48 ±	0.16
PC O-22:1_20:3	22.95	896.6769	0.98 ±	0.33	0.64 ±	0.19	22.94	852.6830	0.71 ±	0.28	0.48 ±	0.14
PC O-22:2_20:3	22.34	894.6610	0.20 ±	0.09	0.12 ±	0.05	22.34	850.6668	0.16 ±	0.07	0.09 ±	0.03
PC O-22:2_20:4	21.01	892.6458	0.38 ±	0.10	0.26 ±	0.08	21.04	848.6528	0.36 ±	0.13	0.23 ±	0.08
PC O-22:1_20:5	21.79	892.6470	0.13 ±	0.05	0.36 ±	0.12	21.81	848.6522	0.14 ±	0.05	0.39 ±	0.11
PC O-22:1_22:6	22.16	918.6596	0.14 ±	0.13	0.34 ±	0.10	22.15	874.6648	0.11 ±	0.05	0.35 ±	0.10
PC O-24:1_22:6	23.06	946.6914	1.3 ±	0.4	2.0 ±	0.5	23.07	902.6991	1.2 ±	0.4	1.9 ±	0.52
PE O-18:0_18:2	22.27	728.5621	0.22 ±	0.07	0.15 ±	0.06	22.39	754.5755	1.1 ±	0.5	0.63 ±	0.25
PE O-18:2_18:2	18.37	724.5299	0.30 ±	0.10	0.20 ±	0.10	18.42	726.5440	0.63 ±	0.26	0.36 ±	0.17
PE O-16:0_20:5	13.98	722.5136	0.10 ±	0.06	0.25 ±	0.14	13.99	724.5265	0.16 ±	0.11	0.40 ±	0.20
PE O-17:1_20:5	14.74	734.5113	0.02 ±	0.02	0.09 ±	0.08	14.71	736.5297	0.03 ±	0.03	0.11 ±	0.11
PE O-17:1_20:5	15.56	734.5164	0.05 ±	0.03	0.18 ±	0.10	15.57	736.5285	0.04 ±	0.02	0.13 ±	0.07
PE O-18:1_20:3	22.38	752.5615	1.5 ±	0.6	0.84 ±	0.38	22.65	804.5913	0.60 ±	0.22	0.85 ±	0.31
PE O-16:1_22:4	19.73	750.5427	0.31 ±	0.09	0.17 ±	0.04	19.73	752.5598	0.47 ±	0.152	0.22 ±	0.07
PE O-18:1_20:5	17.99	748.5267	1.3 ±	0.7	3.9 ±	1.8	17.97	750.5425	1.64 ±	0.953	4.7 ±	2.3
PE O-18:2_20:5	13.48	746.5126	0.42 ±	0.19	1.3 ±	0.4	13.52	748.5267	0.42 ±	0.187	1.2 ±	0.4
PE O-17:1_22:6	16.52	760.5264	0.09 ±	0.05	0.15 ±	0.07	16.47	762.5457	0.12 ±	0.075	0.19 ±	0.09
PE O-20:1_20:5	22.27	776.5620	0.46 ±	0.23	0.84 ±	0.35	22.26	778.5732	0.40 ±	0.200	0.76 ±	0.34
PE O-20:2_20:5	17.94	774.5448	0.05 ±	0.04	0.17 ±	0.25	17.88	776.5595	0.06 ±	0.063	0.25 ±	0.38
PE O-18:2_22:6	15.29	772.5299	1.3 ±	0.4	2.1 ±	0.6	15.29	774.5432	1.38 ±	0.416	2.0 ±	0.5
PE O-20:1_22:6	22.65	802.5764	0.70 ±	0.23	1.1 ±	0.41	22.28	730.5731	0.20 ±	0.069	0.13 ±	0.05
PE O-20:2_22:6	19.69	800.5613	0.08 ±	0.04	0.15 ±	0.10	19.69	802.5731	0.12 ±	0.051	0.20 ±	0.13
PE O-16:1_22:4	19.73	750.5427	0.31 ±	0.09	0.17 ±	0.04	19.73	752.5598	0.47 ±	0.152	0.22 ±	0.07
PE O-18:1_20:5	17.99	748.5267	1.3 ±	0.7	3.9 ±	1.8	17.97	750.5425	1.64 ±	0.953	4.7 ±	2.3
PE O-18:2_20:5	13.48	746.5126	0.42 ±	0.19	1.3 ±	0.45	13.52	748.5267	0.42 ±	0.187	1.2 ±	0.44
PE O-17:1_22:6	16.52	760.5264	0.09 ±	0.05	0.15 ±	0.07	16.47	762.5457	0.12 ±	0.075	0.19 ±	0.09

Chapter 3

Table 8.6: Inclusion list used for the Full MS/ddMS^2 TOP *N* acquisition. Shown are the *m/z* of ions of PI, PS, PC, PC-P, PC-O, PE, and PE-P bearing biologically relevant oxidized PUFA selected for the inclusion list, considering the common (adduct) ions of the individual lipid classes in ESI(-). NCE of 35 relative to *m/z* 500 was used for the fragmentation of ions corresponding to oxPI species.

		m/z	
species level	**molecular species level**	**ESI(-)**	**NCE**
PI 34:2;O	PI 16:0_18:2;O	849.5135	35
PI 36:2;O	PI 18:0_18:2;O	877.5448	35
PI 36:3;O	PI 18:1_18:2;O	875.5291	35
PI 36:4;O	PI 16:0_20:4;O	873.5135	35
PI 36:5;O	PI 16:0_20:5;O	871.4978	35
PI 38:2;O	PI 18:0_20:2;O	905.5761	35
PI 38:3;O	PI 18:0_20:3;O	903.5604	35
PI 38:4;O	PI 18:0_20:4;O	901.5448	35
PI 38:5;O	PI 18:1_20:4;O/PI 18:0_20:5;O	899.5291	35
PI 38:6;O	PI 18:1_20:5;O/PI 16:0_22:6;O	897.5134	35
PI 40:6;O	PI 18:0_22:6;O	925.5448	35
PI 40:7;O	PI 18:1_22:6;O	923.5291	35
PS 34:2;O	PS 16:0_18:2;O	774.4927	25,30
PS 36:2;O	PS 18:0_18:2;O	802.5240	25,30
PS 36:4;O	PS 16:0_20:4;O	798.4927	25,30
PS 38:4;O	PS 18:0_20:4;O	826.5240	25,30
PS 38:5;O	PS 18:1_20:4;O/PS 18:0_20:5;O	824.5083	25,30
PS 38:6;O	PS 18:1_20:5;O/PS 16:0_22:6;O	822.4927	25,30
PS 40:6;O	PS 18:0_22:6;O	850.5240	25,30
PC 34:2;O	PC 16:0_18:2;O	818.5553	25,30
PC 34:3;O	PC 16:1_18:2;O/PC 16:0_18:3;O	816.5396	25,30
PC 34:4;O	PC 14:0_20:4;O	814.5240	25,30
PC 35:3;O	PC 17:1_18:2;O	830.5553	25,30
PC 36:2;O	PC 18:0_18:2;O/PC 16:0_20:2;O	846.5866	25,30
PC 36:3;O	PC 18:1_18:2;O/PC 18:0_18:3;O	844.5709	25,30
PC 36:4;O	PC 16:0_20:4;O/PC 18:2_18:2;O	842.5553	25,30
PC 36:5;O	PC 16:0_20:5;O	840.5396	25,30
PC 38:4;O	PC 18:0_20:4;O/PC 16:0_22:4;O	870.5866	25,30
PC 38:5;O	PC 18:0_20:5;O/PC 16:0_22:5;O	868.5709	25,30
PC 38:6;O	PC 18:2_20:4;O/PC 16:0_22:6;O	866.5553	25,30
PC 40:4;O	PC 18:O_22:4;O	898.6179	25,30
PC 40:6;O	PC 18:0_22:6;O	894.5866	25,30

Table 8.6: Continued. Inclusion list used for the Full MS/ddMS^2 TOP *N* acquisition.

		m/z	
species level	**molecular species level**	**ESI(-)**	**NCE**
PC P-34:2;O	PC P-16:0_18:2;O	802.5604	25,30
PC P-36:4;O	PC P-16:0_20:4;O	826.5604	25,30
PC P-36:5;O	PC P-16:0_20:5;O	824.5447	25,30
PC P-38:6;O	PC P-16:0_22:6;O	850.5604	25,30
PC O-34:2;O	PC O-16:0_18:2;O	804.5761	25,30
PC O-36:3;O	PC O-18:1_18:2;O	830.5917	25,30
PC O-36:4;O	PC O-16:0_20:4;O	828.5761	25,30
PC O-36:5;O	PC O-16:0_20:5;O	826.5604	25,30
PC O-38:4;O	PC O-16:0_22:4;O	856.6074	25,30
PC O-38:5;O	PC O-18:1_20:4;O	854.5917	25,30
PC O-38:6;O	PC O-16:0_22:6;O/PC O-18:1_20:5;O	852.5761	25,30
PC O-40:7;O	PC O-18:1_22:6;O	878.5917	25,30
PE 34:2;O	PE 16:0_18:2;O	730.5028	25,30
PE 34:3;O	PE 16:1_18:2;O	728.4871	25,30
PE 36:2;O	PE 18:0_18:2;O	758.5341	25,30
PE 36:3;O	PE 18:1_18:2;O	756.5185	25,30
PE 36:4;O	PE 16:0_20:4;O	754.5028	25,30
PE 36:5;O	PE 16:0_20:5;O	752.4871	25,30
PE 38:4;O	PE 18:0_20:4;O	782.5341	25,30
PE 38:5;O	PE 18:1_20:4;O/PE 18:0_20:5;O	780.5185	25,30
PE 38:6;O	PE 18:1_20:5;O/PE 16:0_22:6;O	778.5028	25,30
PE 40:4;O	PE 18:0_22:4;O	810.5654	25,30
PE 40:6;O	PE 18:0_22:6;O	806.5341	25,30
PE 40:7;O	PE 18:1_22:6;O	804.5185	25,30
PE P-34:2;O	PE P-16:0_18:2;O	714.5079	25,30
PE P-36:3;O	PE P-18:1_18:2;O/PC P-16:0_20:3;O	740.5236	25,30
PE P-36:2;O	PE P-18:0_18:2;O	742.5392	25,30
PE P-36:4;O	PE P-16:0_20:4;O	738.5080	25,30
PE P-36:5;O	PE P-16:0_20:5;O	736.4922	25,30
PE P-38:4;O	PE P-16:0_22:4;O	766.5393	25,30
PE P-38:5;O	PE P-18:0_20:5;O/PE P-16:0_22:5;O	764.5235	25,30
PE P-38:6;O	PE P-16:0_22:6;O	762.5079	25,30
PE P-40:5;O	PE P-18:1_22:4;O	792.5549	25,30
PE P-40:6;O	PE P-18:0_22:6;O	790.5392	25,30
PE P-40:7;O	PE P-18:1_22:6;O	788.5236	25,30

Fig. 8.8: Optimization of NCE for untargeted LC-HRMS. Shown are the MS^2 spectra in ESI(-) mode of **A** PC 16:0/15-HETE $[M + HCOO^-]^-$ and **B** PE 16:0/15-HETE $[M - H]^-$ using differently stepped NCE. Shown are data from an injection of a mixture of oxPL standards (each 500 nmol L^{-1}). Suggested sites of fragmentation are indicated in the structures.

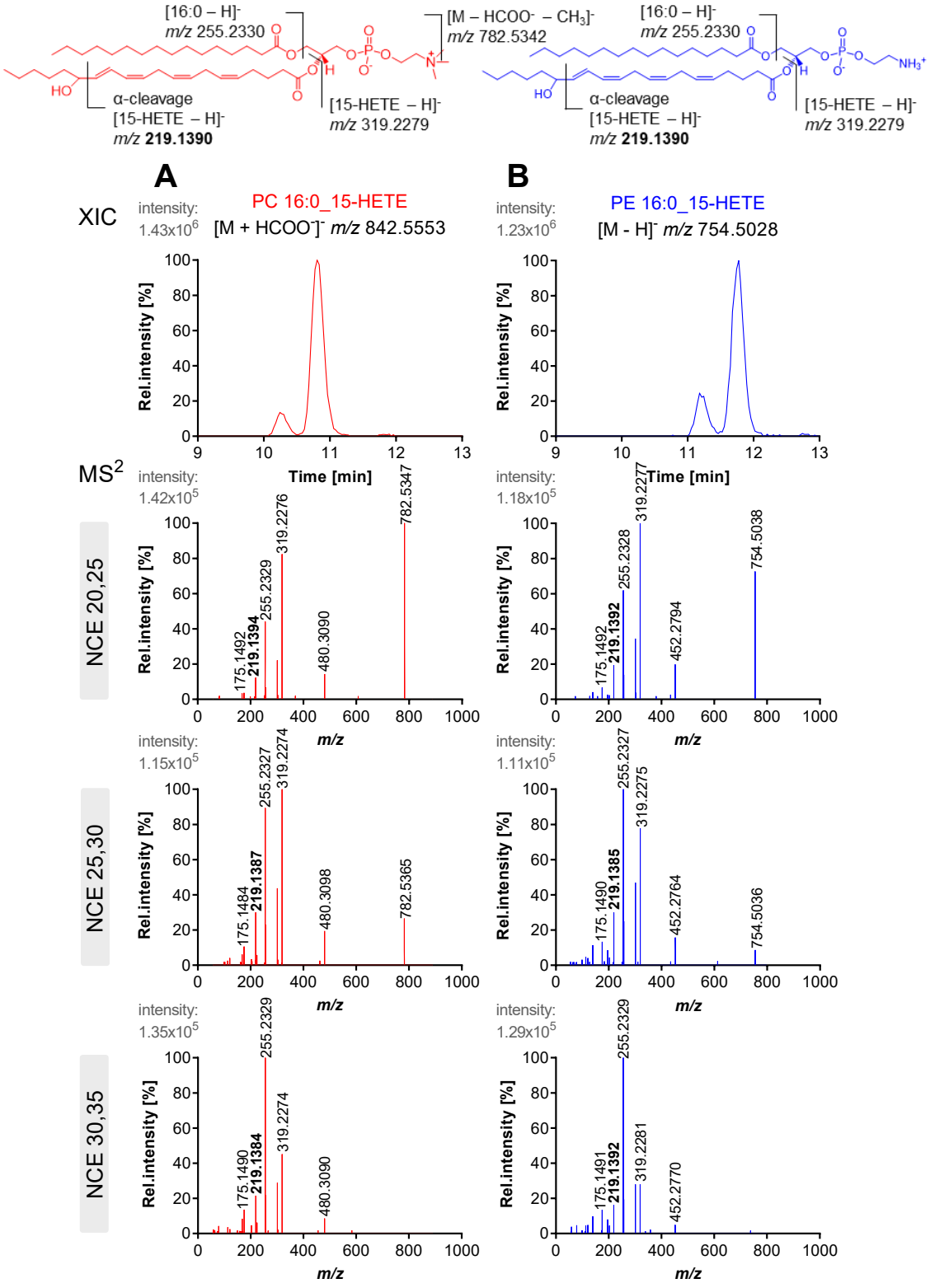

Fig. 8.8: Continued. Optimization of NCE for untargeted LC-HRMS. Shown are the MS^2 spectra in ESI(-) mode of **C** PC 16:0/17-HDHA $[M + HCOO^-]^-$ and **D** PE 16:0/17-HDHA $[M - H]^-$ using differently stepped NCE. Shown are data from an injection of a mixture of oxPL standards (each 500 nmol L^{-1}). Suggested sites of fragmentation are indicated in the structures.

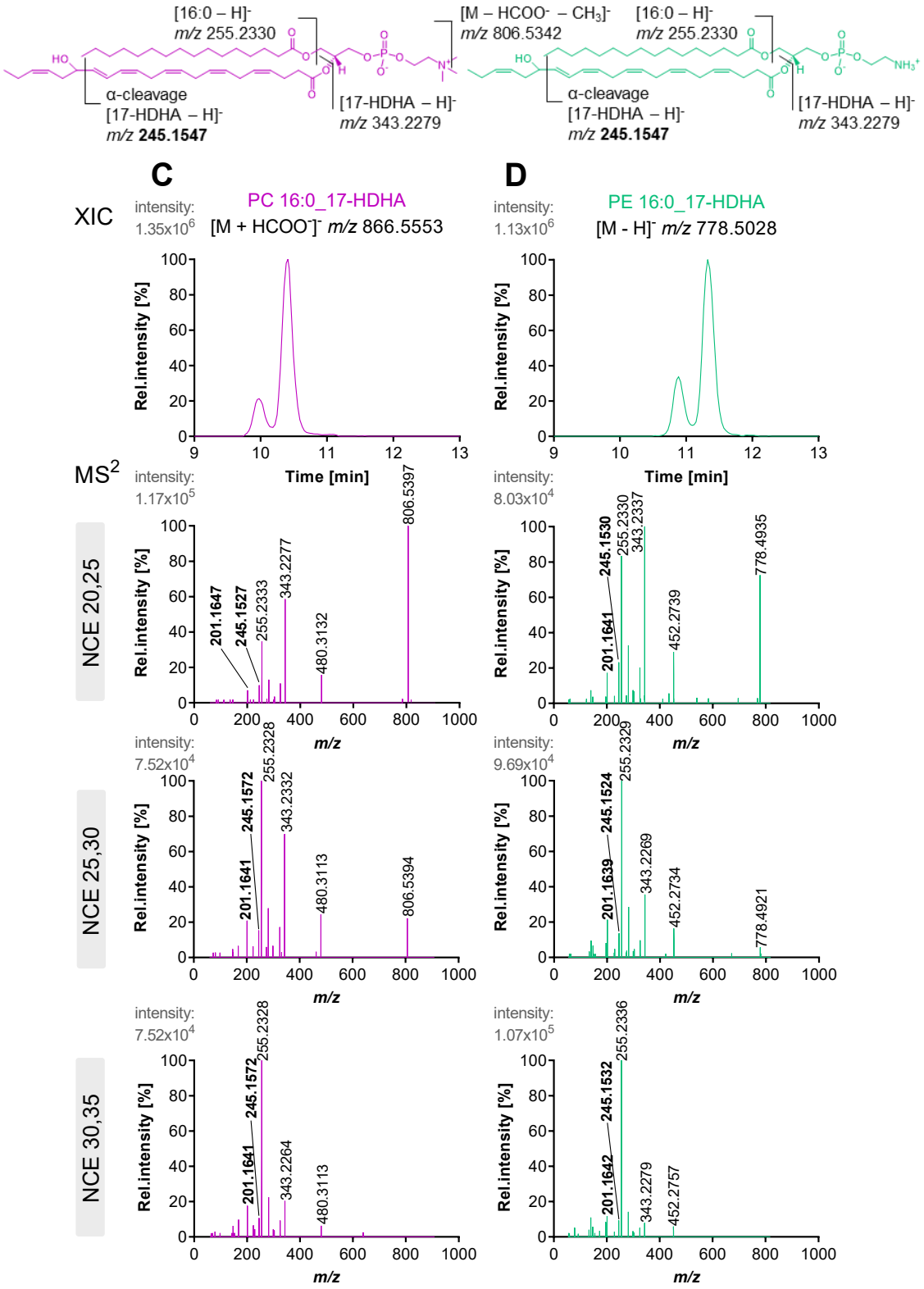

Table 8.7: Total and non-esterified oxylipins in human serum. Total and non-esterified oxylipins were analyzed by targeted LC-MS/MS following SPE as described [1-4]. Shown is the mean ± SD (n = 3). This commercial human serum was used for chromatographic optimization and identification of PL bearing hydroxy-PUFA by untargeted LC-HRMS. Note that the commercial serum contains high concentrations of oxylipins presumably formed by autoxidation during sample collection and storage.

		concentration in human serum [nmol L^{-1}]	
	analyte	**total**	**non-esterified**
hydroxy-LA	13-HODE	61000 ± 5900	1800 ± 53
	9-HODE	36000 ± 3500	1200 ± 44
epoxy-LA	12(13)-EpOME	330 ± 11	65 ± 3
	9(10)-EpOME	420 ± 8	85 ± 4
dihydroxy-LA	12,13-DiHOME	33 ± 5	9.4 ± 0.3
	9,10-DiHOME	43 ± 4	12.4 ± 0.8
hydroxy-ALA	13-HOTrE	1900 ± 160	46 ± 3
	9-HOTrE	970 ± 82	32.3 ± 0.4
hydroxy-ARA	15-HETE	12000 ± 1100	490 ± 26
	11-HETE	13000 ± 1100	530 ± 46
	12-HETE	14000 ± 1500	470 ± 36
	8-HETE	11000 ± 770	350 ± 38
	9-HETE	21000 ± 1300	470 ± 27
	5-HETE	10000 ± 540	2100 ± 170
epoxy-ARA	14(15)-EpETrE	81 ± 6	3.9 ± 0.4
	11(12)-EpETrE	48 ± 8	1.9 ± 0.2
	8(9)-EpETrE	< 5.0	< 0.50
dihydroxy-ARA	14,15-DiHETrE	< 0.25	0.86 ± 0.04
	11,12-DiHETrE	2.08 ± 0.06	0.78 ± 0.06
	8,9-DiHETrE	< 0.68	< 0.068
	5,6-DiHETrE	24 ± 2	7.1 ± 0.3

Table 8.7: Continued. Total and non-esterified oxylipins in human serum.

		concentration in human serum [nmol L^{-1}]	
	analyte	**total**	**non-esterified**
hydroxy-EPA	18-HEPE	870 ± 71	33 ± 1
	15-HEPE	720 ± 64	31 ± 3
	11-HEPE	460 ± 34	20 ± 1
	12-HEPE	850 ± 75	37 ± 2
	8-HEPE	420 ± 37	18.2 ± 0.8
	9-HEPE	1200 ± 110	38 ± 3
	5-HEPE	460 ± 45	200 ± 10
epoxy-EPA	17(18)-EpETE	< 7.5	< 0.75
	14(15)-EpETE	< 2.5	< 0.25
	11(12)-EpETE	59 ± 6	< 0.25
	8(9)-EpETE	< 7.5	< 0.75
dihydroxy-EPA	17,18-DiHETE	< 1.1	< 0.11
	14,15-DiHETE	< 0.50	< 0.050
	11,12-DiHETE	150 ± 16	42 ± 2
	8,9-DiHETE	< 1.0	< 0.10
hydroxy-DHA	20-HDHA	2200 ± 190	110 ± 6
	16-HDHA	1700 ± 120	70 ± 5
	17-HDHA	1600 ± 160	67 ± 5
	13-HDHA	1600 ± 170	78 ± 6
	14-HDHA	1400 ± 150	70 ± 6
	10-HDHA	1300 ± 120	66 ± 6
	11-HDHA	1900 ± 82	92 ± 4
	7-HDHA	1000 ± 60	36.8 ± 1.7
	8-HDHA	1500 ± 70	60 ± 3
epoxy-DHA	19(20)-EpDPE	< 5.0	< 0.50
	16(17)-EpDPE	< 2.5	< 0.25
	13(14)-EpDPE	< 1.0	< 0.10
	10(11)-EpDPE	< 0.25	< 0.025
	7(8)-EpDPE	< 6.5	< 0.65
dihydroxy-DHA	19,20-DiHDPE	< 5.0	1.3 ± 0.1
	16,17-DiHDPE	21.1 ± 1.4	1.20 ± 0.06
	13,14-DiHDPE	< 1.0	< 0.10
	10,11-DiHDPE	< 1.0	< 0.10
	7,8-DiHDPE	< 5.0	< 0.50

Table 8.8: Non-esterified oxylipins in HEK293T cells. 0.5×10^6 cells were used per experiment. HEK293T cells were supplemented with either a mixture of 18:2;Ep, 20:4;OH, 20:4;Ep, 20:5;Ep, or 22:6;Ep positional isomers (Table 3.1). Controls received DMSO. Non-esterified oxylipins were analyzed by targeted LC-MS/MS following SPE as described [1-4]. Shown is the mean ± SD (n = 3) of the concentration per mg of cell protein.

	concentration of non-esterified oxylipins in human cells [pmol mg^{-1}]					
analyte	**DMSO**	**+18:2;Ep**	**+20:4;OH**	**+20:4;Ep**	**+20:5;Ep**	**+22:6;Ep**
13-HODE	< 0.10	< 0.10	< 0.10	< 0.10	< 0.10	< 0.10
9-HODE	0.85 ± 0.11	1.9 ± 0.4	0.85 ± 0.11	1.9 ± 0.4	0.85 ± 0.11	1.9 ± 0.4
12(13)-EpOME	0.43 ± 0.15	50 ± 7	0.43 ± 0.15	50 ± 7	0.43 ± 0.15	50 ± 7
9(10)-EpOME	0.51 ± 0.09	45 ± 6	0.51 ± 0.09	45 ± 6	0.51 ± 0.09	45 ± 6
12,13-DiHOME	0.34 ± 0.23	0.48 ± 0.05	0.34 ± 0.23	0.48 ± 0.05	0.34 ± 0.23	0.48 ± 0.05
9,10-DiHOME	0.36 ± 0.21	1.3 ± 0.2	0.36 ± 0.21	1.3 ± 0.2	0.36 ± 0.21	1.3 ± 0.2
13-HOTrE	< 0.25	< 0.25	< 0.25	< 0.25	< 0.25	< 0.25
9-HOTrE	< 0.10	< 0.10	< 0.10	< 0.10	< 0.10	< 0.10
14(15)-EpEDE	< 0.03	4.4 ± 0.8	< 0.03	< 0.03	< 0.03	< 0.03
15-HETE	< 0.11	< 0.11	29.0 ± 0.8	< 0.11	< 0.11	< 0.11
11-HETE	< 0.022	< 0.022	<0.022	< 0.022	< 0.022	< 0.022
12-HETE	< 0.10	< 0.10	34.9 ± 0.5	< 0.10	< 0.10	< 0.10
8-HETE	< 0.095	< 0.095	<0.095	< 0.095	< 0.095	< 0.095
9-HETE	< 0.27	< 0.27	<0.27	< 0.27	< 0.27	< 0.27
5-HETE	< 0.018	< 0.018	23 ± 3	< 0.018	< 0.018	< 0.018
14(15)-EpETrE	< 0.10	0.72 ± 0.27	< 0.10	92 ± 27	< 0.10	< 0.10
11(12)-EpETrE	< 0.051	< 0.051	< 0.051	70 ± 26	< 0.051	< 0.051
8(9)-EpETrE	< 0.25	< 0.25	< 0.25	28 ± 13	< 0.25	< 0.25
14,15-DiHETrE	< 0.010	< 0.010	< 0.010	2.7 ± 0.7	< 0.010	< 0.010
11,12-DiHETrE	< 0.032	< 0.032	< 0.032	3.3 ± 0.7	< 0.032	< 0.032
8,9-DiHETrE	< 0.034	< 0.034	< 0.034	0.86 ± 0.21	< 0.034	< 0.034
5,6-DiHETrE	< 0.051	< 0.051	< 0.051	< 0.051	< 0.051	< 0.051
18-HEPE	< 0.25	< 0.051	< 0.051	< 0.051	< 0.051	< 0.051
15-HEPE	< 0.10	< 0.051	< 0.051	< 0.051	< 0.051	< 0.051
11-HEPE	< 0.03	< 0.031	< 0.031	< 0.031	< 0.031	< 0.031
12-HEPE	< 0.11	< 0.051	< 0.051	< 0.051	< 0.051	< 0.051
8-HEPE	< 0.022	< 0.030	< 0.030	< 0.030	< 0.030	< 0.030
9-HEPE	< 0.10	< 0.10	< 0.10	< 0.10	< 0.10	< 0.10
5-HEPE	< 0.095	< 0.030	< 0.030	< 0.030	< 0.030	< 0.030

Table 8.8: Continued. Non-esterified oxylipins in HEK293T cells.

	concentration of non-esterified oxylipins in human cells [pmol mg^{-1}]				
analyte	**DMSO**	**+18:2;Ep**	**+20:4;OH**	**+20:4;Ep**	**+20:5;Ep**	**+22:6;Ep**
17(18)-EpETE	< 0.51	< 0.51	< 0.51	< 0.51	130 ± 40	6.7 ± 2.4
14(15)-EpETE	< 0.10	< 0.10	< 0.10	< 0.10	65 ± 21	4.0 ± 0.7
11(12)-EpETE	< 0.10	< 0.10	< 0.10	< 0.10	50 ± 16	2.8 ± 0.4
8(9)-EpETE	< 0.51	< 0.51	< 0.51	< 0.51	46 ± 16	< 0.51
17,18-DiHETE	< 0.084	< 0.084	< 0.084	< 0.084	6.2 ± 2.2	< 0.084
14,15-DiHETE	< 0.025	< 0.025	< 0.025	< 0.025	4.5 ± 1.6	0.27 ± 0.21
11,12-DiHETE	< 0.025	< 0.025	< 0.025	< 0.025	10 ± 0.1	0.42 ± 0.01
8,9-DiHETE	< 0.051	< 0.051	< 0.051	< 0.051	5.7 ± 2.0	< 0.051
20-HDHA	< 0.32	< 0.32	< 0.32	< 0.32	< 0.32	< 0.32
16-HDHA	< 0.10	< 0.10	< 0.10	< 0.10	< 0.10	< 0.10
17-HDHA	< 0.34	< 0.34	< 0.34	< 0.34	< 0.34	< 0.34
13-HDHA	< 0.051	< 0.051	< 0.051	< 0.051	6.9 ± 5.7	< 0.051
14-HDHA	< 0.056	< 0.056	< 0.056	< 0.056	< 0.056	< 0.056
10-HDHA	0.026 ± 0.002	0.035 ± 0.009	0.04 ± 0.02	0.029 ± 0.003	0.048 ± 0.010	0.076 ± 0.035
11-HDHA	< 0.10	< 0.10	< 0.10	< 0.10	< 0.10	< 0.10
7-HDHA	< 0.051	< 0.051	< 0.051	< 0.051	< 0.051	< 0.051
8-HDHA	< 0.038	< 0.038	< 0.038	< 0.038	< 0.038	< 0.038
19(20)-EpDPE	< 0.25	< 0.25	< 0.25	< 0.25	< 0.25	110 ± 23
16(17)-EpDPE	< 0.10	< 0.10	< 0.10	< 0.10	< 0.10	79 ± 15
13(14)-EpDPE	< 0.051	< 0.051	< 0.051	< 0.051	< 0.051	79 ± 17
10(11)-EpDPE	0.023 ± 0.049	< 0.010	< 0.010	0.34 ± 0.13	< 0.010	89 ± 19
7(8)-EpDPE	< 0.44	< 0.44	< 0.44	< 0.44	< 0.44	73 ± 16
19,20-DiHDPE	< 0.25	< 0.25	< 0.25	< 0.25	< 0.25	5.6 ± 0.5
16,17-DiHDPE	< 0.051	< 0.051	< 0.051	< 0.051	< 0.051	5.6 ± 0.5
13,14-DiHDPE	< 0.051	< 0.051	< 0.051	< 0.051	< 0.051	16 ± 1.4
10,11-DiHDPE	< 0.051	< 0.051	< 0.051	< 0.051	< 0.051	5.7 ± 0.6
7,8-DiHDPE	< 0.25	< 0.25	< 0.25	< 0.25	< 0.25	3.7 ± 0.8

Table 8.9: Total oxylipins in HEK293T cells. 0.5 × 10^6 cells were used per experiment. HEK293T cells were supplemented with either a mixture of 18:2;Ep, 20:4;OH, 20:4;Ep, 20:5;Ep, or 22:6;Ep positional isomers (Table 3.1). Controls received DMSO. Total oxylipins were analyzed by targeted LC-MS/MS following alkaline hydrolysis and SPE as described [1-4]. Shown is the mean ± SD (n = 3) of the concentration per mg of cell protein.

	concentration of total oxylipins in human cells [pmol mg^{-1}]					
analyte	**DMSO**	**+18:2;Ep**	**+20:4;OH**	**+20:4;Ep**	**+20:5;Ep**	**+22:6;Ep**
13-HODE	< 2.0	< 2.0	< 2.0	< 2.0	< 2.0	< 2.0
9-HODE	10 ± 3	260 ± 17	140 ± 34	130 ± 47	100 ± 20	260 ± 17
12(13)-EpOME	1.9 ± 0.4	9100 ± 1100	41 ± 7	89 ± 25	27 ± 8	28 ± 14
9(10)-EpOME	2.8 ± 0.8	14000 ± 1900	54 ± 3	110 ± 28	41 ± 8	53 ± 30
12,13-DiHOME	1.4 ± 0.3	100 ± 53	46 ± 5	51 ± 27	36 ± 14	48 ± 32
9,10-DiHOME	2.0 ± 0.5	210 ± 63	59 ± 3	70 ± 44	45 ± 21	91 ± 84
13-HOTrE	< 5.1	< 5.1	< 5.1	< 5.1	< 5.1	< 5.1
9-HOTrE	< 2.0	< 2.0	< 2.0	< 2.0	< 2.0	< 2.0
14(15)-EpEDE	< 0.53	630 ± 68	< 0.53	< 0.53	< 0.53	< 0.53
15-HETE	< 2.2	< 2.2	1200 ± 180	< 2.2	< 2.2	< 2.2
11-HETE	1.2 ± 0.1	< 0.44	< 0.44	< 0.44	< 0.44	< 0.44
12-HETE	2.1 ± 0.1	< 2.0	1700 ± 260	< 2.0	< 2.0	< 2.0
8-HETE	< 1.9	< 1.9	< 1.9	< 1.9	< 1.9	< 1.9
9-HETE	< 5.4	< 5.4	< 5.4	< 5.4	< 5.4	< 5.4
5-HETE	2.9 ± 0.2	5.2 ± 0.5	3300 ± 510	12 ± 1	14 ± 2	7.3 ± 1.7
14(15)-EpETrE	< 2.0	120 ± 11	< 2.0	5800 ± 550	< 2.0	< 2.0
11(12)-EpETrE	< 1.0	50 ± 6	< 1.0	3200 ± 470	< 1.0	< 1.0
8(9)-EpETrE	< 5.0	< 5.0	< 5.0	4300 ± 620	< 5.0	< 5.0
14,15-DiHETrE	< 0.20	< 0.20	< 0.20	74 ± 13	< 0.20	< 0.20
11,12-DiHETrE	< 0.65	< 0.65	< 0.65	55 ± 9	< 0.65	< 0.65
8,9-DiHETrE	< 0.69	< 0.69	< 0.69	38 ± 6	< 0.69	< 0.69
5,6-DiHETrE	< 1.0	< 1.0	< 1.0	1000 ± 170	< 1.0	< 1.0
18-HEPE	< 1.0	< 1.0	< 1.0	<1.0	< 1.0	< 1.0
15-HEPE	< 1.0	< 1.0	< 1.0	<1.0	< 1.0	< 1.0
11-HEPE	< 0.63	< 0.63	< 0.63	<0.63	< 0.63	< 0.63
12-HEPE	< 1.0	< 1.0	< 1.0	<1.0	< 1.0	< 1.0
8-HEPE	< 0.61	< 0.61	< 0.61	<0.61	< 0.61	< 0.61
9-HEPE	< 2.0	< 2.0	< 2.0	<2.0	< 2.0	< 2.0
5-HEPE	< 0.60	< 0.60	< 0.60	<0.60	< 0.60	< 0.60

Table 8.9: Continued. Total oxylipins in HEK293T cells.

	concentration of total oxylipins in human cells [pmol mg^{-1}]					
Analyte	**DMSO**	**+18:2;Ep**	**+20:4;OH**	**+20:4;Ep**	**+20:5;Ep**	**+22:6;Ep**
17(18)-EpETE	< 10	< 10	< 10	7900 ± 1200	1200 ± 87	
14(15)-EpETE	< 2.0	< 2.0	< 2.0	2800 ± 390	390 ± 19	
11(12)-EpETE	< 2.0	< 2.0	< 2.0	1300 ± 110	120 ± 5	
8(9)-EpETE	< 10	< 10	< 10	4600 ± 644	230 ± 8	
17,18-DiHETE	< 1.7	< 1.7	< 1.7	63 ± 6	< 1.7	
14,15-DiHETE	< 0.51	< 0.51	< 0.51	39 ± 5	< 0.51	
11,12-DiHETE	< 0.51	< 0.51	< 0.51	133 ± 22	< 0.51	
8,9-DiHETE	< 1.0	< 1.0	< 1.0	140 ± 18	< 1.0	
20-HDHA	< 2.0	< 2.0	< 2.0	< 2.0	< 2.0	
16-HDHA	< 2.0	< 2.0	< 2.0	< 2.0	< 2.0	
17-HDHA	< 7.0	< 7.0	< 7.0	< 7.0	< 7.0	
13-HDHA	< 1.0	< 1.0	< 1.0	< 1.0	< 1.0	
14-HDHA	< 1.0	< 1.0	< 1.0	< 1.0	< 1.0	
10-HDHA	1.4 ± 0.1	2.2 ± 0.3	2.1 ± 1.2	1.9 ± 1.3	2.2 ± 0.7	3.4 ± 2.1
11-HDHA	< 2.0	< 2.0	< 2.0	< 2.0	< 2.0	< 2.0
7-HDHA	< 1.0	< 1.0	< 1.0	< 1.0	< 1.0	< 1.0
8-HDHA	< 0.77	< 0.77	< 0.77	< 0.77	< 0.77	< 0.77
19(20)-EpDPE	< 5.1	< 5.1	57 ± 7	< 5.1	4400 ± 56	
16(17)-EpDPE	< 2.0	< 2.0	< 2.0	< 2.0	1900 ± 52	
13(14)-EpDPE	< 1.0	< 1.0	< 1.0	< 1.0	1700 ± 95	
10(11)-EpDPE	< 0.20	< 0.20	36 ± 7	< 0.20	2700 ± 36	
7(8)-EpDPE	< 8.8	< 8.8	< 8.8	< 8.8	2000 ± 64	
19,20-DiHDPE	< 5.1	< 5.1	< 5.1	< 5.1	124 ± 8	
16,17-DiHDPE	< 1.0	< 1.0	< 1.0	< 1.0	86 ± 6	
13,14-DiHDPE	< 1.0	< 1.0	< 1.0	< 1.0	190 ± 12	
10,11-DiHDPE	< 1.0	< 1.0	< 1.0	< 1.0	110 ± 8	
7,8-DiHDPE	< 5.1	< 5.1	< 5.1	< 5.1	100 ± 8	

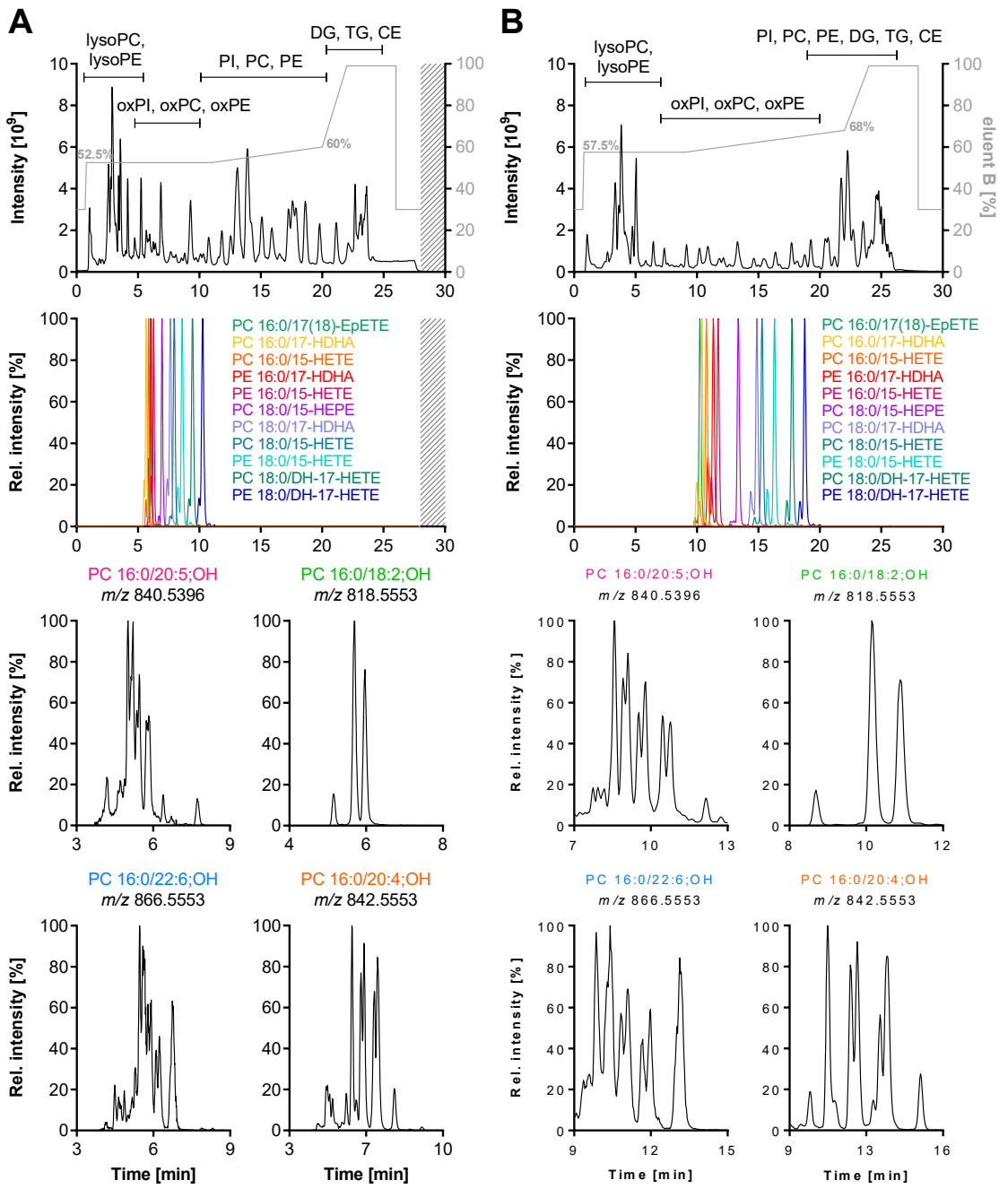

Fig. 8.9: Chromatographic separation efficiency of oxPL using two different solvent gradients (A and B) by untargeted RP-LC-HRMS. Shown is the separation of (**top**) a lipid extract from human serum (full scan *m/z* 200 – 1200) in ESI(+) mode; (**middle**) oxPL standards (XIC, in ESI(-)) (**two bottom rows**) XIC of PC species bearing hydroxy-PUFA positional isomers in a lipid extract from human serum (ESI(-)). Separation was carried out on an ACQUITY Premier CSH C18 column (2.1 × 100 mm, 1.7 µm, 130 Å) using as solvents **A** eluent A (H_2O/ACN, 40/60, v/v) and B (IPA/ACN, 90/10, v/v + 1% H_2O) and **B** A (H_2O/ACN, 60/40, v/v) and B (IPA/ACN, 80/20, v/v, + 1% H_2O), all eluents contain 10 mmol L^{-1} ammonium formate and 0.1% formic acid.

Table 8.10: List of detected oxPL in human serum and in oxylipin-supplemented HEK293T cells by untargeted LC-ESI(-)-HRMS in Full MS/ddMS^2 TOP *N* mode. Shown is the t_R, *m/z* of precursor ion and product ions measured in ESI(-). *Tentative identification of oxPL. OxPL highlighted in light grey were confirmed using authentic standards. n.d. = not detected.

		measured *m/z*						
analyte	**t_R [min]**	**precursor ion**	**molecular ion**	**neutral loss**	***sn*-2 (ox)FA**	***sn*-1 (ox)FA**	**α-cleavage**	**PI group**
PI 16:0/18:2;13OH	7.65	849.5133	n.d.	553.2747	295.2273	255.2326	195.1389	241.0114
PI 16:0/18:2;9OH	8.16	849.5131	n.d.	553.2767	295.2277	255.2327	171.1025	241.0117
PI 18:2;12Ep_16:0	9.24	849.5136	n.d.	n.d.	255.2331	295.2281	195.1391	241.0126
PI 16:0_18:2;12Ep	9.49	849.5137	n.d.	n.d.	295.2281	255.2331	195.1391	241.0118
PI 18:2;9Ep_16:0	9.81	849.5139	n.d.	n.d.	255.2327	295.2275	171.1030	241.0118
PI 16:0_18:2;9Ep	10.15	849.5137	n.d.	n.d.	295.2281	255.2330	171.1023	241.0116
PI 18:0/18:2;13OH	11.07	877.5444	n.d.	581.3082	295.2276	283.2640	195.1385	241.0119
PI 18:0/18:2;9OH	11.90	877.5443	n.d.	581.3087	295.2278	283.2640	171.1027	241.0113
PI 18:0/18:2;12Ep	13.58	877.5443	877.5449	581.3101	295.2271	283.2634	195.1385	241.0123
PI 18:0/18:2;9Ep	14.38	877.5449	877.5446	581.3089	295.2271	283.2640	171.1024	241.0126
PI 18:1_18:2;12Ep	9.89	875.5296	n.d.	n.d.	295.2275	281.2485	195.1390	241.0120
PI 18:1_18:2;Ep	10.73	875.5297	875.5255	n.d.	295.2271	281.2483	n.d.	241.0124
PI 16:0_20:4;15OH	7.99	873.5133	n.d.	n.d.	319.2270	255.2326	219.1389	241.0115
PI 16:0_20:4;11OH	8.73	873.5131	n.d.	n.d.	319.2272	255.2329	167.1074	241.0116
PI 16:0/20:4;12OH	8.89	873.5133	n.d.	553.2748	319.2280	255.2328	179.1080	241.0116
PI 16:0_20:4;8OH	9.77	873.5132	n.d.	n.d.	319.2270	255.2326	155.0712	241.0122
PI 16:0_20:4;9OH	10.04	873.5123	n.d.	n.d.	319.2283	255.2328	167.0711	241.0123
PI 16:0/20:4;5OH	11.49	873.5146	n.d.	#REF!	n.d.	255.2333	115.0399	241.0111
PI 16:0/20:4;14Ep	9.52	873.5136	873.5142	553.2775	319.2279	255.2329	219.1392	241.0117
PI 16:0/20:4;11Ep	10.53	873.5139	873.5125	553.2786	319.2284	255.2326	167.1079	241.0118
PI 16:0/20:4;8Ep	11.31	873.5139	873.5159	553.2757	319.2274	255.2327	167.0704	241.0121
PI 16:0/20:5;17Ep	7.75	871.4974	871.4971	553.2788	317.2112	255.2325	259.1687	241.0115
PI 16:0/20:5;14Ep	8.27	871.4976	871.4976	553.2781	317.2109	255.2339	207.1385	241.0120
PI 36:5;O	8.55	871.4988	871.4985	n.d.	n.d.	255.2333	n.d.	241.0122
PI 36:5;O	9.08	871.4982	n.d.	n.d.	n.d.	255.2328	n.d.	241.0122
PI 18:0/20:2;Ep	17.07	905.5764	905.5764	581.3071	323.2581	283.2658	n.d.	241.0125
PI 18:0/20:2;Ep	17.55	905.5767	905.5715	581.3114	323.2612	283.2642	n.d.	241.0123
PI 18:0/20:3;14Ep	15.11	903.5607	903.5627	581.3105	321.2436	283.2640	221.1534	241.0120
PI 18:0/20:3;Ep	16.47	903.5616	903.5637	581.3097	321.2443	283.2632	n.d.	241.0110
PI 18:1_20:3;14Ep	11.23	901.5456	n.d.	n.d.	321.2437	281.2489	221.1552	241.0117

Table 8.10: Continued 1/14. List of detected oxPL in human serum and in oxylipin-supplemented HEK293T cells by untargeted LC-ESI(-)-HRMS in Full MS/ddMS^2 TOP *N* mode. n.d. = not detected.

		measured *m/z*						
analyte	**t_R [min]**	**precursor ion**	**molecular ion**	**neutral loss**	***sn*-2 (ox)FA**	***sn*-1 (ox)FA**	**α-cleavage**	**PI group**
PI 18:0_20:4;13OH	10.74	901.5441	901.5439	n.d.	319.2270	283.2640	193.1236	241.0128
PI 18:0/20:4;15OH	11.58	901.5440	901.5447	581.3116	319.2271	283.2645	219.1389	241.0116
PI 18:0/20:4;11OH	12.66	901.5439	901.5437	581.3114	319.2274	283.2650	167.1069	241.0119
PI 18:0/20:4;12OH	12.94	901.5440	901.5441	581.3085	319.2271	283.2656	179.1072	241.0112
PI 18:0/20:4;7OH	13.86	901.5450	901.5449	581.3089	319.2273	283.2660	141.0557	241.0126
PI 18:0/20:4;8OH	14.10	901.5447	901.5444	581.3090	319.2270	283.2631	155.0716	241.0115
PI 18:0/20:4;9OH	14.37	901.5441	901.5440	581.3062	319.2279	283.2647	167.0712	241.0113
PI 18:0/20:4;5OH	15.97	901.5450	901.5451	581.3096	319.2289	283.2650	115.0402	241.0118
PI 18:0/20:4;14Ep	13.75	901.5441	901.5457	599.3188	319.2276	283.2641	219.139	241.0116
PI 18:0/20:4;11Ep	14.90	901.5443	901.5453	599.3165	319.2273	283.2642	167.1076	241.0118
PI 18:0/20:4;8Ep	15.77	901.5443	901.5457	599.3196	319.2278	283.2640	155.0714	241.0117
PI 18:0/20:4;5Ep	16.92	901.5446	901.5447	599.3168	319.2275	283.2641	191.1807	241.0118
PI 18:1/20:4;15OH	8.44	899.5294	899.5272	579.2947	319.2278	281.2488	219.1387	241.0119
PI 18:1/20:4;14Ep	9.91	899.5289	899.5289	579.2950	319.2285	281.2486	219.1383	241.0114
PI 18:1/20:4;11Ep	10.94	899.5292	899.5294	579.2942	319.2268	281.2498	167.1081	241.0116
PI 18:1/20:4;8Ep	11.83	899.5292	899.53	579.2941	319.2268	281.2498	155.0715	241.0117
PI 18:0/20:5;17Ep	11.15	899.5283	899.5284	581.3090	317.2115	283.2643	259.1711	241.0117
PI 18:0/20:5;14Ep	11.96	899.5284	899.5286	581.3080	317.2119	283.2637	207.1393	241.0117
PI 18:0/20:5;11Ep	12.36	899.5289	899.5280	581.3061	317.2124	283.2637	167.1074	241.0123
PI 18:0/20:5;8Ep	13.15	899.5291	899.5284	581.3064	317.2122	283.2652	155.0714	241.0124
PI 18:1_20:5;17Ep	8.03	897.5135	897.5128	579.2917	317.2123	281.2473	259.1729	241.0116
PI 18:1_20:5;14Ep	8.62	897.5129	897.5122	579.2927	317.2134	281.2492	207.1386	241.0121
PI 18:1_20:5;11Ep*	8.96	897.5140	n.d.	n.d.	n.d.	281.2490	167.1073	241.0120
PI 18:1_20:5;8Ep*	9.55	897.5139	n.d.	n.d.	n.d.	281.2485	155.0713	241.0123
PI 38:6;O	8.92	897.5140	n.d.	n.d.	n.d.	255.2329	n.d.	241.0120
PI 38:6;O	9.51	897.5142	n.d.	n.d.	n.d.	255.2330	n.d.	241.0124
PI 38:6;O	9.76	897.5141	n.d.	n.d.	n.d.	255.2330	n.d.	241.0120
PI 16:0_22:6;10Ep*	10.24	897.5140	n.d.	n.d.	n.d.	255.2325	153.0918	241.0115
PI 38:6;O	11.08	897.5137	n.d.	n.d.	n.d.	255.2330	n.d.	241.0116
PI 18:0/22:6;19Ep	12.82	925.5449	925.5458	581.3112	343.2293	283.2645	241.1960	241.0109

Table 8.10: Continued 2/14. List of detected oxPL in human serum and in oxylipin-supplemented HEK293T cells by untargeted LC-ESI(-)-HRMS in Full MS/ddMS^2 TOP *N* mode. n.d. = not detected.

			measured *m/z*				
analyte	**t_R [min]**	**precursor ion**	**molecular ion**	**neutral loss**	***sn*-2 (ox)FA**	***sn*-1 (ox)FA**	**α-cleavage**	**PI group**
PI 18:0/22:6;13Ep	13.94	925.5447	925.5460	581.3123	343.2292	283.2639	193.1237	241.0127
PI 18:0/22:6;10Ep*	14.49	925.5449	925.5455	581.3089	n.d.	283.2641	153.0923	241.0130
PI 40:6;O	15.41	925.5449	925.5444	581.3113	n.d.	283.2652	n.d.	241.0114
PI 38:7;O	9.28	923.5300	n.d.	n.d.	n.d.	281.2486	n.d.	241.0124
PI 38:7;O	9.92	923.5297	n.d.	n.d.	n.d.	281.2487	n.d.	241.0114
PI 18:1_22:6;13Ep*	10.24	923.5292	n.d.	n.d.	n.d.	281.2479	193.1239	241.0129
PI 18:1_22:6;10Ep*	10.68	923.5300	n.d.	n.d.	n.d.	281.2492	153.0919	241.0108
PI 38:7;O	11.64	923.5297	n.d.	n.d.	n.d.	281.2486	n.d.	241.0119
			measured *m/z*				
analyte	**t_R [min]**	**precursor ion**	**[M-H-$C_3H_5O_2N$]$^-$**	**neutral loss**	***sn*-2 (ox)FA**	***sn*-1 (ox)FA**	**α-cleavage**	**-**
PS 18:0/18:2;Ep*	14.21	802.5243	715.4860	437.2686	295.2277	283.2639	n.d.	-
PS 18:0/18:2;Ep*	15.02	802.5240	715.4956	437.2677	295.2273	283.2643	n.d.	-
			measured *m/z*					
analyte	**t_R [min]**	**precursor ion**	**[M-CH_3-COOH]$^-$**	**neutral loss**	***sn*-2 (ox)FA**	***sn*-1 (ox)FA**	**α-cleavage**	
PC 16:0/18:2;OH	8.72	818.5549	758.5350	480.3089	295.2274	255.2325	n.d.	-
PC 16:0/18:2;13OH	10.19	818.5558	758.5349	480.3084	295.2278	255.2330	195.1399	-
PC 16:0/18:2;9OH	10.91	818.5558	758.5352	480.3071	295.2277	255.2330	171.1027	-
PC 18:2;12Ep/16:0	12.59	818.5554	758.5341	520.3024	255.2328	295.2273	195.1390	-
PC 16:0/18:2;12Ep	12.89	818.5551	758.5339	480.3068	295.2275	255.2329	195.1389	-
PC 18:2;9Ep/16:0	13.25	818.5554	758.5339	520.3018	255.2329	295.2277	171.1030	-
PC 16:0/18:2;9Ep	13.67	818.5549	758.5341	480.3090	295.2275	255.2329	171.1022	-
PC 16:1/18:2;13OH	7.41	816.5410	756.5183	478.2941	295.2279	253.2173	195.1392	-
PC 16:1/18:2;9OH	7.87	816.5411	756.5197	478.2957	295.2280	253.2184	171.1028	-
PC 18:2;12Ep/16:1	9.13	816.5399	756.5217	520.3050	253.2172	295.2277	195.1377	-
PC 16:1/18:2;12Ep	9.32	816.5400	756.5186	758.2945	295.2276	253.2173	195.1386	-
PC 18:2;9Ep/16:1	9.67	816.5401	756.5197	520.3065	253.2173	295.2275	171.1030	-
PC 16:1/18:2;9Ep	9.95	816.5402	756.5175	478.2955	295.2276	253.2173	171.1025	-
PC 16:0/18:3;16OH	8.35	816.5401	756.5184	480.3081	293.2124	255.2330	235.1707	-
PC 16:0/18:3;13OH	8.63	816.5401	756.5198	480.3064	293.2126	255.2334	195.1387	-

Table 8.10: Continued 3/14. List of detected oxPL in human serum and in oxylipin-supplemented HEK293T cells by untargeted LC-ESI(-)-HRMS in Full MS/ddMS^2 TOP *N* mode. n.d. = not detected.

		measured *m/z*					
analyte	**t_R [min]**	**precursor ion**	**[M-CH_3-COOH]$^-$**	**neutral loss**	***sn*-2 (ox)FA**	***sn*-1 (ox)FA**	**α-cleavage**
PC 16:0/18:3;9OH	8.73	816.5405	756.5197	480.3096	293.2133	255.2333	171.1030
PC 16:0/18:3;O	10.25	816.5410	756.5201	480.3127	293.2123	255.2331	n.d.
PC 16:0/18:3;O	11.30	816.5407	756.5202	480.3083	293.2124	255.2331	n.d.
PC 14:0/20:4;14Ep*	8.95	814.5237	n.d.	452.2776	319.2275	227.2017	219.1400
PC 14:0/20:4;11Ep*	9.86	814.5240	n.d.	452.2801	319.2271	227.2013	167.1076
PC 14:0_20:4;8Ep*	10.55	814.5243	n.d.	n.d.	319.2284	227.2014	155.0707
PC 17:1_18:2;Ep	11.16	830.5570	770.5346	n.d.	295.2272	267.2333	n.d.
PC 18:2;Ep_17:1	11.69	830.5565	n.d.	n.d.	267.2336	295.2280	n.d.
PC 17:1_18:2;Ep	12.01	830.5564	770.5382	n.d.	295.2280	267.2325	171.1020
PC 18:0/18:2;OH	12.72	846.5847	786.5651	508.3410	295.2274	283.2642	n.d.
PC 18:0/18:2;13OH	14.60	846.5866	786.5660	508.3404	295.2276	283.2644	195.1391
PC 18:0/18:2;9OH	15.45	846.5866	786.5667	508.3416	295.2280	283.2641	171.1024
PC 18:0/18:2;12Ep	17.50	846.5863	786.5656	508.3402	295.2275	283.2643	195.1387
PC 18:0/18:2;9Ep	18.31	846.5864	786.564	508.3399	295.2275	283.2631	171.1035
PC 16:0_20:2;Ep	16.53	846.5867	786.5586	n.d.	323.2595	255.2327	n.d.
PC 18:2;12Ep/18:1	13.25	844.5707	784.5504	520.3061	281.2484	295.2277	195.1391
PC 18:1/18:2;12Ep	13.42	844.5704	784.5498	506.3241	295.2275	281.2483	195.1392
PC 18:2;9Ep/18:1	14.03	844.5707	784.5494	520.3054	281.2483	295.2275	171.1026
PC 18:1/18:2;9Ep	14.21	844.5706	784.5505	506.3222	295.2277	281.2484	171.1031
PC 18:2;13OH/18:2	7.87	842.5553	782.5344	520.3049	279.2327	295.2280	195.1386
PC 18:2/18:2;13OH	8.02	842.5553	782.5348	504.3055	295.2280	279.2329	195.1385
PC 18:2;9OH/18:2	8.32	842.5553	782.5345	520.3053	279.2329	295.2278	171.1018
PC 18:2/18:2;9OH	8.63	842.5553	782.5345	504.3092	295.2278	279.2330	171.1025
PC 16:0/20:4;13OH	9.95	842.5555	782.5349	480.3092	319.2274	255.2328	193.1231
PC 15-HETE/16:0	10.24	842.5549	782.5302	544.3007	255.2327	319.2265	n.d.
PC 16:0/15-HETE	10.77	842.5555	782.5346	480.3082	319.2275	255.2329	219.1389
PC 16:0/20:4;10OH	11.05	842.5551	782.5353	480.3109	319.2274	255.2326	181.0866
PC 16:0/20:4;11OH	11.79	842.5555	782.5349	480.3092	319.2278	255.2333	167.1076
PC 16:0/20:4;12OH	12.12	842.5555	782.5343	480.3100	319.2279	255.2332	179.1079
PC 16:0/20:4;7OH	12.81	842.5555	782.5344	480.3117	319.2274	255.2330	141.0556

Table 8.10: Continued 4/14. List of detected oxPL in human serum and in oxylipin-supplemented HEK293T cells by untargeted LC-ESI(-)-HRMS in Full MS/ddMS^2 TOP *N* mode. n.d. = not detected.

		measured *m/z*				
analyte	**t_R [min]**	**precursor ion**	**[M-CH$_3$-COOH]$^-$**	**neutral loss**	***sn*-2 (ox)FA**	***sn*-1 (ox)FA**	**α-cleavage**
PC 16:0/20:4;8OH	13.13	842.5555	782.5347	480.3093	319.2275	255.2329	155.0711
PC 16:0/20:4;9OH	13.49	842.5555	782.5345	480.3065	319.2277	255.2329	167.0709
PC 16:0/20:4;5OH	14.99	842.5555	782.5351	480.3076	319.2277	255.2331	115.0399
PC 20:4;14Ep/16:0	12.58	842.5570	782.5349	544.3043	255.2330	319.2273	219.1396
PC 16:0/20:4;14Ep	13.10	842.5557	782.5353	480.3091	319.2275	255.2330	219.1389
PC 20:4;11Ep/16:0	13.60	842.5557	782.5347	544.3049	255.2330	319.2278	179.1073
PC 20:4;5OH_16:0	13.95	842.5552	782.5308	n.d.	319.2270	255.2328	115.0396
PC 16:0/20:4;11Ep	14.25	842.5557	782.5345	480.3106	319.2278	255.2330	179.1077
PC 16:0/20:4;8Ep	15.00	842.5557	782.5347	480.3087	319.2278	255.2330	155.0709
PC 16:0/20:4;5Ep	16.13	842.5557	782.5334	480.3092	319.2281	255.2325	191.1801
PC 20:4;14Ep/16:1	9.11	840.5392	780.5206	544.3034	253.2170	319.2273	219.1411
PC 16:1/20:4;14Ep	9.43	840.5394	780.5192	478.2939	319.2277	253.2173	219.1395
PC 20:4;11Ep/16:1	10.39	840.5399	780.5175	544.3090	253.2170	319.2278	167.1081
PC 16:1/20:4;8Ep	11.14	840.5401	780.5163	478.2966	319.2281	253.2175	167.0714
PC 16:0/20:5;18OH	8.60	840.5401	780.5185	480.3128	317.2120	255.2345	259.1703
PC 16:0/20:5;14OH	8.95	840.5401	780.5184	480.3119	317.2120	255.2334	207.1389
PC 16:0/20:5;15OH	9.10	840.5401	780.5193	480.3090	317.2120	255.2344	219.1387
PC 16:0/20:5;11OH	9.57	840.5401	780.5194	480.3123	317.2121	255.2347	167.1078
PC 16:0/20:5;12OH	9.80	840.5401	780.5187	480.3103	317.2121	255.2336	179.1080
PC 16:0/20:5;8OH	10.53	840.5401	780.5192	480.3096	317.2119	255.2348	155.0709
PC 16:0/20:5;9OH	10.83	840.5401	780.5195	480.3077	317.2121	255.2336	167.0710
PC 16:0/20:5;5OH	12.18	840.5401	780.5123	480.3092	317.2124	255.2340	115.0394
PC 20:5;Ep/16:0	9.98	840.5400	780.5212	542.2913	255.2331	317.2125	n.d.
PC 16:0/17(18)-EpETE	10.36	840.5392	780.5178	480.3088	317.2119	255.2336	259.1708
PC 20:5;14Ep/16:0	10.70	840.5402	780.5228	542.2861	255.2330	317.2121	207.1397
PC 16:0/20:5;14Ep	11.13	840.5390	780.5223	480.3105	317.2109	255.2340	207.1399
PC 16:0/20:5;11Ep	11.55	840.5391	780.5161	480.3071	317.2113	255.2331	167.1081
PC 16:0/20:5;8Ep	12.26	840.5392	780.5185	480.3084	317.2115	255.2337	155.0718
PC 18:0/20:4;13OH	14.37	870.5867	810.5650	508.3411	319.2276	283.2646	193.1229
PC 15-HETE/18:0	14.66	870.5856	n.d.	n.d.	319.2279	283.2635	n.d.

Table 8.10: Continued 5/14. List of detected oxPL in human serum and in oxylipin-supplemented HEK293T cells by untargeted LC-ESI(-)-HRMS in Full MS/ddMS^2 TOP *N* mode. n.d. = not detected.

		measured *m/z*					
analyte	**t_R [min]**	**precursor ion**	**[M-CH_3-COOH]$^-$**	**neutral loss**	***sn*-2 (ox)FA**	***sn*-1 (ox)FA**	**α-cleavage**
PC 18:0/15-HETE	15.29	870.5869	810.5657	508.3422	319.2277	283.2640	219.1390
PC 18:0/20:4;11OH	16.40	870.5867	810.5657	508.3422	319.2276	283.2640	167.1075
PC 18:0/20:4;12OH	16.71	870.5867	810.5656	508.3407	319.2277	283.2645	179.1074
PC 18:0/20:4;7OH	17.52	870.5867	810.5660	508.3413	319.2272	283.2642	141.0554
PC 18:0/20:4;8OH	17.80	870.5867	810.5658	508.3381	319.2276	283.2643	155.0715
PC 18:0/20:4;9OH	18.11	870.5867	810.5661	508.3403	319.2278	283.2643	167.0717
PC 18:0/20:4;5OH	19.66	870.5867	810.5657	508.3400	319.2276	283.2642	115.0400
PC 18:0/20:4;14Ep	17.66	870.5878	810.5676	508.3415	319.2275	283.2636	219.1388
PC 18:0_20:4;11Ep	18.86	870.5878	810.5640	n.d.	319.2276	283.2632	179.1073
PC 18:0/20:4;8Ep	19.72	870.5878	810.5650	508.3426	319.2280	283.2654	155.0713
PC 18:0_20:4;Ep	20.81	870.5877	810.5674	n.d.	319.2277	283.2629	n.d.
PC 16:0/22:4;17OH	13.19	870.5869	810.5647	480.3092	347.2592	255.2329	247.1693
PC 16:0/22:4;13OH	13.93	870.5867	810.5645	480.3104	347.2588	255.2326	195.1389
PC 16:0_22:4;16Ep	16.12	870.5861	810.5629	n.d.	347.2592	255.2319	247.1683
PC 22:4;Ep_16:0	16.59	870.5865	n.d.	n.d.	255.2335	347.2573	n.d.
PC 16:0/22:4;13Ep	16.97	870.5873	n.d.	480.3046	347.2587	255.2329	195.1384
PC 18:1/20:4;12OH	12.46	868.5709	808.5491	506.3266	319.2280	281.2484	179.1073
PC 18:1/20:4;5OH	15.44	868.5714	808.5441	506.3235	319.2271	281.2493	115.0400
PC 18:1/20:4;14Ep	13.55	868.5709	808.5485	506.3255	319.2280	281.2485	219.1391
PC 18:1/20:4;11Ep	14.70	868.5710	808.5500	506.3208	319.2277	281.2491	167.1077
PC 18:1/20:4;8Ep	15.54	868.5711	808.5499	506.3226	319.2279	281.2483	155.0715
PC 16:0/22:5;19Ep	13.23	868.5712	808.5543	480.3050	345.2433	255.2329	287.2013
PC 22:5;Ep/16:0	13.73	868.5712	808.5422	570.3197	255.2329	345.2419	n.d.
PC 16:0/22:5;13Ep	14.14	868.5714	808.5468	480.3113	345.2429	255.2330	207.1389
PC 16:0/22:5;10Ep	14.55	868.5712	808.5475	480.3094	345.2432	255.2325	195.1030
PC 16:0/22:5;7Ep	15.01	868.5713	808.5504	480.3084	345.2441	255.2340	143.0716
PC 18:0/15-HEPE	13.35	868.5721	808.5518	508.3427	317.2127	283.2648	219.1396
PC 18:0/20:5;17Ep	14.86	868.5715	808.5432	508.3427	317.2125	283.2641	259.1710
PC 18:0/20:5;14Ep	15.77	868.5712	n.d.	508.3423	317.2119	283.2645	207.1389
PC 18:0_20:5;11Ep*	16.18	868.5712	n.d.	n.d.	317.2146	283.2647	n.d.

Table 8.10: Continued 6/14. List of detected oxPL in human serum and in oxylipin-supplemented HEK293T cells by untargeted LC-ESI(-)-HRMS in Full MS/ddMS^2 TOP *N* mode. n.d. = not detected.

			measured *m/z*				
analyte	**t_R [min]**	**precursor ion**	**[M-CH$_3$-COOH]$^-$**	**neutral loss**	***sn*-2 (ox)FA**	***sn*-1 (ox)FA**	**α-cleavage**
PC 18:0/20:5;8Ep	16.92	868.5712	808.5546	508.3383	317.2119	283.2644	155.0714
PC 18:2;13OH/20:4	7.60	866.5547	806.5353	520.3021	303.2325	295.2274	195.1384
PC 18:2;OH/20:4	8.00	866.5547	806.5315	520.3075	303.2326	295.2273	n.d.
PC 18:2/20:4;15OH	8.50	866.5555	806.5351	504.3132	319.2276	279.2330	219.1389
PC 18:2/20:4;11OH	9.36	866.5549	806.5369	504.3109	319.2273	279.2327	167.1076
PC 18:2/20:4;12OH	9.59	866.5560	806.5345	504.3115	319.2280	279.2327	179.1073
PC 18:1/20:5;17Ep	10.80	866.5558	806.5361	506.3242	317.2119	281.2486	259.1697
PC 20:5;14Ep/18:1	11.30	866.5557	806.5334	542.2888	281.2486	317.2118	207.1383
PC 18:1/20:5;14Ep	11.64	866.5557	806.5374	506.3232	317.2130	281.2484	207.1386
PC 18:1_20:5;Ep	12.17	866.5558	806.5294	n.d.	317.2116	281.2487	167.1077
PC 18:1/20:5;8Ep	12.79	866.5557	806.5350	506.3254	317.2121	281.2486	155.0713
PC 16:0/22:6;20OH	9.86	866.5557	806.5349	480.3085	343.2278	255.2328	241.1959
PC 16:0/22:6;16OH	10.28	866.5557	806.5341	480.3096	343.2273	255.2327	233.1548
PC 17-HDHA/16:0	10.05	866.5546	806.5351	568.2973	255.2327	343.2301	n.d.
PC 16:0/17-HDHA	10.41	866.5558	806.5348	480.3107	343.2279	255.2331	201.1645
PC 16:0/22:6;13OH	10.83	866.5557	806.5345	480.3094	343.2277	255.2330	193.1234
PC 16:0/22:6;14OH	11.08	866.5558	806.5345	480.3108	343.2278	255.2330	205.1230
PC 16:0/22:6;10OH	11.64	866.5557	806.5347	480.3077	343.2281	255.2330	153.0920
PC 16:0/22:6;11OH	11.91	866.5556	806.5350	480.3086	343.2275	255.2333	121.1021
PC 16:0/22:6;7OH	12.94	866.5558	806.5346	480.3076	343.2276	255.2328	141.0556
PC 16:0/22:6;8OH	13.13	866.5556	806.5347	480.3104	343.2280	255.2330	189.1646
PC 22:6;19Ep/16:0	11.66	866.5550	806.5341	568.3048	255.2327	343.2273	241.1952
PC 16:0/22:6;19Ep	12.05	866.5552	806.5341	480.3096	343.2277	255.2329	241.1966
PC 22:6;Ep/16:0	12.47	866.5555	806.5341	480.3075	343.2271	255.2329	n.d.
PC 16:0/22:6;16Ep	12.78	866.5549	806.5340	480.3094	343.2266	255.2328	233.1554
PC 16:0/22:6;13Ep	13.15	866.5548	806.5351	568.3039	255.2328	343.2277	193.1228
PC 16:0/22:6;10Ep	13.68	866.5550	806.5353	480.3079	343.2275	255.2328	153.0918
PC 16:0/22:6;7Ep	14.55	866.5548	806.5334	568.3019	255.2328	343.2270	189.1650
PC DH-17-HETE_18:0	17.30	898.6191	838.5984	n.d.	283.2645	347.2603	n.d.
PC 18:0/DH-17-HETE	17.73	898.6192	838.5984	508.3404	347.2595	283.2644	247.1715

Table 8.10: Continued 7/14. List of detected oxPL in human serum and in oxylipin-supplemented HEK293T cells by untargeted LC-ESI(-)-HRMS in Full MS/ddMS^2 TOP *N* mode. n.d. = not detected.

		measured *m/z*					
analyte	**t_R [min]**	**precursor ion**	**[M-CH_3-COOH]$^-$**	**neutral loss**	***sn*-2 (ox)FA**	***sn*-1 (ox)FA**	**α-cleavage**
PC 18:0/22:6;2OH	14.24	894.5870	834.5657	508.3433	343.2281	283.2641	241.1964
PC 18:0/22:6;16OH	14.69	894.5869	834.5660	508.3425	343.2277	283.2643	233.1549
PC 17-HDHA_18:0	14.35	894.5859	834.5680	n.d.	283.2636	343.2274	n.d.
PC 18:0/17-HDHA	14.86	894.5872	834.5660	508.3418	343.2284	283.2650	201.1656
PC 18:0/22:6;13OH	15.32	894.5869	834.5662	508.3406	343.2285	283.2640	193.1227
PC 18:0/22:6;14OH	15.60	894.5872	834.5658	508.3414	343.2282	283.2645	205.1232
PC 18:0/22:6;10OH	16.18	894.5866	834.5657	508.3403	343.2278	283.2643	153.0920
PC 18:0/22:6;11OH	16.49	894.5872	834.5667	508.3413	343.2274	283.2645	121.1018
PC 18:0/22:6;7OH	17.59	894.5864	834.5657	508.3390	343.2283	283.2632	141.0555
PC 18:0/22:6;8OH	17.74	894.5868	834.5660	508.3419	343.2280	283.2641	189.1651
PC 18:0/22:6;19Ep	16.59	894.5861	834.5670	508.3398	343.2285	283.2646	241.1953
PC 18:0/22:6;16Ep	17.46	894.5864	834.5590	508.3410	343.2268	283.2638	233.1531
PC 18:0/22:6;O	17.76	894.5871	n.d.	508.3395	343.2297	283.2638	n.d.
PC 18:0/22:6;10Ep	18.30	894.5865	834.5616	508.3412	343.2289	283.2654	153.0921
PC 18:0/22:6;7Ep	19.17	894.5876	834.5632	508.3373	343.2268	283.2650	189.1650
PC 22:6;19Ep/18:1	12.29	892.5715	832.5507	568.3044	281.2489	343.2278	241.1967
PC 18:1/22:6;19Ep	12.54	892.5716	832.5564	506.3251	343.2278	281.2502	241.1956
PC 22:6;16Ep/18:1	13.10	892.5713	832.5510	568.3040	281.2480	343.2276	233.1548
PC 18:1/22:6;16Ep	13.35	892.5710	832.5549	506.3251	343.2273	281.2489	233.1550
PC 18:1/22:6;13Ep	13.74	892.5714	832.5579	506.3260	343.2280	281.2490	193.1236
PC 22:6;10Ep/18:1	13.74	892.5714	832.5579	568.3057	343.2280	281.2490	153.0922
PC 18:1/22:6;10Ep	14.24	892.5715	832.5471	506.3262	343.2270	281.2495	153.0921
PC 22:6;Ep/18:1	14.55	892.5715	832.5471	568.3027	343.2268	281.2487	n.d.
PC 18:1/22:6;7Ep	15.06	892.5715	832.5476	506.3269	343.2285	281.2496	189.1654
PC P-16:0/18:2;OH	10.08	802.5607	742.5400	464.3152	295.2275	-	n.d.
PC P-16:0/18:2;13OH	11.88	802.5599	742.5388	464.3132	295.2272	-	195.1392
PC P-16:0/18:2;9OH	12.60	802.5601	742.5394	464.3137	295.2272	-	171.1025
PC P-16:0/18:2;12Ep	14.71	802.5613	742.5359	464.3139	295.2281	-	195.1390
PC P-16:0/18:2;9Ep	15.52	802.5607	742.5386	464.3139	295.2275	-	171.1021
PC P-16:0/20:4;13OH	11.55	826.5604	766.5381	464.3118	319.2270	-	193.1232

Table 8.10: Continued 8/14. List of detected oxPL in human serum and in oxylipin-supplemented HEK293T cells by untargeted LC-ESI(-)-HRMS in Full MS/ddMS^2 TOP *N* mode. n.d. = not detected.

			measured *m/z*				
analyte	**t_R [min]**	**precursor ion**	**[M-CH$_3$-COOH]$^-$**	**neutral loss**	***sn*-2 (ox)FA**	***sn*-1 (ox)FA**	**α-cleavage**
PC P-16:0/20:4;15OH	12.47	826.5598	766.5383	464.3145	319.2272	-	219.1392
PC P-16:0/20:4;11OH	13.52	826.5609	766.5390	464.3149	319.2273	-	167.1073
PC P-16:0/20:4;12OH	13.86	826.5606	766.5388	464.3136	319.2274	-	179.1073
PC P-16:0/20:4;7OH	14.69	826.5600	766.5381	464.3130	319.2278	-	141.0555
PC P-16:0/20:4;8OH	14.99	826.5604	766.5391	464.3158	319.2277	-	155.0714
PC P-16:0/20:4;9OH	15.19	826.5605	766.5396	464.3143	319.2273	-	167.0711
PC P-16:0/20:4;5OH	16.85	826.5597	766.5375	464.3151	319.2269	-	115.0399
PC P-16:0/20:4;14Ep	14.86	826.5611	766.5383	464.3145	319.2278	-	219.1397
PC P-16:0/20:4;11Ep	16.04	826.5614	766.5405	464.3145	319.2267	-	167.1069
PC P-16:0/20:4;8Ep	16.83	826.5611	766.5409	464.3123	319.2276	-	155.0708
PC P-16:0/20:5;17Ep	12.05	824.5455	764.5200	464.3146	317.2125	-	215.1819
PC P-16:0/20:5;14Ep*	12.89	824.5454	n.d.	464.3134	317.2118	-	207.1391
PC P-36:5;O*	13.31	n.d.	n.d.	n.d.	343.2276	-	n.d.
PC P-16:0/20:5;8Ep	14.00	824.5453	764.5214	464.3154	317.2122	-	155.0721
PC P-16:0/22:6;19Ep	13.77	850.5609	790.5373	464.3154	343.2276	-	241.1948
PC P-16:0/22:6;16Ep*	14.56	850.5618	n.d.	464.3140	343.2295	-	233.1556
PC P-16:0/22:6;Ep	14.88	850.5623	n.d.	464.3134	343.2270	-	n.d.
PC P-16:0/22:6;10Ep*	15.41	850.5610	n.d.	464.3131	343.2289	-	153.0921
			measured *m/z*				
analyte	**t_R [min]**	**precursor ion**	**[M-CH$_3$-COOH]$^-$**	**neutral loss**	***sn*-2 (ox)FA**	***sn*-1 (ox)FA**	**α-cleavage**
PC O-16:0/18:2;13OH	12.60	804.5752	744.5538	466.3281	295.2272	-	195.1386
PC O-16:0/18:2;OH	13.34	804.5755	744.5545	n.d.	295.2275	-	n.d.
PC O-16:0/18:2;12Ep	15.44	804.5760	744.5552	466.3337	295.2277	-	195.1387
PC O-16:0/18:2;9Ep	16.24	804.5762	744.5557	466.3317	295.2276	-	171.1024
PC O-18:1/18:2;12Ep	15.75	830.5920	770.5690	492.3419	295.2279	-	195.1396
PC O-18:1/18:2;9Ep	16.60	830.5923	770.5676	492.3477	295.2276	-	171.1031
PC O-16:0/20:4;13OH	12.37	828.5754	768.5529	466.3286	319.2271	-	193.1234
PC O-16:0/20:4;15OH	13.22	828.5756	768.5543	466.3306	319.2272	-	219.1385
PC O-16:0/20:4;11OH	14.27	828.5759	768.5541	466.3273	319.2275	-	167.1073

Table 8.10: Continued 9/14. List of detected oxPL in human serum and in oxylipin-supplemented HEK293T cells by untargeted LC-ESI(-)-HRMS in Full MS/ddMS^2 TOP *N* mode. n.d. = not detected.

		measured *m/z*					
analyte	**t_R [min]**	**precursor ion**	**[M-CH_3-COOH]$^-$**	**neutral loss**	***sn*-2 (ox)FA**	***sn*-1 (ox)FA**	**α-cleavage**
PC O-16:0/20:4;12OH	14.63	828.5761	768.5535	466.3289	319.2274	-	179.1078
PC O-16:0/20:4;8OH	15.70	828.5754	768.5546	466.3295	319.2272	-	155.0712
PC O-16:0/20:4;9OH	15.97	828.5761	768.5551	466.3303	319.2273	-	167.0708
PC O-16:0/20:4;5OH	17.59	828.5756	768.5539	466.3311	319.2279	-	115.0397
PC O-16:0/20:4;14Ep	15.58	828.5765	768.5565	466.3286	319.2274	-	219.1392
PC O-16:0/20:4;11Ep	16.76	828.5760	768.5557	466.3289	319.2269	-	167.1074
PC O-16:0/20:4;8Ep	17.59	828.5763	768.5553	466.3321	319.2272	-	167.0710
PC O-16:0/20:5;17Ep	12.72	826.5602	766.5384	466.3273	317.2120	-	215.1798
PC O-16:0/20:5;14Ep	13.59	826.5612	766.539	466.3286	317.2116	-	207.1388
PC O-16:0/20:5;11Ep	14.03	826.5606	766.5444	466.3320	317.2123	-	167.1077
PC O-16:0/20:5;8Ep	14.76	826.5604	766.5397	466.3313	317.2117	-	155.0717
PC O-16:0/22:4;16Ep	18.65	856.6078	796.5887	466.3308	347.2587	-	247.1708
PC O-16:0/22:4;13Ep	19.57	856.6079	796.5874	466.3307	347.2600	-	195.1386
PC O-18:1/20:4;13OH	12.69	854.5907	794.5682	492.3427	319.2264	-	193.1226
PC O-18:1/20:4;15OH	13.59	854.5908	794.5695	492.3476	319.2275	-	219.1390
PC O-18:1/20:4;11OH	14.69	854.5902	794.5702	492.3433	319.2276	-	167.1073
PC O-18:1/20:4;12OH	14.99	854.5915	794.5705	492.3424	319.2278	-	179.1077
PC O-18:1/20:4;7OH	15.73	854.5909	794.5696	492.3449	319.2270	-	141.0551
PC O-18:1/20:4;8OH	16.11	854.5915	794.5699	492.3458	319.2275	-	155.0714
PC O-18:1/20:4;9OH	16.36	854.5909	794.5705	492.3474	319.2273	-	167.0723
PC O-18:1/20:4;5OH	18.11	854.5909	794.5695	492.3457	319.2278	-	115.0396
PC O-18:1/20:4;14Ep	15.94	854.5917	794.5688	492.3451	319.2288	-	219.1399
PC O-18:1/20:4;11Ep	17.13	854.5921	794.5676	492.3410	319.2282	-	167.1075
PC O-18:1/20:4;8Ep	17.96	854.5923	794.5688	492.3443	319.2275	-	167.0708
PC O-18:1/20:5;17Ep	13.08	852.5768	792.5515	492.3443	317.2116	-	215.1790
PC O-18:1/20:5;14Ep*	13.97	852.5771	n.d.	492.3448	317.2114	-	207.1382
PC O-18:1/20:5;11Ep*	14.41	852.5769	n.d.	n.d.	317.2126	-	167.1074
PC O-18:1/20:5;8Ep	15.11	852.5769	792.5588	492.3471	317.2122	-	167.0710
PC O-16:0/22:6;19Ep	14.49	852.5757	792.5537	466.3288	343.2271	-	241.1968
PC O-16:0/22:6;16Ep	15.31	852.5757	792.5535	466.3333	343.2273	-	233.1541

Table 8.10: Continued 10/14. List of detected oxPL in human serum and in oxylipin-supplemented HEK293T cells by untargeted LC-ESI(-)-HRMS in Full MS/ddMS^2 TOP *N* mode. n.d. = not detected.

			measured *m/z*				
analyte	**t_R [min]**	**precursor ion**	**[M-CH_3-COOH]$^-$**	**neutral loss**	***sn*-2 (ox)FA**	***sn*-1 (ox)FA**	**α-cleavage**
PC O-16:0/22:6;13Ep	15.64	852.5756	792.5567	466.3279	343.2274	-	193.1234	-
PC O-16:0/22:6;10Ep	16.16	852.5759	792.5531	466.3309	343.2273	-	153.0920	-
PC O-16:0/22:6;7Ep	17.06	852.5754	792.5521	466.3305	343.2285	-	189.1652	-
PC O-18:1/22:6;19Ep	14.85	878.5912	818.5733	492.3435	343.2252	-	241.1969	-
PC O-18:1/22:6;16Ep	15.67	878.5914	818.5765	492.3474	343.2271	-	233.1552	-
PC O-18:1/22:6;13Ep	15.97	878.5917	818.5680	492.3454	343.2287	-	193.1239	-
PC O-18:1/22:6;10Ep	16.54	878.5919	818.5662	492.3477	343.2284	-	153.0919	-
			measured *m/z*				
analyte	**t_R [min]**	**precursor ion**	**molecular ion**	**neutral loss**	***sn*-2 (ox)FA**	***sn*-1 (ox)FA**	**α-cleavage**	**PE group**
PE 16:0/18:2;13OH	11.11	730.5024	730.5027	452.2787	295.2274	255.2333	195.1386	140.0120
PE 16:0/18:2;9OH	11.88	730.5023	730.5044	452.2766	295.2274	255.2334	171.1023	140.0118
PE 16:0/18:2;12Ep	13.90	730.5031	730.5031	452.2758	295.2274	255.2335	195.1388	140.0117
PE 16:0/18:2;9Ep	14.68	730.5032	730.5027	452.2776	295.2272	255.2328	171.1023	140.0118
PE 16:1_18:2;12Ep*	10.04	728.4875	n.d.	n.d.	295.2280	253.2166	195.1394	n.d.
PE 18:2;9Ep_16:1*	10.54	728.4882	n.d.	n.d.	253.2171	295.2285	171.1027	n.d.
PE 16:1_18:2;9Ep*	10.82	728.4882	n.d.	n.d.	295.2275	253.2175	171.1024	n.d.
PE 18:0/18:2;13OH	15.60	758.5336	758.5348	480.3105	295.2274	283.2640	195.1391	140.0117
PE 18:0/18:2;9OH	16.42	758.5333	758.5325	480.3067	295.2274	283.2635	171.1024	140.0115
PE 18:0/18:2;12Ep	18.56	758.5344	758.5289	480.3087	295.2278	283.2638	195.1393	140.0124
PE 18:0/18:2;9Ep	19.34	758.5343	758.5349	480.3069	295.2278	283.2636	171.1023	140.0116
PE 18:1/18:2;12Ep	14.38	756.5189	756.5193	478.2950	295.2274	281.2484	195.1386	140.0112
PE 18:1/18:2;9Ep	15.21	756.5187	756.5173	478.2918	295.2276	281.2481	171.1026	140.0116
PE 15-HETE/16:0	11.18	754.5040	754.5019	516.2704	255.2333	319.2283	219.1397	n.d.
PE 16:0/15-HETE	11.73	754.5040	754.5045	452.2782	319.2277	255.2330	219.1391	140.0112
PE 16:0/20:4;11OH	12.79	754.5026	754.5037	452.2775	319.2270	255.2332	167.1075	140.0111
PE 16:0/20:4;12OH	13.10	754.5020	754.5027	452.2787	319.2277	255.2332	179.1077	140.0110
PE 16:0/20:4;8OH	14.06	754.5031	754.4974	452.2746	319.2271	255.2336	155.0707	140.0111
PE 16:0/20:4;9OH	14.44	754.5029	754.5021	452.2762	319.2269	255.2327	167.0721	140.0115
PE 16:0/20:4;5OH*	16.01	754.5031	n.d.	452.2757	319.2271	255.2325	115.0396	n.d.

Table 8.10: Continued 11/14. List of detected oxPL in human serum and in oxylipin-supplemented HEK293T cells by untargeted LC-ESI(-)-HRMS in Full MS/ddMS^2 TOP *N* mode. n.d. = not detected.

		measured *m/z*						
analyte	**t_R [min]**	**precursor ion**	**molecular ion**	**neutral loss**	***sn*-2 (ox)FA**	***sn*-1 (ox)FA**	**α-cleavage**	**PE group**
PE 16:0/20:4;14Ep	14.12	754.5034	754.4970	452.2789	319.2275	255.2331	219.1395	140.0126
PE 16:0/20:4;11Ep	15.30	754.5006	754.5070	452.2793	319.2276	255.2320	179.1080	n.d.
PE 16:0/20:4;8Ep	16.14	754.5045	754.5052	452.2795	319.2276	255.2330	155.0715	140.0115
PE 16:0_20:4;5Ep*	17.24	754.5009	n.d.	n.d.	319.2285	255.2327	191.1805	n.d.
PE 16:0/20:5;17Ep*	11.31	752.4877	n.d.	452.2805	317.2119	255.2340	215.1811	140.0119
PE 16:0/20:5;14Ep*	12.18	752.4875	n.d.	452.2766	317.2143	255.2330	207.1392	n.d.
PE 16:0_20:5;11Ep*	12.57	752.4877	n.d.	n.d.	n.d.	255.2334	167.1071	n.d.
PE 16:0/20:5;8Ep	13.21	752.4877	752.4877	452.2765	317.2123	255.2339	155.0714	140.0119
PE 15-HETE/18:0	15.71	782.5357	782.5356	516.2745	283.2641	319.2277	n.d.	n.d.
PE 18:0/15-HETE	16.30	782.5353	782.5365	480.3101	319.2281	283.2646	219.1388	140.0114
PE 18:0/20:4;11OH	17.37	782.5341	782.5341	480.3113	319.2272	283.2637	167.1074	140.0120
PE 18:0/20:4;12OH	17.74	782.5333	782.5315	480.3090	319.2273	283.2637	179.1077	140.0114
PE 18:0/20:4;8OH	18.77	782.5337	782.5331	480.3060	319.227	283.263	155.0713	140.0119
PE 18:0/20:4;9OH	19.08	782.5344	782.539	480.3084	319.2274	283.2639	167.0712	140.0117
PE 18:0_20:4;5OH	20.70	782.5345	n.d.	n.d.	319.2262	283.2638	115.0395	n.d.
PE 18:0/20:4;14Ep	18.73	782.5356	782.5323	480.3078	319.2281	283.2639	219.14	140.0116
PE 18:0/20:4;11Ep	19.85	782.5351	782.5316	480.3117	319.2275	283.2637	179.108	140.0117
PE 18:0/20:4;8Ep	20.70	782.5350	782.5346	480.3097	319.2279	283.2646	155.0709	140.0118
PE 18:1_20:4;12OH*	13.71	780.5187	n.d.	n.d.	319.2278	281.2473	179.1075	n.d.
PE 18:1_20:4;5OH*	16.61	780.5186	n.d.	n.d.	319.2267	281.2477	115.0401	n.d.
PE 18:1/20:4;14Ep	14.57	780.5186	780.518	478.2913	319.2278	281.2483	219.1388	140.0124
PE 18:1/20:4;11Ep	15.74	780.5187	780.5136	478.2930	319.2274	281.2485	167.1076	140.0116
PE 18:1/20:4;8Ep	16.56	780.5186	780.5182	478.2950	319.2275	281.2484	155.0709	140.0113
PE 18:0/20:5;17Ep	15.90	780.5184	780.5238	480.3090	317.2119	283.2639	259.1707	140.0117
PE 18:0/20:5;14Ep	16.76	780.5180	780.5125	480.3091	317.2111	283.2645	207.1385	n.d.
PE 18:0_20:5;11Ep	17.19	780.5187	n.d.	n.d.	317.2106	283.2644	167.1077	n.d.
PE 18:0/20:5;8Ep	17.91	780.5181	780.5208	480.3073	317.2122	283.2642	155.0715	140.0119
PE 18:1/20:5;17Ep	11.84	778.5023	778.5013	478.2936	317.2121	281.2476	259.1711	140.0118
PE 18:1_20:5;14Ep*	12.66	778.5026	778.5052	n.d.	317.2137	281.2491	207.1391	140.0118
PE 18:1_20:5;11Ep*	13.08	778.5035	n.d.	n.d.	317.2124	281.2488	167.1070	n.d.

Table 8.10: Continued 12/14. List of detected oxPL in human serum and in oxylipin-supplemented HEK293T cells by untargeted LC-ESI(-)-HRMS in Full MS/ddMS^2 TOP *N* mode. n.d. = not detected.

		measured *m/z*					
analyte	**t_R [min]**	**precursor ion**	**molecular ion**	**neutral loss**	***sn*-2 (ox)FA**	***sn*-1 (ox)FA**	**α-cleavage**	**PE group**
PE 18:1/20:5;8Ep	13.75	778.5026	778.5034	478.2927	317.2117	281.2487	167.0713	140.0119
PE 16:0/22:6;20OH	10.74	778.5022	778.4993	452.2768	343.2276	255.2334	241.1961	140.0119
PE 16:0/22:6;16OH	11.17	778.5021	778.5056	452.2797	343.2278	255.2325	233.1548	140.0116
PE 17-HDHA/16:0	10.89	778.5040	778.5025	540.2756	255.2331	343.2282	201.1655	140.0112
PE 16:0/17-HDHA	11.30	778.5040	778.5053	452.2787	343.2278	255.2331	201.1650	140.0111
PE 16:0/22:6;13OH	11.73	778.5023	778.4984	452.2771	343.2267	255.2331	193.1236	140.0116
PE 16:0/22:6;14OH	11.97	778.5021	778.5060	452.2804	343.2274	255.2327	205.1235	140.0110
PE 16:0/22:6;10OH	12.57	778.5030	778.4964	452.2745	343.2267	255.2331	153.0923	n.d.
PE 16:0/22:6;11OH	12.88	778.5025	778.5043	452.2768	343.2287	255.2322	121.1026	140.0113
PE 16:0/22:6;7OH	13.86	778.5023	778.5039	452.2785	343.2268	255.2320	141.0544	140.0104
PE 16:0/22:6;8OH	13.99	778.5028	778.5056	452.2767	343.2263	255.2323	189.1637	140.0117
PE 16:0/22:6;19Ep	13.06	778.5029	778.5032	452.2758	343.2278	255.2330	241.1969	140.0115
PE 16:0/22:6;16Ep	13.83	778.5024	778.5042	452.2805	343.2277	255.2328	233.1549	140.0114
PE 16:0/22:6;13Ep	14.15	778.5035	778.5035	452.2816	343.2289	255.2329	193.1241	140.0114
PE 16:0/22:6;10Ep	14.71	778.5026	778.4951	452.2818	343.2278	255.2325	153.0922	140.0120
PE 16:0/22:6;8Ep*	15.51	778.5032	n.d.	452.2776	n.d.	255.2328	189.1648	n.d.
PE DH-17-HETE_18:0	18.39	810.5673	810.5677	n.d.	283.265	347.2589	247.1698	140.0117
PE 18:0/DH-17-HETE	18.78	810.5665	810.5662	480.3097	347.259	283.2645	247.1706	140.0113
PE 18:0/22:6;19Ep	17.66	806.5338	806.5334	480.3103	343.2278	283.2636	241.1955	140.0118
PE 18:0/22:6;16Ep	18.50	806.5336	806.5329	480.3067	343.2271	283.2634	233.1546	140.0124
PE 18:0_22:6;Ep	18.80	806.5338	806.5292	n.d.	343.2268	283.2633	n.d.	n.d.
PE 18:0/22:6;10Ep	19.30	806.5342	806.5282	480.3051	343.2271	283.2632	153.0921	n.d.
PE 18:1/22:6;19Ep	13.58	804.5194	n.d.	478.2954	343.2280	281.2498	241.1971	140.0118
PE 18:1/22:6;16Ep	14.36	804.5194	n.d.	478.2943	343.2284	281.2493	233.1547	n.d.
PE 18:1/22:6;13Ep	14.71	804.5196	n.d.	478.2928	343.2292	281.2491	193.1238	140.0119
PE 18:1/22:6;10Ep	15.21	804.5194	n.d.	478.2910	343.2269	281.2487	153.0917	140.0117
PE P-16:0/18:2;13OH	13.01	714.5081	714.5040	436.2836	295.2274	-	195.1392	140.0113
PE P-16:0/18:2;9OH	13.72	714.5084	714.5048	436.2808	295.2275	-	171.1027	140.0112
PE P-16:0/18:2;12Ep	15.98	714.5083	714.5110	436.2817	295.2276	-	195.1382	140.0119
PE P-16:0/18:2;9Ep	16.70	714.5084	714.5112	436.2856	295.2275	-	171.1021	140.0114

Table 8.10: Continued 13/14. List of detected oxPL in human serum and in oxylipin-supplemented HEK293T cells by untargeted LC-ESI(-)-HRMS in Full MS/ddMS^2 TOP *N* mode. n.d. = not detected.

		measured *m/z*						
analyte	**t_R [min]**	**precursor ion**	**molecular ion**	**neutral loss**	***sn*-2 (ox)FA**	***sn*-1 (ox)FA**	**α-cleavage**	**PE group**
PE P-18:1/18:2;12Ep	16.38	740.5239	n.d.	462.3028	295.2272	-	195.1391	n.d.
PE P-18:1/18:2;9Ep	17.13	740.5239	n.d.	462.2975	295.2281	-	171.1027	n.d.
PE P-16:0/20:3;11Ep	18.71	740.5244	n.d.	436.2851	321.2436	-	197.1184	n.d.
PE P-16:0/20:4;13OH	12.66	738.5082	738.5085	436.2834	319.2275	-	193.1235	n.d.
PE P-16:0/20:4;15OH	13.59	738.5079	738.5082	436.2819	319.2273	-	219.1385	140.0117
PE P-16:0/20:4;10OH	13.93	738.5080	738.5064	436.2841	319.2274	-	181.0869	140.0117
PE P-16:0/20:4;11OH	14.63	738.5079	738.5080	436.2828	319.2273	-	167.1074	140.0113
PE P-16:0/20:4;12OH	14.99	738.5081	738.5077	436.2823	319.2272	-	179.1075	140.0115
PE P-16:0/20:4;8OH	16.04	738.5083	738.5085	436.2837	319.2273	-	155.0711	140.0115
PE P-16:0/20:4;9OH	16.27	738.5091	738.5074	436.2828	319.2274	-	167.0717	140.0119
PE P-16:0/20:4;5OH	17.83	738.5075	738.5150	436.2836	319.2275	-	115.0401	n.d.
PE P-16:0/20:4;14Ep	16.04	738.5085	738.5087	436.2830	319.2277	-	219.1389	140.0116
PE P-16:0/20:4;11Ep	17.23	738.5083	738.5093	436.2826	319.2274	-	167.1075	140.0119
PE P-16:0/20:4;8Ep	18.00	738.5082	738.5086	436.2830	319.2278	-	155.0712	140.0117
PE P-16:0/20:5;17Ep	13.21	736.4922	736.4941	436.2831	317.2117	-	259.1697	140.0118
PE P-16:0/20:5;14Ep	14.08	736.4924	736.4887	436.2827	317.2120	-	207.1390	n.d.
PE P-16:0/20:5;11Ep	14.48	736.4927	736.4890	436.2840	317.2123	-	167.1073	n.d.
PE P-16:0/20:5;8Ep	15.14	736.4924	736.494	436.2833	317.2119	-	155.0718	140.0113
PE P-16:0/22:4;16Ep	19.03	766.5399	766.5349	436.2833	347.2589	-	247.1699	140.0111
PE P-16:0/22:4;13Ep	19.90	766.5397	766.5403	436.2838	347.2590	-	195.1389	140.0113
PE P-16:0/22:5;19Ep	16.27	764.5233	764.5234	436.2827	345.2422	-	287.2025	140.0120
PE P-16:0/22:5;16Ep	16.99	764.5244	764.5295	436.2814	345.2426	-	235.1702	140.0115
PE P-16:0/22:5;13Ep	17.16	764.5239	764.5217	436.2826	345.2430	-	207.1391	n.d.
PE P-16:0/22:5;10Ep	17.53	764.5238	764.5234	436.2837	345.2428	-	195.1026	140.0117
PE P-16:0/22:5;7Ep	17.91	764.5236	764.5219	436.2859	345.2426	-	143.0709	n.d.
PE P-18:0/20:5;17Ep	17.91	764.5236	764.5219	464.3118	317.2116	-	259.1689	n.d.
PE P-18:0/20:5;8Ep	19.81	764.5237	764.5231	464.3147	317.2114	-	155.0717	n.d.
PE P-16:0/22:6;20OH	12.50	762.5071	762.5069	436.2825	343.2274	-	241.1960	140.0120
PE P-16:0/22:6;16OH	12.94	762.5081	762.5073	436.2831	343.2274	-	233.1544	140.0118
PE P-16:0/22:6;17OH	13.13	762.5078	762.5100	436.2838	343.2267	-	201.1643	140.0116

Table 8.10: Continued 14/14. List of detected oxPL in human serum and in oxylipin-supplemented HEK293T cells by untargeted LC-ESI(-)-HRMS in Full MS/ddMS^2 TOP *N* mode. n.d. = not detected.

		measured *m/z*						
analyte	**t_R [min]**	**precursor ion**	**molecular ion**	**neutral loss**	***sn*-2 (ox)FA**	***sn*-1 (ox)FA**	**α-cleavage**	**PE group**
PE P-16:0/22:6;13OH	13.79	762.5080	762.5078	436.2829	343.2280	-	193.1234	140.0117
PE P-16:0/22:6;14OH	13.86	762.5082	762.5054	436.2832	343.2280	-	205.1234	140.0124
PE P-16:0/22:6;10OH	14.37	762.5088	n.d.	436.2816	343.2280	-	153.0918	140.0119
PE P-16:0/22:6;11OH	14.69	762.5078	762.5068	436.2810	343.2276	-	121.1021	n.d.
PE P-16:0/22:6;7OH	15.66	762.5082	762.5036	436.2832	343.2274	-	141.0557	140.0115
PE P-16:0/22:6;8OH	15.80	762.5081	762.5029	436.2829	343.2277	-	189.1648	140.0115
PE P-16:0/22:6;19Ep	14.95	762.5076	762.5071	436.2829	343.2274	-	241.1959	140.0115
PE P-16:0/22:6;16Ep	15.77	762.5077	762.5067	436.2838	343.2274	-	233.1539	140.0116
PE P-16:0/22:6;13Ep	16.09	762.5079	762.5091	436.2825	343.2278	-	193.1232	140.0115
PE P-16:0/22:6;10Ep	16.56	762.5075	762.5074	436.2833	343.2274	-	153.0919	140.0117
PE P-16:0/22:6;7Ep	17.43	762.5078	762.5040	436.2829	343.2277	-	189.1646	140.0117
PE P-18:1/20:5;17Ep	13.62	762.5077	762.5037	462.2975	317.2119	-	259.1706	n.d.
PE P-18:1/20:5;8Ep	15.50	762.5078	762.5050	462.2999	317.2116	-	155.0714	n.d.
PE P-18:1/22:4;16Ep	19.35	792.5565	n.d.	462.2986	347.2585	-	247.1716	n.d.
PE P-18:1/22:4;13Ep	20.25	792.5555	n.d.	462.2983	347.2593	-	195.1387	n.d.
PE P-18:0/22:6;19Ep	19.60	790.5395	790.5362	464.3143	343.2271	-	241.1963	140.0116
PE P-18:0/22:6;16Ep	20.43	790.5384	790.5377	464.3111	343.2278	-	233.1536	n.d.
PE P-18:0/22:6;13Ep	20.69	790.5391	790.5361	464.3129	343.2282	-	193.1239	n.d.
PE P-18:0/22:6;10Ep	21.20	790.5374	790.5374	464.3125	343.2263	-	153.0920	140.0116
PE P-18:1/22:6;19Ep	15.34	788.5244	n.d.	462.2988	343.2269	-	241.1963	140.0118
PE P-18:1/22:6;16Ep	16.16	788.5246	n.d.	462.2970	343.2279	-	233.1543	n.d.
PE P-18:1/22:6;13Ep	16.41	788.5241	n.d.	462.2968	343.2268	-	193.1240	140.0124
PE P-18:1/22:6;10Ep	16.96	788.5243	n.d.	462.2977	343.2284	-	153.0921	140.0118

Table 8.11: Comparison of ionization efficiency of oxPL and PL of the same lipid class. Three solutions containing the IS (i.e., PC 12:0/13:0, PE 12:0/13:0) and oxPL standards at the same concentration level (i.e., 50 nmol L^{-1}, 125 nmol L^{-1}, or 500 nmol L^{-1}) were measured by untargeted LC-ESI(-)-HRMS in Full MS/ddMS^2 mode. Differences in ionization efficiency were calculated as the ratio of the peak height of oxPL to the peak height of PL. This indicates only a minor effect of the oxylipin on ionization efficiency, with signal differences of less than 26%.

	concentration [nmol L^{-1}]	50	125	500	mean
	analyte	**ionization efficiency difference**			
$\frac{Area_{oxPC}}{Area_{PC\ 12:0/13:0}}$	PC 16:0/17(18)-EpETE	0.84	0.74	0.94	0.84
	PC 16:0/17-HDHA	1.0	0.98	1.1	1.1
	PC 16:0/15-HETE	1.1	1.03	1.23	1.1
	PC 18:0/15-HEPE	0.97	1.02	1.02	1.0
	PC 18:0/17-HDHA	0.88	0.75	0.94	0.86
	PC 18:0/15-HETE	1.3	1.2	1.2	1.2
$\frac{Area_{oxPE}}{Area_{PE\ 12:0/13:0}}$	PE 16:0/17-HDHA	0.97	1.2	1.07	1.07
	PE 16:0/15-HETE	0.86	1.0	0.94	0.94
	PE 18:0/15-HETE	1.2	1.3	1.3	1.3

Table 8.12: Comparison of retention time differences of analogue oxPL classes/species. oxPL were detected by untargeted RP-LC-ESI(-)-HRMS in human serum and oxylipin-supplemented cells. Precursor ion and product ions of each oxPL can be found in Table 8.10.

oxPC *vs.* oxPC-O					
Δt_R = 2.44 ± 0.10 (4.1%)					
lipid species	**t_R [min]**	**Δt_R**	**lipid species**	**t_R [min]**	**Δt_R**
PC 16:0/18:2;13OH	10.19	2.41	PC 16:0/20:5;14Ep	11.13	2.46
PC O-16:0/18:2;13OH	12.60		PC O-16:0/20:5;14Ep	13.59	
PC 16:0/18:2;12Ep	12.89	2.55	PC 16:0/20:5;11Ep	11.55	2.48
PC O-16:0/18:2;12Ep	15.44		PC O-16:0/20:5;11Ep	14.03	
PC 16:0/18:2;9Ep	13.67	2.57	PC 16:0/20:5;8Ep	12.26	2.50
PC O-16:0/18:2;9Ep	16.24		PC O-16:0/20:5;8Ep	14.76	
PC 18:1/18:2;12Ep	13.42	2.33	PC 18:1/20:5;17Ep	10.80	2.28
PC O-18:1/18:2;12Ep	15.75		PC O-18:1/20:5;17Ep	13.08	
PC 18:1/18:2;9Ep	14.21	2.39	PC 18:1/20:5;14Ep	11.64	2.33
PC O-18:1/18:2;9Ep	16.60		PC O-18:1/20:5;14Ep*	13.97	
PC 16:0/20:4;13OH	9.95	2.42	PC 18:1/20:5;8Ep	12.79	2.32
PC O-16:0/20:4;13OH	12.37		PC O-18:1/20:5;8Ep	15.11	
PC 16:0/20:4;15OH	10.77	2.45	PC 16:0/22:6;19Ep	12.05	2.44
PC O-16:0/20:4;15OH	13.22		PC O-16:0/22:6;19Ep	14.49	
PC 16:0/20:4;11OH	11.79	2.48	PC 16:0/22:6;16Ep	12.78	2.53
PC O-16:0/20:4;11OH	14.27		PC O-16:0/22:6;16Ep	15.31	
PC 16:0/20:4;12OH	12.12	2.51	PC 16:0/22:6;13Ep	13.15	2.49
PC O-16:0/20:4;12OH	14.63		PC O-16:0/22:6;13Ep	15.64	
PC 16:0/20:4;8OH	13.13	2.57	PC 16:0/22:6;10Ep	13.68	2.48
PC O-16:0/20:4;8OH	15.70		PC O-16:0/22:6;10Ep	16.16	
PC 16:0/20:4;9OH	13.49	2.48	PC 16:0/22:6;7Ep	14.55	2.51
PC O-16:0/20:4;9OH	15.97		PC O-16:0/22:6;7Ep	17.06	
PC 16:0/20:4;5OH	14.99	2.60	PC 18:1/22:6;19Ep	12.54	2.31
PC O-16:0/20:4;5OH	17.59		PC O-18:1/22:6;19Ep	14.85	
PC 16:0/20:4;14Ep	13.10	2.48	PC 18:1/22:6;16Ep	13.35	2.32
PC O-16:0/20:4;14Ep	15.58		PC O-18:1/22:6;16Ep	15.67	
PC 16:0/20:4;11Ep	14.25	2.51	PC 18:1/22:6;13Ep	13.74	2.23
PC O-16:0/20:4;11Ep	16.76		PC O-18:1/22:6;13Ep	15.97	
PC 16:0/20:4;8Ep	15.00	2.59	PC 18:1/22:6;10Ep	14.24	2.30
PC O-16:0/20:4;8Ep	17.59		PC O-18:1/22:6;10Ep	16.54	
PC 16:0/20:5;17Ep	10.36	2.36			
PC O-16:0/20:5;17Ep	12.72				

Table 8.12: Continued 1/5. Comparison of retention time differences of analogue oxPL classes/species.

oxPC *vs.* oxPC-P Δt_R = 1.76 ± 0.07 (4.0%)			oxPE *vs.* oxPE-P Δt_R = 1.90 ± 0.09 (4.8%)		
lipid species	**t_R [min]**	**Δt_R**	**lipid species**	**t_R [min]**	**Δt_R**
PC 16:0/18:2;13OH	10.19	1.69	PE 16:0/18:2;13OH	11.11	1.90
PC P-16:0/18:2;13OH	11.88		PE P-16:0/18:2;13OH	13.01	
PC 16:0/18:2;9OH	10.91	1.69	PE 16:0/18:2;12Ep	13.90	2.08
PC P-16:0/18:2;9OH	12.60		PE P-16:0/18:2;12Ep	15.98	
PC 16:0/18:2;12Ep	12.89	1.82	PE 16:0/20:4;15OH	11.73	1.86
PC P-16:0/18:2;12Ep	14.71		PE P-16:0/20:4;15OH	13.59	
PC 16:0/18:2;9Ep	13.67	1.85	PE 16:0/20:4;14Ep	14.12	1.92
PC P-16:0/18:2;9Ep	15.52		PE P-16:0/20:4;14Ep	16.04	
PC 16:0/20:4;13OH	9.95	1.60	PE 16:0/20:5;17Ep*	11.31	1.90
PC P-16:0/20:4;13OH	11.55		PE P-16:0/20:5;17Ep	13.21	
PC 16:0/20:4;15OH	10.77	1.70	PE 16:0/20:5;8Ep	13.21	1.93
PC P-16:0/20:4;15OH	12.47		PE P-16:0/20:5;8Ep	15.14	
PC 16:0/20:4;11OH	11.79	1.73	PE 16:0/22:6;19Ep	13.06	1.89
PC P-16:0/20:4;11OH	13.52		PE P-16:0/22:6;19Ep	14.95	
PC 16:0/20:4;12OH	12.12	1.74	PE 16:0/22:6;10Ep	14.71	1.85
PC P-16:0/20:4;12OH	13.86		PE P-16:0/22:6;10Ep	16.56	
PC 16:0/20:4;7OH	12.81	1.88	PE 18:1/18:2;12Ep	14.38	2.00
PC P-16:0/20:4;7OH	14.69		PE P-18:1/18:2;12Ep	16.38	
PC 16:0/20:4;8OH	13.13	1.86	PE 18:0/20:5;17Ep	15.90	2.01
PC P-16:0/20:4;8OH	14.99		PE P-18:0/20:5;17Ep	17.91	
PC 16:0/20:4;9OH	13.49	1.70	PE 18:1/20:5;17Ep	11.84	1.78
PC P-16:0/20:4;9OH	15.19		PE P-18:1/20:5;17Ep	13.62	
PC 16:0/20:4;5OH	14.99	1.82	PE 18:0/22:6;19Ep	17.66	1.94
PC P-16:0/20:4;5OH	16.81		PE P-18:0/22:6;19Ep	19.60	
PC 16:0/20:4;14Ep	13.10	1.76	PE 18:0/22:6;10Ep	19.30	1.90
PC P-16:0/20:4;14Ep	14.86		PE P-18:0/22:6;10Ep	21.20	
PC 16:0/20:4;11Ep	14.25	1.79	PE 18:1/22:6;19Ep	13.58	1.76
PC P-16:0/20:4;11Ep	16.04		PE P-18:1/22:6;19Ep	15.34	
PC 16:0/20:4;8Ep	15.00	1.83	PE 18:1/22:6;10Ep	15.21	1.75
PC P-16:0/20:4;8Ep	16.83		PE P-18:1/22:6;10Ep	16.96	
PC 16:0/20:5;17Ep	10.36	1.69			
PC P-16:0/20:5;17Ep	12.05				
PC 16:0/20:5;14Ep	11.13	1.76			
PC P-16:0/20:5;14Ep*	12.89				
PC 16:0/20:5;8Ep	12.26	1.74			
PC P-16:0/20:5;8Ep	14.00				
PC 16:0/22:6;19Ep	12.05	1.72			
PC P-16:0/22:6;19Ep	13.77				
PC 16:0/22:6;16Ep	12.78	1.78			
PC P-16:0/22:6;16Ep*	14.56				
PC 16:0/22:6;10Ep	13.68	1.73			
PC P-16:0/22:6;10Ep*	15.41				

Table 8.12: Continued 2/5. Comparison of retention time differences of analogue oxPL classes/species.

oxPC bearing 16:0 *vs.* 18:0 at the *sn*-1 position Δt_R = 4.57 ± 0.09 (2.0%)					
lipid species	**t_R [min]**	**Δt_R**	**lipid species**	**t_R [min]**	**Δt_R**
PC 16:0/18:2;13OH	10.19	4.41	PC 16:0/22:6;20OH	9.86	4.38
PC 18:0/18:2;13OH	14.60		PC 18:0/22:6;20OH	14.24	
PC 16:0/18:2;9OH	10.91	4.54	PC 16:0/22:6;16OH	10.28	4.41
PC 18:0/18:2;9OH	15.45		PC 18:0/22:6;16OH	14.69	
PC 16:0/18:2;12Ep	12.89	4.61	PC 16:0/22:6;17OH	10.41	4.45
PC 18:0/18:2;12Ep	17.50		PC 18:0/22:6;17OH	14.86	
PC 16:0/18:2;9Ep	13.67	4.64	PC 16:0/22:6;13OH	10.83	4.49
PC 18:0/18:2;9Ep	18.31		PC 18:0/22:6;13OH	15.32	
PC 16:0/20:4;13OH	9.95	4.42	PC 16:0/22:6;14OH	11.08	4.52
PC 18:0/20:4;13OH	14.37		PC 18:0/22:6;14OH	15.60	
PC 16:0/20:4;15OH	10.77	4.52	PC 16:0/22:6;10OH	11.64	4.54
PC 18:0/20:4;15OH	15.29		PC 18:0/22:6;10OH	16.18	
PC 16:0/20:4;11OH	11.79	4.61	PC 16:0/22:6;11OH	11.91	4.58
PC 18:0/20:4;11OH	16.40		PC 18:0/22:6;11OH	16.49	
PC 16:0/20:4;12OH	12.12	4.59	PC 16:0/22:6;7OH	12.94	4.65
PC 18:0/20:4;12OH	16.71		PC 18:0/22:6;7OH	17.59	
PC 16:0/20:4;7OH	12.81	4.71	PC 16:0/22:6;8OH	13.13	4.61
PC 18:0/20:4;7OH	17.52		PC 18:0/22:6;8OH	17.74	
PC 16:0/20:4;8OH	13.13	4.67	PC 16:0/22:6;19Ep	12.05	4.54
PC 18:0/20:4;8OH	17.80		PC 18:0/22:6;19Ep	16.59	
PC 16:0/20:4;9OH	13.49	4.62	PC 16:0/22:6;16Ep	12.78	4.68
PC 18:0/20:4;9OH	18.11		PC 18:0/22:6;16Ep	17.46	
PC 16:0/20:4;5OH	14.99	4.67	PC 16:0/22:6;10Ep	13.68	4.62
PC 18:0/20:4;5OH	19.66		PC 18:0/22:6;10Ep	18.30	
PC 16:0/20:4;14Ep	13.10	4.56	PC 16:0/22:6;7Ep	14.55	4.62
PC 18:0/20:4;14Ep	17.66		PC 18:0/22:6;7Ep	19.17	
PC 16:0/20:4;11Ep	14.25	4.61	PC 16:0/22:4;17OH	13.19	4.54
PC 18:0/20:4;11Ep	18.86		PC 18:0/22:4;17OH	17.73	
PC 16:0/20:4;8Ep	15.00	4.72			
PC 18:0/20:4;8Ep	19.72				

Table 8.12: Continued 3/5. Comparison of retention time differences of analogue oxPL classes/species.

oxPL bearing 16:0 *vs.* 18:0 at the *sn*-1 position					
oxPE			**oxPI**		
Δt_R = 4.61 ± 0.06 (1.3%)			**Δt_R = 4.05 ± 0.35 (8.7%)**		
lipid species	**t_R [min]**	**Δt_R**	**lipid species**	**t_R [min]**	**Δt_R**
PE 16:0/18:2;13OH	11.11	4.49	PI 16:0/18:2;13OH	7.65	3.42
PE 18:0/18:2;13OH	15.60		PI 18:0/18:2;13OH	11.07	
PE 16:0/18:2;9OH	11.88	4.54	PI 16:0/18:2;9OH	8.16	3.74
PE 18:0/18:2;9OH	16.42		PI 18:0/18:2;9OH	11.90	
PE 16:0/18:2;12Ep	13.90	4.66	PI 16:0/18:2;12Ep	9.49	4.09
PE 18:0/18:2;12Ep	18.56		PI 18:0/18:2;12Ep	13.58	
PE 16:0/18:2;9Ep	14.68	4.66	PI 16:0/18:2;9Ep	10.15	4.23
PE 18:0/18:2;9Ep	19.34		PI 18:0/18:2;9Ep	14.38	
PE 16:0/20:4;15OH	11.73	4.57	PI 16:0/20:4;15OH	7.99	3.59
PE 18:0/20:4;15OH	16.30		PI 18:0/20:4;15OH	11.58	
PE 16:0/20:4;11OH	12.79	4.58	PI 16:0/20:4;11OH	8.73	3.93
PE 18:0/20:4;11OH	17.37		PI 18:0/20:4;11OH	12.66	
PE 16:0/20:4;12OH	13.10	4.64	PI 16:0/20:4;12OH	8.89	4.05
PE 18:0/20:4;12OH	17.74		PI 18:0/20:4;12OH	12.94	
PE 16:0/20:4;8OH	14.06	4.71	PI 16:0/20:4;8OH	9.77	4.33
PE 18:0/20:4;8OH	18.77		PI 18:0/20:4;8OH	14.10	
PE 16:0/20:4;9OH	14.44	4.64	PI 16:0/20:4;9OH	10.04	4.33
PE 18:0/20:4;9OH	19.08		PI 18:0/20:4;9OH	14.37	
PE 16:0/20:4;5OH*	16.01	4.69	PI 16:0/20:4;5OH	11.49	4.48
PE 18:0/20:4;5OH	20.70		PI 18:0/20:4;5OH	15.97	
PE 16:0/20:4;14Ep	14.12	4.61	PI 16:0/20:4;14Ep	9.52	4.23
PE 18:0/20:4;14Ep	18.73		PI 18:0/20:4;14Ep	13.75	
PE 16:0/20:4;11Ep	15.30	4.55	PI 16:0/20:4;11Ep	10.53	4.37
PE 18:0/20:4;11Ep	19.85		PI 18:0/20:4;11Ep	14.90	
PE 16:0/20:4;8Ep	16.14	4.56	PI 16:0/20:4;8Ep	11.31	4.46
PE 18:0/20:4;8Ep	20.70		PI 18:0/20:4;8Ep	15.77	
PE 16:0/20:5;17Ep*	11.31	4.59	PI 16:0/20:5;17Ep	7.67	3.48
PE 18:0/20:5;17Ep	15.90		PI 18:0/20:5;17Ep	11.15	
PE 16:0/20:5;14Ep*	12.18	4.58	PI 16:0/20:5;14Ep	8.19	3.77
PE 18:0/20:5;14Ep	16.76		PI 18:0/20:5;14Ep	11.96	
PE 16:0_20:5;11Ep*	12.57	4.62	PI 16:0/22:6;10Ep*	10.24	4.25
PE 18:0_20:5;11Ep	17.19		PI 18:0/22:6;10Ep*	14.49	
PE 16:0/20:5;8Ep	13.21	4.70			
PE 18:0/20:5;8Ep	17.91				
PE 16:0/22:6;19Ep	13.06	4.60			
PE 18:0/22:6;19Ep	17.66				
PE 16:0/22:6;16Ep	13.83	4.67			
PE 18:0/22:6;16Ep	18.50				
PE 16:0/22:6;10Ep	14.71	4.59			
PE 18:0/22:6;10Ep	19.30				

Table 8.12: Continued 4/5. Comparison of retention time differences of analogue oxPL classes/species.

oxPL bearing 16:0 *vs.* 18:1 at the *sn*-1 position

oxPI

Δt_R = 0.42 ± 0.09 (21%)

lipid species	t_R [min]	Δt_R
PI 16:0/18:2;12Ep	9.49	0.40
PI 18:1/18:2;12Ep*	9.89	
PI 16:0/18:2;9Ep	10.15	0.58
PI 18:1/18:2;9Ep*	10.73	
PI 16:0/20:4;15OH	7.99	0.45
PI 18:1/20:4;15OH	8.44	
PI 16:0/20:4;14Ep	9.52	0.39
PI 18:1/20:4;14Ep	9.91	
PI 16:0/20:4;11Ep	10.53	0.41
PI 18:1/20:4;11Ep	10.94	
PI 16:0/20:4;8Ep	11.31	0.52
PI 18:1/20:4;8Ep	11.83	
PI 16:0/20:5;17Ep	7.75	0.28
PI 18:1/20:5;17Ep	8.03	
PI 16:0/20:5;14Ep	8.27	0.35
PI 18:1/20:5;14Ep	8.62	
PI 16:0/22:6;10Ep*	10.24	0.44
PI 18:1/22:6;10Ep*	10.68	

oxPC-O

Δt_R = 0.35 ± 0.02 (6.6%)

lipid species	t_R [min]	Δt_R
PC O-16:0/18:2;12Ep	15.44	0.31
PC O-18:1/18:2;12Ep	15.75	
PC O-16:0/20:4;14Ep	15.58	0.36
PC O-18:1/20:4;14Ep	15.94	
PC O-16:0/20:5;17Ep	12.72	0.36
PC O-18:1/20:5;17Ep	13.08	
PC O-16:0/20:5;8Ep	14.76	0.35
PC O-18:1/20:5;8Ep	15.11	
PC O-16:0/22:6;19Ep	14.49	0.36
PC O-18:1/22:6;19Ep	14.85	
PC O-16:0/22:6;10Ep	16.16	0.38
PC O-18:1/22:6;10Ep	16.54	

oxPC

Δt_R = 0.50 ± 0.06 (13%)

lipid species	t_R [min]	Δt_R
PC 16:0/18:2;12Ep	12.89	0.53
PC 18:1/18:2;12Ep	13.42	
PC 16:0/18:2;9Ep	13.67	0.54
PC 18:1/18:2;9Ep	14.21	
PC 16:0/20:4;12OH	12.12	0.34
PC 18:1/20:4;12OH	12.46	
PC 16:0/20:4;5OH	14.99	0.45
PC 18:1/20:4;5OH	15.44	
PC 16:0/20:4;14Ep	13.10	0.45
PC 18:1/20:4;14Ep	13.55	
PC 16:0/20:4;11Ep	14.25	0.45
PC 18:1/20:4;11Ep	14.70	
PC 16:0/20:4;8Ep	15.00	0.54
PC 18:1/20:4;8Ep	15.54	
PC 16:0/20:5;17Ep	10.36	0.44
PC 18:1/20:5;17Ep	10.80	
PC 16:0/20:5;14Ep	11.13	0.51
PC 18:1/20:5;14Ep	11.64	
PC 16:0/20:5;8Ep	12.26	0.53
PC 18:1/20:5;8Ep	12.79	
PC 16:0/22:6;19Ep	12.05	0.49
PC 18:1/22:6;19Ep	12.54	
PC 16:0/22:6;16Ep	12.78	0.57
PC 18:1/22:6;16Ep	13.35	
PC 16:0/22:6;13Ep	13.15	0.59
PC 18:1/22:6;13Ep	13.74	
PC 16:0/22:6;10Ep	13.68	0.56
PC 18:1/22:6;10Ep	14.24	
PC 16:0/22:6;7Ep	14.55	0.51
PC 18:1/22:6;7Ep	15.06	

Table 8.12: Continued 5/5. Comparison of retention time differences of analogue oxPL classes/species.

oxPL bearing 16:0 *vs.* 18:1 at the *sn*-1 position

oxPE

Δt_R = 0.51 ± 0.05 (11%)

lipid species	t_R [min]	Δt_R
PE 16:0/18:2;12Ep	13.90	0.48
PE 18:1/18:2;12Ep	14.38	
PE 16:0/18:2;9Ep	14.68	0.53
PE 18:1/18:2;9Ep	15.21	
PE 16:0/20:4;12OH	13.10	0.61
PE 18:1/20:4;12OH*	13.71	
PE 16:0/20:4;5OH*	16.01	0.60
PE 18:1/20:4;5OH*	16.61	
PE 16:0/20:4;14Ep	14.12	0.45
PE 18:1/20:4;14Ep	14.57	
PE 16:0/20:4;11Ep	15.30	0.44
PE 18:1/20:4;11Ep	15.74	
PE 16:0/20:4;8Ep	16.14	0.42
PE 18:1/20:4;8Ep	16.56	
PE 16:0/20:5;17Ep*	11.31	0.53
PE 18:1/20:5;17Ep	11.84	
PE 16:0/20:5;14Ep*	12.18	0.48
PE 18:1/20:5;14Ep*	12.66	
PE 16:0/20:5;11Ep*	12.57	0.51
PE 18:1/20:5;11Ep*	13.08	
PE 16:0/20:5;8Ep	13.21	0.54
PE 18:1/20:5;8Ep	13.75	
PE 16:0/22:6;19Ep	13.06	0.52
PE 18:1/22:6;19Ep	13.58	
PE 16:0/22:6;16Ep	13.83	0.53
PE 18:1/22:6;16Ep	14.36	
PE 16:0/22:6;10Ep	14.71	0.50
PE 18:1/22:6;10Ep	15.21	

oxPE bearing 16:0 *vs.* 18:1

Δt_R = 4.37 ± 0.04 (0.8%)

lipid species	t_R [min]	Δt_R
PE 16:1/18:2;12Ep	10.04	4.34
PE 18:1/18:2;12Ep	14.38	
PE 16:1/18:2;9Ep	10.82	4.39
PE 18:1/18:2;9Ep	15.21	

oxPE-P

Δt_R = 0.40 ± 0.06 (16%)

lipid species	t_R [min]	Δt_R
PE P-16:0/18:2;12Ep	15.98	0.40
PE P-18:1/18:2;12Ep	16.38	
PE P-16:0/18:2;9Ep	16.70	0.43
PE P-18:1/18:2;9Ep	17.13	
PE P-16:0/20:5;17Ep	13.21	0.41
PE P-18:1/20:5;17Ep	13.62	
PE P-16:0/20:5;8Ep	15.14	0.36
PE P-18:1/20:5;8Ep	15.50	
PE P-16:0/22:4;16Ep	19.03	0.32
PE P-18:1/22:4;16Ep	19.35	
PE P-18:1/22:4;16Ep	19.35	0.55
PE P-16:0/22:4;13Ep	19.90	
PE P-16:0/22:6;19Ep	14.95	0.39
PE P-18:1/22:6;19Ep	15.34	
PE P-16:0/22:6;16Ep	15.77	0.39
PE P-18:1/22:6;16Ep	16.16	
PE P-16:0/22:6;13Ep	16.09	0.32
PE P-18:1/22:6;13Ep	16.41	
PE P-16:0/22:6;10Ep	16.56	0.40
PE P-18:1/22:6;10Ep	16.96	

oxPC bearing 16:0 *vs.* 18:1

Δt_R = 4.22 ± 0.14 (3.3%)

lipid species	t_R [min]	Δt_R
PC 16:1/18:2;12Ep	9.32	4.10
PC 18:1/18:2;12Ep	13.42	
PC 16:1/18:2;9Ep	9.95	4.26
PC 18:1/18:2;9Ep	14.21	
PC 16:1/20:4;14Ep	9.43	4.12
PC 18:1/20:4;14Ep	13.55	
PC 16:1/20:4;8Ep	11.14	4.40
PC 18:1/20:4;8Ep	15.54	

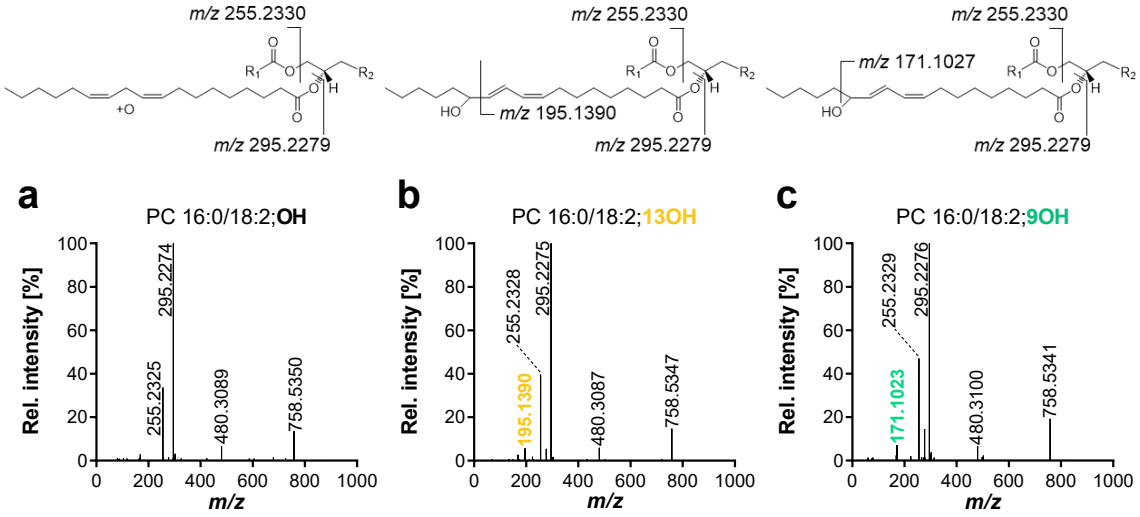

Fig. 8.10: Fragmentation spectra of PC bearing hydroxy-18:2 positional isomers. Shown are the MS^2 spectra in ESI(-) mode of PC species from human serum bearing 16:0 and 18:2;OH positional isomers recorded at **a** 8.70 min, **b** 10.2 min, and **c** 10.9 min. In the structures, suggested sites of fragmentation are indicated. R_1 = $C_{15}H_{31}$ and R_2 = $C_5H_{13}NPO_4$. Lipid extracts were analyzed by untargeted LC-HRMS operating in Full MS/ddMS^2 TOP *N* mode (orbitrap Q Exactive HF).

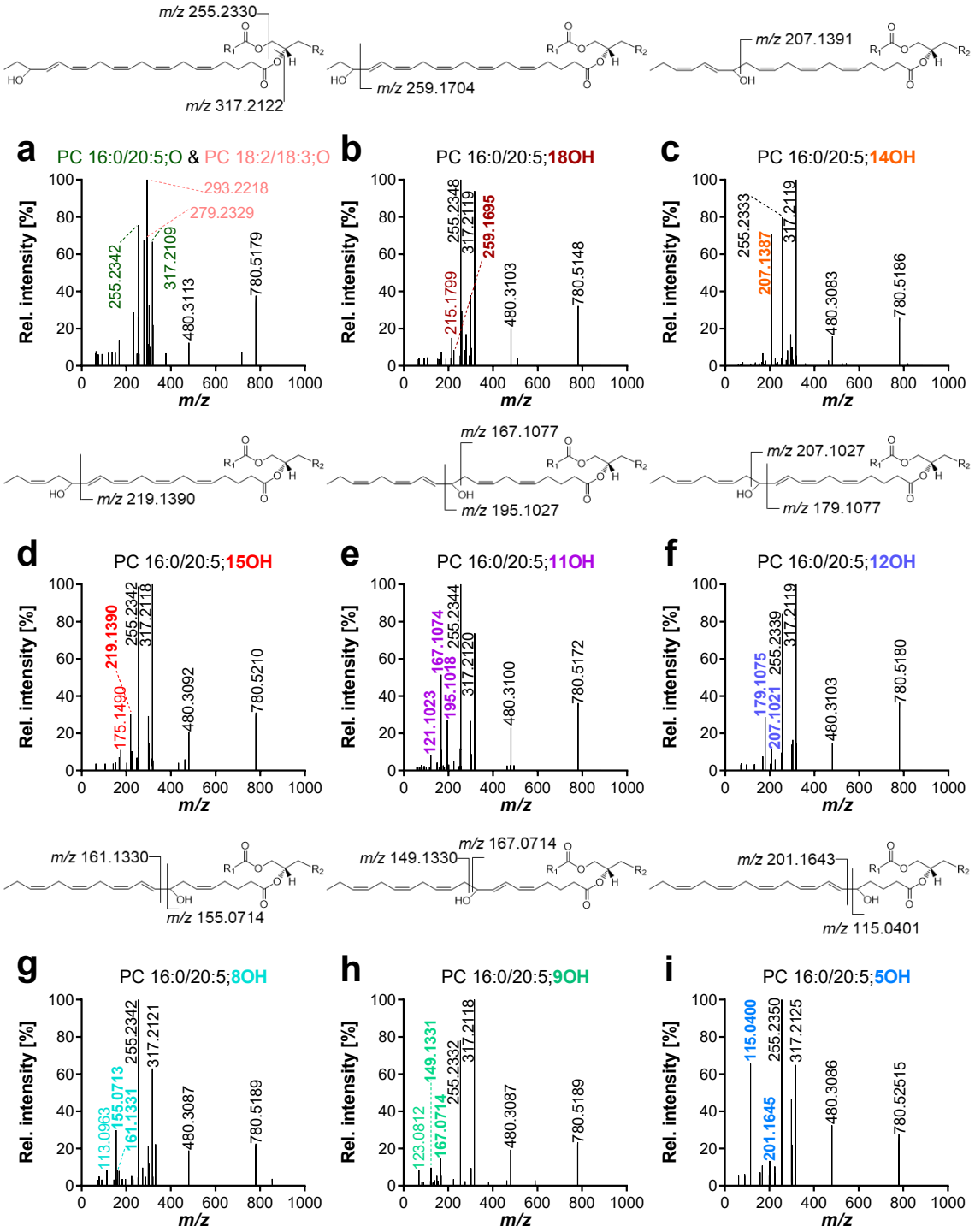

Fig. 8.11: Fragmentation spectra of PC bearing hydroxy-20:5 positional isomers. Shown are the MS^2 spectra in ESI(-) mode of PC species from human serum bearing 16:0 and 20:5;OH positional isomers recorded at **a** 8.19 min, **b** 8.61 min, **c** 8.95 min, **d** 9.19 min, **e** 9.63 min, **f** 9.89 min, **g** 10.6 min, **h** 10.8 min, and **i** 12.2 min. In the structures, suggested sites of fragmentation are indicated. R_1 = $C_{15}H_{31}$ and R_2 = $C_5H_{13}NPO_4$. Lipid extracts were analyzed by untargeted LC-HRMS operating in Full MS/ddMS^2 TOP *N* mode (orbitrap Q Exactive HF).

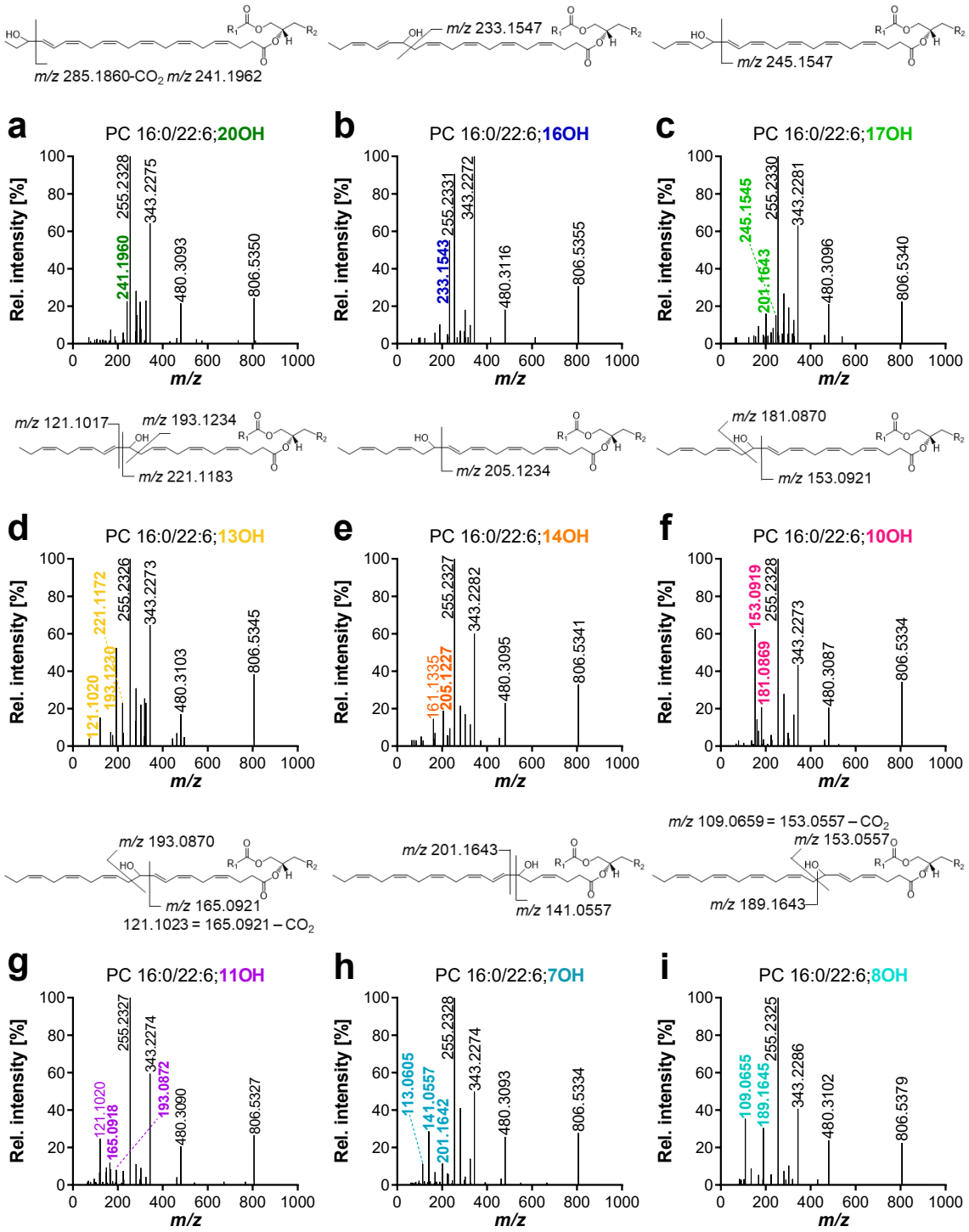

Fig. 8.12: Fragmentation spectra of PC bearing hydroxy-22:6 positional isomers. Shown are the MS^2 spectra in ESI(-) mode of PC species from human serum bearing 16:0 and 22:6;OH positional isomers recorded at **a** 9.85 min, **b** 10.3 min, **c** 10.4 min, **d** 10.8 min, **e** 11.1 min, **f** 11.7 min, **g** 12.0 min, **h** 12.9 min, and **i** 13.1 min. In the structures, suggested sites of fragmentation are indicated. R_1 = $C_{15}H_{31}$ and R_2 = $C_5H_{13}NPO_4$. Lipid extracts were analyzed by untargeted LC-HRMS operating in Full MS/ddMS^2 TOP *N* mode (orbitrap Q Exactive HF).

Table 8.13: Comparison of the elution order of oxPL. The retention times of those oxPL described in a previous study [5] are compared with the retention times determined with the presented method. Separation was carried out on an ACQUITY Premier CSH C18 column using as eluents A (H_2O/ACN, 60/40, v/v) and B (IPA/ACN, 80/20, v/v + 1% H_2O), both containing 10 mmol L^{-1} ammonium formate and 0.1% formic acid. In the previous study, lipids were separated on an ACQUITY BEH peptide C18 column using as eluents A (MeOH/ACN/H_2O, 1/1/3, v/v/v) with 5 mmol L^{-1} ammonium acetate and B 100% IPA with 5 mmol L^{-1} ammonium acetate and 10 nmol L^{-1} EDTA.

this article		**[5]**	
Untargeted RP-LC-HRMS		**Targeted RP-LC-MS/MS**	
structure defined level	**t_R [min]**	**structure defined level**	**t_R [min]**
PI 16:0/18:2;13OH	7.7	PI 16:0/13-HODE	7.2
PI 16:0/18:2;9OH	8.2	PI 16:0/9-HODE	7.4
PI 18:0/18:2;9OH	11.9	PI 18:0/9-HODE	8.4
PC 14:0/20:4;14Ep	9.0	PC 14:0/14(15)-EpETrE	7.7
PC 14:0/20:4;11Ep	9.9	PC 14:0/11(12)-EpETrE	7.9
PC 14:0/20:4;8Ep	10.6	PC 14:0/8(9)-EpETrE	8.1
PI 16:0/20:4;15OH	8.0	PI 16:0/15-HETE	7.5
PI 16:0/20:4;12OH	8.9	PI 16:0/12-HETE	7.8
PI 16:0/20:4;11Ep	10.5	PI 16:0/11(12)-EpETrE	8.3
PI 16:0/20:4;8Ep	11.3	PI 16:0/8(9)-EpETrE	8.5
PI 18:0/20:4;15OH	11.6	PI 18:0/15-HETE	8.5
PI 18:0/20:4;12OH	12.9	PI 18:0/12-HETE	8.8
PI 18:0/20:4;14Ep	13.8	PI 18:0/14(15)-EpETrE	9.2
PI 18:0/20:4;8Ep	15.8	PI 18:0/8(9)-EpETrE	9.7
PI 18:0/20:5;17Ep	11.2	PI 18:0/17(18)-EpETE	8.5
PI 18:0/20:5;14Ep	12.0	PI 18:0/14(15)-EpETE	8.7
PI 18:0/20:5;11Ep	12.4	PI 18:0/11(12)-EpETE	8.8
PI 18:1/20:5;17Ep	8.0	PI 18:1/17(18)-EpETE	7.6
PI 18:1/20:5;14Ep	8.5	PI 18:1/14(15)-EpETE	7.8
PI 18:1/20:5;11Ep	8.9	PI 18:1/11(12)-EpETE	7.9
PI 18:1/20:5;8Ep	9.4	PI 18:1/8(9)-EpETE	8.1
PI 18:0/22:6;16Ep	13.6	PI 18:0/16(17)-EpETE	9.2
PC 16:0/18:2;13OH	10.2	PC 16:0/13-HODE	7.9
PC 14:0_20:4;14Ep	9.0	PC 14:0_14(15)-EpETrE	7.7
PC 14:0_20:4;11Ep	9.9	PC 14:0_11(12)-EpETrE	7.9
PC 18:0/18:2;9OH	15.5	PC 18:0/9-HODE	9.2
PC 16:0/20:4;15OH	10.8	PC 16:0/15-HETE	8.2
PC 16:0/20:4;12OH	12.1	PC 16:0/12-HETE	8.5
PC 16:0/20:4;8OH	13.1	PC 16:0/8-HETE	8.7
PC 16:0/20:4;5OH	15.0	PC 16:0/5-HETE	9.2
PC 16:0/20:4;14Ep	13.1	PC 16:0/14(15)-EpETrE	8.8
PC 16:1/20:4;14Ep	9.4	PC 16:1/14(15)-EpETrE	7.9
PC 16:1/20:4;8Ep	11.1	PC 16:1/8(9)-EpETrE	8.4
PC 16:0/20:5;15OH	9.1	PC 16:0/15-HEPE	7.5
PC 16:0/20:5;8OH	10.5	PC 16:0/8-HEPE	8.1
PC 16:0/20:5;5OH	12.2	PC 16:0/5-HEPE	8.6
PC 16:0/20:5;17Ep	10.4	PC 16:0/17(18)-EpETE	8.1
PC 16:0/20:5;14Ep	11.1	PC 16:0/14(15)-EpETE	8.3
PC 16:0/20:5;11Ep	11.6	PC 16:0/11(12)-EpETE	8.4
PC 16:0/20:5;8Ep	12.3	PC 16:0/8(9)-EpETE	8.6

Table 8.13: Continued. Comparison of the elution order of oxPL.

this article		[5]	
Untargeted RP-LC-HRMS		Targeted RP-LC-MS/MS	
structure defined level	t_R [min]	structure defined level	t_R [min]
PC 18:1/20:4;12OH	12.7	PC 18:1/12-HETE	8.7
PC 18:0/20:5;15OH	13.4	PC 18:0/15-HETE	8.9
PC 18:2/20:4;12OH	9.4	PC 18:2/12-HETE	8.0
PC 16:0/22:6;20OH	9.9	PC 16:0/20-HDHA	8.0
PC 16:0/22:6;17OH	10.4	PC 16:0/17-HDHA	8.2
PC 16:0/22:6;10OH	11.6	PC 16:0/10-HDHA	8.4
PC 16:0/22:6;7OH	12.9	PC 16:0/7-HDHA	8.8
PC 16:0/22:6;19Ep	12.1	PC 16:0/19(20)-EpDPE	8.6
PC 18:0/22:6;17OH	14.9	PC 18:0/17-HDHA	9.3
PC 18:0/22:6;10OH	16.2	PC 18:0/10-HDHA	9.7
PC O-16:0/18:2;13OH	12.6	PC O-16:0/13-HODE	8.5
PC O-16:0/20:4;15OH	13.2	PC O-16:0/15-HETE	8.8
PC O-16:0/20:4;12OH	14.6	PC O-16:0/12-HETE	9.1
PC O-16:0/20:4;5OH	17.6	PC O-16:0/5-HETE	10.0
PC O-16:0/20:4;14Ep	15.6	PC O-16:0/14(15)-EpETrE	9.5
PC O-16:0/20:4;11Ep	16.8	PC O-16:0/11(12)-EpETrE	10.0
PC O-16:0/20:5;17Ep	12.7	PC O-16:0/17(18)-EpETE	8.8
PC O-16:0/20:5;14Ep	13.6	PC O-16:0/14(15)-EpETE	9.0
PC O-16:0/20:5;11Ep	14.0	PC O-16:0/11(12)-EpETE	9.1
PC O-16:0/20:5;8Ep	14.8	PC O-16:0/8(9)-EpETE	9.3
PC O-16:0/22:6;19Ep	14.5	PC O-16:0/19(20)-EpDPE	9.3
PE 16:0/18:2;9OH	11.9	PE 16:0/9-HODE	8.2
PE 18:0/18:2;9OH	16.4	PE 18:0/9-HODE	9.4
PE 16:0/20:4;15OH	11.7	PE 16:0/15-HETE	8.4
PE 16:0/20:4;8OH	14.1	PE 16:0/8-HETE	8.9
PE 16:0/20:4;14Ep	14.1	PE 16:0/14(15)-EpETrE	9.0
PE 16:0/20:4;11Ep	15.3	PE 16:0/11(12)-EpETrE	9.5
PE 16:0/20:4;8Ep	16.1	PE 16:0/8(9)-EpETrE	9.8
PE 18:0/20:4;12OH	17.7	PE 18:0/12-HETE	9.9
PE 18:0/20:4;8OH	18.8	PE 18:0/8-HETE	10.2
PE 18:0/20:4;14Ep	18.7	PE 18:0/14(15)-EpETrE	10.3
PE 18:0/20:4;8Ep	20.7	PE 18:0/8(9)-EpETrE	10.8
PE 16:0/20:5;17Ep	11.3	PE 16:0/17(18)-EpETE	8.3
PE 16:0/20:5;14Ep	12.2	PE 16:0/14(15)-EpETE	8.6
PE 16:0/20:5;11Ep	12.6	PE 16:0/11(12)-EpETE	8.7
PE 16:0/20:5;8Ep	13.2	PE 16:0/8(9)-EpETE	8.8
PE 16:0/22:6;17OH	11.3	PE 16:0/17-HDHA	8.4
PE 16:0/22:6;14OH	12.0	PE 16:0/14-HDHA	8.5
PE 16:0/22:6;10OH	12.6	PE 16:0/10-HDHA	8.6
PE 16:0/22:6;7OH	13.9	PE 16:0/7-HDHA	9.0
PE 16:0/22:6;19Ep	13.1	PE 16:0/19(20)-EpDPE	8.8
PE 18:1/20:4;14Ep	14.6	PE 18:1/14(15)-EpETrE	9.3
PE 18:1/20:4;11Ep	15.7	PE 18:1/11(12)-EpETrE	9.6
PE 18:1/20:4;8Ep	16.6	PE 18:1/8(9)-EpETrE	9.8
PE 18:0/20:5;17Ep	15.9	PE 18:0/17(18)-EpETE	9.5
PE 18:0/20:5;11Ep	17.2	PE 18:0/11(12)-EpETE	9.9
PE 18:0/20:5;8Ep	17.9	PE 18:0/8(9)-EpETE	10.1
PE 18:0/22:6;19Ep	17.7	PE 18:0/19(20)-EpDPE	10.1

References

1. N.M. Hartung, M. Mainka, R. Pfaff, M. Kuhn, S. Biernacki, L. Zinnert, et al., (2023) Development of a quantitative proteomics approach for cyclooxygenases and lipoxygenases in parallel to quantitative oxylipin analysis allowing the comprehensive investigation of the arachidonic acid cascade, *Anal. Bioanal. Chem*. **415**, 913–933.
2. L. Kutzner, K. Rund, A. Ostermann, N. Hartung, J. Galano, L. Balas, et al., (2019) Development of an optimized LC-MS method for the detection of specialized proresolving mediators in biological samples, *Front in Pharma*. **10**, 169.
3. A.I. Ostermann, E. Koch, K.M. Rund, L. Kutzner, M. Mainka, N.H. Schebb, (2020) Targeting esterified oxylipins by LC–MS-Effect of sample preparation on oxylipin pattern, *Prostag. Other Lipid Mediat.* **146**, 106384.
4. K.M. Rund, A.I. Ostermann, L. Kutzner, J.-M. Galano, C. Oger, C. Vigor, et al., Development of an LC-ESI (-)-MS/MS method for the simultaneous quantification of 35 isoprostanes and isofurans derived from the major n3-and n6-PUFAs, *Anal. Chim. Acta* **1037,** (2018) 63–74.
5. R. Aoyagi, K. Ikeda, Y. Isobe, M. Arita, (2017) Comprehensive analyses of oxidized phospholipids using a measured MS/MS spectra library, *J. Lipid Res*. **58,** 2229–223.

Chapter 4

Table 8.14: Instrument parameters of the transitions monitored in the targeted LC-ESI(-)-MS/MS.

Analyte	Mass transition		CE	t_R
	Q1	Q3		[min]
PI 16:0/18:2;OH	849.5	295.2	-60	8.19
PI 16:0/18:2;OH (2)	849.5	255.2	-65	8.19
PI 16:0/18:2;13OH	849.5	195.2	-65	8.19
PI 18:0/18:2;OH	877.6	295.2	-60	11.95
PI 18:0/18:2;OH (2)	877.6	283.3	-65	11.95
PI 18:0/18:2;13OH	877.6	195.2	-65	11.95
PI 16:0/20:4;OH	873.5	319.2	-55	8.63
PI 16:0/20:4;OH (2)	873.5	255.2	-65	8.63
PI 16:0/20:4;15OH	873.5	219.2	-55	8.63
PI 16:0/20:5;OH	871.5	317.2	-50	7.41
PI 16:0/20:5;OH (2)	871.5	255.2	-60	7.41
PI 16:0/20:5;15OH	871.5	219.2	-55	7.41
PI 18:0/20:4;OH	901.5	319.2	-55	12.62
PI 18:0/20:4;OH (2)	901.5	283.2	-65	12.62
PI 18:0/20:4;15OH	901.5	219.2	-55	12.62
PI 18:1/20:4;OH	899.5	319.2	-50	8.95
PI 18:1/20:4;OH (2)	899.5	281.2	-65	8.95
PI 18:1/20:4;15OH	899.5	219.2	-55	8.95
PI 18:0/20:5;OH	899.5	317.2	-50	10.77
PI 18:0/20:5;OH (2)	899.5	283.2	-65	10.77
PI 18:0/20:5;15OH	899.5	219.2	-55	10.77
PI 16:0/22:5;OH	899.5	345.2	-55	9.01
PI 16:0/22:5;OH (2)	899.5	255.2	-65	9.01
PI 16:0/22:5;17OH	899.5	247.2	-55	9.01
PI 18:1/20:5;OH	897.5	317.2	-50	7.67
PI 18:1/20:5;OH (2)	897.5	281.2	-65	7.67
PI 18:1/20:5;15OH	897.5	219.2	-55	7.67
PI 16:0/22:6;OH	897.5	343.3	-50	8.34
PI 16:0/22:6;OH (2)	897.5	255.2	-60	8.34
PI 16:0/22:6;17OH	897.5	201.3	-55	8.34
PI 16:0/22:6;17OH (2)	897.5	245.2	-55	8.34
PI 18:0/22:5;OH	927.6	345.2	-55	13.07
PI 18:0/22:5;OH (2)	927.6	283.2	-65	13.07
PI 18:0/22:5;17OH	927.6	247.2	-60	13.07
PI 18:0/22:6;OH	925.5	343.3	-50	12.19
PI 18:0/22:6;OH (2)	925.5	283.2	-65	12.19
PI 18:0/22:6;17OH	925.5	201.3	-60	12.19
PI 18:0/22:6;17OH (2)	925.5	245.2	-55	12.19
PI 18:1/22:6;OH	923.5	343.3	-55	8.64
PI 18:1/22:6;OH (2)	923.5	281.2	-65	8.64
PI 18:1/22:6;17OH	923.5	201.3	-55	8.64
PI 18:1/22:6;17OH (2)	923.5	245.2	-55	8.64

Table 8.14: Continued 1/4. Instrument parameters of the transitions monitored in the targeted LC-ESI(-)-MS/MS.

Analyte	Mass transition		CE	t_R
	Q1	Q3		[min]
PC 16:0/18:2;OH	818.5	295.2	-50	10.80
PC 16:0/18:2;OH (2)	818.5	255.2	-55	10.80
PC 16:0/18:2;13OH	818.5	195.1	-60	10.80
PC 16:1/18:2;OH	816.5	295.2	-50	7.75
PC 16:1/18:2;OH (2)	816.5	253.2	-55	7.75
PC 16:1/18:2;13OH	816.5	195.2	-60	7.75
PC 18:0/18:2;OH	846.6	295.2	-50	15.30
PC 18:0/18:2;OH (2)	846.6	283.3	-55	15.30
PC 18:0/18:2;13OH	846.6	195.1	-60	15.30
PC 18:1/18:2;OH	844.6	295.2	-50	11.16
PC 18:1/18:2;OH (2)	844.6	281.2	-55	11.16
PC 18:1/18:2;13OH	844.6	195.1	-60	11.16
PC 16:0/15-HETE	842.4	319.2	-50	11.42
PC 16:0/15-HETE (2)	842.4	255.2	-55	11.42
PC 16:0/15-HETE (3)	842.4	219.2	-50	11.42
PC 16:0/20:5;OH	840.5	317.2	-45	9.64
PC 16:0/20:5;OH (2)	840.5	255.2	-55	9.64
PC 16:0/20:5;15OH	840.5	219.2	-50	9.64
PC 18:0/15-HETE	870.6	319.2	-50	15.99
PC 18:0/15-HETE (2)	870.6	283.3	-55	15.99
PC 18:0/15-HETE (3)	870.6	219.2	-55	15.99
PC 16:0/22:5;OH	868.5	345.2	-50	11.93
PC 16:0/22:5;OH (2)	868.5	255.2	-55	11.93
PC 16:0/22:5;17OH	868.5	247.2	-50	11.93
PC 18:0/15-HEPE	868.5	317.2	-50	14.04
PC 18:0/15-HEPE (2)	868.5	283.3	-55	14.04
PC 18:0/15-HEPE (3)	868.5	219.2	-50	14.04
PC 18:1/20:5;OH	866.4	317.2	-45	10.00
PC 18:1/20:5;OH (2)	866.4	281.2	-55	10.00
PC 18:1/20:5;15OH	866.4	219.2	-50	10.00
PC 16:0/17-HDHA	866.4	343.3	-45	11.02
PC 16:0/17-HDHA (2)	866.4	255.2	-55	11.02
PC 16:0/17-HDHA (3)	866.4	201.3	-50	11.02
PC 16:0/17-HDHA (4)	866.4	245.2	-50	11.02
PC 18:0/DH-17-HETE	898.5	347.3	-50	18.43
PC 18:0/DH-17-HETE (2)	898.5	283.3	-55	18.43
PC 18:0/DH-17-HETE (3)	898.5	247.3	-55	18.43
PC 18:1/22:5;OH	894.5	345.2	-50	12.33
PC 18:1/22:5;OH (2)	894.5	283.3	-55	12.33
PC 18:1/22:5;17OH	894.5	247.2	-55	12.33
PC 18:0/17-HDHA	894.5	343.3	-50	15.54
PC 18:0/17-HDHA (2)	894.5	283.3	-60	15.54
PC 18:0/17-HDHA (3)	894.5	201.3	-55	15.54
PC 18:0/17-HDHA (4)	894.5	245.2	-50	15.54
PC 18:1/22:6;OH	892.6	343.3	-45	11.39
PC 18:1/22:6;OH (2)	892.6	281.2	-55	11.39
PC 18:1/22:6;17OH	892.6	201.3	-50	11.39
PC 18:1/22:6;17OH (2)	892.6	245.2	-50	11.39

Table 8.14: Continued 2/4. Instrument parameters of the transitions monitored in the targeted LC-ESI(-)-MS/MS.

Analyte	Mass transition		CE	t_R
	Q1	Q3		[min]
PC P-16:0/18:2;OH	802.6	295.2	-50	12.55
PC P-16:0/18:2;13OH	802.6	195.1	-60	12.55
PC P-16:0/20:4;OH	826.6	319.2	-45	13.16
PC P-16:0/20:4;15OH	826.6	219.2	-50	13.16
PC P-16:0/22:5;OH	852.6	345.2	-45	13.68
PC P-16:0/22:5;17OH	852.6	247.2	-55	13.68
PC O-16:0/18:2;OH	804.6	295.2	-50	13.27
PC O-16:0/18:2;13OH	804.6	195.1	-60	13.27
PC O-16:0/20:4;OH	828.6	319.2	-50	13.90
PC O-16:0/20:4;15OH	828.6	219.2	-50	13.90
PC O-18:1/20:4;OH	854.6	319.2	-50	14.22
PC O-18:1/20:4;15OH	854.6	219.2	-55	14.22
PC O-16:0/22:5;OH	854.6	345.2	-50	14.43
PC O-16:0/22:5;17OH	854.6	247.2	-55	14.43
PC O-16:0/22:6;OH	852.6	343.3	-45	13.44
PC O-16:0/22:6;17OH	852.6	201.3	-50	13.44
PC O-16:0/22:6;17OH (2)	852.6	245.2	-50	13.44
PC O-18:1/22:5;OH	880.6	345.2	-50	14.72
PC O-18:1/22:5;17OH	880.6	247.2	-55	14.72
PC O-18:1/22:6;OH	878.6	343.3	-45	13.72
PC O-18:1/22:6;17OH	878.6	201.3	-60	13.72
PC O-18:1/22:6;17OH (2)	878.6	245.2	-50	13.70
PE 16:0/18:2;OH	730.5	295.2	-40	11.76
PE 16:0/18:2;OH (2)	730.5	255.2	-45	11.76
PE 16:0/18:2;13OH	730.5	195.2	-50	11.76
PE 18:0/18:2;OH	758.5	295.2	-45	16.33
PE 18:0/18:2;OH (2)	758.5	283.3	-45	16.33
PE 18:0/18:2;13OH	758.5	195.2	-55	16.33
PE 16:0/20:4;OH	754.4	319.4	-40	12.39
PE 16:0/20:4;OH (2)	754.4	255.2	-45	12.39
PE 16:0/20:4;15OH	754.4	219.2	-45	12.39
PE 16:0/20:5;OH	752.4	317.2	-40	10.48
PE 16:0/20:5;OH (2)	752.4	255.2	-50	10.48
PE 16:0/20:5;15OH	752.4	219.2	-40	10.48
PE 18:0/15-HETE	782.5	319.2	-40	17.01
PE 18:0/15-HETE (2)	782.5	283.2	-50	17.01
PE 18:0/15-HETE (3)	782.5	219.2	-45	17.01
PE 18:1/20:4;OH	780.5	319.2	-40	12.84
PE 18:1/20:4;OH (2)	780.5	281.2	-50	12.84
PE 18:1/20:4;15OH	780.5	219.2	-45	12.84
PE 18:0/20:5;OH	780.5	317.2	-40	15.03
PE 18:0/20:5;OH (2)	780.5	283.2	-50	15.03
PE 18:0/20:5;15OH	780.5	219.2	-45	15.03
PE 18:1/20:5;OH	778.4	317.2	-40	10.91
PE 18:1/20:5;OH (2)	778.4	281.2	-50	10.91
PE 18:1/20:5;15OH	778.4	219.2	-45	10.91
PE 16:0/17-HDHA	778.4	343.3	-40	11.97
PE 16:0/17-HDHA (2)	778.4	255.2	-45	11.97

Table 8.14: Continued 3/4. Instrument parameters of the transitions monitored in the targeted LC-ESI(-)-MS/MS.

Analyte	Mass transition		CE	t_R
	Q1	Q3		[min]
PE 16:0/17-HDHA (3)	778.4	201.3	-45	11.97
PE 16:0/17-HDHA (4)	778.4	245.2	-45	11.97
PE 18:0/DH-17-HETE	810.7	347.2	-45	19.49
PE 18:0/DH-17-HETE (2)	810.7	283.2	-50	19.49
PE 18:0/DH-17-HETE (3)	810.7	247.1	-48	19.49
PE 18:0/22:5;OH	808.5	345.2	-40	17.50
PE 18:0/22:5;OH (2)	808.5	283.2	-50	17.50
PE 18:0/22:5;17OH	808.5	247.2	-45	17.50
PE 18:0/22:6;OH	806.5	343.2	-40	16.56
PE 18:0/22:6;OH (2)	806.5	283.2	-50	16.56
PE 18:0/22:6;17OH	806.5	201.3	-45	16.56
PE 18:0/22:6;17OH (2)	806.5	245.2	-40	16.56
PE 18:1/22:5;OH	806.5	345.2	-40	13.35
PE 18:1/22:5;OH (2)	806.5	281.2	-55	13.35
PE 18:1/22:5;17OH	806.5	247.2	-50	13.35
PE 18:1/22:6;OH	804.5	343.3	-40	12.40
PE 18:1/22:6;OH (2)	804.5	281.2	-50	12.40
PE 18:1/22:6;17OH	804.5	201.3	-45	12.40
PE 18:1/22:6;17OH (2)	804.5	245.2	-45	12.40
PE P-16:0/18:2;OH	714.5	295.2	-40	13.68
PE P-16:0/18:2;13OH	714.5	195.2	-50	13.68
PE P-16:0/20:4;OH	738.5	319.2	-40	14.28
PE P-16:0/20:4;15OH	738.5	219.2	-45	14.28
PE P-16:0/20:5;OH	736.5	317.2	-35	12.31
PE P-16:0/20:5;15OH	736.5	219.2	-40	12.31
PE P-18:0/20:4;OH	766.5	319.2	-40	18.96
PE P-18:0/20:4;15OH	766.5	219.2	-45	18.96
PE P-16:0/22:4;OH	766.5	347.2	-40	16.83
PE P-16:0/22:4;17OH	766.5	247.2	-45	16.83
PE P-18:1/20:4;OH	764.5	319.2	-40	14.63
PE P-18:1/20:4;15OH	764.5	219.2	-45	14.63
PE P-18:0/20:5;OH	764.5	317.2	-40	16.98
PE P-18:0/20:5;15OH	764.5	219.2	-40	16.98
PE P-16:0/22:5;OH	764.5	345.2	-40	14.85
PE P-16:0/22:5;17OH	764.5	247.2	-45	14.85
PE P-18:1/20:5;OH	762.5	317.2	-40	12.65
PE P-18:1/20:5;15OH	762.5	219.2	-45	12.65
PE P-16:0/22:6;OH	762.5	343.3	-40	13.80
PE P-16:0/22:6;17OH	762.5	201.5	-45	13.80
PE P-16:0/22:6;17OH (2)	762.5	245.0	-40	13.80
PE P-18:0/22:4;OH	794.6	347.2	-40	19.49
PE P-18:0/22:4;17OH	794.6	247.2	-45	19.49
PE P-18:0/22:5;OH	792.5	345.2	-40	19.49
PE P-18:0/22:5;17OH	792.5	247.2	-45	19.49
PE P-18:1/22:5;OH	790.5	345.2	-40	15.17
PE P-18:1/22:5;17OH	790.5	247.2	-45	15.17
PE P-18:0/22:6;OH	790.5	343.3	-40	18.43
PE P-18:0/22:6;17OH	790.5	201.3	-45	18.43

Table 8.14: Continued 4/4. Instrument parameters of the transitions monitored in the targeted LC-ESI(-)-MS/MS.

Analyte	Mass transition		CE	t_R
	Q1	Q3		[min]
PE P-18:0/22:6;17OH (2)	790.5	245.2	-45	18.43
PE P-18:1/22:6;OH	788.5	343.3	-40	14.13
PE P-18:1/22:6;17OH	788.5	201.3	-45	14.13
PE P-18:1/22:6;17OH (2)	788.5	245.2	-45	14.13
PI 12:0/13:0 (IS)	711.4	241.0	-48	7.36
PI 12:0/13:0 (2) (IS)	711.4	213.0	-55	7.36
PC 12:0/13:0 (IS)	680.4	213.0	-42	9.75
PC 12:0/13:0 (2) (IS)	680.4	199.1	-42	9.75
PE 12:0/13:0 (IS)	592.0	213.0	-38	10.73
PE 12:0/13:0 (2) (IS)	592.0	199.1	-33	10.73
PG 12:0/13:0 (IS)	623.2	213.0	-42	7.73
PG 12:0/13:0 (2) (IS)	623.2	199.1	-42	7.73

Table 8.15: Standards used for the quantification of oxPL by targeted LC-ESI(-)-MS/MS. The standards were assigned to the analytes based on the head group and the fatty acyl chains. For oxPI analytes, standards from the PC class were selected. Correcting factors for the MRM signal of the analyte and the compounds used for quantification. n.d. = not determined.

analyte quantified	standard used for quantification	correcting factor
PI 16:0/18:2;13OH	PC 16:0/15-HETE	1.01
PI 18:0/18:2;13OH	PC 18:0/15-HETE	n.d.
PI 16:0/20:4;15OH	PC 16:0/15-HETE	1.41
PI 16:0/20:5;15OH	PC 18:0/15-HEPE	0.92
PI 18:0/20:4;15OH	PC 18:0/15-HETE	1.44
PI 18:1/20:4;15OH	PC 18:0/15-HETE	1.18
PI 18:0/20:5;15OH	PC 18:0/15-HEPE	1.38
PI 16:0/22:5;17OH	PC 16:0/17-HDHA	n.d.
PI 18:1/20:5;15OH	PC 18:0/15-HEPE	n.d.
PI 16:0/22:6;17OH	PC 16:0/17-HDHA	n.d.
PI 18:0/22:5;17OH	PC 18:0/17-HDHA	n.d.
PI 18:0/22:6;17OH	PC 18:0/17-HDHA	1.24
PI 18:1/22:6;17OH	PC 18:0/17-HDHA	0.88
PC 16:0/18:2;13OH	PC 16:0/15-HETE	1.10
PC 16:1/18:2;13OH	PC 16:0/15-HETE	n.d.
PC 18:0/18:2;13OH	PC 18:0/15-HETE	0.80
PC 18:1/18:2;13OH	PC 18:0/15-HETE	1.00
PC 16:0/20:5;15OH	PC 18:0/15-HEPE	0.92
PC 16:0/22:5;17OH	PC 16:0/17-HDHA	0.59
PC 18:1/20:5;15OH	PC 18:0/15-HEPE	n.d.
PC 18:1/22:5;17OH	PC 18:0/17-HDHA	n.d.
PC 18:1/22:6;17OH	PC 18:0/17-HDHA	n.d.
PC P-16:0/18:2;13OH	PC 16:0/15-HETE	0.60
PC P-16:0/20:4;15OH	PC 16:0/15-HETE	0.91
PC P-16:0/22:5;17OH	PC 16:0/17-HDHA	n.d.
PC O-16:0/18:2;13OH	PC 16:0/15-HETE	0.75
PC O-16:0/20:4;15OH	PC 16:0/15-HETE	0.95
PC O-18:1/20:4;15OH	PC 18:0/15-HETE	0.85
PC O-16:0/22:5;17OH	PC 16:0/17-HDHA	0.44
PC O-16:0/22:6;17OH	PC 16:0/17-HDHA	1.39
PC O-18:1/22:5;17OH	PC 18:0/17-HDHA	n.d.
PC O-18:1/22:6;17OH	PC 18:0/17-HDHA	n.d.

Table 8.15: Continued. Standards used for the quantification of oxPL by targeted LC-ESI(-)-MS/MS.

analyte quantified	standard used for quantification	correcting factor
PE 16:0/18:2;13OH	PE 18:0/15-HETE	0.65
PE 18:0/18:2;13OH	PE 18:0/15-HETE	0.75
PE 16:0/20:4;15OH	PE 18:0/15-HETE	0.94
PE 16:0/20:5;15OH	PE 18:0/15-HETE	n.d.
PE 18:1/20:4;15OH	PE 18:0/15-HETE	n.d.
PE 18:0/20:5;15OH	PE 18:0/15-HETE	n.d.
PE 18:1/20:5;15OH	PE 18:0/15-HETE	n.d.
PE 18:0/22:5;17OH	PE 16:0/17-HDHA	n.d.
PE 18:0/22:6;17OH	PE 16:0/17-HDHA	1.39
PE 18:1/22:5;17OH	PE 16:0/17-HDHA	n.d.
PE 18:1/22:6;17OH	PE 16:0/17-HDHA	0.98
PE P-16:0/18:2;13OH	PE 18:0/15-HETE	0.51
PE P-16:0/20:4;15OH	PE 18:0/15-HETE	0.91
PE P-16:0/20:5;15OH	PE 18:0/15-HETE	0.78
PE P-18:0/20:4;15OH	PE 18:0/15-HETE	n.d.
PE P-16:0/22:4;17OH	PE 18:0/DH-17-HETE	0.44
PE P-18:1/20:4;15OH	PE 18:0/15-HETE	n.d.
PE P-18:0/20:5;15OH	PE 18:0/15-HETE	n.d.
PE P-16:0/22:5;17OH	PE 16:0/17-HDHA	0.67
PE P-18:1/20:5;OH	PE 18:0/15-HETE	n.d.
PE P-16:0/22:6;17OH	PE 16:0/17-HDHA	1.23
PE P-18:0/22:4;OH	PE 18:0/DH-17-HETE	n.d.
PE P-18:0/22:5;17OH	PE 16:0/17-HDHA	n.d.
PE P-18:1/22:5;17OH	PE 16:0/17-HDHA	0.68
PE P-18:0/22:6;17OH	PE 16:0/17-HDHA	1.49
PE P-18:1/22:6;17OH	PE 16:0/17-HDHA	0.95

Table 8.16: Concentration of oxPL formed following supplementation, endogenously via 15-LOX-2 or exogenously via added 15-LOX-2. 5×10^6 cells were used per experiment. HEK293T cells supplemented with either 15(*S*)-HETE, 15(*S*)-HEPE, 17(*S*)-HDHA, or 13(*S*)-HODE (300 nmol L^{-1}, 2 h). Endogenous formation of oxPL elicited by overexpression of 15-LOX-2 in HEK293T_15-LOX-2 cells (200 ng mL^{-1} doxycycline, 24 h). Direct 15-LOX-2 conversion by addition of exogenous 15-LOX-2 human enzyme to HEK293T cell homogenate (6.9×10^{-3} U mL^{-1} in assay, 2 h at 37 °C). Shown is the mean ± SD (n = 3) of the concentration per mg of cell protein determined by targeted LC-ESI(-)-MS/MS using external calibration.

		concentration of individual oxPL species [pmol mg^{-1}]		
	analyte	oxylipin-supplemented HEK293T cells	HEK293T_15-LOX-2 cells overexpressing 15-LOX-2	exogenous 15-LOX-2 added in HEK293T cell homogenate
20:4;15OH	PC P-16:0/20:4;15OH	< LOD	< LOD	4.6 ± 0.4
	PC O-18:1/20:4;15OH	< LOD	< LOD	3.7 ± 0.8
	PE 16:0/20:4;15OH	< LOD	< LOD	30 ± 4
	PC 18:0/15-HETE	0.24 ± 0.05	0.32 ± 0.06	4.6 ± 0.8
	PC O-16:0/20:4;15OH	0.83 ± 0.03	0.80 ± 0.10	4.8 ± 0.7
	PE 18:1/20:4;15OH	0.26 ± 0.23	1.4 ± 0.2	45 ± 6
	PC 16:0/15-HETE	1.6 ± 0.3	1.6 ± 0.1	21 ± 6
	PE 18:0/15-HETE	0.17 ± 0.01	2.4 ± 0.1	53 ± 6
	PE P-16:0/20:4;15OH	3.2 ± 0.6	9.1 ± 0.6	53 ± 6
	PI 16:0/20:4;15OH	30 ± 2	11.4 ± 0.5	58 ± 6
	PI 18:1/20:4;15OH	67 ± 4	20 ± 1	64 ± 6
	PI 18:0/20:4;15OH	246 ± 17	114 ± 3	222 ± 56
20:5;15OH	PC 18:0/15-HEPE	2.8 ± 0.3	0.45 ± 0.15	< LOD
	PC 16:0/20:5;15OH	15 ± 2	3.6 ± 0.3	6.0 ± 1.1
	PE P-16:0/20:5;15OH	1.700 ± 0.3	7.1 ± 0.2	11 ± 1.0
	PI 18:0/20:5;15OH	189 ± 11	49 ± 2	7.2 ± 1.4

Table 8.16: Continued 1/2. Concentration of oxPL formed following supplementation, endogenously via 15-LOX-2 or exogenously via added 15-LOX-2.

	concentration of individual oxPL species [pmol mg^{-1}]		
analyte	**oxylipin-supplemented HEK293T cells**	**HEK293T_15-LOX-2 cells overexpressing 15-LOX-2**	**exogenous 15-LOX-2 added in HEK293T cell homogenate**
22:6;17OH			
PI 18:1/22:6;17OH	3.0 ± 0.3	1.7 ± 0.2	7.9 ± 1.3
PE 16:0/17-HDHA	2.9 ± 0.5	2.4 ± 0.2	36 ± 4
PC 18:0/17-HDHA	4.9 ± 0.3	2.6 ± 0.2	6.5 ± 1.1
PC O-18:1/22:6;17OH	8.5 ± 0.8	< LOD	< LOD
PC O-16:0/22:6;17OH	20 ± 1	9.2 ± 0.4	7.6 ± 1.3
PC 16:0/17-HDHA	21.7 ± 0.4	10.6 ± 0.6	27 ± 4
PE 18:1/22:6;17OH	6.6 ± 1.0	12.5 ± 0.8	52 ± 7
PE 18:0/22:6;17OH	3.2 ± 0.09	13.7 ± 0.3	78 ± 11
PI 18:0/22:6;17OH	10.1 ± 1.1	17.0 ± 1.4	33 ± 6
PE P-18:1/22:6;17OH	34 ± 2	23.3 ± 0.7	35 ± 4
PE P-18:0/22:6;17OH	46 ± 1	24.9 ± 0.6	23 ± 3
PE P-16:0/22:6;17OH	61 ± 1	33.9 ± 0.4	39 ± 4

Table 8.16: Continued 2/2. Concentration of oxPL formed following supplementation, endogenously via 15-LOX-2 or exogenously via added 15-LOX-2.

	concentration of individual oxPL species [pmol mg^{-1}]			
	analyte	oxylipin-supplemented HEK293T cells	HEK293T_15-LOX-2 cells overexpressing 15-LOX-2	exogenous 15-LOX-2 added in HEK293T cell homogenate
18:2;13OH	PE 16:0/18:2;13OH	0.39 ± 0.30	< LOD	3.1 ± 0.1
	PE 18:0/18:2;13OH	0.22 ± 0.03	0.61 ± 0.64	0.64 ± 0.07
	PC P-16:0/18:2;13OH	0.65 ± 0.12	0.86 ± 0.19	< LOD
	PC 16:1/18:2;13OH	1.1 ± 0.07	0.89 ± 0.18	3.4 ± 0.2
	PE P-16:0/18:2;13OH	1.6 ± 0.1	1.3 ± 0.1	7.6 ± 1.3
	PC 18:0/18:2;13OH	1.3 ± 0.1	1.8 ± 0.2	< LOD
	PI 16:0/18:2;13OH	3.1 ± 0.2	< LOD	1.2 ± 0.3
	PC 18:1/18:2;13OH	4.4 ± 0.2	2.5 ± 0.1	6.4 ± 0.3
	PI 18:0/18:2;13OH	5.7 ± 0.4	2.8 ± 0.2	4.6 ± 1.2
	PC O-16:0/18:2;13OH	3.1 ± 0.3	3.0 ± 0.2	< LOD
	PC 16:0/18:2;13OH	13 ± 1	13.4 ± 0.4	13 ± 1

Table 8.17: Concentration of oxPL in cells depending on amount of the cells used for LLE. Endogenous formation of oxPL elicited by overexpression of 15-LOX-2 in 5×10^6 HEK293T_15-LOX-2 cells (200 ng mL^{-1} doxycycline, 24 h). LLE was performed using different volumes of sonicated cells — 10 µL (0.076 mg protein), 25 µL (0.19 mg protein), 50 µL (0.38 mg protein), 75 µL (0.57 mg protein), and 100 µL (0.76 mg protein) — while maintaining identical extraction solvent volumes. Analytes are sorted by t_R. Shown is the mean ± SD (n = 3) of the concentration per mg of cell protein of the analytes depicted in Fig. 4.6A. OxPL were quantified by targeted LC-ESI(-)MS/MS using external calibration (Tables 4.2, 8.15).

analyte	t_R	concentration of individual oxPL species [pmol mg^{-1}]				
	[min]	0.076 mg protein	0.19 mg protein	0.38 mg protein	0.57 mg protein	0.76 mg protein
PI 16:0/20:4;15OH	8.63	19 ± 2	14.4 ± 0.9	14.9 ± 1.3	14.3 ± 0.6	15.2 ± 1.2
PI 18:1/20:4;15OH	8.95	18 ± 1	15.9 ± 0.6	16.4 ± 1.4	18 ± 1	19 ± 2
PI 18:0/20:5;15OH	10.80	52 ± 5	46 ± 2	50 ± 3	54 ± 3	58 ± 5
PC 16:0/18:2;13OH	10.80	13 ± 1	12.3 ± 0.9	12.5 ± 0.6	13.2 ± 0.9	13.6 ± 0.8
PC 16:0/17-HDHA	11.00	6.1 ± 1.0	6.4 ± 0.7	7.3 ± 1.0	7.8 ± 0.2	8.2 ± 0.8
PC 16:0/22:5;17OH	11.90	6.7 ± 1.7	6.9 ± 1.3	7.4 ± 0.70	7.7 ± 0.2	7.8 ± 0.5
PE P-16:0/20:5;15OH	12.00	4.7 ± 0.4	4.5 ± 0.1	4.9 ± 0.50	4.7 ± 0.4	4.7 ± 0.5
PI 18:0/20:4;15OH	12.60	97 ± 10	92 ± 4	96 ± 5	103 ± 7	106 ± 6
PE P-16:0/18:2;13OH	13.70	0.95 ± 0.16	1.1 ± 0.1	1.1 ± 0.1	1.0 ± 0.2	1.0 ± 0.2
PE P-16:0/22:6;17OH	13.80	40 ± 2	38 ± 2	41 ± 2	39 ± 3	40 ± 3
PE P-18:1/22:6;17OH	14.10	16 ± 2	15.1 ± 0.9	16.1 ± 1.4	16 ± 1	16.0 ± 1.6
PE P-16:0/20:4;15OH	14.30	6.1 ± 0.7	5.8 ± 0.3	6.5 ± 0.4	6.2 ± 0.4	6.1 ± 0.6
PC O-16:0/22:5;17OH	14.40	6.2 ± 0.6	7.0 ± 0.3	7.1 ± 0.2	7.8 ± 0.6	7.9 ± 0.7
PE P-16:0/22:5;17OH	14.90	53 ± 4	48 ± 2	51 ± 4	51 ± 4	51 ± 5
PE P-18:1/22:5;17OH	15.20	11 ± 1	9.9 ± 0.6	11 ± 1	11 ± 1	10.6 ± 0.8
PE 18:0/22:6;17OH	16.60	7 ± 1	5.6 ± 0.4	6.7 ± 0.3	7.4 ± 0.4	8.9 ± 1.3
PE P-16:0/22:4;17OH	16.80	3.7 ± 0.2	3.6 ± 0.2	3.8 ± 0.3	3.8 ± 0.4	3.7 ± 0.3
PE 18:0/15-HETE	17.00	1.3 ± 0.2	1.3 ± 0.1	1.5 ± 0.1	1.6 ± 0.2	1.9 ± 0.2
PE P-18:0/22:6;17OH	18.50	20 ± 2	18.9 ± 1.5	20 ± 2	20.8 ± 1.6	21 ± 2
PE P-18:0/22:5;17OH	19.50	23 ± 3	35.1 ± 1.4	61 ± 4	81 ± 10	109 ± 12

Table 8.18: Intra- and inter-day extraction efficiency of IS and spiked oxPL in human cells. HEK293T cell samples were extracted by liquid-liquid extraction on three different days. IS and a mixture of oxPL (2.5 pmol of each) were added to the cell sample at the beginning of sample preparation. Shown are the mean values and RSD (n = 3 for intra- and n = 3 for inter-day). Extraction recovery was calculated relative to an IS/oxPL solution directly injected. Lipid extracts were analyzed by targeted LC-ESI(-)-MS/MS operating in scheduled MRM mode (QTRAP6500+).

analyte	Day 1		Day 2		Day 3		Days 1 – 3
	recovery [%]	RSD [%]	recovery [%]	RSD [%]	recovery [%]	RSD [%]	$RSD_{interday}$ [%]
PI 12:0/13:0 (IS)	80	8	75	3	80	8	4
PC 12:0/13:0 (IS)	99	6	92	1	99	6	4
PE 12:0/13:0 (IS)	87	7	83	1	87	7	3
PC 16:0/17-HDHA	107	10	100	13	84	4	12
PC 16:0/15-HETE	100	9	93	4	102	4	5
PE 16:0/17-HDHA	93	7	81	12	78	10	10
PC 18:0/15-HEPE	89	4	97	10	91	11	4
PC 18:0/17-HDHA	115	7	88	19	87	7	16
PC 18:0/15-HETE	102	2	92	12	93	7	6
PE 18:0/15-HETE	87	5	80	14	78	7	6
PC 18:0/DH-17-HETE	78	3	69	7	67	8	8
PE 18:0/DH-17-HETE	370	5	327	7	305	3	10

Table 8.19: Oxylipin-supplementation in cells with lower concentrations of hydroxy-PUFA (~ 50 nmol L^{-1}, 2 h) results in a similar distribution into NL and PL as 15-LOX-2 oxylipins endogenously formed in HEK293T_15-LOX-2 cells. HEK293T cells were supplemented with either 15(*S*)-HETE, 15(*S*)-HEPE, 17(*S*)-HDHA, or 13(*S*)-HODE (~ 50 nmol L^{-1}, 2 h at 37 °C). Endogenous formation of oxPL was elicited by overexpression of 15-LOX-2 in HEK293T_15-LOX-2 (200 ng mL^{-1} doxycycline, 24 h at 37 °C). Esterified oxylipins were quantified in the HILIC-separated lipid fractions – PI/PS, PE, PC, PG, and NL – by targeted LC-MS/MS following alkaline hydrolysis and SPE as described [1-4]. Shown is the mean ± SD (n = 3) of the relative distribution of oxylipins in NL and PL.

	oxylipin-supplemented HEK293T cells		**15-LOX-2 overexpressing HEK293T_15-LOX-2 cells**	
Analyte	**NL [%]**	**PL [%]**	**NL [%]**	**PL [%]**
15-HETE	25 ± 3	75 ± 3	18 ± 1	82 ± 1
15-HEPE	15 ± 1	85 ± 1	12.3 ± 1.6	88 ± 2
17-HDHA	14 ± 2	86 ± 2	5.2 ± 0.9	95 ± 1
13-HODE	19 ± 2	81 ± 2	13 ± 2	87 ± 2

References

1. N.M. Hartung, M. Mainka, R. Pfaff, M. Kuhn, S. Biernacki, L. Zinnert, et al., (2023) Development of a quantitative proteomics approach for cyclooxygenases and lipoxygenases in parallel to quantitative oxylipin analysis allowing the comprehensive investigation of the arachidonic acid cascade, *Anal. Bioanal. Chem*. **415**, 913–933.
2. L. Kutzner, K. Rund, A. Ostermann, N. Hartung, J. Galano, L. Balas, et al., (2019) Development of an optimized LC-MS method for the detection of specialized proresolving mediators in biological samples, *Front in Pharma*. **10**, 169.
3. A.I. Ostermann, E. Koch, K.M. Rund, L. Kutzner, M. Mainka, N.H. Schebb, (2020) Targeting esterified oxylipins by LC–MS-Effect of sample preparation on oxylipin pattern, *Prostag. Other Lipid Mediat.* **146**, 106384.
4. K.M. Rund, A.I. Ostermann, L. Kutzner, J.-M. Galano, C. Oger, C. Vigor, et al., Development of an LC-ESI (-)-MS/MS method for the simultaneous quantification of 35 isoprostanes and isofurans derived from the major n3-and n6-PUFAs, *Anal. Chim. Acta* **1037,** (2018) 63–74.

Abbreviations

12-LOX	12-lipoxygenase
15-LOX	15-lipoxygenase
15-LOX-1	15-lipoxygenase-1
15-LOX-2	15-lipoxygenase-2
5-LOX	5-lipoxygenase
acc.	accuracy
ACN	acetonitrile
ACS	acyl-CoA synthetase
ACSL	long-chain acyl-CoA synthetase
AdA	adrenic acid (22:4(7*Z*,10*Z*,13*Z*,16*Z*))
AGC	automatic gain control
Akt/PKB	protein kinase B
ALA	α-linolenic acid (18:3(9*Z*,12*Z*,15*Z*))
AMP	acyl-adenosine monophosphate
ARA	arachidonic acid (20:4(5*Z*,8*Z*,11*Z*,14*Z*))
CDP-DG	diphosphate-diacylglycerol
CE	collision energy
$CHCl_3$	chloroform
Chol Ester	cholesteryl ester
CoA	coenzyme A
COX	cyclooxygenase
CXP	collision exit potential
CYP	cytochrome monooxygenases
D	deuterium
dd	data-dependent
DG	diacylglycerol
DGLA	dihomo-γ-linolenic acid (20:3(8*Z*,11*Z*,14*Z*))
DHA	docosahexaenoic acid (22:6(4*Z*,7*Z*,10*Z*,13*Z*,16*Z*,19*Z*))
DH-HETE	dihomo-hydroxyeicosatetraenoic acid
DiH	dihydroxy
DiHDPE	dihydroxydocosapentaenoic acid
DiHETE	dihydroxyeicosatetraenoic acid
DiHETrE	dihydroxyeicosatrienoic acid
DiHOME	dihydroxyoctadecamonoenoic acid

DMEM	Dulbecco's Modified Eagle Medium
DMSO	dimethylsulfoxide
DP	declustering potential
EDTA	ethylenediaminetetraacetic acid
EP	entrance potential
EPA	eicosapentaenoic acid (20:5(5*Z*,8*Z*,11*Z*,14*Z*,17*Z*))
EpDPE	epoxydocosapentaenoic acid
EpETE	epoxyeicosatetraenoic acid
EpETrE	epoxyeicosatrienoic acid
EpOME	epoxyoctadecamonoenoic acid
ER	endoplasmic reticulum
ESI	electrospray ionization
ESI(-)	negative electrospray ionization
ESI(+)	positive electrospray ionization
FA	fatty acid
FC	free cholesterol
FCS	fetal calf serum
FWHM	full width at half maximum
GPX	glutathione peroxidase
HDHA	hydroxydocosahexaenoic acid
HEK293T	human embryonic kidney 293 cell line
HEPE	hydroxyeicosapentaenoic acid
HESI	heated electrospray ionization
HETE	hydroxyeicosatetraenoic acid
HILIC	hydrophilic interaction liquid chromatography
HODE	hydroxyoctadecadienoic acid
HOTrE	hydroxyoctadecatrienoic acid
HpETE	hydroperoxyeicosatetraenoic acid
HRMS	high resolution mass spectrometry
IPA	isopropanol
IS	internal standard
IT	injection time
LA	linoleic acid (18:2(9*Z*,12*Z*))
LC	liquid chromatography
LLE	liquid-liquid extraction
LLOQ	lower limit of quantification
LOD	limit of detection
LPCAT	lysoPC acyl transferase
LPLAT	lysoPL acyl transferase
lysoPC	lysophosphatidylcholine
lysoPE	lysophosphatidylethanolamine

lysoPL	lysophospholipid
m/z	mass-to-charge ratio
mCPBA	*meta*-chloroperoxybenzoic acid
MeOH	methanol
MG	monoacylglycerol
MRM	multiple reaction monitoring
MS	mass spectrometry
MS/MS	tandem mass spectrometry
MS^2	tandem mass spectrometry
MTBE	*tert*-butyl methyl ether
n3-PUFA	omega 3 polyunsaturated fatty acid
n6-PUFA	omega 6 polyunsaturated fatty acid
NCE	normalized collision energy
NL	neutral lipids
NP-LC	normal phase liquid chromatography
oxPL	oxidized phospholipids
oxPUFA	oxidized polyunsaturated fatty acids
PA	phosphatidic acid
PBS	phosphate-buffered saline
PC	phosphatidylcholine
PC-O	ether phosphatidylcholine
PC-P	plasmalogen phosphatidylcholine
PDK1	phosphoinositide-dependent kinase-1
PE	phosphatidylethanolamine
PE-P	plasmalogen phosphatidylethanolamine
PG	phosphatidylglycerol
PI	phosphatidylinositol
PI3K	phosphoinositide 3-kinase
PIP	phosphatidylinositol 4-biphosphate
PIP_2	phosphatidylinositol 4,5-biphosphate
PIP_3	phosphatidylinositol 3,4,5-trisphosphate
PL	phospholipid
PLA_1	phospholipase 1
PLA_2	phospholipase 2
PLC	phospholipase C
PL-O	ether phospholipid
PL-P	plasmalogen phospholipid
prec.	precision
PS	phosphatidylserine
PUFA	polyunsaturated fatty acids
R	resolution

RF	radio frequency
RP	reversed phase
RP-LC	reversed-phase liquid chromatography
RSD	relative standard deviation
RvE_4	5(*S*),15(*S*)-DiHEPE
S/N	signal-to-noise ratio
SD	standard deviation
SIM	selected ion monitoring
SL	sphingolipid
SM	sphingomyelin
sn	stereospecific numbering
SPE	solid-phase extraction
SPM	specialized pro-resolving mediators
SRM	selected reaction monitoring
TG	triacylglycerol
TIC	total ion chromatogram
TLC	thin-layer chromatography
TPPU	1-(1-propanoylpiperidin-4-yl)-3-[4-(trifluoromethoxy)phenyl]urea
t_R	retention time
XIC	extracted ion chromatogram

Acknowledgement

This thesis was carried out from April 2021 to December 2024 at the University of Wuppertal and at the Chair of Food Chemistry (University of Wuppertal) in the research group of Prof. Dr. Nils Helge Schebb.

First and foremost, I would like to express my sincere gratitude to **Prof. Dr. Nils Helge Schebb** for giving me the opportunity to pursue my PhD within his research group. I am deeply thankful for his invaluable supervision, continuous support, and unwavering commitment throughout the course of my doctoral studies. His guidance and encouragement have been key in the successful completion of this work. I am also grateful for the opportunity to attend international conferences where I could present and discuss my results. I would like to thank him for showing such genuine interest and enthusiasm in my research and for reviewing this thesis.

I would like to express my sincere gratitude to **Prof. Dr. Dieter Steinhilber** for reviewing this thesis and offering valuable feedback. Moreover, I am thankful to him for his trust in our collaborative projects and for kindly providing the transfected cell lines, which were key to the success of my work.

Furthermore, I would like thank **Prof. Dr. Nils Helge Schebb**, **Prof. Dr. Claudia Bohrmann-Linde**, **Prof. Dr. Julia Bornhorst** and **Prof. Dr. Fabian Mohr** for accepting to be members of the examination committee.

Importantly, I want to thank **Dr. Katharina Maria Rund** who provided me a strong support and invaluable help at the beginning of my PhD. Your support undeniably helped me progress – not only in scientific writing but also in designing my experiments. We also successfully co-authored a paper on the development and optimization of an LC-HRMS method for PL analysis. Once again, your expertise was pivotal in making this project a success. During our conference in Vienna, we had some truly fun, almost sleepless nights working on the

manuscript – memories that I won't forget! But fortunately, we also had the chance to share a delicious Aperol Spritz at the "Aperol Spritz Corner" and enjoy some tasty pizza during our time in Vienna.

I would like to sincerely thank **Dr. Nadja Kampschulte** for always sharing so many helpful computer tips and giving valuable advice for my work. Thanks for your help and support. We'd be lost without you! I especially appreciated your remarkable ability to apply just the right amount of force – or, when necessary, the right amount of violence – to persuade the mass spectrometer to cooperate during the disassembling process. I'll also never forget the fun moments we shared, enjoying barbecues in Lilli's garden – and of course, sipping, or not… Aperol Spritz!

Luca Marcel Wende, intergalactically known as the expert in HILIC-based SPE. I sincerely thank you for your invaluable contributions throughout my entire thesis, especially for analyzing samples and creating this huge oxPL MS-DIAL data list. You were always ready with a joke, and I truly enjoyed the fun we had traveling together to the conference in Vienna, especially during that unforgettable 10-hour train ride. I will also always laugh when I think about the time you carefully selected all the data… only to lose the entire selection! Thanks for all these hilarious moments.

I want to express my sincere gratitude to **Susanne Reif** for your valuable contributions during your Master's thesis. Your efforts in analyzing the samples for our collaborative project with Frankfurt have been immensely helpful. Thanks for your work, dedication, and good mood! I also want to thank both **Tim Wermund** and **Robin Lauterbach** for their contribution, specifically the work in the development of the untargeted LC-HRMS method.

Moreover, I would also like to express my gratitude to **Dr. Bjarne Goebel** and **Dr. Ann-Kathrin Häfner**, who, under the supervision of Prof. Dr. Dieter Steinhilber, kindly provided cryovials of HEK293T cells transfected with 15-LOX-2. This cell line was pivotal in the development of the targeted oxPL LC-MS/MS method, and I would like to thank all of you for reviewing my most recent paper and providing helpful suggestions.

Je voudrais remercier chaleureusement **Michelle Wiebel** – alias *Madame Wiebél* – qui a été un véritable pilier tout au long de mon doctorat. J'espère que tu auras le courage de goûter à nouveau ce délicieux (mais ô combien calorique) cookie vendu à l'université. Et bien sûr, j'espère que nous aurons de nouveau le plaisir de nous retrouver autour d'une gaufre, accompagnée – comme il se doit – de sa savoureuse glace à la pistache… et qui sait, peut-être irons-nous un jour goûter ce fameux tiramisu à la pistache? Merci pour tous ces bons moments de rigolade!

I want to sincerely thank **Lilli Scholz** – a.k.a. *Chili Lilli*. You were such a friendly and lovely colleague. Thank you all for the wonderful moments we've shared. I hope we'll have the chance to enjoy another barbecue – whether in your garden or somewhere else – sometime soon! We also had such a fun time at the carnival in Düsseldorf – truly, we were the most beautiful grapes the world has ever seen! The carnival in Köln was a blast too, and I just wish I could have joined earlier… as originally planned!

Many thanks to **Michel André Chromik** for always being so friendly and such a funny colleague. Thanks for taking the time to analyze the overexpression of the LOX enzymes and for testing their activity. I truly enjoyed the way we teased each other, though I must admit, I wasn't a fan of when you tortured my ears with the paper shredding! I'll get my revenge, Auge um Auge, Zahn um Zahn!

I am grateful to **Rebecca Kirchhoff** for introducing me to cell culture techniques and for consistently taking the time to answer all my questions. Thanks for your kindness, and of course, for the chewing gum! A big thank you to **Ariane Löwen** as well, especially for always providing so many chocolates and sweet treats. You were always there for a friendly chat and ready to listen. Thank you for giving me a personal box full of caramelized hazelnut – it was delicious!

I am thankful to **Dr. Elisabeth Koch** for warmly welcoming me to the group and for generously taking the time to teach me the oxylipin procedure. Your energy always brought good (though sometimes noisy!) vibes to the group. A big thank you to **Dr. Nicole Hartung** and **Dr. Malwina Mainka** as well, for your kindness, your help, and for making me feel so welcome in the group.

I want to thank **Dr. Rei-ichi Ohno** for always being here to help. Together, we were able to resolve the artificial formation issue, and I appreciated working with you. I also want to thank **Dr. Kathrin Plitzko** for your good mood and for bringing delicious cakes. To **Katja Mosel**, it was so funny when Till accidentally sprayed us both with whipped cream! Thanks for your kindness and positivity.

I would like to express my sincere thanks to **Claudia Steinhage** and **Marion Fischer** for their valuable support during the supervision of the students in the practical course. I want to thank **Sabine Scalet** for her dedicated support and assistance with all administrative matters. I also want to thank members of the group, including **Anne Kaufmann**, **Carina Rothweiler**, **Evelynn Butsch**, **Michel Kuhn**, **Olivia Stroka**, and **Henrik Reuter**. Thanks to all of you for always bringing good vibes to the group!

To **Dr. Gürbüz Dursun** and **Katerina Mathianaki**, thank you for all the fun moments we shared during our private breaks! We also had some really lovely evenings at Laurentiusplatz. I hope we'll get the chance to meet again soon!

Enfin et surtout, Je tiens à remercier du fond du cœur ma famille pour son amour, son soutien inconditionnel et sa patience tout au long de ce parcours. Sans vous, rien de tout cela n'aurait été possible. Votre présence, vos encouragements et votre confiance m'ont porté dans les moments les plus difficiles. Merci d'avoir toujours cru en moi et d'avoir été mon pilier au quotidien. Je tiens également à adresser une attention toute particulière à Till, avec qui je partage ma vie.

Curriculum Vitae

The Curriculum Vitae is not available on the online version.

List of Publications

PUBLICATIONS IN PEER-REVIEWED JOURNALS

WITHIN THE SCOPE OF THIS THESIS

CARPANEDO L, WENDE LM, GOEBEL B, HÄFNER AK, CHROMIK MA, KAMPSCHULTE N, STEINHILBER D, AND SCHEBB NH, TARGETED LC-MS/MS (**2025**) SUBSTRATE-DEPENDENT INCORPORATION OF 15-LIPOXYGENASE PRODUCTS IN LIPIDS: 15-HETE AND 15-HEPE IN PI, 17-HDHA IN PLASMALOGEN PE, AND 13-HODE IN PC, JLR (ACCEPTED FOR PUBLICATION)

CARPANEDO L, RUND KM, WENDE LM, KAMPSCHULTE N, AND SCHEBB NH, (**2024**) LC-HRMS ANALYSIS OF PHOSPHOLIPIDS BEARING OXYLIPINS, *ANAL. CHIM. ACTA*. **1326**, 343139.

RUND KM*, CARPANEDO L*, LAUTERBACH R, WERMUND T, WEST AL, WENDE LM, CALDER PC, AND SCHEBB NH, (**2024**) LC-ESI-HRMS - LIPIDOMICS OF PHOSPHOLIPIDS – CHARACTERIZATION OF EXTRACTION, CHROMATOGRAPHY AND DETECTION PARAMETERS, *ANAL. BIOANAL. CHEM*. **416**, 925 – 944.

*AUTHORS CONTRIBUTED EQUALLY TO THIS WORK.

FURTHER PUBLICATIONS

GOEBEL B, CARPANEDO L, REIF S, GÖBEL T, SIMONYI S, SCHEBB NH, STEINHILBER D, AND HÄFNER AK, (**2023**) DEVELOPMENT OF A CELL-BASED MODEL SYSTEM FOR THE INVESTIGATION OF FERROPTOSIS, *FRONT CELL DEATH*. **2**, 1182239.

WENDE LM, CARPANEDO L, RUND KM, KAMSCHULTE N, AND SCHEBB NH (**2024**) TARGETING OXYLIPINS BOUND TO PHOSPHOLIPIDS IN HUMAN CELLS QUANTIFICATION OF ESTERIFIED OXYLIPINS FOLLOWING HILIC BASED FRACTIONATION OF POLAR LIPID CLASSES. GORDON RESEARCH CONFERENCES (GRC), WEEK 5TH – 10TH MAY, LUCCA, ITALY.

CARPANEDO L, WENDE LM, KAMSCHULTE N, AND SCHEBB NH (**2024**) TOWARDS AND ANALYSIS OF ESTERIFIED OXYLIPINS (OXIDIZED PHOSPHOLIPIDS). GORDON RESEARCH CONFERENCE (GRC), WEEK 5TH – 10TH MAY, LUCCA, ITALY.

WENDE LM, CARPANEDO L, RUND KM, KAMSCHULTE N, AND SCHEBB NH (**2023**) MATRIX EFFECTS OF PLASMA IN UNTARGETED LC-MS. INTERNATIONAL LIPIDOMICS SOCIETY (ILS), WEEK 27TH – 30TH AUGUST 2023, VIENNA, AUSTRIA.

CARPANEDO L, REIF S, KAMPSCHULTE N, AND SCHEBB NH, (**2023**) ANALYSIS OF ESTERIFIED OXYLIPINS IN THE MEMBRANES (OXIDIZED PHOSPHOLIPIDS) BY MEANS OF TARGETED AND UNTARGETED LC-MS. INTERNATIONAL LIPIDOMICS SOCIETY (ILS), WEEK 27TH – 30TH AUGUST 2023, VIENNA, AUSTRIA.

CARPANEDO L, REIF S, RUND KM, AND SCHEBB NH, (**2023**) UNTARGETED LIPIDOMICS OF OXIDIZED PHOSPHOLIPIDS BY LC-ESI-HRMS/MS – OPTIMIZATION OF CHROMATOGRAPHIC SEPARATION. INTERNATIONAL SOCIETY FOR THE STUDY OF FATTY ACIDS AND LIPIDS (ISSFAL), WEEK 2ND – 5TH JULY 2023, NANTES, FRANCE.

CARPANEDO L, RUND KM, WERMUND T, KAMPSCHULTE N, CALDER PC, AND SCHEBB NH, (**2022**) ANALYSIS OF POLAR LIPIDS IN PLASMA OF OMEGA-3 PUFA SUPPLEMENTED HUMAN SUBJECTS BY COMBINATION OF UNTARGETED LC-HRMS/MS AND TARGETED LC-MS/MS. EUROPEAN WORKSHOP ON LIPID MEDIATORS (EWLM), WEEK 29TH JUNE – 1ST JULY 2022, STOCKOLM, SWEDEN.

CARPANEDO L, RUND KM, AND SCHEBB NH, (**2021**) INVESTIGATION OF OXIDIZED LIPIDS IN BIOLOGICAL SAMPLES BY COMBINATION OF TARGETED OXYLIPIN ANALYSIS AND UNTARGETED LIPIDOMICS. INTERNATIONAL LIPIDOMICS SOCIETY (ILS), WEEK 5TH – 8TH OCTOBER 2021, REGENSBURG, GERMANY.